UNIVERSITY OF EAST ANGLIA

JOHN INNES CENTRE

Investigating the regulation of nuclear calcium oscillation in plant endosymbiosis

LAUREN ELIZABETH GRUBB

Thesis submitted to the University of East Anglia for the degree of Doctor of Philosophy

Research conducted at the John Innes Centre

2022

This copy of the thesis has been supplied on condition that anyone who consults it is understood to recognize that its copyright rests with the author and that use of any information derived there-from must be in accordance with current UK Copyright Law. In addition, any quotation or extract must include full attribution. Copyright © Lauren E. Grubb, 2022.

Abstract

Plants associate with beneficial microorganisms such as nitrogen-fixing bacteria, rhizobia, or arbuscular mycorrhizal (AM) fungi to access nutrients in a biologically available form. Successful colonization results in *de novo* organogenesis of a nodule structure for symbiotic nitrogen fixation or formation of a branched arbuscule structure in root cortical cells for AM fungi. Following perception of lipochitooligosaccharide Nod factors or short-chain chitooligosaccharide Myc factors, respectively, an important early signaling events in both symbiotic associations is the generation of nuclear calcium (Ca^{2+}) oscillation at the nuclear envelope. This requires three nuclear-localized ion channels, DOES NOT MAKE INFECTIONS1 (DMI1), cyclic nucleotide gated channel 15 (CNGC15) a/b/c and a SERCA-type ATPase, MCA8. While much is known about Nod and Myc factor perception as well as the requirement for these channels at the nuclear envelope, it is thus far unclear how these channels are activated.

This work presents a novel player in the common symbiosis signaling pathway, a kinase termed AUK. Using CRISPR-Cas9 experiments in *M. truncatula* hairy roots, AUK was shown to be required for nodulation. Overexpression of AUK in hairy roots as well as a gain-of-function EMS mutant resulted in spontaneous nuclear Ca^{2+} oscillation, and the generation of spontaneous nodule-like structures. In addition, there was increased nodulation and AM colonization upon inoculation with the respective symbionts, indicating an important role for AUK within the common symbiosis signaling pathway. Further epistasis analysis also indicated a role for AUK upstream of DMI1. Finally, preliminary evidence for a mechanism by which AUK may be activating the nuclear Ca^{2+} oscillation is investigated.

Overall, this thesis presents a novel player in the common symbiosis pathway and provides insight into a possible mechanism for activation of nuclear Ca^{2+} oscillation involved in plant association with beneficial symbiotic microorganisms.

Access Condition and Agreement

Each deposit in UEA Digital Repository is protected by copyright and other intellectual property rights, and duplication or sale of all or part of any of the Data Collections is not permitted, except that material may be duplicated by you for your research use or for educational purposes in electronic or print form. You must obtain permission from the copyright holder, usually the author, for any other use. Exceptions only apply where a deposit may be explicitly provided under a stated licence, such as a Creative Commons licence or Open Government licence.

Electronic or print copies may not be offered, whether for sale or otherwise to anyone, unless explicitly stated under a Creative Commons or Open Government license. Unauthorised reproduction, editing or reformatting for resale purposes is explicitly prohibited (except where approved by the copyright holder themselves) and UEA reserves the right to take immediate ‘take down’ action on behalf of the copyright and/or rights holder if this Access condition of the UEA Digital Repository is breached. Any material in this database has been supplied on the understanding that it is copyright material and that no quotation from the material may be published without proper acknowledgement.

Acknowledgements

To Myriam, many thanks for all you have taught me, your kind and supportive mentorship and your many edits throughout my PhD. I couldn't have done it without you!

To my secondary supervisor and committee member, Mark Banfield and David Lawson for many helpful discussions and suggestions during review meetings. To Allan Downie, for suggestions and useful insights during lab meetings.

To the John Innes Foundation, for the funding of the JIC/TSL/EI Rotation PhD Programme, which provided me with this amazing experience. To Steph Bornemann, for the welcoming start to my time in this programme and your dedication to student well-being. And to Ant Dodd for continuing the programme.

To Mark Banfield and Lars Ostergaard, for the opportunity to undertake rotations in your groups, in which I learned many skills useful for my final PhD project.

To the current and former members of the Charpentier Lab, namely: Aisling Cooke, Anson Lam, Catherine Jacott, Clemence Marchal, Edmund Bridge, Emily Tipper, Giulia Gobbato, Janni Seppä, Nicola Cooke, Pablo del Cerro, Pierre Dangeville. To Shouchao Yan, rotation student mentee, for your help with the DMI1-AUK wild-type co-IP.

To Sergio Lopez and Eva Wegel, for much help with microscopy. To Clare Stevenson and Julia Mundy for help with setting up and analysis of crystal screens. To Gerhard Saalbach and Carlo Oliveira-Martins for the LC-MS/MS analysis and answering of many questions. To lab support and horticultural services, who keep everything running smoothly and ensure our plants stay alive. In particular, thanks to Tim Wells for taking care of all the *Medicago* plants in B5110, and to Eleanor Rickaby for always knowing where to find things/who to ask. And to Gary Creissen, for introduction to and problem solving any equipment in the Bateson building. And of course to Steve the security guard for always being a friendly face and conversation on weekends and late nights in the lab.

To my fellow rotation students (virtually the best rotation year), Anna Backhaus, Jenny Jo, Jiawen Chen and Thomas Gate. From journal clubs (online and otherwise), to figure club, to exploring restaurants around Norwich, my PhD experience wouldn't have been nearly as enjoyable without you guys.

To everyone at Hill Farm Riding Centre and the Norwich lindy hoppers, and to everyone in my virtual French classes, thank you for providing an outlet to allow me to break from research for a while and keep me sane.

To the podcast ‘Help I Sexted My Boss’, for the countless hours of hilarity and laughter during long days in the flow hood or screening roots. And to Radio Norfolk for being the only radio station we could access in the lab, providing entertainment no matter how cheesy.

And finally, to all my friends and family. Thank you for putting up with me and always lending an ear to me chattering away about my research. In particular, thanks to my dad for always being willing to read over my thesis drafts and making a huge effort to understand what my research is about.

Table of Contents

List of Figures

List of Tables

Acronyms and abbreviations

AM	Arbuscular mycorrhiza
ABA	Abscisic acid
ABI1	ABA INSENSITIVE1
ACN	Acetonitrile
AD	Activation domain
AKT1	ARABIDOPSIS K^+ TRANSPORTER1
AMP-PNP	Adenylyl-imidodiphosphate
ANOVA	Analysis of variance
AON	Autoregulation of nodulation
ARB	Arbuscule
ASL18	ASYMMETRIC LEAVES2-LIKE18
AU	Arbitrary units
AUK	Auxiliary unit kinase of DMI1
AVG	Aminoethoxyvinylglycine
BAK1	BRI1-ASSOCIATED RECEPTOR KINASE1
BCP1	BLUE COPPER PROTEIN1
BCS	Basic chemicals screen
BD	Binding domain
BES1	BRI1 EMS SUPPRESSOR1
BiFC	Bifluorecence complementation
BIK1	BOTRYTIS INDUCED KINASE1
BIN2	BR-INSENSITIVE2
BK	CA^{2+}-ACTIVATED POTASSIUM CHANNEL
BKI1	BRI1 KINASE INHIBITOR1
BLI	Biolayer interferometry
BNM	Buffered nodulation media
BR	Brassinosteroid
BRI1	BRASSINOSTEROID INSENSITIVE1
BSK	BR-SIGNALING KINASE
BZR1	BRASSINAZOLE RESISTANT1
Ca^{2+}	Calcium ion
CaM	Calmodulin (Ca^{2+} mediated protein)
CAX	Ca^{2+}/H^+-exchanger
CBL	Calcineurin B-like
CBP	Consecutive base pairs

CCaMK	Ca^{2+}/CaM-dependent protein kinase
CDKA	CYCLIN-DEPENDENT KINASE A
CDPK	Calcium-dependent protein kinase
CEP	C-TERMINALLY ENCODED PEPTIDE
CFP	Cyan fluorescent protein
CID	Collision-induced dissociation
CIPK	CBL-interacting protein kinase
CLE	CLAVATA3/EMBRYO-SURROUNDING REGION
CML	CaM-like protein
CNGC	Cyclic nucleotide gated channel
CO	Chitooligosaccharide
co-IP	co-immunoprecipitation
CPA	Cyclopiazonic acid
CRE1	Cytokinin receptor
CRISPR	Clustered regularly interspaced short palindromic repeats
cryo-EM	Cryogenic electron microscopy
Ct	C-terminus
C-term	Carboxy terminus
DAG	Diacylglycerol
DGK	DAG KINASE
DMI1	DOES NOT MAKE INFECTIONS
DNA	Deoxyribonucleic acid
dNTPs	Deoxyribonucleotide triphosphate
dpi	Days post inoculation/infiltration
DTT	Dithiothreitol
ECL	Enhanced chemiluminescence
EDTA	Ethylenediaminetetraacetic acid
EMS	Ethylmethylsulfonate
ENOD	EARLY NODULIN
EtOH	Ethanol
EV	Empty vector
FER	FERONIA
FL	Full-length
FLS2	FLAGELLIN SENSING2
FRET	Förster resonance energy transfer
GA	Gibberellic acid

GF	Gel filtration
GFP	Green fluorescent protein
GLR	Glutamate-like receptor
GoF	Gain of function
HA1	H^{+}-ATPase
HCD	Higher-energy C-trap dissociation
HEPES	4-(2-hydroxyethyl)-1-piperazineethanesulfonic acid
Het	Heterozygous
His	Histidine
HMGR1	3-hydroxy-3-methylglutaryl CoA reductase1
Hmz	Homozygous
HRP	Horseradish peroxidase
IAA	Iodoacetamide
IBP	Internal base pairs
IP	Immunoprecipitation
IP3	Inositol (1,4,5)-trisphosphate
IPD3	INTERACTING PROTEIN OF DMI3
IPTG	Isopropyl β- d-1-thiogalactopyranoside
IRH	Intraradical hyphae
IT	Infection thread
JIC	John Innes Centre
KASP	Kompetitive allele-specific PCR
KD	Kinase domain
Kd	Dissociation constant
kDa	Kilodaltons
KIN10	KINASE10
Km	Kinase mutant
LB	Luria broth
LBD16	LATERAL ORGAN BOUNDARIES DOMAIN16
LC-MS/MS	Liquid chromatography tandem mass spectrometry
LCO	Lipochitooligosaccharide
Leu	Leucine
LHK1	LOTUS HISTIDINE KINASE
LRR	Leucine-rich repeat
LYK	LysM domain-containing receptor-like kinase
LysM	Lysin-motif

MAPK	Mitogen activated protein kinase
Mas7	Mastoparan7 analog
MBP	Maltose binding protein
MCA8	*M. truncatula* Ca^{2+}-ATP-ase
Mod FP	Modified fahreus plant media
MthK	Ca^{2+}-gated potassium channel
MVA	Mevalonate
NADP	Nicotinamide adenine dinucleotide phosphate
NEB	New England Biolabs
NFP	Nod factor perception
NFR	Nod factor receptor
NF-Y	Nuclear factor-Y
Ni^{2+}-NTA	Ni^{2+} Nitriloacetic acid
NIN	Nodule Inception
NLS	Nuclear localization signal
Nod	Nodulin
NPL	NODULE PECTATE LYASE
N-term	Amino terminus
NUP	NUCLEOPORIN
OE	Overexpression
OST1	OPEN STOMATA1
PA	Phosphatidic acid
PAM	Protospacer adjacent motif
PCR	Polymerase chain reaction
PDB	Protein data bank
PIP2	Phosphatidylinositol (4,5)-bisphosphate
PIT	Pre-infection thread
PKA	PROTEIN KINASE A
PKC	PROTEIN KINASE C
PKG	PROTEIN KINASE G
PLC	Phospholipase C
PLD	Phospholipase D
PLT	PLETHORA
PPA	Pre-penetration apparatus
PT4	*PHOSPHATE TRANSPORTER 4*
PUB	Plant U-box protein

PVDF	Polyvinylidene fluoride
RCK	Regulator of K^+ conductance
REM	Remorin
RLCK	Receptor-like cytoplasmic kinase
RLK	Receptor-like kinase
RLP	Receptor-like protein
RNA	Ribonucleic acid
rpm	Revolutions per minute
RT	Room temperature
SCR	SCARECROW
SD	Synthetic dextrose
SDS-PAGE	Sodium dodecyl sulphate- polyacrylamide gel electrophoresis
SFM	*Spodoptera frugiperda* medium
sgRNA	Small guide RNA
SHR	SHORTROOT
SIE3	SYMRK-INTERACTING E3 LIGASE
SINA4	SEVEN IN ABSENTIA4
SIRK1	SUCROSE INSENSITIVE KINASE1
SLAC1	SLOW ANION CHANNEL1
SNP	Single nucleotide polymorphism
SnRK	SNF-related protein kinase
SOC	Super optimal broth with catabolite repression
SPCH	SPEECHLESS
SUMO	Small ubiquitin-like modifier
SUNN	SUPER NUMERIC NODULE
Sym	Symbiosis
SYMREM	SYMBIOSIS REMORIN
SYMRK	SYMBIOSIS RECEPTOR KINASE
TAE	Tris acetate EDTA
TBP	Total base pairs
TBS	Tris buffered saline
TCEP	Tris(2-carboxyethyl)phosphine
TML	TOO MUCH LOVE
Trp	Tryptophan
TY	Tryptone yeast extract
UBI	Ubiquitin

UV	Ultraviolet
VES	Vesicle
WT	Wild-type
X-Gal	5-bromo-4-chloro-3-indolyl-beta-D-galacto-pyranoside
Y2H	Yeast 2-hybrid
YC	Yellow cameleon
YCE	YFP C-terminus
YFP	Yellow fluorescent protein
YNE	YFP N-terminus
YPAD	Yeast extract-peptone-adenine dextrose

1- Introduction

1.1- Calcium as a second messenger in plants

The calcium ion (Ca^{2+}), which is a ubiquitous second messenger in plants, plays a key role in signaling processes that govern the plant response to environmental cues and stressors, both biotic and abiotic. As Ca^{2+} is key to such a wide variety of signaling responses, ion levels must be tightly regulated as high cytosolic Ca^{2+} concentration can be detrimental for the cell. It can cause precipitation of calcium salts with inorganic phosphate, which would otherwise be used for metabolic processes and ATP (Sanders *et al.*, 1999). Thus, during resting state, the plant maintains a low cytosolic Ca^{2+} concentration of around 50-100 nM (Clapham, 2007). Upon recognition of a stimulus, Ca^{2+} is rapidly mobilized from internal stores such as the vacuole and endoplasmic reticulum, and from the external environment and cell wall, which can host Ca^{2+} levels of 0.1-10 mM (Stael *et al.*, 2012). The spatiotemporal pattern of Ca^{2+} release changes during stimulus response, including variation in frequency, amplitude, spike duration and shape, and was hypothesized to encode information about the type of external signal in the form of a 'calcium signature' (Figure 1.1; McAinsh & Hetherington, 1998; McAinsh & Pittman, 2009). Information about stimulus nature is relayed by Ca^{2+} binding proteins containing EF-hand motifs, which allow for signal decoding and activation of appropriate genes and downstream targets, creating signaling cascades which culminate in the appropriate plant response to the stimulus or stressor. Release of calcium requires Ca^{2+} channels, and re-uptake requires Ca^{2+} transporters. Many plant Ca^{2+} channels have been cloned and characterized and fall into several different classes. Some of the most studied channels regulating Ca^{2+} influx across membranes include ligand-gated Ca^{2+} permeable channels known as cyclic nucleotide gated channels (CNGCs), and glutamate receptors (GLRs), as well as several other channel types (Demidchik *et al.*, 2018). Channels required for the uptake of Ca^{2+} have been identified as Ca^{2+}-ATPase (e.g. ACAs and ECAs) and Ca^{2+}/H^{+} exchangers (CAXs; Demidchik *et al.*, 2018).

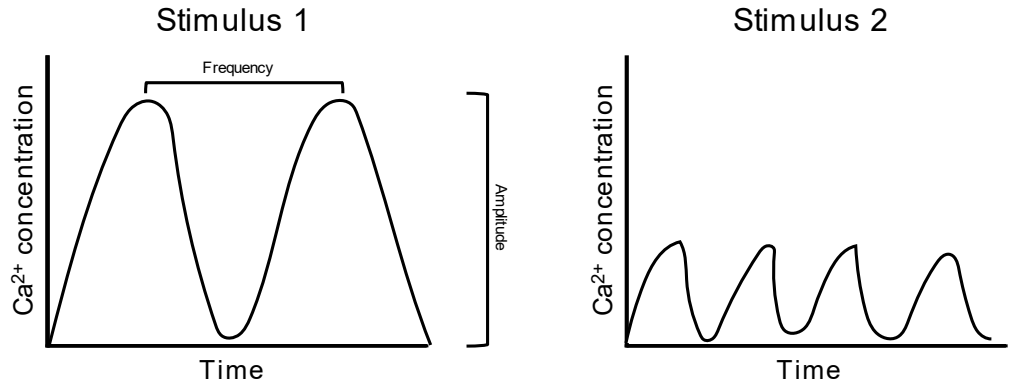

Figure 1.1. Calcium signature hypothesis.

Hypothetical examples of two different types of 'calcium signatures' produced by different stimuli. There is variation seen in amplitude, and frequency of the calcium oscillation. Calcium signatures can also differ in oscillation shape and duration of the signal.

The Ca^{2+} signature must be interpreted and transduced through a signaling cascade to culminate in the appropriate plant response dependent on the external stimulus. The interpretation takes place via Ca^{2+}-binding proteins, many of which possess classical helix-loop-helix EF-hand motifs, to which Ca^{2+} binding induces a conformational change, allowing it to interact with downstream targets to propagate the signal. In accordance with the diversity of Ca^{2+} signature locations and patterns, these Ca^{2+} sensor proteins are proposed to possess variety in Ca^{2+} binding characteristics, subcellular localization, and downstream interactions. There are several types of Ca^{2+}-binding sensor proteins, and they can be classified as sensor responders or sensor relay proteins (Sanders *et al.*, 2002). The sensor responders are proteins which couple a sensing function (Ca^{2+} binding and conformational change) with response activity, such as kinase activity. Calcium-dependent protein kinases (CDPKs) and Ca^{2+}/CaM protein kinases (CCaMKs) are classified as sensor responders. The sensor relay proteins possess Ca^{2+} binding domains and usually undergo a conformational change upon binding, but they lack effector domains and must interact with downstream targets to modulate their activity for generation of a response. Classes of sensor relay proteins include calmodulins (CaMs), CaM-like proteins (CMLs), and calcineurin-B like proteins (CBLs). CBL targets are CBL-interacting protein kinases (CIPKs), dividing the sensor and responder across two proteins, with signal translated to phosphorylation upon complex formation (Kudla *et al.*, 2018). The types of calcium-binding sensor proteins are illustrated in Figure 1.2. Often the Ca^{2+} signal transduction and interpretation consists of cascades of phosphorylation by kinases and phosphatases and the regulation of transcription factors leading to appropriate gene

expression changes (Sanders *et al.*, 1999). The diversity in Ca^{2+} sensors allow the plant to respond to a diverse range of responses.

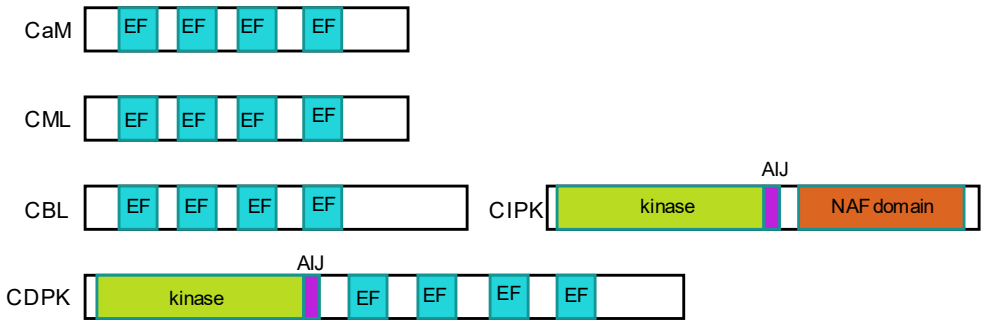

Figure 1.2. Types of calcium-binding sensor proteins.
Different classes of calcium-binding sensor proteins are shown with their domain structure. Calcium-binding EF hands are denoted in blue, kinase domains in green and autoinhibitory junctions (AIJ) in purple. CBLs and CIPKs are illustrated on the same line as they function in pairs and the CIPKs possess and regulatory NAF domain.

1.1.1- The CaM-binding protein ZAR1 in *Arabidopsis*

An interesting CaM-binding LRR-RLK, ZYGOTIC ARREST1 (ZAR1) has been studied in *Arabidopsis.* ZAR1 was shown to be an essential gene in *Arabidopsis*, with a *zar1* mutant zygote elongating normally, but failing to perform asymmetric cell division, resulting in a lethal phenotype (Yu et al., 2016). The authors found its localization in protoplasts to the plasma membrane and nucleus, and it was also found to have a putative CaM-binding domain and Gβ- binding motif, which were both required for its activation. A phylogenetic tree of ZAR1 close homologues in legumes is shown in Figure 1.3. As described later in Section 1.3, the *M. truncatula* homolog was the focus of this thesis and will hereafter be referred to as AUK. There are three *ZAR1* homologs in *Arabidopsis*, however only one in *M. truncatula*, which is also quite diverged, suggesting its mechanism and function may differ in legumes.

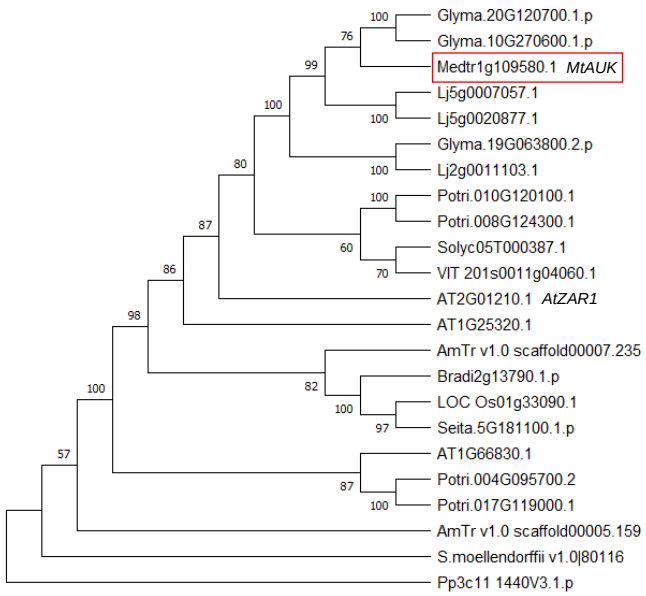

Figure 1.3. Phylogenetic tree of *Mt*AUK homologs

Phylogeny was produced using the Neighbour-joining method (Saitou & Nei, 1987). 1000 bootstraps were used (Felsenstein, 1985). All gaps and missing data were eliminated. Analysis conducted in MEGA-X (Kumar et al., 2018). No branches were condensed. *Mt*AUK and *At*ZAR1 are indicated, with *Mt*AUK indicated with a red box. *Glma, Glycine max; Medtr, M. truncatula; Lj, L. japonicus; Potri, Populus trichocarpa; Solyc, Solanum lycopersicum; VIT, Vitis vinifera; AT, A. thaliana; Am, Amborella trichopoda; Bradi, Brachypodium distachyon; Os, Oryza sativa; Seita, Setaria italica; Pp, Physcomitrella patens.*

1.1.2- Nuclear calcium

Approaches for measuring calcium responses in plants have become more sophisticated over time. Early measurements involved microinjection with Ca^{2+}-responsive dyes, which were used to identify induction of nuclear-localized Ca^{2+} oscillations within legume root hair cells in response to rhizobial Nod factor signaling molecules (Ehrhardt *et al*., 1996). However, these dyes are not restricted to the nucleus, and thus the measurement could only surmise that there was Ca^{2+} oscillation within the nuclear region. Next was the eventual development of methods that make use of genetically encoded Ca^{2+}-responsive proteins, such as the naturally-occurring aequorin (Knight *et al.*, 1991) or the synthetic cameleon (Miyawaki *et al*., 1997). Aequorin is composed of an apoprotein and luminophore coelenterazine. Ca^{2+} binds the three Ca^{2+}-binding EF-hand domains within the protein and induces a conformational change allowing the oxidation of coelenterazine to coelenteramide, producing CO_2 (Shimomura *et al.*, 1974). Blue light is emitted when coelenteramide relaxes to its ground state (Shimomura & Johnson, 1970). Yellow cameleons (YC) are the most commonly used ratiometric sensor in plants and make use of Förster resonance energy transfer (FRET) between yellow fluorescent protein (YFP)

and cyan fluorescent protein (CFP) linked by CaM. Binding of Ca^{2+} to CaM induces a conformational change to bring the fluorescent proteins closer together, inducing an increase in YFP and decrease in CFP fluorescence intensity (Miyawaki *et al.*, 1997).

Although initially debated, it is now widely accepted that the nucleus and cytoplasm can have distinct Ca^{2+} responses (Charpentier & Oldroyd, 2013). Use of the cameleon calcium sensors mentioned above has led to conclusive observation of nuclear Ca^{2+} signals in plant protoplasts and cell culture responses to sphingolipids (Lachaud *et al.*, 2010), to wind and cold (van der Luit *et al.*, 1999), the G protein agonist, mastoparan (Pauly *et al.*, 2000), osmotic shock (Pauly *et al.*, 2001), pathogen elicitors (Lecourieux *et al.*, 2005), and jasmonic acid (Walter *et al.*, 2007). Nuclear Ca^{2+} has been uncovered in whole plant responses to symbiotic signals (Chabaud *et al.*, 2011; Sieberer *et al.*, 2009), and playing a role in root development (Leitão *et al.*, 2019). Changes in nuclear Ca^{2+} dynamics have also been shown in pollen tube growth (Moser *et al.*, 2020), in response to some pathogenic elicitors (Yuan *et al.*, 2020), and to NaCl and cold responses (Kelner *et al.*, 2018), although the molecular players behind these signals are unclear. In addition, many Ca^{2+}-binding proteins are nuclear localized, including CaMs and CMLs (Bender *et al.*, 2013; Choi *et al.*, 2005; Wu *et al.*, 2012), CDPKs (Boudsocq *et al.*, 2010; Choi *et al.*, 2005; Dammann *et al.*, 2003; Ishida *et al.*, 2008), CCaMKs (Singh & Parniske, 2012), CBL-CIPKs (Batistič *et al.*, 2010), IQD proteins (Bürstenbinder *et al.*, 2017), and a Ca^{2+}-binding ATP/GDP protein (Guan *et al.*, 2013). One of the most widely studied nuclear Ca^{2+} oscillations occurs upon perception of symbiotic stimuli (Chabaud *et al.*, 2011; Ehrhardt *et al.*, 1996; Miwa *et al.*, 2006; Sieberer *et al.*, 2009), which is the focus of this thesis.

1.2- Signaling in endosymbiosis

1.2.1- Nuclear Ca^{2+} oscillation in endosymbiosis

For symbiosis with nitrogen fixing bacteria, called rhizobia, in nitrogen-limited soils the host plant root secretes flavonoid signals, which can confer host-specificity (Lerouge *et al.*, 1990; Peters *et al.*, 1986). These host-specific flavonoids activate the rhizobia transcription factor, NodD to induce the expression of Nodulation (Nod) genes. From these Nod genes, Nod factors are produced, which are lipochitooligosaccharide (LCO) molecules with a conserved chitin backbone. Different side chain decorations can confer specificity to the interaction with the appropriate plant host (Liu & Murray, 2016). These LCO molecules are recognized by LysM receptors at the plasma membrane and activate the early signal transduction pathway to nuclear Ca^{2+} oscillation and symbiosis gene expression.

One of the first physiological events occurring upon perception of Nod factors is a nuclear Ca^{2+} oscillation. First described in 1996 from microinjection experiments of Ca^{2+}-responsive dextran dye in alfalfa root hairs (Ehrhardt *et al.*, 1996), similar Ca^{2+} oscillation was observed in *Pisum sativum* (Walker *et al.*, 2000a), in *Lotus japonicus* (Harris *et al.*, 2003), and

in *Phaseolus vulgaris* (Cárdenas *et al.,* 1999). The Ca^{2+} oscillation preferentially starts in the nucleus, as determined by the dual Ca^{2+} reporter NRCG-GECO1.2, allowing simultaneous recording of cytoplasmic and nuclear Ca^{2+} oscillation (Kelner *et al.,* 2018). It begins approximately 10-30 min after Nod factor addition, and has a period of approximately 60 s (Ehrhardt *et al.,* 1996; Walker *et al.,* 2000). The spikes are asymmetrical, consisting of a quick rise to a peak, followed by a more gradual fall back to baseline, indicating different kinetics for Ca^{2+} influx and reuptake. In addition, the Ca^{2+} oscillations are cell autonomous. This Nod factor-induced spiking could be induced at low concentrations, of just 10^{-12}- 10^{-9} M, and showed a structural specificity of the host for Nod factors produced by the appropriate colonizing rhizobia (Ehrhardt *et al.,* 1996; Oldroyd, Mitra, *et al.,* 2001; Shaw & Long, 2003). Interestingly, Miwa *et al.,* (2006) have shown that an average of 36 calcium spikes are sufficient for induction of early nodulin genes, such as *ENOD11* in root hairs. The nuclear Ca^{2+} oscillation is most regular in the zone of growing root hairs (Sieberer *et al.,* 2009).

Perception of AM fungal, 'Myc' factors also induces nuclear Ca^{2+} oscillation, differing from that induced by Nod factors (Kosuta *et al.,* 2008). Chabaud *et al.,* (2011) observed Ca^{2+} oscillation in cells in contact with AM hyphopodia, with the highest frequency spiking in the cells with nuclei facing the fungal contact site. In addition, the path of both rhizobial and fungal infection seems to be determined by a switch from low- to high-frequency Ca^{2+} oscillation, which ceases upon completion of the colonization (Sieberer *et al.,* 2012). This led to the proposal that the Ca^{2+} oscillation may allow for cell adaptation of the plant for colonization (Charpentier & Oldroyd, 2013).

1.2.2- Symbiotic perception and the common symbiosis signaling pathway

1.2.2.1- Perception of Nod and Myc factors

Perception occurs through recognition of Nod factors and Myc, which are LCOs and short-chain chitooligosaccharides (COs), respectively. Recognition of Nod factors occurs through the Lysin motif (LysM) receptor complexes consisting of receptor pairs, termed NOD FACTOR RECEPTOR1/5 (NFR1/NFR5) in *L. japonicus* or NOD FACTOR PERCEPTION/LYSM DOMAIN RECEPTOR-LIKE KINASE3 (NFP/LYK3) in *M. truncatula* (Arrighi *et al.,* 2006; Broghammer *et al.,* 2012; Limpens *et al.,* 2003; Madsen *et al.,* 2003; Radutoiu *et al.,* 2003; Smit *et al.,* 2007). Myc factor recognition occurs through the LysM receptor kinase *Mt*LYK9 (Gibelin-Viala *et al.,* 2019; Leppyanen *et al.,* 2018). Intriguingly, overexpression of *LjNFR1* and *LjNFR5* was found to trigger the formation of spontaneous nodule structures in absence of rhizobia (Ried *et al.,* 2014). This correlated with induction of symbiosis genes *NODULE INCEPTION (NIN)* and *SbtS*, and the action of NFR5 was dependent on NFR1 and a proposed co-receptor SYMBIOSIS RECEPTOR KINASE (SYMRK). Interestingly, *NFR1* and *NFR5* expression solely in the root epidermis is sufficient for infection thread formation and cortical cell division for nodule organogenesis (Hayashi *et*

al., 2014), suggesting that their expression might be confined to the epidermis. In *M. truncatula*, a screen for interactors of LYK3, identified a Plant U-box protein, PUB1, which was induced by Nod factor and found to interact with the LYK3 kinase domain (Mbengue *et al.*, 2010). The authors determined that PUB1 could be phosphorylated by LYK3 but could not detect ubiquitination or degradation of LYK3 by PUB1, suggesting that the post-translational modifications such as phosphorylation and ubiquitination may have important roles in symbiotic signaling, but further work needs to be done to determine the mechanism.

1.2.2.2- Nuclear Ca^{2+} oscillation encoding

Downstream of perception, there are several common factors required for nuclear Ca^{2+} oscillation for both rhizobial and AM fungal symbionts, termed the common symbiosis (sym) pathway. Originally characterized based on the inability of *M. truncatula* mutants to form nodules or be colonized by AM fungi, the *DOES NOT MAKE INFECTIONS (DMI)* genes *DMI1* and *DMI2* have been found to be required for nuclear Ca^{2+} oscillation with both rhizobia (Sieberer *et al.*, 2009; Wais *et al.*, 2000), and AM fungi (Chabaud *et al.*, 2011; Kosuta *et al.*, 2008). *MtDMI2/LjSYMBIOSIS RECEPTOR KINASE (LjSYMRK)* encodes a leucine-rich repeat receptor-like kinase (LRR-RLK), which is believed to act as a co-receptor through its interaction with the LysM-RLKs at the plasma membrane (Antolín-Llovera *et al.*, 2014; Endre *et al.*, 2002; Stracke *et al.*, 2002). Although not found to ubiquitinate LYK3, a report identified PUB1 as a negative regulator of DMI2 through polyubiquitination leading to turnover by the 26S proteasome (Vernié *et al.*, 2016). In addition, two E3 ligases have been reported to ubiquitinate *Lj*SYMRK, including SymRK-INTERACTING E3 ligase (SIE3), which is a positive regulator of nodulation (Yuan *et al.*, 2012), and SEVEN IN ABSENTIA4 (SINA4), which destabilizes SYMRK and negatively impacts rhizobial infection (Den Herder *et al.*, 2007). In addition, another PUB E3 ligase, PUB2 was reported to be phosphorylated by DMI2, activating its ubiquitination activity on DMI2 for its polyubiquitination and turnover by the 26S proteasome to maintain a homeostasis during nodulation (Liu *et al.*, 2018). Interestingly, Ried *et al.*, (2014) also identified spontaneous nodules upon overexpression of *LjSYMRK*, as well as observation of induced expression of *NIN*, and of other AM marker genes, *SbtS*, and *SbtM1*. Saha *et al.*, 2014 also observed spontaneous nodulation with the overexpression of *M. truncatula SYMRK*, *MtDMI2* kinase domain, and with the overexpression of *Arachis hypogaea SYMRK* kinase domain. These studies all implicate DMI2 as playing an important role in symbiosis with both rhizobia and AM, and as an important point in the symbiosis pathway for regulation.

MtDMI1 encodes a cation permeable channel (Ané *et al.*, 2004), which localizes to the nuclear envelope (Riely *et al.*, 2007). In *L. japonicus*, the role of *Mt*DMI1 is performed by its ortholog *Lj*POLLUX and another potassium-permeable channel *Lj*CASTOR, which similarly localize to the nuclear envelope and are required for generation of symbiotic nuclear

Ca^{2+} (Charpentier *et al.,* 2008; Miwa *et al.,* 2006). Recently, researchers identified a gain-of-function allele of *Mt*DMI1 possessing a point mutation within the RCK2 domain, which could produce spontaneous nodules (Liu *et al.,* 2022). This constitutively active version of DMI1 corresponded to a point mutation of Ser760, which disrupts a hydrogen bond and salt bridge network connecting the RCK2 domains of neighbouring subunits in the DMI1 tetramer. The gain-of-function activity was only observed in a heterozygous mutant, through a mechanism not fully understood. In addition, this constitutively active *DMI1* mutant was also able to produce spontaneous Ca^{2+} oscillations, indicating an involvement of DMI1 in the activation of nuclear Ca^{2+} oscillation and in the generation of nodule structures. The authors additionally observed constitutive expression of the nodulation-related *NIN* and *EARLY NODULIN GENE 11 (ENOD11),* and the AM-related *H^+-ATPase1 (HA1), BLUE COPPER PROTEIN1 (BCP1)* and *PHOSPHATE TRANSPORTER4 (PT4).* Finally, they reported that *DMI1* overexpression could result in spontaneous nodule formation. Therefore, DMI1 also plays a key role in symbiosis signal transduction, and identification of its activation mechanism will be important for understanding how symbiosis is activated and regulated.

There are two other channels located on the nuclear envelope, which are required for the symbiosis-induced nuclear Ca^{2+}, including a SarcoEndoplasmic reticulum (SERCA)-type ATPase (MCA8) (Capoen *et al.,* 2011), and a channel of CYCLIC NUCLEOTIDE GATED CHANNEL15 (CNGC15) a/b/c units (Charpentier *et al.,* 2016). DMI1 and CNGC15 have been shown to associate in a complex at the nuclear envelope via the C-terminus of DMI1 and the N-terminus of CNGC15s (Charpentier *et al.,* 2016). Recently, a calmodulin (*Mt*CaM2) was identified to associate with CNGC15 and function to close the channel, therefore providing the negative feedback of the nuclear Ca^{2+} oscillation (Del Cerro *et al.,* 2022). In addition to the ion channels, components of the nucleoporin complex, NUP85, NUP133 and NENA are also required for the symbiotic nuclear Ca^{2+} oscillation (Groth *et al.,* 2010; Kanamori *et al.,* 2006; Saito *et al.,* 2007). Mathematical modeling has indicated that *Mt*DMI1 functions to not only counter-balance the ion flux of positive charge generated by CNGC15s, but also to regulate the calcium signal with simultaneous activation of DMI1 and CNGCs for oscillation to occur (Charpentier *et al.,* 2013, 2016; Granqvist *et al.,* 2015), indicating an interplay between the interacting channels to activate and regulate the nuclear Ca^{2+} oscillation.

1.2.2.3- Decoding of nuclear Ca^{2+} oscillation

A third *dmi* mutant, *dmi3,* was found to act downstream of the nuclear Ca^{2+} oscillation (Wais *et al.,* 2000). It encodes a Ca^{2+}/CaM kinase, *Mt*DMI3 or *Lj*CCaMK, with a role in decoding the nuclear Ca^{2+} oscillations. This CCaMK associates with and phosphorylates INTERACTING PROTEIN OF DMI3 (IPD3)/*Lj*CYCLOPS (Horváth *et al.,* 2011; Lévy *et al.,* 2004; Messinese *et al.,* 2007; Mitra *et al.,* 2004; Yano *et al.,* 2008), and together they induce expression of appropriate symbiosis-related genes, such *NIN* (Schauser *et al.,* 1999; Singh *et*

al., 2014), which itself is a transcription factor that regulates expression of the *NUCLEAR FACTOR-Y SUBINIT* genes (*NF-YA1* and *NF-YB1*), which control cell division (Soyano *et al.,* 2013; Yoro *et al.,* 2014). CCaMK possesses a catalytic domain followed by a CaM-binding/autoinhibitory domain and three Ca^{2+}-binding EF-hand motifs, allowing for regulation by both Ca^{2+} and Ca^{2+}-loaded CaM (Figure 1.4). CCaMK kinase domain alone, lacking the autoinhibitory domain, has been reported to generate spontaneous nodules when expressed in absence of rhizobia (Gleason *et al.,* 2006), indicating the importance of the autoinhibitory domain in regulation of its activity. Miller *et al.,* (2013) identified a mechanism for activation and inactivation of CCaMK through determination of different binding affinities of CaM and EF-hands whereby at basal levels of calcium, Ca^{2+} is bound to CCaMK, promoting its autophosphorylation on Thr271, and the protein is maintained in an inactive state. However, at elevated Ca^{2+} levels, such as when nuclear Ca^{2+} oscillation is occurring, Ca^{2+}-bound CaM can bind to CCaMK and activate it by overriding the autoinhibitory domain autophosphorylation. This is consistent with autoactive mutation previously shown by mutating Thr271 inducing spontaneous nodules (Hayashi *et al.,* 2014; Takeda *et al.,* 2012; Tirichine *et al.,* 2006), where the inability of CCaMK activity to be suppressed by phosphorylation at this Thr residue led to its autoactivation. In addition, phosphorylation at Ser343/344 has been shown to inhibit CaM binding, preventing the activation of CCaMK (Liao *et al.,* 2012; Routray *et al.,* 2013). Interestingly, a recent report showed a mutation W342F, which increased the binding of CaM to CCaMK, even in the absence of Ca^{2+}. However, there was an impact on nodulation, implying the need for proper CaM kinetics for the regulation of CCaMK activity (Jauregui *et al.,* 2017). Importantly, downstream of CCaMK is the *Mt*IPD3/*Lj*CYCLOPS, which is phosphorylated by CCaMK. A phosphomimetic variant of *Lj*CYCLOPS can also induce spontaneous nodulation without rhizobia present (Horváth *et al.,* 2011; Ovchinnikova *et al.,* 2011; Singh *et al.,* 2014; Yano *et al.,* 2008). Thus, CCaMK acts as an important step within the nodulation and AM signaling pathways and its activity is subjected to multiple regulatory mechanisms to ensure its proper activity. Altogether, DMI2, DMI1, CNGC15a/b/c, CaM2, MCA8, CCaMK and CYCLOPS form the common symbiosis signaling pathway, required for endosymbiosis with both rhizobia and AM fungi. Figure 1.5 illustrates the important components for symbiosis-induced nuclear Ca^{2+} oscillation in response to rhizobial Nod factors.

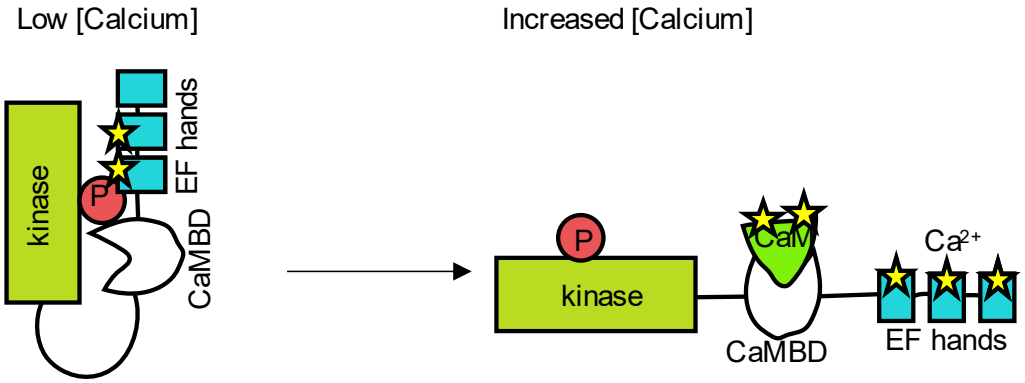

Figure 1.4. CCaMK activation mechanism.

CCaMK possesses a kinase domain (green), a CaM-binding domain (CaMBD; white) and three EF hands (blue). In a low calcium state not all EF hands have Ca^{2+} bound. This promotes autophosphorylation, which maintains the kinase domain in an inactive state. An increase in calcium results in binding of all three EF hands with calcium and the binding of calcium-bound CaM to the CaMBD. This results in release of the autoinhibition of the kinase domain, allowing it to interact with and phosphorylate downstream targets. Figure adapted from Sathyanarayanan et al., 2001.

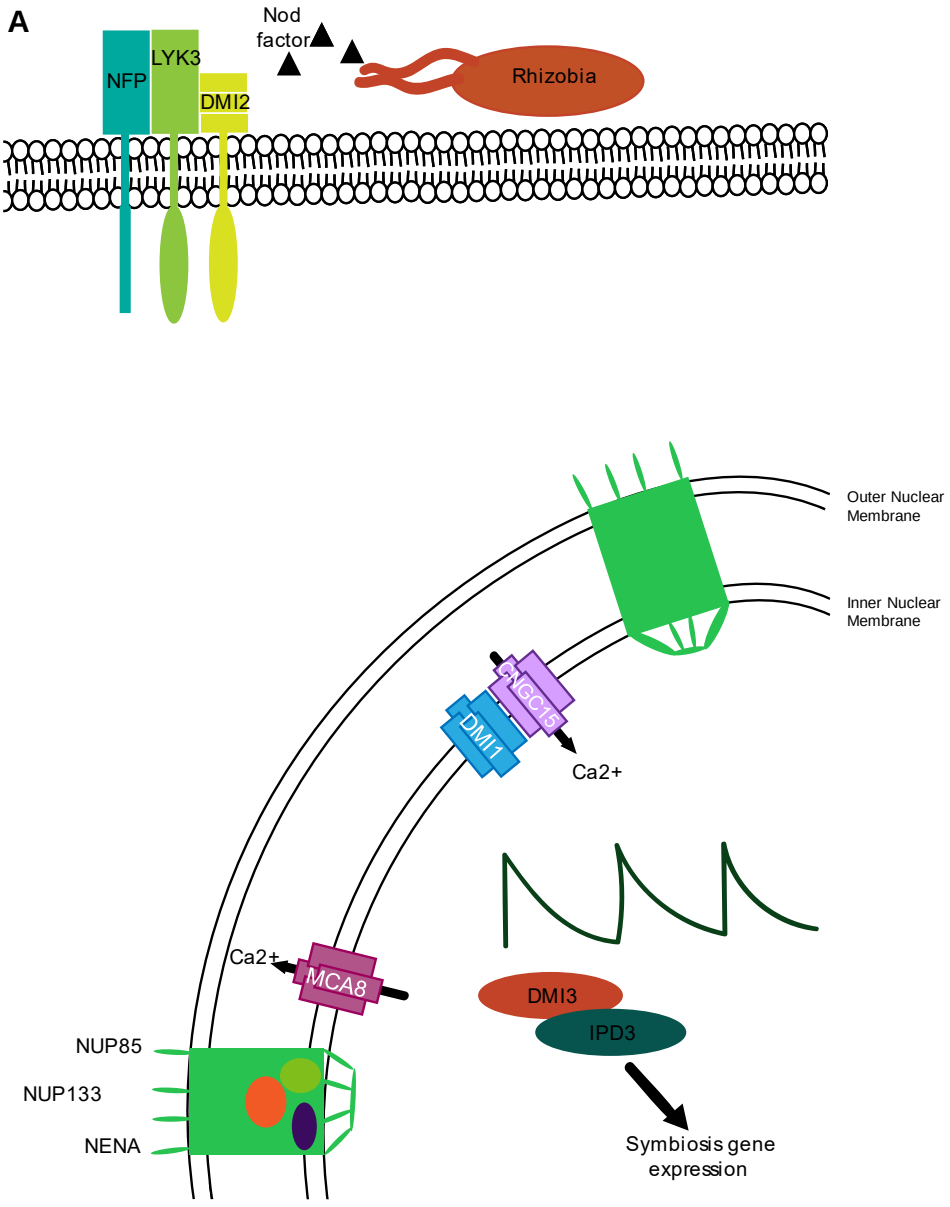

B

M. truncatula Gene Name	*L. japonicus* Gene Name
NOD FACTOR PERCEPTION (NFP)	*NOD FACTOR RECEPTOR1 (NFR1)*
LYSM- RECEPTOR-LIKE KINASE3 (LYK3)	*NOD FACTOR RECEPTOR5 (NFR5)*
DOES NOT MAKE INFECTIONS2 (DMI2)	*SYMBIOSIS RECEPTOR KINASE (SYMRK)*
DOES NOT MAKE INFECTIONS1 (DMI1)	*CASTOR/POLLUX*
DOES NOT MAKE INFECTIONS3 (DMI3)	*CALCIUM/CALMODULIN KINASE (CCaMK)*
INTERACTING PROTEIN OF DMI3(IPD3)	*CYCLOPS*

Figure 1.5. Molecular components required for the generation of rhizobia-induced nuclear Ca^{2+}.

A. Rhizobia produce Nod factors, which are perceived by the LysM-RLKs at the plasma membrane, which in *M. truncatula* are NFP, with an inactive kinase domain, and LYK3. Together with an LRR-RLK DMI2, they perceive the rhizobial Nod factors. At the nuclear envelope, three ion channels, MCA8, DMI1 and CNGC15s are required for generation of a nuclear Ca^{2+} oscillation. Components of the nucleoporin complex, NUP85, NUP133 and NENA are also required for this Ca^{2+} spiking. The Ca^{2+} spiking is decoded by DMI3 and its interacting protein IPD3, which activate transcription of symbiosis gene expression allowing for host plant association with symbiont. **B.** Table showing the common sym gene names for *M. truncatula* compared to those of *L. japonicus.*

In addition to these players, the overexpression of the nodulation-related transcription factor, *NIN*, could also produce spontaneous nodules in both *L. japonicus* and *M. truncatula* (Soyano *et al.,* 2013; Vernié *et al.,* 2015). Interestingly, the spontaneous organogenesis could be induced by the expression of *NIN* under either an epidermal or cortical promoter (Vernié *et al.,* 2015). Exogenous application of the phytohormones cytokinin, auxin and gibberellin can also lead to production of pseudonodules in absence of rhizobia (Akamatsu *et al.,* 2021; Jin *et al.,* 2016; Tirichine *et al.,* 2007), and a gain-of-function mutation in the cytokinin receptor LjLHK1/MtCRE1 can also produce nodule-like structures (Tirichine *et al.,* 2007), indicating that the crosstalk between many different pathways is responsible for development of a nodule structure.

1.2.3- Pharmacological perturbation of symbiotic nuclear Ca^{2+}

Several pharmacological studies have been performed to uncover finer details of early signaling in endosymbiosis, such as factors that may perturb the Ca^{2+} oscillation. One of these came from the identification that the 3-hydroxy-3-methylglutaryl CoA reductase1 (*Mt*HMGR1) associates with DMI2 cytosolic kinase domain and its knockdown by RNAi leads to a reduction in nodulation (Kevei *et al.,* 2007), *ENOD11* expression and Ca^{2+} oscillation in response to both Nod factors and GSE (Venkateshwaran *et al.,* 2015). Additionally, HMGR inhibition by statin drugs also results in reduced nodule number (Kevei *et al.,* 2007). HMGR enzyme activity is the rate-limiting step within the mevalonate (MVA) pathway, with MVA as a direct product from conversion of HMG-CoA. The addition of MVA itself can induce nuclear Ca^{2+} oscillation in wild-type root hairs and restore the abolished Ca^{2+} oscillation in the RNAi of HMGR1. Interestingly, MVA-induced Ca^{2+} oscillation is dependent on DMI1, and partially dependent on the plasma membrane receptor-like kinase DMI2 (Venkateshwaran *et al.,* 2015). Taken together, these experiments all suggest a possible role for MVA or its derivatives as a 2^{nd} messenger linking membrane perception to the nuclear Ca^{2+} oscillation.

Additionally, the use of G protein agonists and antagonists has provided evidence for the involvement of heterotrimeric G protein signaling in symbiosis. The G protein agonist mastoparan, which was initially found in wasp venom and acts by mimicking the intracellular domain of membrane-spanning receptors, as well as its more active peptide analog Mas7, was found to activate expression of the early nodulin gene *ENOD12*, and root hair deformation (den Hartog *et al.*, 2001; Higashijima *et al.*, 1990; Pingret *et al.*, 1998). It was additionally determined that pertussis toxin, an antagonist of G proteins via interference with receptor interaction through ADP-ribosylation of a Gα cysteine residue, could inhibit *ENOD12* expression (Pingret *et al.*, 1998). Interestingly, Mas7 could induce *ENOD11* expression in a *dmi1* and *dmi2* mutant, but not *dmi3* (Charron *et al.*, 2004), implicating activity of the G protein agonist downstream of DMI1 and DMI2, but dependent on DMI3. Sun *et al.*, (2007) went on to show that Mas7 application could activate the nuclear Ca^{2+} oscillation in a similar manner to that of Nod factor, independently of NFP, DMI1, and DMI2. The symbiosis-like nuclear Ca^{2+} oscillation observed in a *dmi1* mutant suggested that DMI1 itself is not the Ca^{2+} channel, but its requirement for nuclear Ca^{2+} oscillation in a wild-type context might be functioning as a regulator of the nuclear Ca^{2+} channel CNGC15.

A pathway often catalyzed by mastoparan and G protein activation is that of phospholipase C (PLC), which cleaves phosphatidylinositol (4,5)-bisphosphate (PIP_2) to produce inositol (1,4,5)-trisphosphate (IP_3) and diacylglycerol (DAG). IP_3 can release Ca^{2+} from internal stores, serving to activate activity of Ca^{2+}-binding proteins. DAG is phosphorylated by DAG kinase (DGK) to produce phosphatidic acid (PA) (Munnik *et al.*, 1998). PA is also a primary product of phospholipase D (PLD) signaling, from the hydrolysis of phophatidylcholine (PC). n-butanol, an inhibitor which competes with water for the phosphatidyl group to inhibit PA production and also inhibited Nod factor-induced root hair deformation (den Hartog *et al.*, 2001), additionally blocks the induction of *ENOD11* activation and nuclear Ca^{2+} oscillation by Mas7 (Charron *et al.*, 2004; Sun *et al.*, 2007). PLC antagonists, neomycin and the aminosteroid PLC inhibitor U73122 could also inhibit Nod factor- and mastoparan-induced *ENOD12* induction and root hair deformation (den Hartog *et al.*, 2001; Engstrom *et al.*, 2002; Pingret *et al.*, 1998). These experiments provided further evidence for the role of G protein signaling and its downstream products in activation of symbiosis.

Calcium agonists and antagonists have also been applied to determine the source of the Ca^{2+} for Nod factor-induced oscillation and transients. Ruthenium red, which inhibits ryanodine receptors could act as an antagonist of Nod factor- and mastoparan-induced *ENOD12* expression, as could the Ca^{2+} chelator, EGTA, and trivalent lanthanum ion La^{3+}, a Ca^{2+} channel blocker (Pingret *et al.*, 1998). These experiments indicated that both extracellular and intracellular Ca^{2+} stores are important for Nod factor- and mastoparan-activated symbiosis signaling responses. In addition, CPA, which inhibits type IIA Ca^{2+} ATPases, blocked

ENOD11 expression and nuclear Ca^{2+} oscillation induced by Mas7 (Charron *et al.,* 2004; Engstrom *et al.,* 2002; Sun *et al.,* 2007), which was later confirmed by the finding of the requirement for the SERCA-type ATPase, MCA8 on the nuclear envelope for symbiosis-induced nuclear Ca^{2+} oscillation (Capoen *et al.,* 2011).

1.2.4- Plant colonization by nitrogen-fixing bacteria

Following chemical communication, rhizobia attach to root hairs, which curl and form a 'shepherd's crook' structure, entrapping the bacteria within a so-called infection pocket. Bacterial proliferation occurs within the root hair curl, leading to a high concentration of Nod factor, and eventually an intracellular tunnel is formed from an inversion of the root hair (Brewin, 2004). Pre-infection thread structures (PIT) form, which are cytoplasmic bridges aligned in radial rows across outer cortical cells (van Brussel *et al.,* 1992), which sets the path for infection thread formation. This precedes the formation and growth of a tunnel-like infection thread (IT) structure, which grows and invades into cortical cells for infection. The infection thread is a tubular ingrowth of cell wall, which is surrounded by plasma membrane and encloses bacteria within a matrix (Brewin, 2004; Gage, 2002). For IT formation and extension, the plant cell wall must be degraded to allow rhizobial entry (van Spronsen *et al.,* 1994), which requires a NODULE PECTATE LYASE (NPL) protein, involved in degrading both polygalacturonic acids and pectin (Xie *et al.,* 2012). Integral membrane proteins are also required to contribute to development of the infection thread as it progresses. Figure 1.6 illustrates the infection progression from Nod factor perception through to nodule primordia development.

Simultaneous with the initiation of ITs within epidermal root hair cells, root pericycle and cortical cells re-enter the cell cycle and begin to divide. This initiates formation of the nodule primordium and vascularization. Nodules such as those formed by *M. truncatula* are organized into developmental zones: meristem, infection zone, nitrogen fixation zone, and senescence zone (Xiao *et al.,* 2014). Development of the various zones requires successive divisions within the root pericycle, endodermis and cortex.

Once the IT reaches the nodule cortex, it branches and releases bacteria into plant cell walls, which then forms a unique organelle called a symbiosome, which are surrounded by plant membrane, similar to the plasma membrane (Tsyganova *et al.,* 2017). Within the symbiosome, bacteria grow and divide and expand to fill the plant cell (Roth & Stacey, 1989). In the final stage of rhizobial symbiosis, there is senescence of nodule tissue. Infected cells are lysed and nodule nutrients recycled by the host plant (Van de Velde *et al.,* 2006).

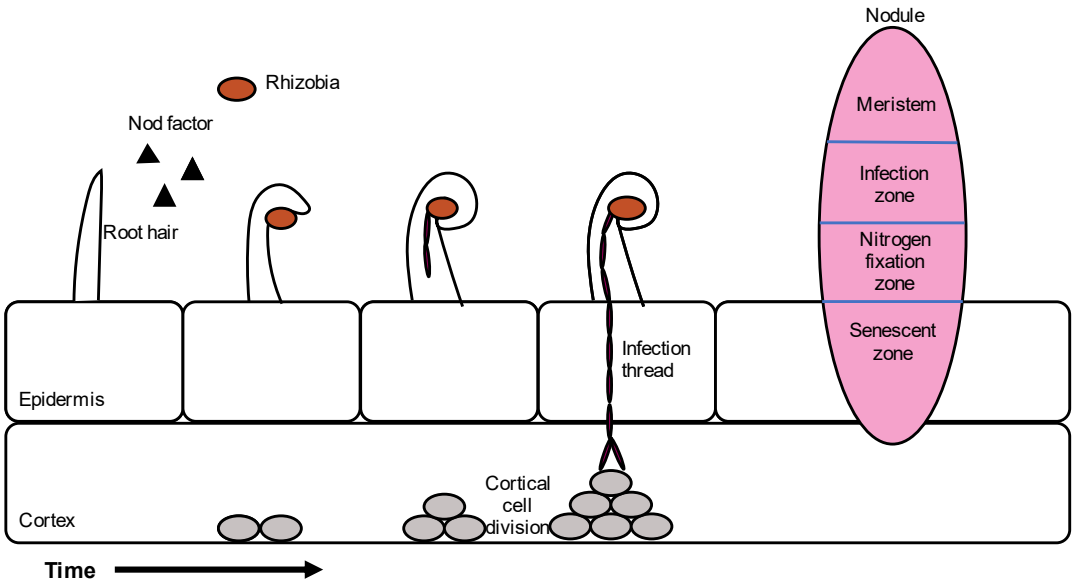

Figure 1.6. Root hair infection and nodule organogenesis.

Upon perception of rhizobial Nod factor, the root hair curls to entrap the bacteria. As infection develops, a growing infection thread extends downward through the root hair and epidermis into the cortex. There is also cortical cell division to initiate nodule primordia formation.

1.2.5- Plant colonization by AM fungi

While nodulation is restricted to the *Fabales, Fagales, Cucurbitales,* and *Rosales,* at least 80% of plants form symbioses with beneficial arbuscular mycorrhizal (AM) fungi (Luginbuehl & Oldroyd, 2017). Similar to the establishment of rhizobial symbiosis, there is first an exchange of chemical signals. The plant secretes strigolactones into the soil, which induces spore germination, fungal metabolism and hyphal branching in the AM fungi (Akiyama *et al.*, 2005). This hyphal branching increases the opportunity for the fungus to encounter the host plant root. In turn, the AM fungi produce 'Myc factors', which are short-chain CO molecules (Genre *et al.*, 2013). Myc factors are perceived by LysM receptors on the plasma membrane, which induces a signal transduction cascade including transcriptional activation of plant symbiosis genes, nuclear Ca^{2+} spiking, starch accumulation, and the formation of lateral roots (Chabaud *et al.*, 2011; Genre *et al.*, 2013; Gutjahr *et al.*, 2009; Kosuta *et al.*, 2003; Oláh *et al.*, 2005). As described above, the nuclear Ca^{2+} oscillation frequency serves as a guide for the progression of colonization by the AM fungus into the plant root (Sieberer *et al.*, 2012).

Upon contact with the plant root, the AM fungal hyphae differentiate into attachment structures called hyphopodia (Bonfante & Genre, 2010), and the plant forms a pre-penetration apparatus (PPA), a cytoplasmic bridge across the vacuole, which guides the fungal penetration and growth from the appressorium (Genre *et al.*, 2005). From initial penetration, the AM fungus grows intercellularly and proceeds to develop tree-shaped arbuscules upon reaching the root inner cortical cells, which provide increased surface area as the site of nutrient

exchange between the AM fungi and the host. The developing arbuscules are continuously surrounded by plant-derived peri-arbuscular membrane (Gutjahr & Parniske, 2013). Arbuscules are short-lived and collapse within days, with subsequent degradation. Both development and collapse of the AM fungi must be tightly regulated, and are highly correlated with changes in plant gene expression (Pimprikar & Gutjahr, 2018). Senescence progresses until the entire arbuscule has collapsed and peri-arbuscular membrane rearranges for host cell to regain previous organization, where it can undergo new colonization. The formation of fungal vesicles and spores are representative of a sustained association between host plant and AM fungus. Vesicles are globular intracellular structures thought to be the fungal lipid storage organs (Jabaji-Hare *et al.*, 1984).Vesicles and new fungal spores represent completion of the fungal life cycle, allowing for subsequent recolonization. The structures scored in studies of AM colonization are detailed in Figure 1.7.

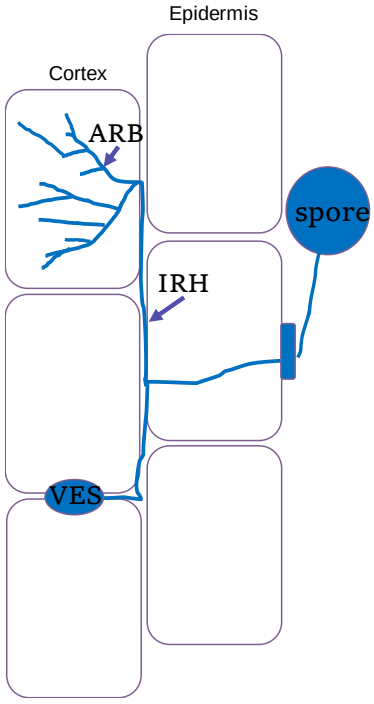

Figure 1.7. Diagram of AM colonization

Upon contact with the plant root, the AM fungi penetrates the epidermal cell layer and intraradical hyphae (IRH) cross around and through cells through a pre-penetration apparatus. Once the IRH reach the cortical cell layer, they form tree-like arbuscules for nutrient exchange. Further along in development of the fungus, vesicle formation occurs and the life cycle restarts.

1.3- Thesis Outline and Objectives

DMI1, along with MCA8 and CNGC15, is required for generation of symbiosis factors-induced nuclear Ca^{2+} oscillation, necessary for establishment of the plant association with beneficial AM fungi and rhizobia for uptake of nutrients required for optimal plant growth and development. Much is known about the mechanism of symbiotic factor perception at the plasma membrane, and about the factors involved at the nucleus in generating the symbiosis-induced nuclear Ca^{2+} oscillation, however very little is known about what happens in between as the link between the plasma membrane perception of symbiotic Nod and Myc factors leading to calcium oscillation at the nucleus. The overarching objective of this thesis is to understand how the nuclear Ca^{2+} oscillation is activated and regulated, with a focus on what might be occurring upstream of the nuclear calcium oscillation. DMI1 is required for nuclear calcium oscillation and symbiotic signaling with both rhizobia and AM fungi. The activation of symbiosis-like calcium oscillation upon Mas7 treatment, along with mathematical modelling suggesting a requirement for interplay between it and its interacting partner channel CNGC15 suggests it might be acting as a gatekeeper for the nuclear calcium oscillation. Prior to the beginning of this thesis, a yeast 2 hybrid screen was performed to identify putative interacting partners of DMI1, with the goal of identifying players that may regulate its activation. One of the players identified was an LRR-RLK (described in Section 1.1.1), hereafter referred to as AUxilliary unit Kinase of DMI1 (AUK).

With a focus on AUK as a putative interactor of DMI1, it could be hypothesized that it was acting upstream of DMI1, as a putative activator or regulator. To study this, the first objective was to confirm the association of AUK and DMI1. As each protein-protein interaction method has its caveats and potential for false positives or negatives, several different experiment types were used, *in vitro*, in heterologous systems and *in planta* in both *N. benthamiana* and the endogenous *M. truncatula*. The results and details of these protein-protein interaction experiments are described in Chapter 3. As the putative interactor of AUK, DMI1 is required for nuclear calcium oscillation and symbiosis with both rhizobia and AM fungi, the second objective was to identify whether AUK plays a role in nuclear calcium oscillation and symbiosis. CRISPR-Cas9 knockout experiments and overexpression experiments, as well as EMS mutant analysis were used to determine assess the requirement and function of AUK in symbiosis signaling. Epistasis analysis was also employed to determine a placement for AUK within the common symbiosis signaling pathway. These phenotyping experiments are described in Chapter 4. Finally, AUK is an LRR-RLK. LRRs are often described in perception of a ligand and RLK kinase activity in transducing a signal down the pathway. Thus, it could be hypothesized that AUK might be activating the nuclear calcium oscillation through its association with DMI1. A putative mechanism through which AUK

might phosphorylate DMI1 to activate the symbiotic nuclear Ca^{2+} oscillation is explored in Chapter 5.

2- Materials & Methods

2.1- Plant methods

2.1.1- *Medicago truncatula* lines and growth conditions

Medicago truncatula wild-type (WT) ecotypes Jemalong A17 (Barker *et al.,* 1990) and R108 (Hoffmann *et al.,* 1997) were used in this study. *dmi1, dmi2,* and *auk* mutants were derived from the A17 genotype and Ca^{2+} oscillation experiments were performed using mutant and WT expressing the Ca^{2+} fluorescence resonance energy transfer (FRET) sensor *Yellow Cameleon (YC) 3.6*. *auk* mutant lines were obtained from reverse screening the ethylmethylsulfonate (EMS) mutagenized population of *M. truncatula* ecotype A17 by UKREVGEN (JIC). See Table 2.1 for lines used in this study.

For sterilization, *M. truncatula* seeds were threshed from pods by grinding, scarified with sandpaper, and sterilized in 10% bleach for 5 min prior to washing with sterile water to remove all trace of bleach. Seeds were left to imbibe in sterile water containing 5 µg/mL nystatin and 50 µg/mL augmentin for 4 h to overnight to avoid fungal contamination. Seeds were then plated on buffered nodulation medium (BNM; Table 2.3) and stratified for 5 days at 4 °C in the dark to synchronize germination, followed by a shift to room temperature overnight to induce germination. Upon germination, seedlings were moved to plates containing Modified Fahreus Plant medium (Mod FP; Table 2.3) and covered with filter paper to avoid the roots growing into the medium. Briefly, Whatman paper (Grade 0858 Cellulose Qualitative Filter paper) was cut to fit square tissue culture dishes (Greiner Bio-One) and autoclaved to sterilize. Seedlings were grown vertically for 7-14 days depending on the assay in a controlled environment chamber at 22 °C, 80% humidity, 16 h photoperiod, 300 µmol m^{-2} s^{-1} light intensity. Plants were watered regularly, as required. Plants for nodulation and mycorrhization assays were transferred to Terragreen/sand (Oil-Dri Company, Wisbech, UK) to a ratio of 1:1 in P40 trays or phytaboxes in a growth chamber under the same growth conditions as above. Plants for line generation and seed bulking were grown in Cereal Mix (Table 2.3).

2.1.2 DNA extraction and genotyping of TILLING lines and crosses

A leaf of each plant for genotyping was collected 7-10 days after planting on soil. The leaves were frozen at -20 °C and then extracted using the QIAamp® 96 DNA QIAcube HT kit (Qiagen) 96-well plate kit following manufacturer's instructions, with elution in 50 µL sterile dH_2O.

Genotyping to determine presence/absence of single nucleotide polymorphism (SNP)s was done using Kompetitive allele-specific Polymerase Chain Reaction (PCR) (KASP) with allele-specific primers including FAM and HEX fluorescence probes indicated in Table 2.6. An assay mix was made consisting of 12 µM of each allele-specific primer and 30 µM of the

common primer. The final reaction consisted of 1 × KASP mix, 5-10 ng/µL DNA and 0.056 ratio of assay mix to sample number. A thermocycler was then used to perform Touch Down PCR with the following conditions: 15 min 94 °C, 10 cycles of 20 s at 94 °C then 1 min 61-55 °C ramp, followed by 40 cycles of 20 s at 94 °C then 1 min 55 °C. A no-template control and wild-type control were included. Fluorescence was detected using a PHERAStar Plate reader and SNPs were determined using KlusterCaller.

2.1.3- Hairy root transformation

M. truncatula R108 or A17 seeds were sterilized and germinated as previously described. Constructs for root transformations were transformed into *Agrobacterium rhizogenes AR1193* by electroporation and incubation at 28 °C on LB plates containing rifampicin, carbenicillin and the appropriate vector selection antibiotic (Table 2.7 or Table 2.8). The *A. rhizogenes* was grown in overnight Luria Broth (LB) culture containing appropriate antibiotics (Table 2.7 or Table 2.8) at 28 °C and then centrifuged at 1 439 × g to pellet the cells. The pellet was resuspended in sterile water and 3 mm root tip was excised. The cut end was dipped in the *Agrobacterium* solution for 1 min prior to transfer to plates containing Mod FP pH 6.0 for growth as described above, with 20 seedlings/plate. At 7 days post transformation, initial untransformed roots were excised to encourage growth of transformed roots from the calli, and seedlings were transferred to Mod FP plates in a with filter paper as described above. Plants were grown for 2 weeks following this excision of untransformed roots prior to screening the roots using the fluorescent dsRed or mCherry fluorescent marker prior to experimental set-up.

2.1.4- Transient protein expression in *N. benthamiana*

Constructs were transformed into *Agrobacterium tumefaciens* GV3101 by electroporation and incubated on LB plates containing rifampicin, gentamycin, and the appropriate selection antibiotic (Table 2.8) for 3 days. The *A. tumefaciens* expressing the desired protein combination or the P19 viral suppressor (Lakatos *et al.*, 2004) were grown overnight at 28 °C with 200 rpm shaking followed by centrifugation at 1 439 × g for 10 min to collect cells. The cells were resuspended in infiltration buffer (10 mM $MgCl_2$, 10 mM MES, pH 6.3) and diluted to OD_{600} of 0.5. Cultures were mixed with P19 viral suppressor according to the experiment and leaves of 4-5 week of *Nicotiana benthamiana* plants were infiltrated using a needleless syringe. Tissue was collected 3 days post-infiltration (dpi), and either a 1 mm leaf disc was taken for confocal analysis, or material was flash-frozen in liquid N_2 and stored at -80 °C until use.

Table 2.1- List of *M. truncatula* lines used in this study (For Description section, mutant lines are denoted as nucleotide change:amino acid substitution)

Line	Description	Background	Reference
A17 Jemalong	Wild-type		(Barker *et al.*, 1990)
R108	Wild-type		(Hoffmann *et al.*, 1997)
dmi1-1	G1264A nucleotide change that occurs at the 5′ splice site of the third intron and that causes a missplicing event	Jemalong A17	(Catoira *et al.*, 2000b; Penmetsa & Cook, 1997)
dmi2-1	Premature STOP codon from residue 368	Jemalong A17	(Catoira *et al.*, 2000b; Sagan *et al.*, 1995)
A17 YC3.6		Jemalong A17	(Sun *et al.*, 2015)
dmi1-1 YC3.6		Jemalong A17	This study; cross done by MC
dmi2-1 YC3.6		Jemalong A17	This study; cross done by MC
auk-1/auk^{GoF}	2293C>T:565P>P/S	Jemalong A17	This study
auk-2	2479G>A:627G>G/R	Jemalong A17	This study
auk-3	2416G>A:606V>V/M	Jemalong A17	This study
auk-4	2401G>A:601E>K	Jemalong A17	This study
auk-5	2285G>A:562G>E	Jemalong A17	This study
auk-6	2177C>T:526P>P/L	Jemalong A17	This study
auk-7	2494G>A:632V>I	Jemalong A17	This study
auk-1 YC3.6		Jemalong A17 YC3.6	This study; cross done by MC

2.2- Microbiological Methods

2.2.1- Bacterial methods

2.2.1.1- Bacterial strains and growth conditions

Escherichia coli cultures used for molecular cloning were grown at 37 °C for 16 h overnight at 200 rpm in 5 mL cultures. *Agrobacterium rhizogenes* strain AR1193 (Stougaard *et al.*, 1987) was used for hairy root transformation of *M. truncatula* and *A. tumefaciens* GV3101 was used for transient transformation of *N. benthamiana. Agrobacterium* was cultured overnight in 5 mL LB culture inoculated from a single colony and grown at 200 rpm at 28 °C. *Sinorhizobium meliloti* 2011 strains were grown overnight at 28 °C under 200 rpm shaking. Long-term storage of bacterial strains was done at a final concentration of 20% glycerol at -80 °C.

2.2.1.2- Transformation of and plasmid purification from bacteria by heat shock or electroporation

For plasmid purification, overnight cultures of *E. coli* were grown overnight at 37 °C with shaking at 200 rpm. Cultures were pelleted at 15 871 × g for 10 min at room temperature. Plasmid was isolated by alkaline lysis method using the Qiagen miniprep kit following manufacturer's instructions. Competent *E. coli* cells were transformed by heat shock at 42 °C for 45 s followed by immediate cold shock on ice for at least 2 min. Super Optimal broth with Catabolite repression (SOC) media was added and cells were allowed to recover for 1 h at 37 °C with shaking. Cells were then plated on LB medium containing appropriate antibiotics (Table 2.7-2.9). Transformation of *Agrobacterium* cells was done by electroporation. Sterile cuvettes were used and 25 µL cells had approximately 100 ng plasmid added. Current was applied at 2.5 V for 10 s at a resistance of 200 Ω and SOC medium was immediately added for cell recovery at 28 °C with shaking for 2 h. Cells were plated and selected on LB plates containing the appropriate antibiotic (Table 2.7-2.9).

2.2.2- Transformation and culture of *Saccharomyces cerevisiae*

2.2.2.1- Yeast transformation

50 mL of Yeast extract- Peptone-Adenine-Dextrose (YPAD; Table 2.3) was inoculated from fresh plates of AH109 yeast (Clontech) and grown at 30 °C overnight to an OD_{600} of >1.5 stationary phase. The culture was then diluted to OD_{600} of 0.3 in 200 mL YPAD and grown for approximately 3 h to OD_{600} of 0.6-0.8. The cultures were pelleted at 1 439 × g for 10 min, followed by resuspension in 25 mL total sterile water. The resuspended culture was centrifuged at 1 000 × g for 5 min followed by resuspension in 2 mL sterile 100 mM LiOAc. Approximately 200 ng of each construct was mixed in Eppendorf tubes for each co-transformation prior to addition of 300 µL PEG/LiOAc master mix containing 40% PEG, 120 mM LiOAc and 160 µg/mL Yeastmaker® denatured carrier DNA (Clontech). This mixture was vortexed prior to addition of 100 µL previously resuspended yeast cells to each transformation tube. The mix was then vortexed for 1 min to mix and incubated first at 30 °C for 30 min, then 42 °C for 30 min. The yeast was pelleted by centrifugation at 700 × g for 5 min, dissolved in 100 µL 0.9% NaCl and plated on SD+ (Table 2.3) plates lacking leucine and tryptophan. The murine p53 and its interacting partner the SV40 large T-antigen were used as control (ClonTech™ PT3024-1).

2.2.2.2- Growing yeast on dropout media

The plates were incubated for 2-3 days at 30 °C. Following this incubation, the successful co-transformants were grown in overnight SD+ culture lacking Leu and Trp overnight at 28 °C and then plated in 15 µL droplets on an SD+ -Leu-Trp plate as control and SD lacking -Leu, -Trp, -Ade, -His as saturated culture and dilutions of 1:10, 1:100, 1:500. Droplets were allowed

to dry and then grown on media at 28 °C. Plates were imaged by a scanner at 5-7 days following plating on dropout media.

2.2.3- Culture of *Spodoptera frugiperda Sf*9 insect cells

Insect cells of *Spodoptera frugiperda* strain *Sf9* were maintained at a density of 1×10^6 cells/mL by passaging in 20 mL of 1 × SF-900™ (SFM; Gibco) every 3-5 days, with density measured using a countess chamber (ThermoFisher). The cells were grown at 26 °C with 200 rpm shaking.

Table 2.2- List of bacterial and culture strains used in this study

Strain	Purpose	Source	Reference
E. coli DH5α	General purpose cloning and plasmid amplifications	Invitrogen (Life Technologies)	
E. coli Top10	General purpose cloning of larger and more difficult constructs		
E. coli STELLAR	InFusion cloning		
E. coli Rosetta pLysS	Bacterial protein expression		
E. coli DB3.1	ccdB resistant propagation of gateway destination vectors	J. A. Downie, JIC	
E. coli DH10Bac, YFP	Amplification of bacmid for insect cell protein expression	C. Stone, JIC	
A. rhizogenes AR1193	Hairy root transformation		(Stougaard *et al.*, 1987)
A. tumefaciens GV3101	Transient protein expression in *N. benthamiana*		
*S. meliloti Sm*2011 *LacZ*	Symbiont of *M. truncatula*		
*Spodoptera frugiperda Sf*9	Insect cell protein expression	C. Stone, JIC	
Saccharomyces cerevisiae AH109	Y2H	Clontech	

Table 2.3- List of media and soil used for growth of bacteria, yeast, and plants

Medium	Composition
Media for bacterial culture	
LB (Luria Broth)	10 $g \cdot L^{-1}$ tryptone, 5 $g \cdot L^{-1}$ yeast extract, 5 $g \cdot L^{-1}$ NaCl. pH adjusted to 7.0 with 1.0 NaOH. For solid medium, addition of Formedium agar was done to final concentration of 1.5%.
SOC (Super Optimal broth with Catabolite repression)	20 $g \cdot L^{-1}$ tryptone, 5 $g \cdot L^{-1}$ yeast extract, 0.58 $g \cdot L^{-1}$ NaCl, 0.19 $g \cdot L^{-1}$ KCl, 2.03 $g \cdot L^{-1}$ $MgCl_2$, 2.46 $g \cdot L^{-1}$ $MgSO_4 \cdot 7H_2O$, 3.6 $g \cdot L^{-1}$ glucose.
TY (*Rhizobium* Complete Medium; Tryptone Yeast extract)	5 $g \cdot L^{-1}$ tryptone, 3 $g \cdot L^{-1}$ yeast extract, 1.32 $g \cdot L^{-1}$ $CaCl_2 \cdot 6H_2O$. For solid medium, addition of Formedium agar was done to concentration of 1.5%.
Media for yeast culture	
YPAD (Yeast extract-Peptone-Adenine-Dextrose)	10 $g \cdot L^{-1}$ yeast extract, 20 $g \cdot L^{-1}$ peptone, 20 $g \cdot L^{-1}$ glucose, 0.02 $g \cdot L^{-1}$ adenine. For solid medium, addition of Formedium agar to final concentration of 2%.
SD+ (Synthetic Dextrose Minimal Media)	6.9 $g \cdot L^{-1}$ yeast nitrogen base without amino acids (Formedium), 20 $g \cdot L^{-1}$ glucose, complete supplement mixture (CSM) dropout (either -leucine-tryptophan at 0.64 $g \cdot L^{-1}$ or -leucine-tryophan-adenine-histidine at 0.61 $g \cdot L^{-1}$). pH was adjusted to 5.8 with NaOH. For solid medium, Formedium agar was added to final concentration of 2%.
Media for plant culture	
Mod FP (Modified Fahreus Plant Medium)	132.3 $mg \cdot L^{-1}$ $CaCl_2 \cdot 2H_2O$, 123.2 $mg \cdot L^{-1}$ $MgSO_4 \cdot 7H_2O$, 95.3 $mg \cdot L^{-1}$ KH_2PO_4, 113.6 $mg \cdot L^{-1}$ Na_2HPO_4, 4.9 $mg \cdot L^{-1}$ Ferric citrate, 40 $mg \cdot L^{-1}$ NH_4NO_3, 0.1 $mg \cdot L^{-1}$ $MnCl_2 \cdot 4H_2O$, 0.1 $mg \cdot L^{-1}$ $CuSO_4 \cdot 5H_2O$, 0.1 $mg \cdot L^{-1}$ $ZnCl_2$, 0.1 $mg \cdot L^{-1}$ H_3BO_4, 0.1 $mg \cdot L^{-1}$ $Na_2MoO_4 \cdot 2H_2O$. pH was corrected to 6.0 with HCl. For solid medium, Sigma agar was added to a final concentration of 1%.
BNM (Buffered Nodulation Medium)	61 $mg \cdot 1L^{-1}$ $MgSO_4 \cdot 7H_2O$, 34 $mg \cdot L^{-1}$ KH_2PO_4, 2.3 $mg \cdot L^{-1}$ $ZnSO_4 \cdot 7H_2O$, 1.5 $mg \cdot L^{-1}$ H_3BO_4, 5.8 $mg \cdot L^{-1}$ $MnSO_4 \cdot 4H_2O$, 0.25 $mg \cdot L^{-1}$ $Na_2MoO_4 \cdot 2H_2O$, 0.025 $mg \cdot L^{-1}$ $CuSO_4 \cdot 5H_2O$, 0.025 $mg \cdot L^{-1}$ $CoCl_2 \cdot 6H_2O$, 9.35 $mg \cdot L^{-1}$ Na_2EDTA, 6.95

	mg·L^{-1} $FeSO_4 \cdot 7H_2O$, 340 mg·L^{-1} $CaSO_4 \cdot 2H_2O$, 390 mg·L^{-1} MES hydrate. pH was adjusted to 6 with KOH. For solid medium, Sigma agar was added to a final concentration of 1.5%.
Soil for plant growth	
TerraGreen & sand Mix	1:1 mix of Terragreen (Oil-dry UK Ltd) and sharp sand (BB Minerals)
Cereal Mix	65% peat, 25% loam, 10% grit, 3kg/m^3 dolomitic limestone, 1.3 kg/m^3 PG mix, 3kg/m^3 osmocote extract.

2.3- Molecular Cloning

2.3.1- Agarose gel electrophoresis

DNA was resolved by running on 1.5% agarose gel at 120 V in 1 × Tris acetate EDTA (TAE). The gel was then placed in an ethidium bromide bath prepared at a concentration of 0.5 µg/mL in dH_2O for visualization of the DNA bands using a Geneflash Syngene Bioimaging System.

2.3.2- PCR Cycling Conditions

All PCR reactions were carried out with thermocyclers. For all cloning purposes, hi-fidelity Phusion Taq (New England Biolabs) was used according to the manufacturer's instructions. For colony PCR and confirmation of KASP genotyping, GoTaq green master mix was used.

Table 2.4- PCR Cycling Parameters for Phusion Taq

Stage	Temperature	Time	Number of cycles
Initial denaturation	98	30 s	× 1
Denaturation	98	10 s	
Annealing	55-60	30 s	× 35
Extension	72	30 s/kb amplified	
Final Extension	72	10 min	× 1

Table 2.5- PCR Cycling Parameters for GoTaq

Stage	Temperature (°C)	Time	Number of cycles
Initial denaturation	95	2 min	× 1
Denaturation	95	30 s	
Annealing	55-60	30 s	× 35
Extension	72	1 min/kb amplified	
Final Extension	72	10 min	× 1

2.3.3- Restriction digest

Digestion of DNA was carried out using restriction enzymes that were specific to the desired sequence. Restriction enzymes used in this study were either from NEB or Roche and were used following the manufacturer's instructions. Reactions used 1 µg plasmid or PCR purified fragments and incubated at 37 °C for 1 h unless otherwise specified. The enzyme was then inactivated by heating to 80 °C for 10 min if required.

2.3.4- DNA gel extraction

DNA stained by ethidium bromide as described in Section 2.3.1 was visualized on a long wavelength UV transilluminator and the desired fragment was excised using a clean scalpel blade. The desired DNA was purified using the Qiaquick gel extraction kit (Qiagen) following the manufacturer's instructions and eluted twice in 15 µL sterile water heated to 70 °C before use in other cloning reactions described below.

2.3.5- Gateway cloning

Gateway® cloning (Invitrogen™, Carlsbad, CA) was used based on site-specific recombination. Firstly, entry vectors were created by amplifying the coding sequence by PCR as described in Section 2.3.2 using GoTaq Green Master Mix (Promega) with primers to generate overhangs for BP reaction into pDONR207 entry vector. The amplicon size was confirmed on a 1.5% agarose gel, and gel extraction used to purify desired DNA fragments. A BP reaction was then performed with the reaction mix containing 1 × BP clonase (Invitrogen), 150 ng gel-purified PCR amplicon, and 150 ng entry vector (pDONR207 containing the *ccdB* 'suicide gene') in a final volume of 5 µL. This was incubated at 25 °C for 1 h to overnight for larger constructs, and 2.5 µL was used to transform 25 µL DH5*α E. coli* by heat shock. Cells were plated on LB plates containing the appropriate antibiotic (Table 2.7) and incubated at 37 °C overnight. Colonies were grown in 5 mL cultures overnight at 37 °C with shaking and minipreps were performed using QiaPrep Spin Miniprep kit (Qiagen) prior to Sanger sequencing by Eurofins Genomics or GeneWiz/Azenta Life Sciences. Once the BP clone was confirmed by sequencing, an LR reaction was performed to shuttle the insert into the appropriate destination vector. The LR reaction mix contained 1 × LR clonase (Invitrogen), 150 ng pDONR207 entry clone, and 150 ng destination vector in a final volume of 2.5 µL. This was transformed into DH5*α E. coli* and plated on appropriate antibiotic as mentioned above through to sequencing confirmation. Primers used and Gateway constructs generated in this study are listed in Tables 2.6 and 2.7, respectively.

2.3.6- InFusion Cloning

InFusion HD (Takara Bio Europe) cloning was used to generate pOPINM, pOPINS3C and pOPINJ constructs for expression of the *AUK* kinase domain for in vitro analyses and pFastBac vectors for insect cell protein expression. PCR was performed using Phusion® High Fidelity DNA Polymerase (New England Biolabs). pOPIN vectors were linearized by *KpnI* and *HindIII*

restriction enzymes. Reaction conditions used for the InFusion reaction consisted of 1 × Phusion HF Buffer, 500 µM $MgCl_2$, 200 µM dNTPs, 0.5 µM each of forward and reverse primer, 3% DMSO, 50-100 ng template DNA and 1 unit of Phusion DNA Polymerase in a final reaction volume of 50 µL. Thermocycler conditions were as detailed in Table 2.4. PCR products were separated on an agarose gel and gel extracted using a gel extraction kit (Macherey-Nagel). DNA concentration was determined with a NanoDrop One (Thermo Scientific). An InFusion reaction was prepared using 1× In-Fusion HD enzyme premix, 50-100 ng linearized vector and 10-50 ng of purified PCR fragment. The reaction was incubated at 50 °C for 15 min and used to transform 50 µL chemically competent STELLAR *E. coli* cells (Clontech) by heat shock. Cells were then plated on LB agar plates containing appropriate antibiotic (Table 2.9), 1 mM Isopropyl β-d-1-thiogalactopyranoside (IPTG) and 200 µg/mL 5-bromo-4-chloro-3-indolyl-beta-D-galacto-pyranoside (X-Gal) for antibiotic and blue-white selection overnight at 37 °C. White colonies were grown in 10 mL culture containing appropriate antibiotic overnight at 37 °C, and plasmids were purified using NucleoSpin® Plasmid (Qiagen) and sent to Azenta Life Sciences for sequencing to assess correct cloning. Primers used and InFusion constructs generated in this study are listed in Tables 2.6 and 2.9, respectively.

2.3.7- Golden Gate cloning

Golden Gate cloning was used to generate constructs for CRISPR, BiFC, co-IP and *pAUK::NLS-GFP* experiments. Firstly, Level 1 constructs were generated using primers that include *BsaI* restriction sites (Table 2.6). DNA amplicons were generated by PCR, and gel purified as described for In-Fusion cloning. A digestion-ligation reaction was performed using 100-200 ng Golden Gate acceptor plasmid, and 2:1 molar ratio of PCR insert:acceptor plasmid, 1X T4 ligase buffer, 1 × BSA, 400 units T4 DNA ligase and 10 units BsaI restriction enzyme. The following cycle was used to assemble the Level 1 Golden Gate construct: 37 °C for 20 s, 26 cycles of 3 min 37 °C then 4 min 16 °C, followed by 5 min 50 °C, 5 min 80 °C, and finally 5 min 16 °C. The reaction was then used to transform Top10 *E. coli* cells by heat shock and plated on LB agar plates containing antibiotic (Table 2.8), and X-Gal for blue-white selection.

Generation of Level 2 Golden Gate constructs was performed as above but using BpiI restriction enzyme and all Level 1 insert parts at a 2:1 molar ratio insert:acceptor. These were plated on appropriate antibiotic selection (Table 2.8). Constructs were confirmed using colony PCR with GoTaq DNA polymerase mix as described above for Gateway Cloning. Following colony PCR, colonies with a PCR amplicon of expected size on a 1.5% agarose gel were purified by miniprep kit and sent for sequencing for both Level 1 and Level 2 Golden Gate reactions as described above.

For generation of CRISPR Cas9 constructs primers were designed using CRISPR-P 2.0 (Liu *et al.*, 2017) to identify appropriate PAM sites. The forward and reverse primers were

diluted to 100 nM and mixed 1:1. This primer mix was heated to 95 °C and allowed to cool slowly to room temperature. 1 µL of this primer mix was then included in a Level 1 Golden Gate reaction with Esp3I restriction enzyme with reaction and thermocycler conditions as detailed above. Level 2 Golden Gate reactions were performed using MtU6 promoter and SpCas9 enzyme. For this thesis, four constructs with three gRNAs in combinations of 2 or 3 were used to determine which were cutting as expected upstream of the kinase domain of AUK (Table 2.7). Primers used and Gateway constructs generated are listed in Tables 2.6 and 2.8, respectively.

2.3.8- Site-directed mutagenesis

Site-directed mutagenesis was performed to generate constructs for Golden Gate domestication, *auk-1*, Y2H and protein expression and purification and generation of Δpocket, KD and Km AUK mutants using a variation on QuikChange™ site-directed mutagenesis protocol as described in (Liu & Naismith, 2008). Partially overlapping primers were designed (Table 2.6) and used in a PCR reaction with Phusion® *Taq* as previously described to amplify the entirety of an entry clone with the desired sequence to be mutated, using 2-10 ng template. The vector amplification was verified on 1.5% agarose gel followed by a restriction digest with *DpnI* (NEB). 2.5 µL of this reaction was used to transform Top10 *E.coli* by heat shock and plated on LB with appropriate antibiotics (Table 2.7). Colonies were grown, and plasmids purified and sequenced by Azenta Life Sciences as described above.

Table 2.6- List of primers used in this work

Primer name	Sequence (5' to 3')
KASP Genotyping	
LG89_RLKTILLING_P526L_fp1	GAAGGTGACCAAGTTCATGCTCTATCTGCATGAG TTCAGCCC
LG90_RLKTILLING_P526L_fp2	GAAGGTCGGAGTCAACGGATTCTATCTGCATGAG TTCAGCCT
LG91_RLKTILLING_P526L_rp	GGCTTTAGATCTCCATGGACAT
LG92_RLKTILLING_G562E_fp1	GAAGGTGACCAAGTTCATGCTGCCTCGCAAACAT CGCTGG
LG93_RLKTILLING_ G562E_fp2	GAAGGTCGGAGTCAACGGATTGCGCCTCGCAAAC ATCGCTGA
LG94_RLKTILLING_ G562E_rp	GTTCGATTGCAGGGTCGGTG
LG95_RLKTILLING_P565S_fp1	GAAGGTGACCAAGTTCATGCTCAAACATCGCTGG AGGTTCAC
LG96_RLKTILLING_ P565S_fp2	GAAGGTCGGAGTCAACGGATTCAAACATCGCTGG AGGTTCAT
LG97_RLKTILLING_ P565S_rp	CCACTCGGTTCGATTGCAG

LG98_RLKTILLING_E601K_fp1	GAAGGTGACCAAGTTCATGCTGAAGTGGTTATCAAGCTCCGG
LG99_RLKTILLING_ E601K_fp2	GAAGGTCGGAGTCAACGGATTGAAGTGGTTATCAAGCTCCGA
LG100_RLKTILLING_ E601K_rp	GTGATGGCTTCACCACTTTAAG
LG101_RLKTILLING_V606M_fp1	GAAGGTGACCAAGTTCATGCTCTCCGGAAGCACTTAAAGTGG
LG102_RLKTILLING_ V606M_fp2	GAAGGTCGGAGTCAACGGATTCTCCGGAAGCACTTAAAGTGA
LG103_RLKTILLING_ V606M_rp	ACATCCCACTTCTGTGATGG
LG104_RLKTILLING_G627R_fp1	GAAGGTGACCAAGTTCATGCTCTTAAAGTGGGAAATGATGACAG
LG105_RLKTILLING_ G627R_fp2	GAAGGTCGGAGTCAACGGATTCTTAAAGTGGGAAATGATGACAA
LG106_RLKTILLING_ G627R_rp	GAGTTACCTACTTGTACAATAGG
LG107_RLKTILLING_V632I_fp1	GAAGGTGACCAAGTTCATGCTCAGAAATGGACCTTGTTCAAG
LG108_RLKTILLING_ V632I_fp2	GAAGGTCGGAGTCAACGGATTCAGAAATGGACCTTGTTCAAA
LG109_RLKTILLING_ V632I_rp	GTCCATTTCTGAGTTACCTAC

Gateway Cloning	
LG01_pDONR_RLKkinase_fp	GGGGACAAGTTTGTACAAAAAAGCAGGCTTCATGCCGCTAACTTGGTCGGAC
LG02_pDONR_RLKkinase_rp	GGGGACCACTTTGTACAAGAAAGCTGGGTGTCTCAATCAGATGAAACAGACAATCTATCC
LG26_RLKkonly_pDONR_fp2	GGGGACAAGTTTGTACAAAAAAGCAGGCTTCATGCCGCTAACTTGGTCGGACCGA
LG27_RLKkonly_pDONR_rp2	GGGGACCACTTTGTACAAGAAAGCTGGGTGTCTCAATCAGATGAAACAGACAATCTATCCAAAGCATCAAGTA
LG81_pDONR_DMI1Ct_fp	GGGGACAAGTTTGTACAAAAAAGCAGGCTTCATGGCAGAAAAGGAAAAGGAGGAAATGGAAATGG
LG82_pDONR_DMI1Ct_rp	GGGGACCACTTTGTACAAGAAAGCTGGGTGTCTCATTCACCTGAGGCTAAAACAACAAAAACATCATC
LG83_pDONR_DMI1Ctmin5_rp	GGGGACCACTTTGTACAAGAAAGCTGGGTGTCTCACCATTTTCTTGGCACAGATTTTTCTGAAGGG
LG84_pDONR_DMI1Ctmin4_rp	GGGGACCACTTTGTACAAGAAAGCTGGGTGTCTCAAGGTAGACGTCTCGACTGTATATCACG

LG85_pDONR_DMI1Ctmin3_rp	GGGGACCACTTTGTACAAGAAAGCTGGGTGTCTC ACTCATCTGCAAGAATAAGGATAGAATCAAAAGT C
LG86_pDONR_DMI1Ctmin2_rp	GGGGACCACTTTGTACAAGAAAGCTGGGTGTCTC A AGTGTCATCATCCTCAGCTATAACAAGGAC
InFusion Cloning	
LG17_RLK kinase_pOPINM_fp	AAGTTCTGTTTCAGGGCCCGCCGCTAACTTGGTCG GACTGA
LG18_RLK kinaseplus_pOPINM_fp	AAGTTCTGTTTCAGGGCCCGTCGAGGGTTTGCGGT TTTACTC
LG24_RLK k_pOPINM_fpb:	AAGTTCTGTTTCAGGGCCCGCCGCTAACTTGGTCG GACCGA
MtRLK_cds_pOPINM_Infusion_F	AAGTTCTGTTTCAGGGCCCGATGTTCCCTTTTTCTT TTCA
BamHIpFASTBAC1-MBP-F	CCACCATCGGGCGCGGATCCCATGAAAATCGAAG AAGGTAA
HindIIIpFASTBAC1-RLK-R	CTAGTACTTCTCGACAAGCTTGTCAATCAGATGAA ACAGACA
Golden Gate Cloning	
LG42_RLK_GG1_SC1_BiFC_fp	CACTCTGTGGTCTCAAATGTTCCCTTTTTCTTTTCA TTTCCTCTTTTTTCTTC
LG43_RLK_GG1_SC1_BiFC_rp	CACTTCGTGGTCTCACACCATCAGATGAAACAGA CAATCTATCCAAAGCATCAAGTACATGCCTCATTG TAGGCCTCTT
LG123_RLKproGG_fwd	CACTCTGTGGTCTCAGGAGGCTCTTTTCACCCCGA GATAAATAATTTC
LG130_pRLKwoUTR_rp	CACTTCGTGGTCTCACATTACGGTATCATTCTCAA TTTCTCACG
LG134_RLKproGG_rev2	CACTTCGTGGTCTCACATTTTTAATTCTTCTTCTCA AACTATGTGAACGTTGGG
LG137_gRLK5UTR_SCI_rp	CACTTCGTGGTCTCACACCATCAGATGAAACAGA CAATCTATCCAAAG
LG173_DMI1trunc3SC1_rp	ATGGTCTCACACCCTCATCTGCAAGAATAAGGAT AGAATCAAAAGTC
Site-directed mutagenesis	
LG45_RLK_GGSDM_domes_fp	TACTGGTTTATCTTCTCTTGAAAAACTTGAC
LG46_RLK_GGSDM_domes_rp	AAGAGAAGATAAACCAGTACCAAATCC

LG128_RLKGOFSDM_fp	TGGAGGTTCATCGACCCTGCAATCGAAC
LG129_RLKGOFSDM_rp	TGCAGGGTCGATGAACCTCCAGCGATGTTTG
LG131_RLKKmSDM_fp	GTCCATGGAGCTCTAAAGCCAAGTAACATAC
LG132_RLKKmSDM_rp	GGCTTTAGAGCTCCATGGACATATTTTTTG
LG133_RLKdelGBBS_fp	ATCGAACCGAGAAGTCACAACAAATATTATTGGA AGTGGTTATCAAG
LG134_RLKdelGBBS_rp	GTTGTGACTTCTCGGTTCGATTGCAGGGTCGGTGA ACCTCCAGCGATATTTG
LG135_gRLKdom3_fp	CTGAAAAGAGGCCTACAATGAGGCATGTAC
LG136_gRLKdom3_rp	CATTGTAGGCCTCTTTTCAGTGCTGCTGTTAAC

Sequencing	
LG87_RLK_SeqF	CCATACATTGTCCATTTGATTC
LG88_RLK_R1	GGTCTCTTTTCAGTGCTGCT
LG119_RLK_CRISPR_seqF	GAGGACCAACTGCTTTTATTGG
LG120_RLK_CRISPR_seqR	GAGCGTTTATGCTAGTAGATAAGC
171_T35S toward	ACACATGAGCGAAACCCTATAAGA
511_DON207fwd	TCGCGTTAACGCT AGCATGGATCTC
512_DON207rev	TGTAACATCAGAGATTTTGAGACAC
1010_GoldenGate-3	CCCGCCAATATATCCTGTC
1011_GoldenGate-4	GCGGACGTTTTTAATGTACTG
1410-Bglob-pA-R	TTTTGGCAGAGGGAAAAAGA
1411-MBP-F	GATGAAGCCCTGAAAGACGCGCAG
1163_Primer_GFP_fwd	ATGCCCGAAGGCTACGTCCAGGA
Seq_1_pFASTBAC-F-	TCAGGAGATCGGAAGACCTC
Seq_2_pFASTBAC-MBP-F-	CTGACTGATGAAGGTCTGGA
Seq_3_pFASTBAC-R-	GATACATTGATGAGTTTGGA

CRISPR-Cas9	
LG_105_RLKCRISPRsg1_fp	AACGTCTCACTTGTTGTTCTCTTTCTTTTACTCGGT TTAGAGACGAA
LG_106RLKCRISPRsg1_rp	TTCGTCTCTAAACCGAGTAAAAGAAAGAGAACAA CAAGTGAGACGTT
LG_107RLKCRISPRsg2_fp	AACGTCTCACTTGCTTTGGCTGTGAGAAGATTGGG TTTAGAGACGAA
LG_108RLKCRISPRsg2_rp	TTCGTCTCTAAACCCAATCTTCTCACAGCCAAAGC AAGTGAGACGTT
LG_109RLKCRISPRsg3_fp	AACGTCTCACTTGTCCGCCTTTGAAGAATCCATGG TTTAGAGACGAA

LG_110RLKCRISPRsg3_rp	TTCGTCTCTAAACCATGGATTCTTCAAAGGCGGACAAGTGAGACGTT

Table 2.7- Gateway vectors generated and used in this work (For source: JS= Joseph Seaman, LG= Lauren Grubb, MC= Myriam Charpentier)

Vector Name	CDS	Entry Vector	Resistance	Source
Entry vectors				
pDONR207: RLK FL noSTOP	RLK FL	-	Gentamycin	JS
pDONR207: gRLK	Genomic RLK	-	Gentamycin	LG
pDONR207: RLK kinase+	RLK kinase+	-	Gentamycin	JS
pDONR207: RLK kinase only	RLK kinase domain	-	Gentamycin	LG
pDONR207: RLK FL w STOP	RLK FL	-	Gentamycin	LG
pDONR207: RLK kinase GOF	RLK kinase domain P565S	-	Gentamycin	LG
pDONR207: RLK kinase ΔGBBS	RLK kinase domain$_{\Delta 571\text{-}586}$	-	Gentamycin	LG
pDONR207: RLK FL KD	RLK kinase domain K535A	-	Gentamycin	LG
pDONR207: DMI1 Ct	DMI1 Ct	-	Gentamycin	LG
pDONR207: DMI1 Ct min5	DMI1 Ct$_{\Delta 870\text{-}882}$	-	Gentamycin	LG
pDONR207: DMI1 Ct min4	DMI1 Ct$_{\Delta 727\text{-}882}$	-	Gentamycin	LG
pDONr207: DMI1 Ct min3	DMI1 Ct$_{\Delta 698\text{-}882}$	-	Gentamycin	LG
pDONR207: DMI1 Ct min2	DMI1 Ct$_{\Delta 585\text{-}882}$	-	Gentamycin	LG
Y2H Expression vectors				
pDEST-GADT7: T	T Y2H Control	-	Ampicillin	Clontech™
pDEST-GBKT7: 53	53 Y2H Control	-	Kanamycin	Clontech™
pDEST-GADT7: DMI1 Ct	DMI1 Ct	pDONR207: DMI1 Ct	Ampicillin	(Charpentier *et al.*, 2016)
pDEST-GBKT7: DMI1 Ct	DMI1 Ct	pDONR207: DMI1 Ct	Kanamycin	(Charpentier *et al.*, 2016)
pDEST-GADT7: RLK kinase+	RLK kinase+	pDONR207: RLK kinase+	Ampicillin	LG

pDEST-GBKT7: RLK kinase+	RLK kinase+	pDONR207: RLK kinase+	Kanamycin	LG
pDEST-GADT7: RLK kinase only	RLK kinase domain	pDONR207: RLK kinase only	Ampicillin	LG
pDEST-GBKT7: RLK kinase only	RLK kinase domain	pDONR207: RLK kinase only	Kanamycin	LG
pDEST-GADT7: DMI1 Ct min5	DMI1 $Ct_{\Delta 870-882}$	pDONR207: DMI1 Ct min5	Ampicillin	LG
pDEST-GBKT7: DMI1 Ct min5	DMI1 $Ct_{\Delta 870-882}$	pDONR207: DMI1 Ct min5	Kanamycin	LG
pDEST-GADT7: DMI1 Ct min4	DMI1 $Ct_{\Delta 727-882}$	pDONR207: DMI1 Ct min4	Ampicillin	LG
pDEST-GBKT7: DMI1 Ct min4	DMI1 $Ct_{\Delta 727-882}$	pDONR207: DMI1 Ct min4	Kanamycin	LG
pDEST-GADT7: DMI1 Ct min3	DMI1 $Ct_{\Delta 698-882}$	pDONR207: DMI1 Ct min3	Ampicillin	LG
pDEST-GBKT7: DMI1 Ct min3	DMI1 $Ct_{\Delta 698-882}$	pDONR207: DMI1 Ct min3	Kanamycin	LG
pDEST-GADT7: DMI1 Ct min2	DMI1 $Ct_{\Delta 585-882}$	pDONR207: DMI1 Ct min2	Ampicillin	LG
pDEST-GBKT7: DMI1 Ct min2	DMI1 $Ct_{\Delta 585-882}$	pDONR207: DMI1 Ct min2	Kanamycin	LG
Plant Expression vectors				
pK7FWG2: free GFP KDEL	GFP KDEL	-	spectinomycin	MC
pK7FWG2: empty	Empty vector	-	spectinomycin	MC
pK7FWG2: RLK-GFP	RLK CDS	pDONR207: RLK FL no stop	spectinomycin	LG
pK7FWG2: gRLK-GFP	Genomic RLK	pDONR207: gRLK	spectinomycin	LG
pK7FWG2: gRLK-GFPminlinker	Genomic RLK	pDONR207: gRLK	spectinomycin	LG

Table 2.8- List of level 2 golden gate vectors generated and used in this work. For identifier, constructs labelled based on the person who generated them: D= Pierre Dangeville, LG= Lauren Grubb

Identifier	Backbone	R1			R2			R3			R4			End linker
		Pro	CDS	Term	Pro	CDS	Term	Pro	CDS	Term	Pro	CDS	Term	
CRISPR-Cas9														
L2-LG5	EC50507	p35S	mCherry	t35S	MtU6.6	sgRNA1/EFScaffold	MtU6.6	MtU6.6	sgRNA2/EFScaffold	MtU6.6	-	-	-	EC41766
L2-LG6	EC50507	p35S	mCherry	t35S	MtU6.6	sgRNA2/EFScaffold	MtU6.6	MtU6.6	sgRNA3/EFScaffold	MtU6.6	-	-	-	EC41766
L2-LG7	EC50507	p35S	mCherry	t35S	MtU6.6	sgRNA1/EFScaffold	MtU6.6	MtU6.6	sgRNA3/EFScaffold	MtU6.6	-	-	-	EC41766
L2-LG8	EC50507	p35S	mCherry	t35S	MtU6.6	sgRNA1/EFScaffold	MtU6.6	MtU6.6	sgRNA2/EFScaffold	MtU6.6	MtU6.6	sgRNA3/EF Scaffold	MtU6.6	EC41780
Split-YFP														
L2-LG13	EC50507	pLjUBI	DMI1-YNE	t35S	pNos	gRLK (WT)-YCE	tNos	pAtUBI10	NESmCherry	t35S	-	-	-	EC41766
L2-LG14	EC50507	pLjUBI	DMI1-YNE	t35S	pNos	gRLK (P565S)-YCE	tNos	pAtUBI10	NESmCherry	t35S	-	-	-	EC41766
L2-LG15	EC50507	pLjUBI	DMI1-YNE	t35S	pNos	free YCE	tNos	pAtUBI10	NESmCherry	t35S	-	-	-	EC41766
L2-LG16	EC50507	pLjUBI	DMI1-YNE	t35S	pNos	gRLK$_{\Delta 571-586}$-YCE	tNos	pAtUBI10	NESmCherry	t35S	-	-	-	EC41766
L2-LG17	EC50507	pLjUBI	DMI1$_{\Delta 698-882}$-YNE	t35S	pNos	gRLK (WT)-YCE	tNos	pAtUBI10	NESmCherry	t35S	-	-	-	EC41766
Gene expression analysis														
L2-LG31	EC50507	p35S	mCherry	t35S	pRLK	NLS-GFP	tACS2	-	-	-	-	-	-	EC41744
L2-LG33	EC50507	p35S	mCherry	t35S	pRLK	GUS	tACS2	-	-	-	-	-	-	EC41744
L2-D7	EC50507	p35S	mCherry	t35S	-	-	-	-	-	-	-	-	-	EC41722

Table 2.9- InFusion vectors generated and used in this work (For source: LG= Lauren Grubb, NCM= Neftaly Cruz Mireles)

Vector Name	CDS	Resistance	Source
pOPINM: His-MBP-DMI1 Ct	DMI1 Ct	carbenicillin	NCM
pOPINM: His-MBP-RLK kinase	RLK kinase domain	carbenicillin	LG
pOPINS3C: His-SUMO-RLK kinase	RLK kinase domain	carbenicillin	LG
pOPINJ: His-GST-RLK kinase	RLK kinase domain	carbenicillin	LG
pOPINM: His-MBP-RLK kinase P565S	RLK kinase domain P565S	carbenicillin	LG
pOPINM: His-MBP-RLK kinase$_{\Delta GBBS}$	RLK kinase domain$_{\Delta 571\text{-}586}$	carbenicillin	LG
pOPINM: His-MBP-RLK FL	RLK FL	carbenicillin	LG
pFastBac: MBP-RLK FL	RLK FL	gentamycin	LG

2.4- Plant assays

2.4.1- Nodulation assay

For all nodulation assays with transformed roots, approximately 14 days after excision of untransformed and transferring plants to plates with filter paper, plants were screened for dsRed fluorescence as a transformation marker and transferred either to TerraGreen and sand mix (Oil-Dri Company, Wisbech, UK) in P40 trays or into phytaboxes placed in the growth chamber as described in Section 2.1.1. For stable lines, following germination plants were grown in a growth chamber for 7-10 days. For all experiments, after 3 days of acclimatization to soil, plants were inoculated with *Sm*2011 expressing hemA-β-galactosidase (LacZ) reporter gene of OD_{600} ~0.01. Roots were harvested 14, 21, 60 or 100 days post inoculation (dpi) and stained overnight for β-galactosidase activity in 0.1 M sodium phosphate (pH 7.2), 5 mM $K_3Fe(CN)_6$, 5 mM $K_4Fe(CN)_6$ and 0.02 M X-Gal at 30 °C. The number of nodules and primordia were scored in each plant using a stereo microscope (Leica MZFLIII with fluorescence screening for transformed roots).

For spontaneous nodulation assays, plants were transferred to sterile phytaboxes with autoclaved TerraGreen and sand mix (Oil-Dri Company, Wisbech, UK) in absence of rhizobia and allowed to grow for 8-10 weeks. Following this, plants were uprooted, roots screened for fluorescence, and spontaneous nodule-like structure sections of roots were fixed in 10% glutaraldehyde and imaged. Fixed roots were sectioned with a VT1000 vibratome (Leica) using 100 µM sections and imaged on a Leica DM6000 microscope.

2.4.2- Mycorrhization assay and ink staining

Mycorrhization assays were performed on plants with transformed roots 14 days following transfer to ModFP plates with filter paper or on stable lines after 7-10 days growth on ModFP plates. Transformed roots were screened for fluorescence marker and transferred to the controlled environment chamber in 20% AM inoculum, 80% TerraGreen and sand mix (Oil-Dri Company, Wisbech, UK). After 3-5 weeks (or until the desired wild-type arbuscule

colonization as indicated), plants were uprooted, washed in water and roots trimmed. The roots were bleached with 10% KOH for 20 min and then stained with a solution of 5% acetic acid and 5% Sheaffer ink for 10 min. Roots were destained in water overnight and scored the following day using a grid method as described in Montero *et al.*, (2019).

2.4.3- Root system architecture phenotyping

Root system architecture analysis was done on segregating populations of EMS mutants where ~120 plants were sterilized and germinated on plates as described above in Section 2.1.1 and then planted in TerraGreen and sand mix (Oil-Dri Company, Wisbech, UK). Three days after planting, the plants were inoculated with *Sm*2011 LacZ at OD_{600} 0.01. They were then left to grow for 14 or 25 days. The genotype of segregating population was determined using KASP as described above, and photos were taken of the roots with a Canon G11 digital camera. The length of primary root, and number and length of lateral roots was assessed using the NeuronJ plugin on Fiji ImageJ software.

2.5- Microscopy methods

2.5.1- Light microscopy

All images were captured using the Leica DM6000 or Leica M205FA stereo microscope. Images were processed using ImageJ.

2.5.2- Confocal laser scanning microscopy

Localization experiments for AUK-GFP and BiFC experiments were performed using a Zeiss 780 confocal laser scanning microscope equipped with an Argon Krypton laser (Zeiss). The seedlings were imaged 2 weeks following transfer to Mod FP plates pH 6.0 containing filter paper following excision of untransformed roots. The 488 nm excitation line of the argon ion laser was used to excite GFP, and emission spectra were collected between 497 and 551 nm. For YFP, excitation was at 514 nm and emission between 520-580 nm. For mCherry excitation was at 587 nm and emission imaged between 600-620 nm. Images were processed in ImageJ software. Protein expression and integrity was assessed by protein extraction and immunoblotting.

2.5.3- Ca^{2+} oscillation analysis

For analysis of Ca^{2+} oscillation in transformed roots, wild-type, *dmi1-1*, *dmi2-1* and *auk-1 M. truncatula* roots expressing *YC3.6* were transformed as described above with empty *pK7FWG2* vector or *pUBI:AUK-GFP* or A17 and *auk-1* plants were transformed with *NLS-YC3.6* as described above. Following 2 weeks root growth on ModFP plates for transformed plants, or 2 days growth on BNM plates with 100 nM aminoethoxyvinylglycine (AVG) for stable lines, on filter paper, these were analyzed for Ca^{2+} oscillation using a Nikon ECLIPSE FN1 with an emission image splitter (Optosplit, Cairn Research, UK) and an electron multiplying cooled charge coupled camera (Rolera™ Thunder EMCDD, QImaging). CFP was

excited at wavelength of 436±20 nm by a light emitting diode (OptoLED, Cairn) and emitted fluorescence was detected at of 480±40 nm for CFP fluorescence and 535±30 nm for YFP fluorescence. Images were collected in 3 s intervals for 1.5 h using MetaFluor software. A chamber of 48 × 64 mm coverglass (Solmedia) using high-vacuum grease (Dow Corning GMBH) was used to place the roots in 2 mL BNM. Nod factor application was done at 40 min into recording at a final concentration of 10^{-8} M. Ca^{2+} imaging was performed on 2 cm long roots and on the root hairs in the induction zone. Ca^{2+} imaging traces were detrended using GNU Octave v6 1.0 with the nan 3.5.0 and io v2.6.3 packages using the script described in (Del Cerro *et al.,* 2022).

2.6- Protein biochemistry methods

2.6.1- Heterologous expression and purification

2.6.1.1- Heterologous expression and purification from E. coli

Protein coding sequences were cloned into pOPIN vectors (-M, -S3C, and -J) as previously described for protein production followed by transformation into Rosetta BL21 pLysS *E. coli* expression strain. Cell cultures were grown in LB at 37 °C until OD_{600} 0.6-0.8 was reached followed by transfer to 16 °C overnight. Cells were harvested by centrifugation in a Sorvall Lynx centrifuge at 5663 x g and resuspended in buffer A1 (50 mM HEPES, 50 mM glycine, 0.5 M NaCl, 20 mM imidazole, 5% (v/v) glycerol) with the addition of cOmplete™ EDTA-free protease inhibitor cocktail tablets (1 tablet per 50 mL). Cells were lysed by sonication using a VibraCell sonicator (SONICS) at 40% maximum amplitude with 1 s pulse with 3 s interval in between pulses. Whole cell lysate was centrifuged at 38, 724 x g for 30 min at 4 °C in a Sorvall Lynx centrifuge. Clarified cell lysate was then injected onto a 5 mL Ni2+-NTA column (GE Healthcare) equilibrated in A1 buffer, followed by step-elution with elution buffer B1 (50 mM Tris-HCl pH 8.0, 50 mM glycine, 0.5 M NaCl, 500 mM imidazole, 5% (v/v) glycerol), and transferred to a Superdex 75 16/60 gel filtration column (for AUK) or 200 16/60 (for DMI1) in buffer A4 (20 mM HEPES pH 7.5, 150 mM NaCl, 1 mM TCEP). Fractions of 2 mL were collected, those corresponding to an absorbance peak were separated on an sodium dodecyl sulphate- polyacrylamide gel electrophoresis (SDS-PAGE) gel, and those containing the protein of interest were pooled and concentrated to 1-3 mg/mL using VivaSpin® centrifugal concentrators (3K MWCO for AUK kinase and 50K for MBP-DMI1). For cleavage of the tag on AUK for BLItz assays, 3C protease (1:100 ratio of protein:protease) was added to the concentrated protein and incubated overnight at 4 °C for cleavage of the 6xHis-MBP tag. This treated sample was then applied to a 5 mL Ni2+-NTA column equilibrated in buffer A1. The column was washed with 3 CV A1 buffer, with collection of the flow-through and wash-through fractions. To remove the tag from the protein sample, the protein was applied to a dextrin sepharose (MBPTrap) column (GE Healthcare) equilibrated in A1 buffer. Three CV

of A1 buffer were used to wash the column, and the collected flow-through and wash-through fractions were separated on an SDS-PAGE gel. Fractions containing the desired protein were pooled and concentrated to 5 mL using VivaSpin® centrifugal concentrators as before. A second gel filtration step was performed using a Superdex 75 16/60 column equilibrated in buffer A4. Fractions of 2 mL were collected, and those corresponding to the absorbance peak separated by SDS-PAGE. Those fractions containing the desired protein were pooled and concentrated and concentration was measured using a NanoDrop spectrophotometer.

2.6.1.2- Heterologous expression and purification from Sf*9 insect cells*

For protein production from insect cells, the full-length coding sequence of AUK was subcloned into pOPINM and then pFASTBAC Dual vectors including MBP tag by InFusion cloning (Takara BioSciences) as described above to allow for purification. The constructs were transformed into STELLAR *E. coli*, transformants selected and plasmids purified to isolate plasmid DNA followed by confirmation by sequencing. Recombinant bacmid was generated by transforming purified plasmid into DH10Bac competent cells expressing YFP as a transformation marker, positive colonies selected and isolated by a modified plasmid purification protocol. From a 5 mL culture incubated overnight at 37 °C with 200 rpm shaking, cells were pelleted at 2 558 × g for 5 min and resuspended in 300 µL buffer P1 (from Qiagen plasmid prep kit). Following addition of 300 µL buffer P2, mixture was incubated at room temperature for 5 min. 400 µL of P3 was added and mixed by inversion. This was allowed to rest on ice for 6 min and then centrifuged at 15 871 × g for 10 min and then an additional 2 min to remove residual chromatin. Supernatant was removed and 500 µL of 70% ethanol was added to the pellet and inverted before centrifugation at 15 871 × g for 5 min at room temperature. This was repeated twice more. Supernatant was removed and the pellet was air-dried for 1 min. DNA was then dissolved in 50 µL buffer EB and bacmid concentration was determined using a nanodrop. Next, recombinant baculovirus was produced using *Sf*9 cells cultured in 1 × SF-900™ (SFM; Gibco). Cells in log phase were added to wells containing 2 mL Grace's Culture Medium seeded at 0.5 $\times 10^6$ cells/mL in a 6-well plate. Cells were allowed to attach for 15 min at room temperature. 6 µL of FuGENE HD transfection reagent was added to 4 µg of bacmid in 200 µL SFM media and incubated for 15 min at room temperature. This was then added dropwise to the cells in 6-well plates and incubated for 3 days at 27 °C for production of the P1 viral stock. P1 virus was harvested and P2 was produced by addition of 1:100 P1 to 50 mL *Sf*9 cells at density of 1-2 × 10^6 cells/mL. This was incubated for 3 d at 27 °C with shaking at 200 rpm to produce the P2 viral stock. P2 viral stock was harvested by centrifugation at 1000 × g for 10 min at 4 °C. P2 viral stock was used to infect 100 mL culture at 2 $\times 10^6$ cells/mL and incubated for 2d at 27 °C with shaking at 200 rpm. Cells were harvested at 2 000 ×g for 20 min and washed in PBS.

For protein purification, cells were centrifuged again at 2 000 × g for 10 min, resuspended and lysed in hypotonic buffer (20 mM Tris-HCl pH 8.0, 5 mM β-mercaptoethanol and 1 × Sigma protease inhibitor tablet). Cell membranes were collected by centrifugation at 29 448 × g for 30 min at 4 °C. Membranes were resuspended and protein further extracted by glass dounce homogenizer in extraction buffer (50 mM HEPES-Na pH 8.58, 150 mM NaCl, 0.5% LMNG, 5 mM β-mercaptoethanol). After incubation in extraction buffer for 1 h, the solubilized membrane was clarified by ultracentrifugation at 111 338 × g for 30 min. Supernatant was added to a 5 mL MBP-Trap column (GE) and washed with 3 CV buffer A (50 mM HEPES-Na pH 5.85, 150 mM NaCl, 0.05% LMNG, 0.15 mM soybean polar lipid extract (Avanti), 5 mM β-mercaptoethanol) and subsequently buffer B (50 mM HEPES-Na pH 7.4, 500 mM NaCl, 0.05% LMNG, 0.15 mM soybean polar lipid extract, 5 mM β-mercaptoethanol). Maltose was added at 20 mM to buffer B for elution. Protein presence and purity was then assessed by 12% SDS-PAGE gel followed by Coomassie staining as previously described.

2.6.2- Protein experiments

2.6.2.1- Bio-layer interferometry (BLItz)

BLItz was used to monitor interaction between DMI1 and the purified AUK kinase domain (wild-type and mutant) using a FortéBio (Menlo Park, CA) Octet RED96 instrument and Ni-NTA biosensors (Sartorius) at room temperature. Baseline was established in A4 buffer for 30 s then 75 µM DMI1 was loaded onto the Ni-NTA biosensor tip for 2 min. A baseline was re-established in A4 buffer for 30 s to wash away unbound DMI1 and then 25-100 µM AUK kinase was added for the association step for 2 min. Finally, the dissociation step was performed in A4 buffer for 2 min. A4 buffer was used as a reference control. Curves were analyzed and K_D values determined using the BLItz Pro software.

2.6.2.2- Crude protein extraction from M. truncatula *roots*

To test protein expression by western blot, roots were ground in liquid nitrogen prior to addition of extraction buffer (100 mM Tris-HCl pH 8, 150 mM NaCl, 5 mM EDTA, 10 mM dithiothreitol (DTT), 5% SDS, 4 M urea, 1 × protease inhibitor cocktail), prewarmed to 65 °C at 1:1 ratio of powder to buffer. Samples were then vortexed in the buffer followed by incubation at 70 °C for 30 min. A brief centrifugation of 2 min at 15 871 × g was performed to pellet debris. The supernatant was then taken and mixed with 1 × Laemmli Sample Buffer (BioRad) with 10 mM DTT prior to loading on SDS-PAGE gel and immunoblotting.

2.6.2.3- SDS-PAGE and immunoblotting

Protein samples were run on a 10% SDS-PAGE pre-cast gel (Bio-Rad for Western blots, Expedeon or Merck for *in vitro* protein samples) using 1 × Tris-Glycine running buffer for 20 min at 75 V then 1 h at 120 V. For immunoblotting, the proteins were transferred from the gel onto Polyvinylidene fluoride (PVDF) membrane (BioRad) with 1 × transfer buffer in 20%

EtOH overnight at 30 V. The next day membranes were blocked for 1 h in 5% milk in tris-buffered saline with 1% Tween-20 (TBS-T) at room temperature (RT) and then blotted with appropriate primary antibody (See Table 2.10) overnight in 1 % milk at 4 °C. For antibodies that were not horseradish peroxidase (HRP)-conjugated, the blots were washed in TBS-T four times for 10 min at RT followed by 2 h incubation at RT with appropriate secondary antibody (See Table 2.10). The blots were then washed 4 times with TBS-T for 15 min each at RT before imaging with Pico enhanced chemiluminescence (ECL; ThermoFisher) on an ImageQuant8000 imager (Cytiva).

2.6.2.4- Immunoprecipitation and mass spectrometry

Co-immunoprecipitation (co-IP) was performed to assess interaction of AUK and DMI1 *in planta*. For co-IP analysis, approximately 40 plants were grown and inoculated as described above and dug out 14 dpi with *Sm*2011. Roots were pulverized in liquid nitrogen with mortar and pestle and lysis buffer (10% glycerol, 50 mM Tris-HCl pH 8.0, 150 mM NaCl, 1% Igepal ca-630, 250 mM Mannitol, 1 mM PMSF, 20 µM MG-132, 1 × cOMPLETE Protease inhibitor cocktail) at a ratio of 10 mL per 3 g root material. The material was further homogenized using a Potter tube homogenizer and then supernatant was clarified by centrifugation three times at 2 558 ×g for 10 min each. An input fraction was collected and then the supernatant was incubated with µMacs HA-trap beads for 2 h at 4 °C. Supernatant was then applied to a µ column in a µMacs magnetic stand and then beads were washed 4 times with 1 mL wash buffer (50 mM Tris-HCl pH 8.0, 150 mM NaCl, 0.1% Triton X-100, 1 × EDTA-free protease inhibitor cocktail). Following washes, beads were eluted by 2 additions of 40 µL µMacs elution buffer preheated to 80 °C and beads were allowed to sit in buffer for 1 min prior to elution from columns. Input and IP samples were then loaded on an SDS-PAGE gel and immunoblotted.

For samples used for phosphosite determination, either 12 infiltrated leaves collected at 3 dpi or transformed roots from TerraGreen and sand grown for 1 week prior to inoculation and excavated at 14 dpi (treated with or without *Sm*2011) were used. Lysis was done as described for co-IP experiments, but 30 µL ChromoTek myc-trap agarose beads were added to supernatant and allowed to incubate for 1h at 4 °C with end-over-end rotation. Beads were collected by centrifugation at 2 000 × g, supernatant was removed and then beads were washed 3x with 1 mL wash buffer with centrifugation at 2 000 × g between each wash step. Finally, protein was eluted from the beads by addition of 80 µL SDS-PAGE Sample buffer (100 mM Tris-Cl pH 6.8, 4% SDS, 20% glycerol, 2% DTT, 0.04% bromophenol blue) and boiling at 95 °C for 10 min. Expression was verified by SDS-PAGE and immunoblotting with α-GFP N-terminal antibody (Sigma G-1544) and the rest of the elution was run on a 10% acrylamide gel and stained with RunBlue Coomassie stain. Bands corresponding to the size of DMI1 were excised with sterilized scalpel blade. The gel slices were destained in 30% EtOH for 30 min

at 65 °C and repeated until clear. A 20 min wash with vortexing was done with 50 mM TEAB/50% acetonitrile (ACN). The gel slices were then incubated with 10 mM DTT in 50 mM TEAB for 30 min at 55 °C. DTT was removed and 30 mM iodoacetamide (IAA) was added and gel slices were incubated in the dark with vortex for 30 min at room temperature. Washes were then performed for 20 min each with 50 mM TEAB/50% ACN followed by 50 mM TEAB alone. Gel slices were cut into 1 × 1 mm pieces and moved to a protein low bind Eppendorf tube where they were washed 20 min each at room temperature, first with TEAB/50%ACN and then with 100% ACN twice. Following washes, 100% ACN was removed, and gel slices were dried for 30 min in a speed vac prior to trypsin digestion and LC-MS/MS.

Aliquots were analyzed using nano-LC-MS/MS on an Orbitrap Fusion™ Tribrid™ mass spectrometer coupled to an UltiMate® 3000 RSLCnano LC system (Thermo Fisher Scientific). The samples were loaded and trapped using a pre-column with 0.1% TFA at 20 µL min^{-1} for 3 min. The trap column was then switched in-line with the analytical column (nanoEase M/Z column, HSS C18 T3, 100 Å, 1.8 µm; Waters, Wilmslow, UK) for separation using the following long gradient of solvents A (water, 0.05% formic acid) and B (80% ACN, 0.05% formic acid) at a flow rate of 0.3 µL min^{-1}; 0-4 min 3% B (trap only); 3-13 min linear increase B to 13%; 13-77 min increase B to 38%; 77-92 min increase to 55%; 92-97 min increase B to 55%; followed by a ramp to 99% B and re-equilibration to 3% B. Data were acquired with the following mass spectrometer settings in positive ion mode: MS1/OT [resolution 60K, profile mode, mass range m/z 300-1800, AGC $4e^5$, fill time 50 ms], MS2/IT [data analysis was performed using Higher-energy C-trap dissociation (HCD) and Collision-induced dissociation (CID) fragmentation with the following parameters: top20 in IT rapid, centroid mode, isolation window 1.6 Da, charge states 2-5, threshold 1.9 e^4, CE = 30, AGC target $1.9e^4$, max. inject time 35 ms, dynamic exclusion 1 count, 15 s exclusion, exclusion mass window ±5 ppm].

Peaklists were generated with MaxQuant 1.6.17.0 (16) in Label-Free Quantitation (LFQ) mode using the *Medicago* protein sequence database [*Medicago truncatula*, BioProject 10791], (57, 585 entries)] and the MaxQuant contaminants database (245 entries). The quantitative LFQ results from MaxQuant with default parameters were used together with search results from an in-house Mascot Server 2.4.1 (Matrixscience, London, UK) on the same databases. A precursor tolerance of 6 ppm and a fragment tolerance of 0.6 Da was used. The enzyme was set to trypsin/P with a maximum of 2 allowed missed cleavages; oxidation (M), acetylation (protein N-term) was set as variable modifications; carbamidomethylation (C) as fixed modification. The Mascot search results were combined into Scaffold 4 (www.proteomesoftware.com) using identification probabilities of 99% for proteins and 20% for peptides.

2.6.2.5- In vitro *kinase assays*

In vitro kinase assays were performed to test phosphorylation of DMI1 by AUK kinase domain. For the assay, 1.8 µg AUK kinase domain and 1 µg DMI1 C-term was incubated in 20 µL 25 mM Tris-HCl (pH 8.0), 15 mM $MgCl_2$, 2 mM $MnCl_2$, 7.5 mM NaCl, 0.05 mM EDTA, 0.05 mM DTT, 5% glycerol and 75 µM ATP at 27 °C for 30 min. Samples were analyzed by 12% SDS-PAGE gel, stained with Pro-Q Diamond phosphoprotein gel stain (Invitrogen), and imaged on Typhoon 4600 fluorescence imager. For protein staining, the gel was stained with RunBlue Coomassie Brilliant Blue stain.

2.6.2.6- Protein x-ray crystallography

For structural analysis of AUK wild-type and gain-of-function, proteins were purified as before, tags cleaved, and final fractions collected in A4 buffer. Protein fractions were run on a native PAGE gel to ensure purity, and fractions were pooled and concentrated. Crystallization 96 well screening plates with one drop of wild-type protein and one drop of mutant at 10 mg/mL were set up in A4 buffer using an Oryx nano robot (Douglas Instruments) with sitting drop by vapour diffusion. Screens tried for this thesis included KISS, Morpheus, BCS, JCSGPlus and Pact Premier.

Table 2.10- Antibodies and titres used in this work

Antibody	Titre Used	Vendor
α-GFP Nterm (G-1544)	1:1 000	Sigma
α-HA(F-7)-HRP	1:500	Santa Cruz Biotechnology
α-HA-HRP (3F10)	1:1 000	Roche
α-c-myc (9E10)	1:500	Roche
α-FLAG-HRP (A8592)	1:5 000	Sigma
α-MBP-HRP (E8038S)	1:2 500	NEB
α-rabbit-HRP sc-2357 (A0120)	1:10 000	Santa Cruz Biotechnology
m-IgGK BP (α-mouse)-HRP (sc-516102)	1:10 000	Santa Cruz Biotechnology

2.7- Computation Methods

2.7.1- Expression analysis from gene atlas

Expression analysis was done by extracting microarray data from the Noble Gene Expression Atlas (http://mtgea.noble.org/jic/).

2.7.2- Protein homology modeling

Amino acid sequence was submitted to i-tasser (Zhang, 2008) or Swiss-Model (Waterhouse *et al.*, 2018) for structure prediction. Effect of mutations was analyzed using Coot (Emsley *et al.*, 2010) and CCP4mg (McNicholas *et al.*, 2011) and change in structure flexibility assessed by PBD file submission to Dynamut (Rodrigues *et al.*, 2018). Final figures were made in ccp4mg.

2.7.3- Phylogenetic analysis

Phylogenetic analysis of amino acid sequences was performed using the parameters indicated in figure legends. MEGA-X was used for alignment and phylogenetic tree construction.

2.7.4- Statistical analyses

Statistical analyses were performed using GraphPad Prism version 8.0 for Windows (GraphPad Software, La Jolla California USA, www.graphpad.com).

3- Analysis of DMI1 association with a putative interacting protein

3.1- Introduction

As detailed in Chapter 1, over the past several decades, many forward and reverse genetic screens been performed in the model legumes, *M. truncatula* and *Lotus japonicus*, to identify key players involved in endosymbiosis signaling with nitrogen fixing bacteria (*Rhizobia*) or arbuscular mycorrhizal (AM) fungi. These identified genes playing a role in perception of the Nod and Myc factors at the plasma membrane (*Lj*NFR1/*Mt*NFP and *Lj*NFR5/*Mt*LYK3 for rhizobia, *Mt*LYK9 for AM fungi as well as the co-receptor *Lj*SYMRK/*Mt*DMI2), a common symbiosis signaling pathway including machinery involved in nuclear calcium oscillation (MCA8, LjLOTUS and LjCASTOR/MtDMI1), and proteins that are involved in decoding the calcium signal (*Lj*CCaMK/*Mt*DMI3 and its interacting partner *Lj*CYCLOPS/*Mt*IPD3) to allow for appropriate gene expression allowing for association with the endosymbiont. As a result of these genetic screens, much is known about perception of Nod and Myc factors at the plasma membrane, and of components at the nuclear envelope involved in Ca^{2+} oscillation, however there is a lack of understanding about the components acting between, that may function as channel activators or regulators downstream of perception.

In addition to these, pharmacological studies have been performed to uncover more detail of early signaling in endosymbiosis, including the use of the G protein agonist, mastoparan, the product of HMGR1, MVA and inhibitors of PLC and PLD (Charron *et al.*, 2004; Engstrom *et al.*, 2002; Kevei *et al.*, 2007; Pingret *et al.*, 1998; Sun *et al.*, 2007; Venkateshwaran *et al.*, 2015). HMGR1 has been observed to interact with DMI2, and is required for symbiosis with *Sinorhizobium* and induction of nuclear Ca^{2+} oscillation by both Nod factor and AM fungal exudates (Kevei *et al.*, 2007; Venkateshwaran *et al.*, 2015). MVA, a direct product of HMGR1, has been shown to be sufficient for activation of nuclear Ca^{2+} oscillation, dependent on NFP and partially on DMI2 (Venkateshwaran *et al.*, 2015). These studies placed MVA upstream of the activation of nuclear Ca^{2+} channels. The G protein agonist, Mas7, has interestingly been shown to induce symbiosis-like nuclear Ca^{2+} oscillations and induction of early nodulin gene expression (Pingret *et al.*, 1998), in a *dmi1* mutant (Charron *et al.*, 2004; Sun *et al.*, 2007), suggesting that DMI1 itself might not be the Ca^{2+} channel involved. In accordance with this observation, mathematical modelling has been performed to test the role of each ion channel in the generation of the nuclear Ca^{2+} oscillation, leading to the proposal that DMI1 is a counter-ion channel, balancing oscillations through movement of another cation such as potassium (Charpentier *et al.*, 2013; Peiter *et al.*, 2007). With the finding that DMI1 associates with CNGC15 channel at the nuclear envelope (Charpentier *et al.*, 2016), it became likely that DMI1 regulates CNGC15 through association and thereby indirectly regulates the nuclear Ca^{2+} oscillation, acting as a gatekeeper.

Additionally, PLC/D were suggested to play a role in symbiosis signaling through biochemical studies in common vetch roots and alfalfa suspension cell cultures (den Hartog *et al.,* 2003). These phospholipases generate secondary messengers, such as IP_3 and PA. The use of n-butanol, an antagonist for production of PA by phospholipase D has been shown to inhibit induction of early nodulin genes (Charron *et al.,* 2004). Importantly, a more recent study has shown the induction of *PLDα1* in rhizobial infection and nodulation, with involvement in control of nodule number, nodulation gene expression, cytoskeletal rearrangement and hormone levels in *Glycine max* (Zhang *et al.,* 2021). Altogether, these experiments suggest a possible role for a secondary messenger in the activation of channels involved in nuclear Ca^{2+} oscillation, or some other factor potentially transducing the signal to the nucleus from perception at the plasma membrane, and that DMI1 may function as a regulator of the Ca^{2+} oscillation rather than as the Ca^{2+} channel itself.

With the hypothesis of DMI1 acting as a regulator for nuclear Ca^{2+} oscillation in symbiosis, a yeast two-hybrid (Y2H) screen was performed to identify putative interacting proteins of DMI1, with several proteins predicted to be localized to the nucleus or nuclear envelope. In this thesis chapter, an analysis and confirmation of the association of DMI1 with one of these candidate interactors, an LRR-RLK, which will hereafter be referred to as AUxilliary Kinase interacting with DMI1 (AUK), is presented. Its interaction with DMI1 was assessed through several different protein-protein interaction experiments, heterologous, *in vitro* and *in planta,* and some indications of finer details of its interaction in a complex at the nuclear envelope are shown.

3.2- Results

3.2.1- DMI1 C-terminus associates with AUK kinase domain in pairwise Y2H

To identify putative interacting partners of DMI1 that may function to regulate its activation for symbiosis factors-induced nuclear Ca^{2+} oscillation, a Y2H screen was previously performed using the C-terminus of DMI1 and a *M. truncatula* root cDNA library. The C-terminus of DMI1 was used as bait owing to the fact it is on the cytoplasmic side of the nuclear membrane and is a soluble domain, whereas the N-terminus is smaller, less conserved, and is predicted to be a disordered region. The screen was performed by Hybrigenics services and identified 44 putative interacting partners in total. These were narrowed down further based on those candidates that were predicted to localize to the nucleus or cytoplasm where they could associate with DMI1 and conceivably transduce a signal upstream of the nuclear calcium oscillation, leaving nine interesting candidates.

At the beginning of this thesis, three of these candidates were chosen for further study confirm their association with DMI1 C-terminus via pairwise GAL4-based Y2H. These candidates included a leucine-rich repeat receptor-like kinase (LRR-RLK), a small

hypothetical protein (hereafter termed HYPO) and an SMI/KNR4-like protein of unknown function (hereafter termed SMI). HYPO and SMI had already been found to localize to the nucleus (Joseph Seaman, unpublished), and thus were deemed plausible interacting partners of DMI1 at the nuclear envelope.

GAL4 is a transcription factor with two separate domains, a DNA-binding domain (BD) that binds to the promoter sequence of the target gene, and the transcription-activation domain (AD) that is responsible for the activation of transcription (Osman, 2004). These domains need to function together for transcriptional activation to occur, and thus if each putative interacting protein is fused to either the AD or BD, there will be transcriptional activation only if protein-protein interaction does truly occur, bringing the domains into contact to allow them to function together. In the case of this experiment, when the fusion proteins interact, the BD and AD are brought into proximity to activate transcription of *HIS3* and *ADE2*, genes which promote biosynthesis of histidine and adenine, respectively. These two amino acids are essential for yeast to grow, and thus when the transformed yeast is plated on quadruple dropout media (lacking leucine, tryptophan, adenine and histidine; -LWAH) there will only be growth for true interacting proteins. Double dropout plates (lacking leucine and tryptophan; -LW) are used as controls of transformation as the plasmids containing the fusion proteins of AD and BD contain either leucine or tryptophan, respectively.

AUK is predicted to possess 5 leucine-rich repeats (LRRs), and a transmembrane domain followed by 157 amino acids upstream of its kinase domain (Figure 3.1b). The interaction of DMI1 C-terminus with the kinase domain (the domain found as interacting in the initial Y2H screen) was tested, as well as the entire C-terminus of AUK (here termed kinase+; Figure 3.1b) to further elucidate how the proteins associate. The C-terminal domain (Ct) of DMI1 was subcloned into pDEST destination vector containing GAL4-AD and AUK kinase domain and kinase+ as well as HYPO and SMI into a pDEST destination vector containing GAL4-BD. As a positive control in the pairwise Y2H, the SV40 large T-antigen (Clontech™ PT30234-1) and its positive interacting partner p53 were included. P53 and the T-antigen were also included in combination with each other protein in the experiment as a negative control to test for autoactivation. If the yeast grew in the negative control, the interaction was deemed autoactive. DMI1 was also included as a positive interactor with itself as previous work has shown its self-association via pairwise Y2H (Charpentier *et al.*, 2016). The pairwise Y2H experiment had growth in the quadruple dropout for DMI1 Ct with AUK kinase domain, but not AUK kinase+ (Figure 3.1a), although a western blot confirmed expression of all proteins (Figure 3.1e-f). This result may suggest that the kinase+ protein folds incorrectly, preventing association or accessibility of the interaction domain. In the immunoblot for DMI1 Ct, there is a higher upper band, which may represent a DMI1 Ct oligomer. It could be expected that the SDS in the SDS-PAGE gel may disrupt this association,

however these upper bands have been shown in previous literature (Charpentier et al., 2016), and perhaps the oligomerization is not completely disturbed. For the T, p53 and AUK kinase immunoblots, lower bands may correspond to non-specific binding of the antibody.

Interestingly, SMI interacted with DMI1 C-terminus (Figure 3.1a), however, it was also seen to associate with the T and p53 positive controls, indicating autoactivation and promiscuous binding. Thus, it was discounted from further investigation as a false positive. Additionally, DMI1 C-terminus was found to interact with HYPO (Figure 3.1a), however as a small hypothetical protein of unknown function, this was not a focus of the rest of the thesis.

AUK as an LRR-RLK was chosen for further study as the most promising candidate that could serve as a player upstream of the nuclear calcium oscillation, perhaps transducing a signal from the plasma membrane perception through phosphorylation of downstream targets. Many RLKs have been shown to act in dimers or multimers to facilitate their function, either through autophosphorylation of the kinase activation loop or through structural changes upon association allowing kinase activation (Heldin, 1995; Li *et al.,* 2002; Liu *et al.,* 2002; Nam & Li, 2002). AUK kinase domain association with itself was tested by Y2H assay and self-association was observed (Figure 3.1c), suggesting AUK may function in a dimer or multimer. Overall, the above results for pairwise Y2H experimental results provide preliminary evidence for an interaction between DMI1 Ct and the kinase domain of AUK, which oligomerizes, implicating AUK as an interesting candidate for further study.

The *Arabidopsis* ortholog of AUK was found to associate with CaM, and this association activated its autophosphorylation capacity when co-expressed in *E. coli* (Yu *et al.*, 2016). Thus, the association of AUK with MtCaM was assessed. *M. truncatula* has three CaMs, so each of these was investigated for putative association with AUK. Interestingly, none of the CaMs was observed to associate with AUK (Figure 3.1d), suggesting possible divergence in function or activation. It would be important to confirm this association in other systems before drawing further conclusions.

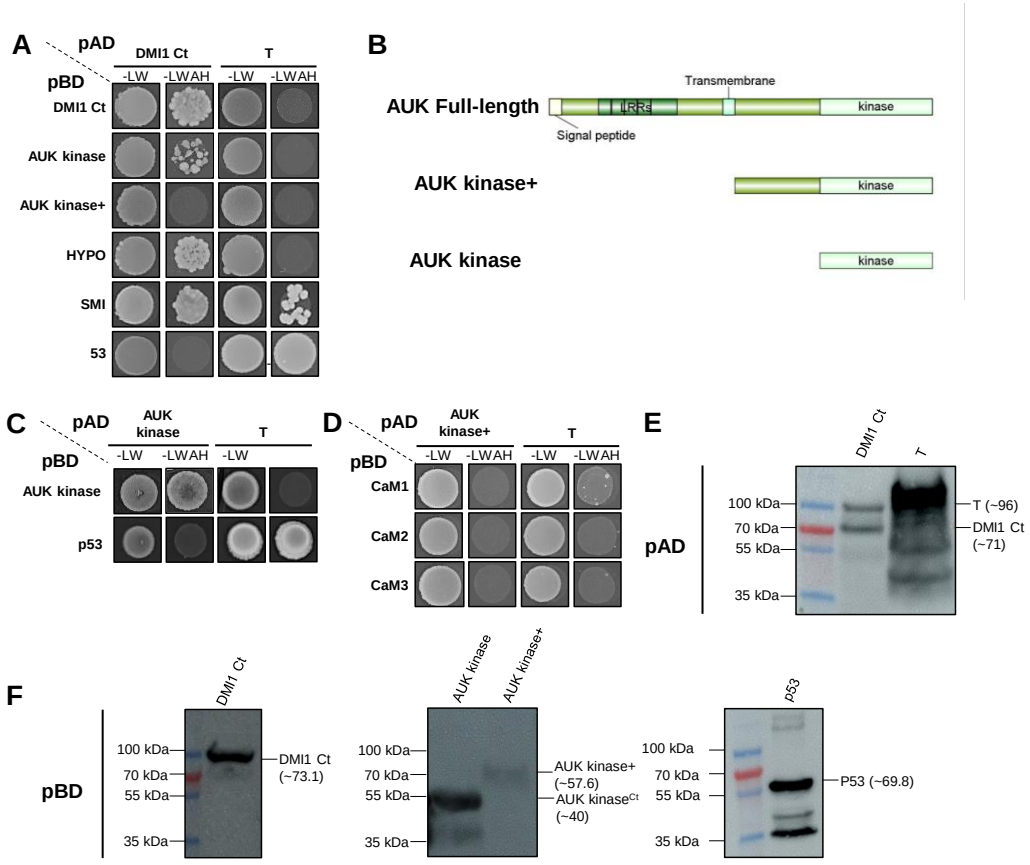

Figure 3.1. DMI1 C-terminus associates with AUK kinase domain via pairwise Y2H.

A. Yeast two-hybrid assays between the C-terminal domain of DMI1 as prey (BD) and AUK kinase domain, AUK kinase+, SMI and HYPO as bait (AD). Murine p53 and its interacting partner SV40 large T antigen (simian virus large tumor antigen) and DMI1 interaction with itself were used as controls. SD-LW, synthetic dropout medium lacking Leu and Trp; SD-LWAH, synthetic dropout medium lacking Ade, His, Leu, and Trp. Data shown are representative of 3 replicates. **B.** Schematic representation of AUK constructs used in the Y2H experiment. LRR repeat domains, transmembrane domain and kinase domain are indicated. **C.** Yeast two-hybrid assays between the AUK kinase domain as bait (AD) and as prey (BD). Murine p53 and its interacting partner SV40 large T antigen was used for a positive control. SD-LW, synthetic dropout medium lacking Leu and Trp; SD-LWAH, synthetic dropout medium lacking Ade, His, Leu, and Trp. Data shown is representative of 3 replicates. **D.** Yeast two-hybrid assays between the AUK kinase+ as bait (AD) and CaM1/2/3 as prey (BD). Murine p53 and its interacting partner SV40 large T antigen was used for a positive control. SD-LW, synthetic dropout medium lacking Leu and Trp; SD-LWAH, synthetic dropout medium lacking Ade, His, Leu, and Trp. Data shown is representative of 3 replicates. **E-F.** Western blot of yeast crude protein extraction to confirm protein expression. Proteins were immunoblotted with α-myc (E) and α-HA (D) antibodies to show protein expression of pBD

(E) and pAD (D) tagged proteins, respectively. Approximate protein sizes are shown in brackets beside each blot.

3.2.2- Truncations of DMI1 C-terminus alter its interaction with AUK kinase domain

To determine more precisely how AUK might associate with DMI1, and to generate negative controls for further analysis of interaction in further *in vivo* and *in planta* studies, truncations of DMI1 C-terminus were generated. DMI1 is a tetrameric cation channel with four transmembrane domains, followed by two Regulator of K^+ conductance (RCK) domains (Kim *et al.,* 2019; Peiter *et al.,* 2007) (Figure 3.2c). The C-terminal construct encompasses the soluble part of the DMI1 protein from Serine343 downstream to the end, from shortly after the fourth transmembrane domain and including both RCK domains. To determine where to make the truncations in the DMI1 protein, the C-terminal protein sequence of DMI1 was submitted to PSIVER (Murakami & Mizuguchi, 2010), which predicts accessible residues that may function as a binding surface with an interacting protein (Figure 3.2a). The truncations of $DMI1_{\Delta 870\text{-}882}$, $DMI1_{\Delta 727\text{-}882}$, $DMI1_{\Delta 698\text{-}882}$, and $DMI1_{\Delta 585\text{-}882}$ were selected for further study. The shortest truncation removes the majority of the second RCK domain (Figure 3.2c). These truncations were tested via pairwise Y2H for interaction with AUK kinase domain (Figure 3.2b). Although Y2H cannot be used for definitive quantification, the results suggested that truncations within the RCK2 domain disrupted the interaction of DMI1 C-terminus with AUK kinase domain. However, the complete removal of RCK2 seemed to enhance the interaction with AUK, indicating that RCK1 might form the interacting interface with AUK kinase. Protein expression was confirmed for all interactions by western blot, with all bands showing the expected size (Figure 3.2d). The results suggest that DMI1 might undergo a conformational change allowing its association with AUK upstream of residue 585, but that the smaller truncated versions affect its interacting domains, whereas when the entire second RCK domain is removed, the binding interface might be more accessible in yeast. Based on these results, DMI1 $Ct_{\Delta 698\text{-}882}$ was used in further *in planta* experiments as a negative control as it severely impacted the ability of yeast to grow on the quadruple dropout medium (See Section 3.2.5).

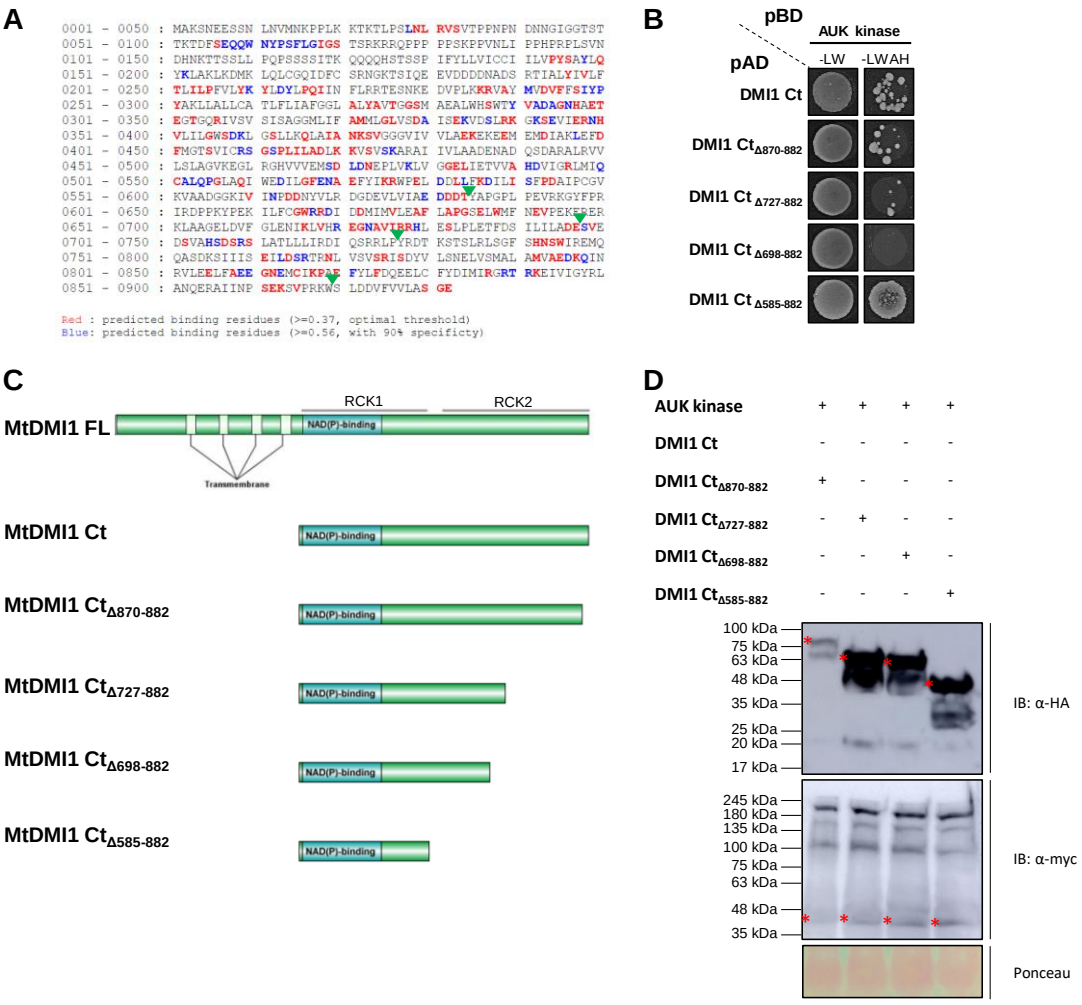

Figure 3.2. Truncations of DMI1 C-terminus alter its interaction with AUK in yeast

A. Output from PSIVER predicting likelihood of DMI1 amino acid residues acting at interaction interfaces for protein-protein interaction. Red, residues with >0.37 predicted optimal threshold for binding interface; blue, residues with >0.56 with 90% specificity for being an interaction interface; green triangles indicate position of DMI1 C-terminal truncations. **B.** Yeast two-hybrid assays between the AUK kinase domain as prey (BD) and DMI1 full-length (FL) and indicated truncations as bait (AD). SD-LW, synthetic dropout medium lacking Leu and Trp; SD-LWAH, synthetic dropout medium lacking Ade, His, Leu, and Trp. Data shown is representative of 2 replicates. **C.** Schematic of DMI1 full-length (FL) and truncations used for Y2H experiment in **(B)**. Transmembrane domains, NAD(P)-binding domain and location of RCK domains is indicated. **D.** Western blot showing expression of DMI1 FL and truncations and AUK kinase domain from yeast crude protein extraction of **(B)**. Proteins were immunoblotted with α-myc and α-HA antibodies to show protein expression of pBD and pAD tagged proteins, respectively. Ponceau stain was included as a loading control. Red asterisks indicate the expected size of the immunoblotted protein.

3.2.3- The AUK kinase domain can be purified from *E. coli* and interacts with DMI1 C-terminus using *in vitro* bio-layer interferometry (BLItz)

When using a yeast heterologous system for analysis of protein-protein interaction, it is difficult to determine quantitatively how strong the interaction is between the two proteins of interest. For a quantitative view of the association strength between DMI1 C-terminus and AUK kinase domain, the *in vitro* system, bio-layer interferometry (BLItz) was used to determine the enzymatic association and dissociation constant (K_D). To perform BLItz experiments, the proteins first had to be heterologously expressed and purified. A protocol for expressing DMI1 C-terminus in *E. coli* and purifying it was already established in the lab, and this was repeated with success (Figure 3.3). However, there was some unspecific protein seen at a lower size (possibly cleaved MBP tag), whereas DMI1 C-terminus is more pure after tag cleavage and subsequent additional gel filtration (as shown in Chapter 5).

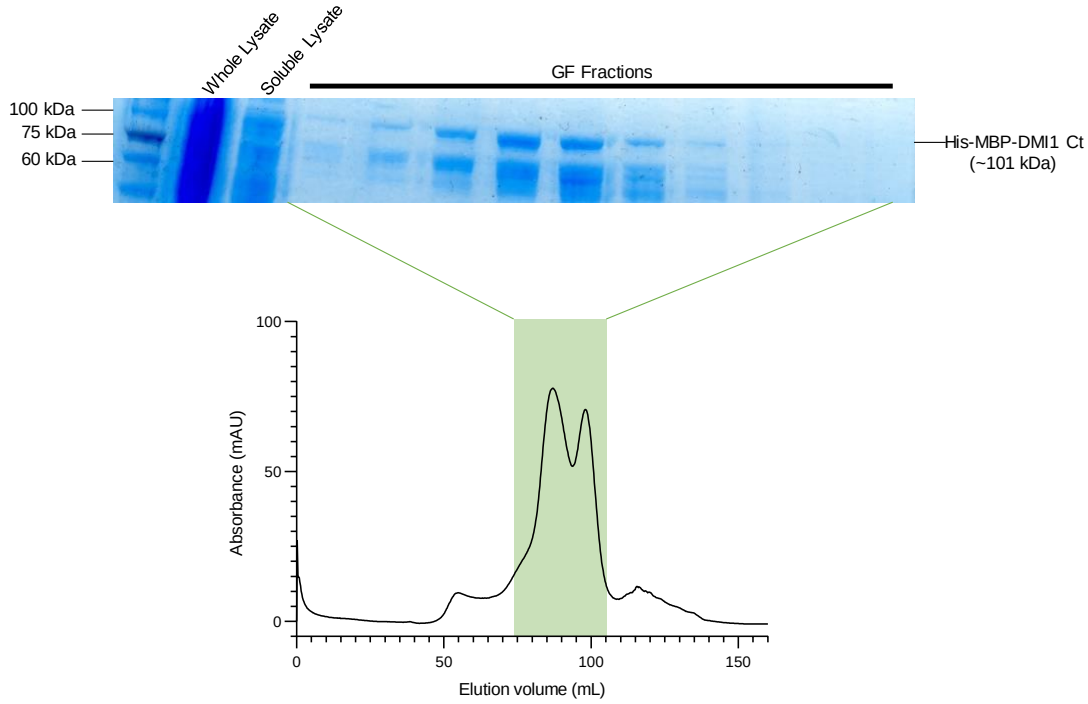

Figure 3.3. His-MBP-DMI1 C-terminus can be purified from *E. coli*

Elution trace of His-MBP-DMI1 C-terminus (~101 kDa size) after expression in *E. coli* and purification using IMAC followed by gel filtration (GF) with Superdex S200 16/60 gel filtration column. The chromatograph shows UV absorbance values at 280 nm (mAU) for protein as it was eluted from the column (elution volume, mL). The green box indicates fractions that were collected for SDS-PAGE purification assessment, shown above. Crude and soluble lysate are also indicated on the SDS-PAGE gel.

To purify AUK kinase domain, its solubility and stability was first examined with different epitope tags. Thus, AUK kinase domain was subcloned into three different expression

vectors to determine which tag was best: pOPINM (His-MBP tag), pOPINJ (His-GST tag), and pOPINS3C (His-SUMO tag). Small-scale expression tests were performed (Figure 3.4a) and indicated that the MBP tag was the best for protein solubility, and to a lesser extent SUMO tag. Next, protein expression was scaled up in *E. coli* using a similar protocol to DMI1 C-terminus purification, and AUK kinase domain expression, purification, and cleavage of the MBP tag was successful (Figure 3.4). AUK kinase domain protein could be purified to a high concentration that was stable in A4 gel filtration buffer (20 mM HEPES pH 7.5, 150 mM NaCl, 1 mM TCEP) without a tag.

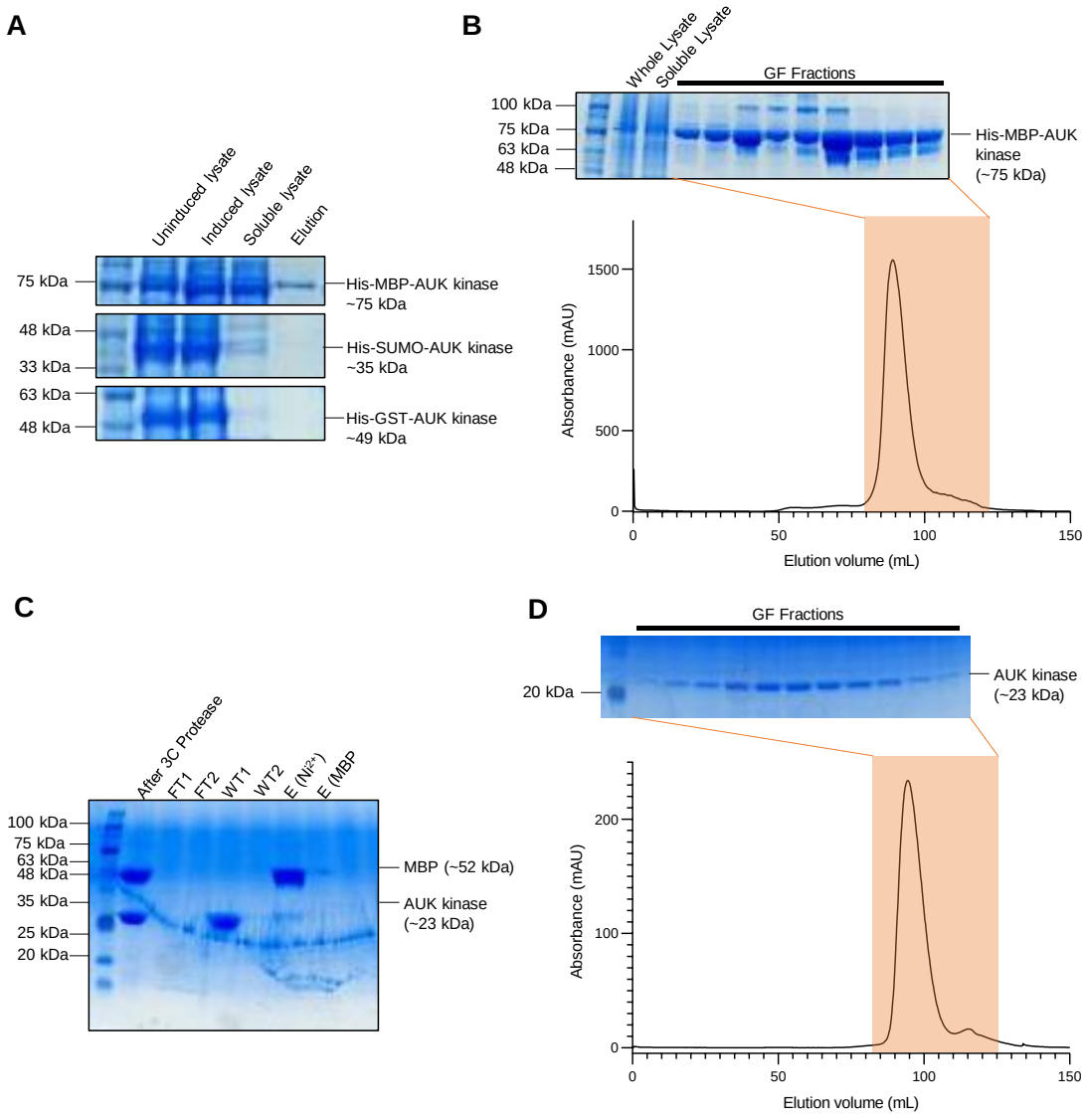

Figure 3.4. AUK kinase domain can be expressed and purified from *E. coli*

A. Expression and purification testing of AUK kinase domain with *pOPINM:His-MBP-AUK* kinase domain (~75 kDa), *pOPINS3C:His-SUMO-AUK* kinase domain (~35 kDa), and *pOPINJ:His-GST-AUK* kinase domain (~49 kDa) in Rosetta BL21 pLysS *E. coli*. Soluble protein was eluted from a 1 mL His-Trap column to analyze efficiency of binding and elution. SDS-PAGE gel shows uninduced, induced, and soluble lysates as well as elution from the

tested columns. The His-MBP-AUK kinase domain was chosen for further purification. **B.** Elution trace of His-MBP-AUK kinase domain (~75 kDa size) after expression in *E. coli* and purification using IMAC followed by gel filtration with Superdex S200 16/60 gel filtration column. The chromatograph shows absorbance values (AU) for protein as it was eluted from the column (elution volume, mL). The orange box indicates fractions that were collected for SDS-PAGE purification assessment, shown above. Crude and soluble lysate are also indicated on the SDS-PAGE gel. **C.** SDS-PAGE analysis of 3C protease cleavage of the His-MBP epitope tags (~52 kDa) from AUK kinase domain (~23 kDa). FT, flow-through fractions; WT, wash-through fractions; E, elution from His-Trap or MBP-Trap columns (GE Healthcare). **D.** Elution trace of untagged AUK kinase domain (~23 kDa size) from purification using gel filtration with Superdex S75 16/60 gel filtration column. The chromatograph shows absorbance values (AU) for protein as it was eluted from the column (elution volume, mL). The orange box indicates fractions that were collected for SDS-PAGE purification assessment, shown above.

The purified DMI1 C-terminus and AUK kinase domain were used to perform a BLItz experiment using Ni^{2+}-NTA biosensors. The tag was not cleaved from DMI1 C-terminus to allow for its attachment to the biosensor as bait protein. AUK kinase domain was purified and was used as the prey. 50 µM DMI1 C-terminus was attached to the biosensor via His tag and either the gel filtration buffer described above minus AUK kinase domain (baseline) or three different concentrations of AUK kinase domain (25 µM, 50 µM or 100 µM) were used to determine binding affinity. From three BLItz experiments with two separate protein purifications, the K_D value was determined from three reps to be 35.44 µM ± 0.85 (Figure 3.5). This result is indicative of moderate strength of association between AUK kinase domain and DMI1 C-terminus and the observation of interaction corroborated the results seen in Y2H experiments (Section 3.2.1). It is important to note, however, that an important negative control using free MBP is missing. Additionally, the impurity and possible tag cleavage of DMI1 C-terminus could affect the BLItz binding results, and thus the later experiment in Chapter 5 where AUK was attached to the Ni^{2+}-NTA biosensor and untagged DMI1 C-terminus was used may be more indicative of binding affinity.

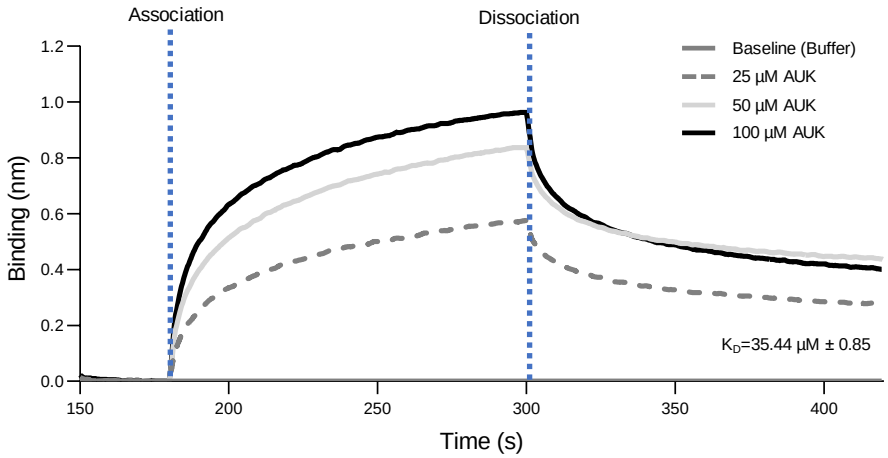

Figure 3.5. DMI1 C-terminus associates with AUK kinase domain in *in vitro* BLItz assay
DMI1 association K_D values were determined for AUK kinase domain by BLItz assay. Baseline was established with A4 buffer and 50 µM His-MBP-DMI1 C-terminus attached to Ni^{2+}-NTA tips. Purified untagged AUK kinase domain was assessed for binding to DMI1 C-terminus at 25 µM, 50 µM and 100 µM for ratios of 1:2, 1:1, 2:1 AUK kinase domain to DMI1 C-terminus. Time of association (when AUK was applied to the tip with DMI1) and dissociation (when AUK was removed and replaced with A4 buffer) are denoted by dashed blue lines. Data shown are averages for 3 replicates from 2 separate protein purifications.

3.2.4- Analysis of *AUK* expression

Genes involved in early symbiosis signal transduction are expressed in root epidermis, and notably root hairs. To assess whether *AUK* is expressed in root epidermis, the Noble *Medicago truncatula* Gene Atlas (He *et al.,* 2009), which includes several RNA-seq and microarray datasets for *Medicago truncatula* gene expression in different tissues and under different conditions, was searched using a probe specific to *AUK*. It was determined that *AUK* is ubiquitously expressed in the *M. truncatula* plant, including in roots and nodules, but also in leaves, stem, and flowers, with the highest expression in seeds (Benedito *et al.*, 2008; Figure 3.6a). In addition, *AUK* is expressed in root hairs, but this expression is not induced by rhizobia (*Sm*1021; Breakspear *et al.*, 2014; Figure 3.6b), nor induced by AM fungal inoculation with *G. intraradices* (Gomez *et al.*, 2009; Figure 3.6c). Future work should include analysis of *AUK* expression under the conditions used in nodulation and AM colonization experiments within the following chapters.

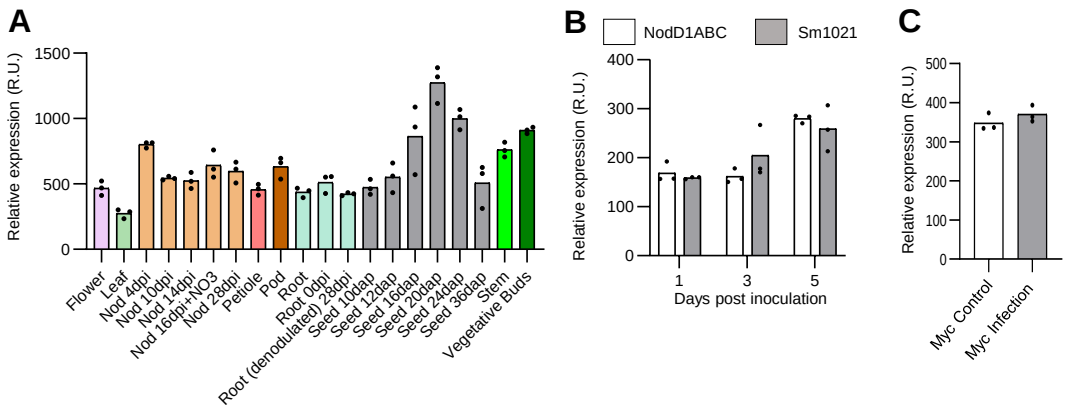

Figure 3.6. *AUK* is expressed in root hairs and not induced by rhizobial or AM infection **A.** Relative expression of *AUK* in different tissues of *M. truncatula* flowers, leaf, nodules (Nod), petiole, root, seed, stem, and vegetative buds. Data is from 3 reps extracted from Benedito *et al.*, (2008) in the Noble Gene Atlas v3 (https://mtgea.noble.org/v3/). **B.** Relative expression of *AUK* in A17 root hairs upon inoculation with NodD1ABC or *Sm*1021 at 1, 3, or 5 days post inoculation (dpi). Data is from 3 reps extracted from Breakspear *et al.* (2014) in the Noble Gene Atlas v3. **C.** Relative expression of *AUK* in A17 roots after 6 weeks mock or inoculation with *G. intraradices*. Data are from 3 reps extracted from Gomez *et al.* (2009) in the Noble Gene Atlas v3.

To test the expression pattern shown in the data from the Noble Gene Atlas, the promoter region of *AUK* was determined. There is a region only 1.1 kb upstream of the *AUK* open reading frame prior to another gene, which was amplified to subclone as the promoter. This was used to generate a *pAUK::NLS-GFP* construct to assess *AUK* gene expression by confocal microscopy. In uninoculated *M. truncatula* hairy roots, *GFP* expression was observed in the nuclei of root hairs (Figure 3.7), corroborating the results from the gene atlas that *AUK* is indeed expressed in root hair cells.

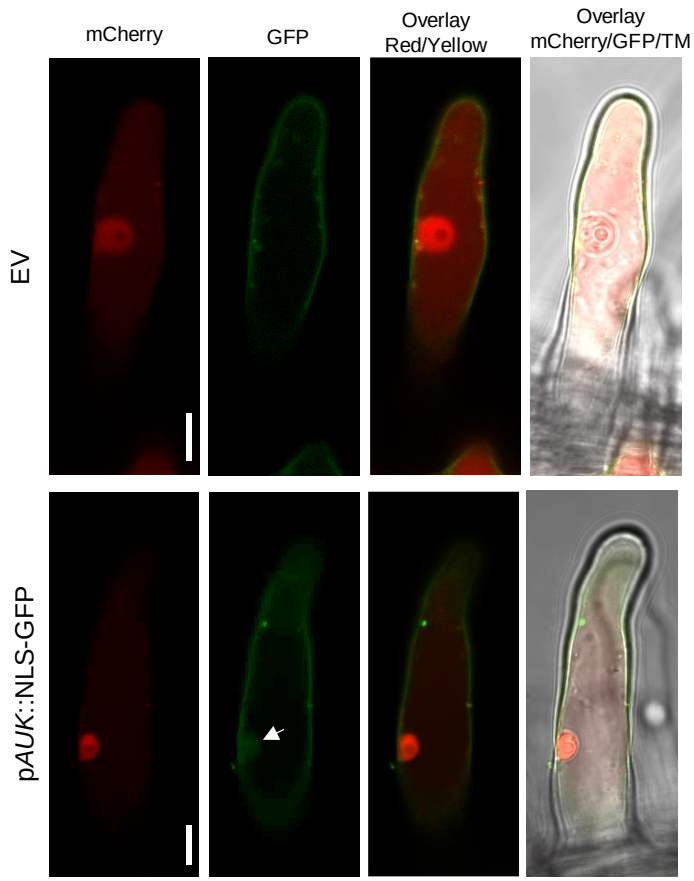

Figure 3.7. *AUK* is expressed in root hairs

Analysis of *pAUK::NLS-GFP* by confocal microscopy in *M. truncatula* hairy roots expressing either empty vector (EV; upper panel) or *pAUK::NLS-GFP* (lower panel) in root hairs. mCherry was used as a transformation marker in all constructs. Scale bar indicates 10 µm. White arrow indicates nuclear *GFP* expression under the *AUK* promoter.

3.2.5- AUK localizes to the nuclear envelope and associates with DMI1 *in planta*

The protein-protein interaction studies described above were performed in heterologous and *in vitro* systems. Although the results both indicated protein association between DMI1 and AUK, they were only certain domains of the proteins, and not under physiologically relevant conditions. Thus, it was important to confirm the results using *in planta* experiments. Firstly, subcellular localization of AUK was investigated to determine whether the proteins localize to cellular compartments where they could conceivably associate. DMI1 possesses four transmembrane domains and has previously been shown to localize to the nuclear envelope in roots of *M. truncatula* (Riely *et al.*, 2007). AUK is also predicted to have one transmembrane domain (Figure 3.1b), and a nuclear localization signal predicted via NLStradamus (Nguyen Ba *et al.*, 2009).

To determine AUK localization, AUK-GFP was first expressed in *M. truncatula* hairy roots under the control of the p*35S* promoter. Very weak GFP signal was observed (data not shown), so it was then cloned under the control of the p*Lj*UBI promoter, and once again there was only very weak expression (data not shown). It was then hypothesized that the very low expression level may be due to some factor in an intron or within the genomic sequence that may be required to help stabilize protein expression, and a genomic AUK construct was generated and transformed into *M. truncatula* hairy roots under the control of the p*Lj*UBI promoter. This construct resulted in a slightly stronger GFP signal, but it was still quite weak. This did, however, show localization of AUK to the nuclear envelope and ER within root hairs of *M. truncatula* (Figure 3.8).

Similar weak expression has been seen with both DMI1 and *L. japonicus* homologs CASTOR and POLLUX and MtCNGC15, but success had been found using immunogold localization (Capoen et al., 2011; Charpentier et al., 2008, 2016). I tried to use immunogold localization for with AUK-GFP expressed under its own promoter (pAUK) and the p*Lj*UBI promoter, however no immunogold labelling was detected (data not shown). This result indicated that AUK and DMI1 both localize to the nuclear envelope or ER, and could thus conceivably associate there.

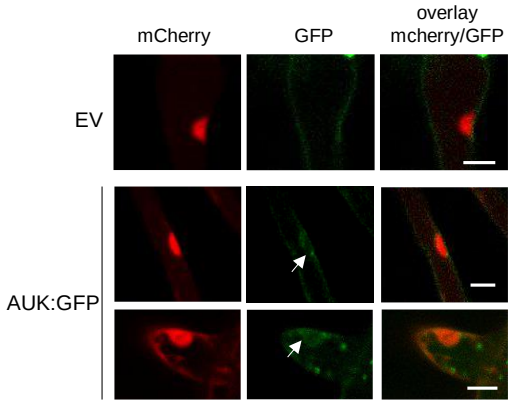

Figure 3.8. AUK localizes to the nuclear envelope in *M. truncatula* root hairs
A. mCherry empty vector (EV) (left panel) and p*Lj*UBI:*gAUK-GFP* (centre, right) expression in *M. truncatula* R108 hairy roots (top: dsRed channel; middle: GFP channel; bottom: composite image). White arrows indicate where GFP can be detected in nuclear envelope. Scale bars represent 10 µm.

The localization of DMI1 and AUK was further analyzed using bi-fluorescence complementation (BiFC) experiments, which can indicate whether proteins are in close proximity to each other. It also corroborates the localization of the proteins as YFP signal is only reconstituted in the compartment when association occurs. Typically, protein-protein interaction for symbiosis-related proteins has been done in *N. benthamiana* due to ease of

transient protein expression in leaves, short experimental time and high expression levels of protein produced. Therefore constructs containing *pNos:DMI1-myc-YNE* and p*LjUBI:gAUK-HA-YCE* (Table 2.8) were transiently expressed in combination with the P19 viral suppressor (Lakatos *et al.,* 2004) in leaves of *N. benthamiana* and reconstitution of YFP signal was observed at 3 dpi in the nuclear envelope (Figure 3.9). Free GFP and the truncated version of DMI1 determined from 3.2.2 not to associate with AUK were used as negative controls. There also was some YFP reconstitution in ER, which is continuous with the nuclear envelope. These results show that AUK and DMI1 are in close proximity when transiently expressed in leaves of *N. benthamiana.*

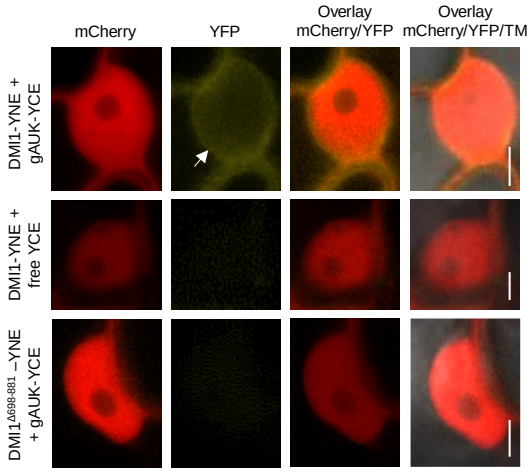

Figure 3.9. DMI1 associates with AUK in BiFC in the nuclear envelope of *N. benthamiana*
N. benthamiana leaves expressing N-terminal YFP (YNE) fused to the C-terminus of DMI1 and truncated DMI1$_{\Delta 698\text{-}881}$ and C-terminal YFP (YCE) fused to the C-terminus of gAUK or free. Images show reconstitution of YFP signal at the nuclear envelope. mCherry was present in all vectors. Scale bars represent 5 µm. White arrow indicates reconstituted YFP signal at the nuclear envelope.

To test the BiFC result in *M. truncatula* roots, hairy root transformations were performed with the same constructs expressing both *DMI1* and *gAUK* (Table 2.8), and reconstitution of YFP was analyzed by confocal microscopy in uninoculated conditions. Free GFP and the truncated version of DMI1 determined from 3.2.2 not to associate with AUK were used as negative controls as in *N. benthamiana*. A version of AUK lacking a segment corresponding to an extension putatively forming a binding pocket within the kinase activation loop (Δpocket; discussed in Chapter 5) was also used to determine whether this possible interaction segment was required for DMI1-AUK interaction. YFP reconstitution was seen at the nuclear envelope in root hairs of *M. truncatula* hairy roots expressing *DMI1* and *gAUK*,

and *DMI1* with *gAUK*$_{\Delta pocket}$ (Figure 3.10). No YFP signal reconstitution was observed in the free GFP construct or that with the truncated version of DMI1.

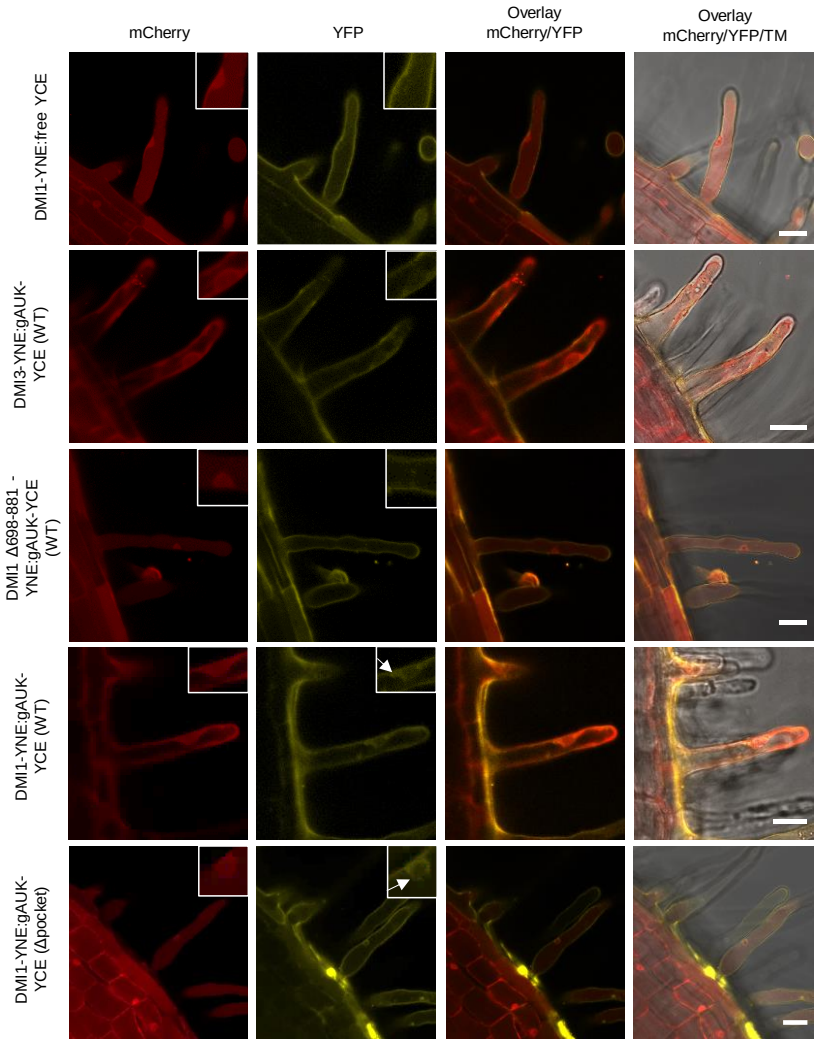

Figure 3.10. DMI1 associates with AUK in BiFC in the nuclear envelope of *M. truncatula* roots

M. truncatula hairy roots expressing N-terminal YFP (YNE) fused to the C-terminus of DMI1 and truncated DMI1$_{\Delta 698\text{-}881}$ or DMI3 and C-terminal YFP (YCE) fused to the C-terminus of gAUK WT and Δpocket or free YCE. mCherry was present in all vectors. Inset shows zoom in on nucleus. White arrows indicate reconstituted YFP at the nuclear envelope. Scale bars represent 20 µm.

Expression of the proteins in *M. truncatula* roots was tested by immunoblotting (Figure 3.11), with all bands the expected size. Protein expression of the truncated DMI1 was not observed, however this could be the result of variable expression within different roots. For each construct, at least 15 roots were screened, and even within the positives not every root has YFP reconstitution as this is dependent on the expression level of each protein within

the individual root system. For each immunoblot, only 3-4 roots were used, thus it is possible that the roots used for the immunoblot with this construct were not expressing the truncated DMI1 well. This immunoblot will need to be repeated. Overall, these results show that AUK associates with DMI1 *in planta* at the nuclear envelope and strengthen the results seen with heterologous yeast and *in vitro* BLItz protein-protein interaction experiments.

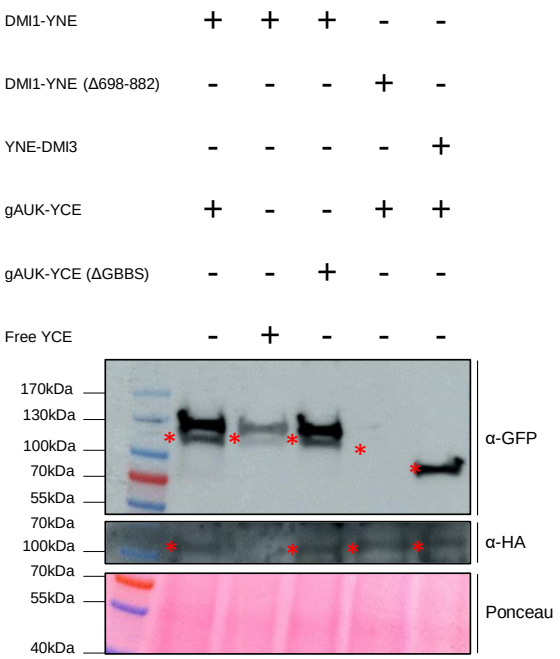

Figure 3.11. Assessing expression of constructs used in *M. truncatula* BiFC experiment
α-GFP and α-HA immunoblots of constructs expressed for BiFC in *M. truncatula* hairy roots (Figure 3.10). Red asterisks indicate expected protein size. Ponceau stain included as loading control.

For further analysis of DMI1 association with AUK *in planta* co-immunoprecipitation (co-IP) in *M. truncatula* hairy roots was performed to test for DMI1 and AUK direct interaction *in planta.* co-IPs of endosymbiosis proteins are typically done using *N. benthamiana* leaves because of the low general expression and high volume of root material needed. To ensure association in the relevant root system, a protocol for use of *M. truncatula* roots for co-IP was designed. It made use of the BiFC constructs, which in addition to nYFP and cYFP, also possess myc and HA epitope tags, respectively. The plants were grown on plates and then transferred to TerraGreen and sand where they were inoculated with *Sm*2011. The roots were dug up 14 dpi and used for the co-IP experiment. The first attempts used ChromoTek myc-trap agarose beads to immunoprecipitated DMI1, however AUK was not visible in the IP samples. There are several possible reasons for this: 1) *AUK* is not expressed well enough and the association with DMI1 may be transient, so it was not detectable, or 2) Our HA antibody is not very sensitive (which is something we had previously observed in

other assays within the lab). For future attempts we used an increased amount of material (3-4 g root powder), and immunoprecipitated AUK using α-HA beads (μMacs) as it had weaker expression than DMI1. Indeed, this did show immunoprecipitation of DMI1 with gAUK in the inoculated roots (Figure 3.12). Interestingly, on the immunoblots, DMI1 showed an upper band, which as discussed in section 3.2.1 may represent oligomerization as DMI is a tetrameric ion channel. AUK also shows a slightly higher band above the expected size, which may correspond to phosphorylated AUK, although this would require further examination and incubation with a phosphatase or kinase inhibitors to determine whether this would prevent the upper band. Overall, the results of subcellular localization, BiFC and co-IPs show that AUK and DMI1 associate in the nuclear envelope under control conditions and when inoculated with *Sm*2011.

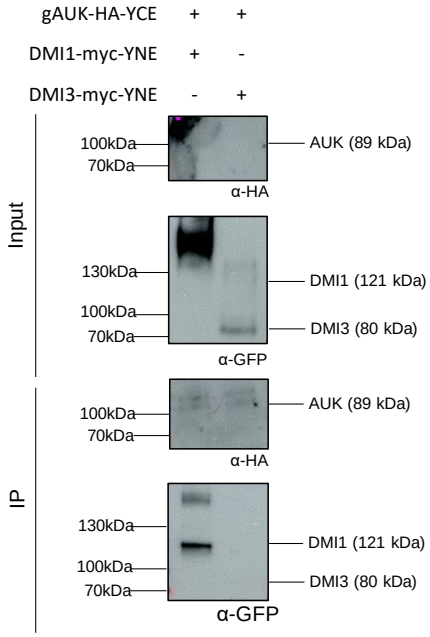

Figure 3.12. DMI1 associates with AUK via co-IP in *M. truncatula* hairy roots

Co-immunoprecipitation from *M. truncatula* hairy roots inoculated with *Sm*2011 for 14 days. Immunoprecipitation was done with α-HA beads (μMacs) and immunoblotting with α-HA to observe AUK and α-GFP N-term to observe DMI1 or DMI3. Input and IP samples are shown.

3.3- Discussion

Nuclear Ca^{2+} oscillation is necessary for the generation of a successful endosymbiosis between host plant and its symbiont: nitrogen-fixing bacteria or AM fungi. Much work has been done to identify key players involved in early signaling mechanisms establishing these associations. Essential components include LysM receptors localized to the plasma membrane with a role in perceiving symbiotic 'Nod' and 'Myc' factors, and several components at the nuclear envelope including ion channels and subunits of the nucleoporin complex. While much focus

has been on initial signal perception and on components directly involved in generating nuclear Ca^{2+} oscillations, little is known about components that link these two compartments. There may be mobile elements, intracellular receptors or proteins inducing post-translational modifications, which may function to activate or regulate the nuclear envelope-localized channels.

In this work, focus was on one putative interacting partner of DMI1, an LRR-RLK, so called AUxilliary unit Kinase of DMI1 (AUK). Multiple protein-protein interaction experiments were used to confirm the association of DMI1 with AUK (results of which are summarized in Table 3.1.

Table 3.1. Summary table of methods and obtained results presented in this chapter.

Method	Summary of Results
Y2H	-DMI1 C-terminus associates with AUK kinase, but not AUK kinase+ -$DMI1_{\Delta 698\text{-}881}$ does not associate with AUK kinase domain
BLItz	-DMI1 C-terminus associates with AUK kinase domain K_D=~35 µM
BiFC	-DMI1 associates with AUK at the nuclear envelope in *N. benthamiana* -DMI1 associates with AUK at the nuclear envelope in *M. truncatula* roots
Co-IP	-DMI1 associates with AUK in *M. truncatula* hairy roots upon inoculation with *Sm*2011

The reasoning behind the use of many methods is that each experiment has its caveats. For instance, the initial screen was done with a Y2H cDNA library from *M. truncatula* roots. While Y2H can be a good method for rapid screening of putative interactors, it is a heterologous system and therefore the conditions in yeast may not reflect those *in planta*. Thus, both false negatives and false positives are inherent. Proteins may not fold correctly outside of their physiological environment, or they may need other proteins or post-translational modifications to induce structural changes allowing for interaction to occur (Rao *et al.*, 2014; Semple *et al.*, 2002). Thus, it is imperative to confirm Y2H results with other methods. One of those used here was *in vitro* BLItz assay, which allowed for determination of K_D value indicative of a moderate interaction strength. While BLItz is also performed outside of physiological environment, and similarly to Y2H was only performed with certain interacting domains of the proteins, the BLItz method did provide more information about the interaction strength and stoichiometry. The association constant was found to be 35 µM, which is considered a moderate strength protein-protein interaction. This is interesting as the binding affinity of protein kinases with their substrate is typically low and involves long-range residue interactions, rather than close range localized to the phosphorylation site (Waas & Dalby, 2002). In addition, the shape of the binding curve, not quite reaching a plateau is indicative of

oligomerization of AUK and DMI1. This is supported by the evidence for DMI1 as a tetramer (Kim *et al.,* 2019; Peiter *et al.,* 2007), and the self-association of AUK kinase domain shown in this chapter (Figure 3.1c).

In addition to heterologous and *in vitro* methods, several *in planta* methods were used, including subcellular localization to determine whether where proteins localize would facilitate interaction, BiFC, which was performed in both *N. benthamiana* and *M. truncatula*, allowing for determination of whether proteins are in close proximity to each other, and co-IP in *M. truncatula* roots. Taken together, the results from the use of each of these protein-protein interaction studies provides strong evidence for the association between AUK and DMI1.

The analysis of interactions of truncations of DMI1 with AUK provided further detail on the complexity of DMI1 channel regulation. Deletion of smaller portions of the DMI1 soluble C-terminus led to subsequently less interaction in yeast, however the largest deletion of the entire second RCK domain led to a stronger association with AUK kinase domain than the full-length. This may provide evidence for the importance of the soluble C-terminus in regulation of interacting partner association, and thus the channel functioning. PSIVER was used to predict potential binding interfaces on DMI1 protein to guide deletion strategy. This indicated several putative sites within the C-terminus of DMI1. With the advent of Alphafold Multimer, it was investigated whether might give more of an indication of binding sites could be predicted, however there was no predicted interaction interface between the two proteins determined (data not shown). This suggests that there may be some structural change or post-translational modification required for their association that cannot currently be predicted computationally.

For the *in planta* experiments, the constitutive promoters, p35S and p*Lj*UBI, were used. It is important to note that these constitutive promoters may give false results as the protein may not otherwise be expressed to those levels. In addition, in these *in planta* methods, the transient expression system in *N. benthamiana* was used as well as the physiologically relevant stable protein expression in *M. truncatula* hairy roots. In *N. benthamiana* AUK and DMI1 YFP signal was reconstituted at the nuclear envelope as it was in *M. truncatula* hairy roots, demonstrating that the system could be used for further experiments. However, it was important to use *M. truncatula* roots as it is the endogenous environment and more likely that AUK and DMI1 were expressed to their physiological levels and with possible other interactors facilitating their association. See Figure 3.13 for a summary of the overall results from this chapter.

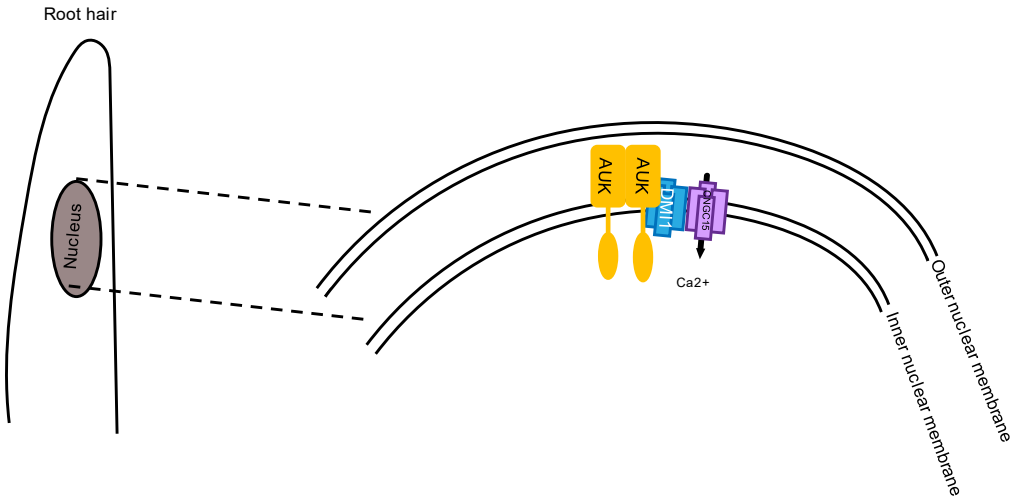

Figure 3.13. Summary of AUK association with DMI1

AUK is expressed in *M. truncatula* root hairs. AUK localizes to the nuclear envelope, where it forms oligomers and associates with DMI1 via its kinase domain.

It is interesting to speculate on what the outcome of AUK association with DMI1 might be. As AUK is a kinase, one could speculate that the interaction might lead to phosphorylation of the channel, which could function in its activation or regulation by inducing a conformational change. This conformational change could facilitate activation of CNGC15 to regulate nuclear Ca^{2+} oscillation. Several plant RLKs have been demonstrated to function as homodimers. For instance, the LRR-RLKs BRI1 and FLS2 has been shown to homodimerize *in planta* (Sun *et al.*, 2012; Wang *et al.*, 2005), and researchers observed BRI1 elution from gel filtration column of the kinase domains in a homodimer (Bojar *et al.*, 2014). They have also been demonstrated to self-associate and autophosphorylate *in planta* and autophosphorylation sites have been mapped (Wang *et al.*, 2005).The authors observed that ligand-induced auto-phosphorylation of these residues within the kinase activation loop activated a functional kinase for downstream signaling. Presumed homodimer elution of AUK kinase domain was observed, as evidenced by a fainter band on SDS-PAGE gel of the purification (Figure 3.4b), and AUK kinase domain self-associated in Y2H experiments (Figure 3.1c). Thus, it is tempting to speculate that the LRRs in the extracellular domain of AUK might sense an as yet unknown ligand, induce autophosphorylation in the kinase activation loop, thereby inducing a functional kinase to phosphorylate its targets for nuclear Ca^{2+} oscillation.

Receptor complexes have been found on membranes involved in many plant processes, including immune signaling, hormone signaling in developmental processes of stomatal development and patterning, floral abscission, shoot apical meristem maintenance,

xylem differentiation, lateral root emergence and many others (reviewed in He *et al.*, 2018). Many of these processes involve RLKs and RLPs. Several RLKs function to phosphorylate ion channels to facilitate their activation. Although fewer ion channels have been found to be phosphorylated by RLKs in plants, some examples include the following: CNGC2/4 are activated by phosphorylation through action of the immune signaling kinase BIK1 (Tian *et al.*, 2019) and the voltage-gated potassium channel AKT1 is phosphorylated by CIPK23 in its C-terminal linker (Xu *et al.*, 2006), which induces a conformational change for channel activation (Lu *et al.*, 2022). Thus, one could hypothesize that AUK might phosphorylate the cation channel DMI1 in its soluble C-terminus to induce a conformational change leading to activation or regulation of CNGC15 and modulation of the symbiosis-induced nuclear Ca^{2+} oscillation.

In summary, this work provides strong evidence for DMI1 association with AUK through several different protein-protein interaction methods. In addition, it was demonstrated that AUK localizes to the nuclear envelope and associates with DMI1 *in planta*, suggesting interaction in a complex of AUK kinases to activate the nuclear Ca^{2+} oscillation via interaction with DMI1.

4- Characterizing the role of AUK in endosymbiosis

4.1- Introduction

Downstream of symbiotic Nod and Myc factor perception by LysM-RLKs, signal transduction pathways converge on a common Sym pathway, with components involved in generating association with both nitrogen-fixing rhizobia bacteria and AM fungi. Briefly, this common sym pathway consists firstly of an LRR-RLK (so-called DMI2 in *M. truncatula* and SYMRK in *L japonicus*) that is believed to act as a co-receptor of the Nod and Myc factor receptors. Downstream, both pathways converge on components involved in nuclear Ca^{2+} oscillation, including three ion channels, MCA8, DMI1 and CNGC15s, and components of the nucleopore complex NUP85, NUP133 and NENA. The Ca^{2+} oscillations are decoded by MtDMI3/LjCCaMK, which phosphorylates the transcriptional activator MtIPD3/LjCYCLOPS to induce gene expression of further symbiosis genes, which may confer specificity for either rhizobial or AM fungal colonization.

Interestingly, gain-of-function alleles or overexpression of several genes involved at various stages within rhizobia perception and the common sym pathways can induce nodule organogenesis in absence of rhizobia. Overexpression of the Nod factor receptors, *LjNFR1* and *LjNFR5* can induce spontaneous nodules possessing peripheral vascular bundles, rather than central root vasculature seen in lateral root primorida, as can overexpression of *LjSYMRK* (Ried *et al.*, 2014). All of these can induce expression of early symbiosis genes, *NIN* and *SbtS*, but both the spontaneous nodule phenotype and expression are most prominent when *SYMRK* is overexpressed, and only *SYMRK* overexpression could induce expression of the AM-related *SbtM1* (Ried *et al.*, 2014). Saha *et al.*, 2014 also observed spontaneous nodulation with the overexpression of *M. truncatula SYMRK, MtDMI2* kinase domain, and with the overexpression of *Arachis hypogaea SYMRK* kinase domain. Furthermore, a gain-of-function allele of the nuclear envelope-localized MtDMI1 possessing a point mutation within the RCK2 domain could produce spontaneous nodules in a heterozygote context (Liu *et al.*, 2022). In addition, this constitutively active *DMI1* mutant was also able to produce spontaneous Ca^{2+} oscillations, indicating an involvement of activation of the nuclear Ca^{2+} oscillation in generation of nodule structures. The authors also observed constitutive expression of the nodulation-related *NIN* and *ENOD11*, and the AM-related *HA1, BCP1* and *PT4*. Specific mutations in the Ca^{2+} decoder and its direct interactor *Mt*DMI3/*Lj*CCAMK and *Mt*IPD3/*Lj*CYCLOPS, respectively, can also lead to generation of nodules in absence of rhizobia (Gleason *et al.*, 2006; Singh *et al.*, 2014; Tirichine *et al.*, 2006). For CCaMK, this gain-of-function can be induced either by deletion of the autoinhibitory domain (Gleason *et al.*, 2006) or by substitution of the threonine at the kinase autophosphorylation site for aspartate (Hayashi *et al.*, 2010; Tirichine *et al.*, 2006). Nuclear localization of the autoactive

CCaMK could further enhance the spontaneous nodulation phenotype and downstream gene expression (Takeda *et al.,* 2012). *Lj*CYCLOPS is phosphorylated by CCaMK (Yano *et al.,* 2008), and a phosphomimetic version of CYCLOPS can also induce formation of nodule-like structures in absence of rhizobia. The overexpression of the nodulation-related transcription factor, *NIN,* could also produce spontaneous nodules in both *L. japonicus* and *M. truncatula* (Soyano *et al.,* 2013; Vernié *et al.,* 2015). Interestingly, the spontaneous organogenesis could be induced by the expression of *NIN* under either an epidermal or cortical promoter (Vernié *et al.,* 2015). Exogenous application of cytokinin, auxin and gibberellin can lead to production of pseudonodules in absence of rhizobia (Akamatsu *et al.,* 2021; Jin *et al.,* 2016; Tirichine *et al.,* 2007), and a gain-of-function mutation in the cytokinin receptor LjLHK1/MtCRE1 can also produce nodule-like structures (Tirichine *et al.,* 2007), indicating crosstalk between many different pathways is responsible for development of a nodule structure.

The infection process for association with both rhizobial and AM fungal endosymbionts consists of several developmental stages, involving coordination of epidermal and cortical cells, which are under tight genetic control to ensure optimal nutrient acquisition and plant fitness. In the case of nodulation, perception of the Nod factor occurs in the epidermis, particularly by a root hair cell. Rhizobia are able to attach the root hairs and accumulate with higher concentration, increasing the opportunity for infection to occur (Fujishige *et al.,* 2006; Goedhart *et al.,* 2000). Expression of *ENODs* is induced, restricted to the zone of actively growing root hairs, referred to as the infection zone (Journet *et al.,* 1994, 2001; Scheres *et al.,* 1990). Ca^{2+} oscillation within all zones is one of the earliest responses upon perception of rhizobia (Ehrhardt *et al.,* 1996; Miwa *et al.,* 2006; Wais *et al.,* 2000; Walker *et al.,* 2000b). Initial stages of infection involve the arrest of root hair growth, followed by a re-initiation of a new growth axis (de Ruijter *et al.,* 1998; van Batenburg *et al.,* 1986). The root hair grows in the direction of the Nod factor, and continues to curl 180-360 ° (Esseling *et al.,* 2003), entrapping the bacteria in a so-called infection pocket. This root hair curling requires the Nod factor receptor NFP (Ben Amor *et al.,* 2003), but is independent of Ca^{2+} spiking (Miwa *et al.,* 2006). Cytoskeletal changes are involved in this reorientation of root hair growth, and these changes are induced within 3-6 minutes after NF application, which is earlier than the Ca^{2+} oscillation begins (Cárdenas *et al.,* 1998; Esseling *et al.,* 2003). There is bacterial proliferation within the root hair curl, and eventually an intracellular tunnel is formed from a kind of inversion of root hair growth (Brewin, 2004). PIT form across outer cortical cells (van Brussel *et al.,* 1992), preceding the development of IT, which grows and invades into cortical cells. Subsequently, the cortical cells are responsible for nodule formation via activation of mitotic cell divisions through cell cycle regulators (Cebolla *et al.,* 1999), requiring several early nodulin genes, such as *ENOD40*, which is only induced in nodule primordia, not in epidermis (Charon *et al.,* 1997, 1999; Crespi *et al.,* 1994). *M. truncatula* produce indeterminate

nodules, consisting of a persistent distal meristem, which differentiates and divides in response to symbiotic factors (Franssen *et al.,* 2015; Xiao *et al.,* 2014). Root pericycle, endodermis and cortical cell layers are all involved in the generation of indeterminate nodules. The development can be divided into 5 stages, defined in a fate map by Xiao *et al.,* 2014: 1) Priming of nodule primordia resulting from anticlinal cell divisions within the pericycle occurring opposite to the protoxylem pole of the root (Timmers *et al.,* 1999), 2) initiation of nodule primordium resulting from anticlinal and periclinal divisions within the inner cortex to form nodule apical meristem, 3) Nodule outgrowth, involving removal of the epidermis and halting of mitosis within the inner cortex, division of the middle cortex and formation of a primordium with activated nodule apical meristem and IT penetration, 4) Nodule maturation where the nodule vascular bundle is formed, and bacteroids within an infection zone can fix nitrogen, and finally 5) Nodule senescence where nitrogen fixation diminishes and programmed cell death of bacteroids and plant cells occurs.

AM colonization of the host plant root is also a highly regulated process. Following chemical communication between the host plant and AM fungi, first contact is established by the formation of a swelling on several epidermal cells of the plant root, followed by branching to develop a so-called hyphopodium (Genre *et al.,* 2005). AM hyphal branching typically concentrates in the vicinity of young lateral roots as the primary site for AM colonization (Kosuta *et al.,* 2003). Expression of *ENOD11* occurs in the area of the hyphopodium (Chabaud *et al.,* 2002), and reorganization of epidermal cell cytoplasm occurs to produce the PPA, which is required for fungal penetration deeper into the root cortex (Genre *et al.,* 2005). Cytoplasm is aggregated at the contact site and a thick column develops, predicting the path for the hypha across the cell (Genre *et al.,* 2005), and interestingly the nucleus moves toward the site of the PPA development. The hyphal tip then grows through the epidermal cell wall along the PPA, with perifungal membrane assembly and PPA secretory vesicles fusing to produce plasma membrane invagination. When the hyphae reach the root inner cortex, there is repeated branching to form the arbuscule, which can swell to fill most of the host cell, and acts as the site of nutrient exchange (Genre *et al.,* 2008; Gutjahr & Parniske, 2013). The accommodation of arbuscules within the root cortex involves reactivation of the cell cycle inducing ectopic cell division for generation of split-cells in advance of development of arbuscules (Russo *et al.,* 2019), and recursive endoreduplication (Carotenuto *et al.,* 2019). Arbuscules have an estimated lifespan of 4-5 days prior to fungal wall collapse and retraction of cytoplasm. This is followed by vesicle formation. Vesicles and new fungal spores represent completion of the fungal life cycle, allowing for subsequent recolonization. Apart from the role of strigolactone in the initial AM-host communication (Akiyama *et al.,* 2005; Akiyama & Hayashi, 2006; Besserer *et al.,* 2006, 2008), several other phytohormones are involved in AM colonization. For instance, abscisic acid (ABA) can serve to promote AM symbiosis at a low concentration,

but inhibit it at high levels, possibly functioning to regulate the symbiotic progression (Charpentier *et al.,* 2014). In addition, gibberellic acid (GA) decreases AM colonization of host root (Floss *et al.,* 2013; Foo *et al.,* 2013), however GA is upregulated during AM development in *L. japonicus* roots (Takeda *et al.,* 2015), suggesting a complex feedback. A role for auxin signaling has also been suggested in AM colonization through the use of miR393, which downregulates auxin and results in defects in arbuscule formation (Etemadi *et al.,* 2014). Overall, there is much complexity in phytohormone signaling during both AM and rhizobial symbioses.

There are several parallels between the development of nodules and of lateral roots, and it is largely thought that nodule development partially evolved from recruitment of elements of lateral root development pathways (Hirsch *et al.,* 1997; Schiessl *et al.,* 2019; Shrestha *et al.,* 2021; Soyano *et al.,* 2019, 2021). Apart from being influenced by plant nutrient status, both processes involve divisions of inner root tissues and are tightly controlled by plant hormone signaling. Lateral root primordia form from activation of cell division in the pericycle, cortex and endodermis, with lateral root primordia receiving a contribution of cells from the endodermis and cortex (Herrbach *et al.,* 2014; Xiao *et al.,* 2019). In *M. truncatula,* cell divisions initiate in cells of the pericycle prior to reactivation of endodermal and inner cortical cells (Xiao *et al.,* 2014). Both lateral root and nodule formation involve several phytohormones. For example, auxin accumulation is found in pericycle cells at the site at which lateral roots emerge (Dubrovsky *et al.,* 2008), and auxin perception may trigger divisions in other cell layers, such as the endodermis and inner cortex as they contribute to lateral root formation (Herrbach *et al.,* 2014). High local auxin accumulation in dividing cortical cells has also been observed at the sites of nodule development (Suzaki *et al.,* 2012). In addition, pseudo-nodules can be formed by application of auxin transport inhibitors (Rightmyer & Long, 2011). Other phytohormones can have complex functions in conjunction with auxin. For instance, cytokinin acts as an antagonist of auxin in lateral root development. Despite having a positive effect on regulating shoot branching, cytokinin negatively regulates lateral root formation through negative regulation of auxin transport (Laplaze *et al.,* 2007). Interestingly, cytokinin seems to play a positive role in nodule development (Gonzalez-Rizzo *et al.,* 2006; Murray *et al.,* 2007), with the a gain-of-function mutant cytokinin receptor *Lj*LHK1 or *Mt*CRE1 producing spontaneous nodules in absence of rhizobia (Tirichine *et al.,* 2007). Cytokinin acts as a key positive regulator of nodule primordia cortical cell division. In addition, there is crosstalk between auxin and ethylene in both root and nodule development processes. Ethylene can inhibit lateral root formation (Negi *et al.,* 2008). It also acts locally to restrict nodule number (Larrainzar *et al.,* 2015; Oldroyd *et al.,* 2001; Penmetsa & Cook, 1997; Penmetsa *et al.,* 2008).

In the previous chapter, AUK was presented as an interactor of DMI1 at the nuclear envelope, expressed in root hairs and root endodermis. Given this localization and expression pattern, it was possible that AUK could play a role in endosymbiosis, and possibly within the common symbiosis pathways with early signaling through nuclear Ca^{2+} oscillation involving DMI1. This chapter provides genetic analysis and phenotypic examination of the role of AUK within the endosymbiotic signaling pathways of both nitrogen-fixing bacteria and AM fungi.

4.2- Results

4.2.1- CRISPR knockout of *AUK* abolishes nodulation

To identify whether AUK plays a role in endosymbiotic signaling, it was important to assess its phenotypes with a gene knockout. There were no available tobacco retrotransposon Tnt1 insertion lines within the *AUK* gene, so three sgRNA guides were designed using CRISPR-P 2.0 (Liu *et al.*, 2017) to assess CRISPR-Cas9 knockout of *AUK* in *Medicago* hairy roots with the cut sites located upstream of or disrupting the AUK kinase domain to affect functionality of the protein kinase (Figure 4.1b). The sgRNA design was based on minimizing off-targets sites (only judged as acceptable if there were at least 4 mismatches within the sequence), having a GC content of more than 20%, having out-of-frame score of at least 60, and having RNA structure features with the following: no more than 7 consecutive base pairs (CBP), no more than 12 total base pairs (TBP) and no more than 6 internal base pairs (IBP). The primers chosen and parameters are listed in Table 4.1. The effect of using different combinations of two or three guides within the same Golden Gate construct was assessed, including the *Mt*U6 promoter and the *Sp*Cas9 enzyme (detailed in Table 2.8).

Genotyping analysis of transformed roots revealed that deletion and/or insertion occurred at the protospacer adjacent motif (PAM) sequences of the sgRNA1 and sgRNA3 sites (Figure 4.1b). In contrast, no alterations were identified with sgRNA2. To knock out *AUK*, *Cas9* was expressed in combination with sgRNA1 and sgRNA3 to assess the nodulation phenotype of the transformed root at 25 dpi with *Sm*2011. Both transformed roots with nodules and those without nodules were collected and DNA was extracted and sent for Sanger sequencing (Figure 4.1c). Those roots transformed with sgRNA1 and sgRNA3 that were genotyped as homozygous knockouts by PCR and subsequent sequencing for *AUK* corresponded to the transformed root systems with complete lack of nodules (Figure 4.1a). The knockout alleles for the lines are indicated in Figure 4.1b. This result indicated that AUK plays an important role and is required for root nodulation.

Table 4.1- CRISPR Cas9 primer design parameters (Bold in sequence indicates the PAM sequence, Structure features CBP, consecutive base pairs; TBP, total base pairs; IBP, internal base pairs)

Position	Sequence	Length (+3 PAM)	Off-targets (=4 nt diff)	GC-content sgRNA nt 1-10 (%)	GC-content sgRNA nt 4-8 (%)	Structure features	Out-of-frame score
sgRNA1 (1st exon)	GCTTTGGCTGTGAGAAGATTGG**GGG**	22	12	60	60	7 CBP;12 TBP;0 IBP	66
sgRNA2 (1st exon)	GTTGTTCTCTTTCTTTTACTCG**AGG**	22	12	40	40	4 CBP;7 TBP;0 IBP	76
sgRNA3 (1st exon)	GTCCGCCTTTGAAGAATCCATG**TGG**	22	0	60	80	5 CBP;5 TBP;0 IBP	60

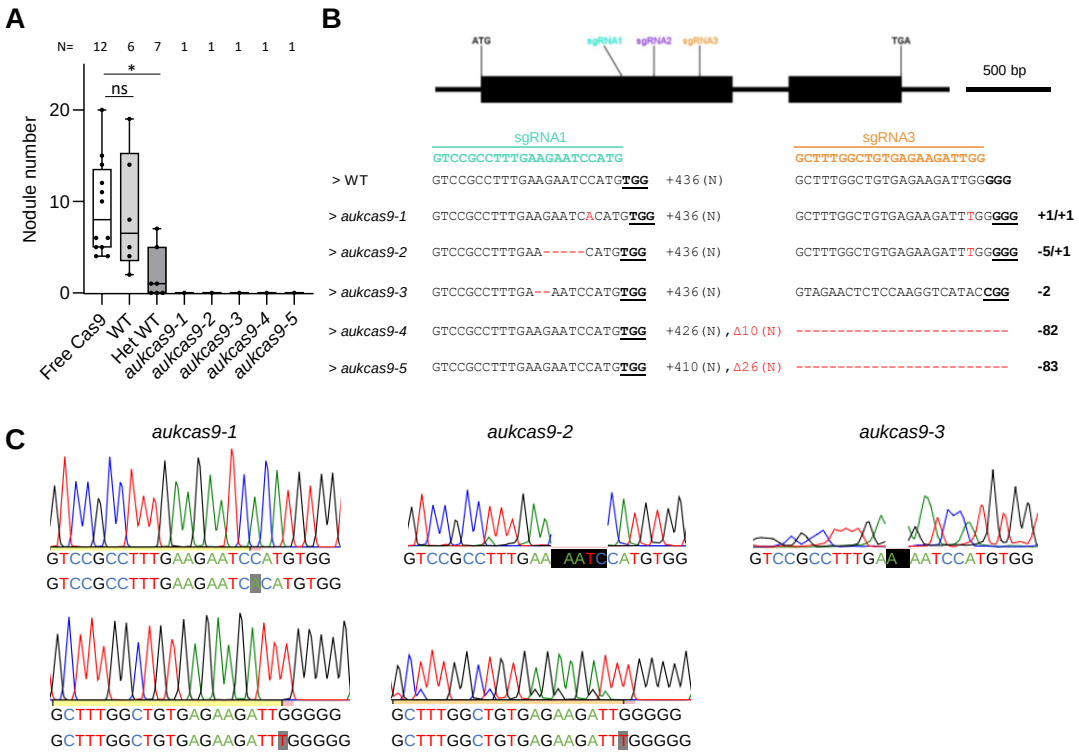

Figure 4.1. CRISPR-Cas9 knockout of *AUK* abolishes nodulation

A. Number of nodules from *M. truncatula* R108 hairy roots transformed with a *CRISPR Cas9* construct with 2 sgRNAs or free *Cas9* inoculated with *Sm*2011 for 25 days. Plants were genotyped by PCR and Sanger sequencing. Wildtype (WT) and heterozygous (Het) roots are indicated as a control. Statistics are from a one-way ANOVA (*, significance level $p<0.05$). **B.** Gene structure and organization indicating the position of the sgRNAs on *AUK* genomic sequence. The PAM site is indicated as bold and underlined. Red letters indicate positions on the sequence where the Cas9 cut occurred and what the consequence was (with dashes indicating deletions and red letters indicating insertions). Five *aukcas9* plants with homozygous CRISPR cuts as indicated in (A) are shown. (N) indicates the number of nucleotides with the number inserted or deleted indicated with + or Δ, respectively. **C.** Sanger sequencing traces of *aukcas9* CRISPR alleles from alignments in Benchling with the *AUK* genomic sequence. sgRNA sequence is indicated with coloured letters corresponding to A, T, G, C nucleotides. Insertions are highlighted in grey with the wild-type sequence shown above the sequence with insertion. Deletions are shown with black highlighting of the nucleotides that have been deleted in the allele. Images are screenshots of sequencing alignment with the wild-type sequence in Benchling.

4.2.2- Analysis of *AUK* overexpression in endosymbiosis

4.2.2.1- AUK *overexpression induces spontaneous Ca^{2+} oscillation dependent on DMI1 and downstream of DMI2*

Given the phenotype of *aukcas9* mutants with no nodules (Figure 4.1), the next step was to determine whether AUK is involved in early signaling for nodulation with rhizobia. An early step in endosymbiosis signaling is the generation of nuclear Ca^{2+} oscillations. For examination of a role for AUK in nuclear Ca^{2+} oscillation, the *pLjUBI:AUK-GFP* construct was used to overexpress *AUK* in hairy roots of A17 plants expressing the nuclear localized *YC3.6* Ca^{2+} reporter. In roots expressing the empty vector (EV), nuclear Ca^{2+} spiking began 5-10 min following application of Nod factor, as reported in previous literature (Figure 4.2; Wais *et al.*, (2000). Interestingly, upon overexpression of *AUK*, spontaneous nuclear Ca^{2+} spikes were observed in absence of Nod factor addition (Figure 4.2). In addition, in wild-type the nuclear Ca^{2+} oscillation often begins with a faster Nod factor-induced oscillation before evening out to a steady ongoing oscillation frequency. This initial phase was not observed in the *AUK-OE* hairy roots, indicating that the roots might have already been primed for the nuclear Ca^{2+} oscillation. It is important to note that the Ca^{2+} oscillations following addition of Nod factor in the *AUK-OE* roots seemed more wild-type in amplitude and frequency than the spontaneous spikes, suggesting Nod factor perception is necessary for full activation of the nuclear Ca^{2+} oscillation response, however this was not fully assessed.

Based on the *AUK-OE* root spontaneous nuclear Ca^{2+}, the next step was to perform epistasis analysis to position *AUK-OE* within the signal transduction pathway for early symbiosis signaling. In the previous chapter of this thesis, it was shown that AUK associates with DMI1 at the nuclear envelope. DMI1 is an ion channel required for nuclear Ca^{2+} oscillation, and a *dmi1-1* mutant has no Ca^{2+} oscillation, even upon Nod factor application (Wais *et al.*, 2000). If AUK is involved in regulation or activation of the nuclear Ca^{2+} oscillation through its interaction with DMI1, it could be expected that the *AUK-OE*-induced spontaneous nuclear Ca^{2+} is dependent on presence of DMI1. Thus, in a *dmi1-1* mutant, it could be predicted that there would be no Ca^{2+} oscillation. Indeed, *AUK-OE* in *dmi1-1 YC3.6* hairy roots had no nuclear Ca^{2+} oscillation before or after Nod factor application. This result demonstrates that AUK-induced nuclear Ca^{2+} oscillation is dependent on DMI1.

Following determination of the dependence of DMI1 for AUK-induced spontaneous nuclear Ca^{2+}, steps further upstream in the signal transduction pathway were examined to determine the genetic interaction of AUK with DMI2. DMI2 is believed to act as a co-receptor of the Nod and Myc factor receptors as it is essential for the induction of nuclear Ca^{2+} oscillation in response to Nod and Myc factor, nodulation and mycorrhization (Antolín-Llovera *et al.*, 2014; Catoira *et al.*, 2000; Wais *et al.*, 2000). Given the previous hypothesis that AUK might act as a link between the perception of signaling molecules at the plasma

membrane and activation of the ion channels at the nuclear envelope for nuclear Ca^{2+} oscillation, and its dependence on and association with DMI1, it could be hypothesized that the spontaneous nodulation induced by *AUK-OE* would still occur in the *dmi2-1* mutant. As predicted, *AUK-OE* in the *dmi2-1 YC3.6* hairy roots induced spontaneous nuclear Ca^{2+} oscillation in absence of Nod factor (Figure 4.2). Interestingly, following Nod factor addition, the nuclear Ca^{2+} oscillation was not induced to the typical wild-type Nod-factor induced amplitude and frequency (although not directly measured, but assessed visually), and instead resembled the less efficient spontaneous nuclear Ca^{2+} prior to Nod factor addition. This result is indicative of AUK playing a role downstream of DMI2 to generate nuclear Ca^{2+} oscillation where DMI2 is still required for proper perception of Nod factor, which subsequently is necessary for full activation of the nuclear Ca^{2+} oscillation. It is important to note that not all of the plants overexpressing *AUK* showed spontaneous nuclear Ca^{2+} oscillation, however within the transformed root system, there can be much variation in the extent of *AUK* overexpression. Overall, the results from these Ca^{2+} imaging epistasis experiments point to a role of AUK in nuclear Ca^{2+} oscillation dependent on DMI1, but downstream DMI2.

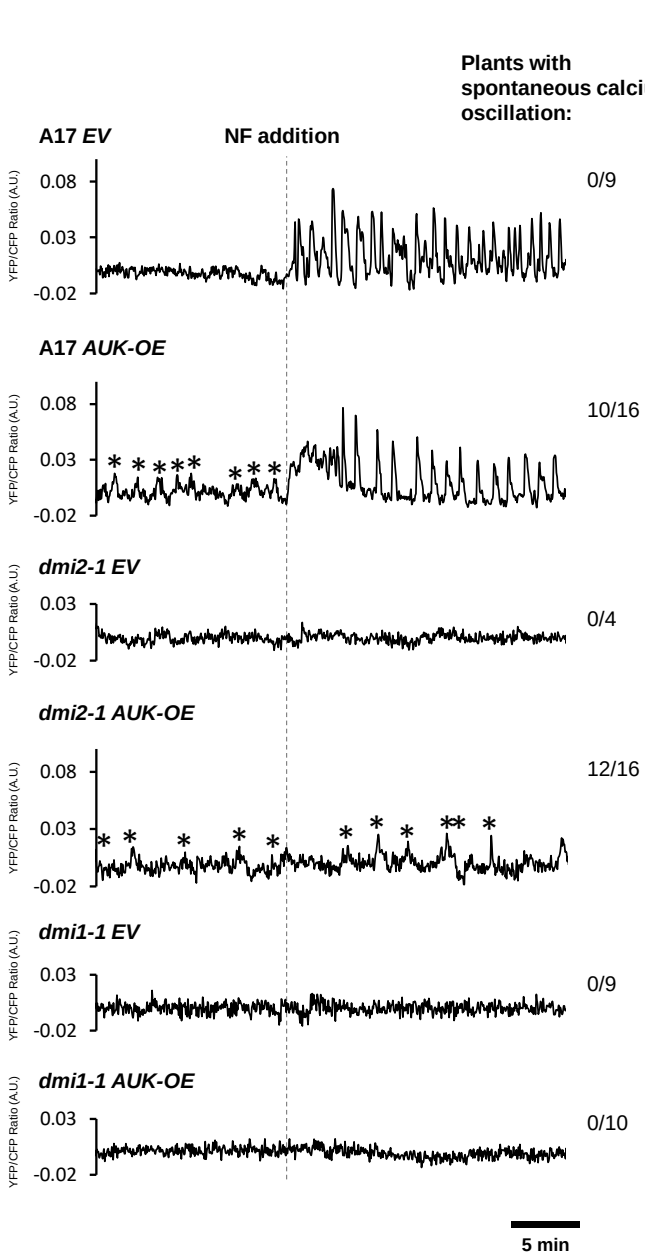

Figure 4.2. *AUK* overexpression induces spontaneous nuclear Ca^{2+} oscillation dependent on DMI1, but downstream or independently of DMI2

A. Representative Ca^{2+} imaging traces, detrended to make oscillation more visible, from transformed roots of A17, *dmi1-1* and *dmi1-2* plants expressing the *YC3.6* Ca^{2+} reporter transformed with EV and *pUBI:AUK-GFP* (*AUK-OE*) measured as the ratio of YFP/CFP (A.U.) under a confocal microscope. The dashed line indicates the addition of Nod Factor (NF), number of plants with spontaneous Ca^{2+} spiking is indicated at the top right of each trace, and spontaneous Ca^{2+} oscillations are denoted by an asterisk.

4.2.2.2- AUK *overexpression induces spontaneous nodulation*

The spontaneous nuclear Ca^{2+} phenotype with *AUK-OE* strongly suggested a role for AUK within the Nod factor-induced early signaling pathway. However, the spontaneous nuclear Ca^{2+} spikes and those induced in the *dmi2-1* mutant were visibly at a lower amplitude than the Nod factor-induced Ca^{2+} oscillation, suggesting inefficient activation of the Ca^{2+} oscillation machinery. The next step was to determine whether the spontaneous nuclear Ca^{2+} oscillations observed in *AUK-OE* hairy roots were sufficient to generate nodules by performing a spontaneous nodulation assay. A17 plant roots were transformed with *pLjUBI:AUK-OE* and planted in sterile TerraGreen and sand mix in phytaboxes for 10 weeks without addition of rhizobia, with empty vector transformed as a control. Interestingly, 60-80% of the roots were observed to have nodule-like bumps (Figure 4.3a). V-shaped nodule vasculature could be seen in some of the larger bumps (Figure 4.3b), and thus these bumps were designated as 'nodule-like structures'. The empty vector control did not have any of these nodule-like bump structures. The nodule-like structures were similar in appearance to those previously reported in the literature, such as for *LjSYMRK* overexpression. Future work should include fine sectioning of the nodule-like structure to assess vasculature phenotypes as well as qPCR analysis to assess whether early nodulation genes, such as *NIN* and *ENOD11,* are induced with AUK overexpression. This phenotype suggests that overexpression of *AUK* generates spontaneous Ca^{2+} oscillation that is sufficient to induce the formation of nodule-like structures in absence of rhizobia.

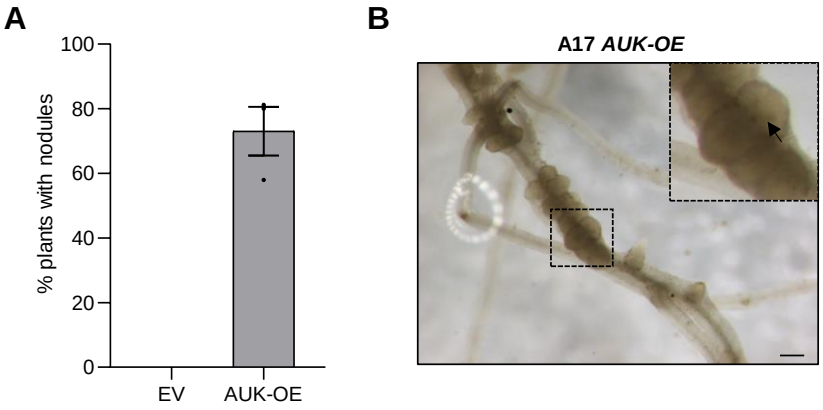

Figure 4.3. *AUK* overexpression is sufficient for induction of spontaneous nodule-like structures

A. Percentage (%) of plants from each of 3 different reps that had spontaneous nodule-like structures after 8 weeks in phytaboxes. Error bars represent standard error. **B.** Bright field image of a representative plant with spontaneous nodule-like structure. Inset zooms in on nodule-like structure where nodule-like vasculature can be observed, indicated by the black arrow. Scale bar represents 5 mm.

4.2.2.3- AUK *overexpression results in increased nodule number*

AUK overexpression resulted in spontaneous nuclear Ca^{2+} oscillation, which seemed to be sufficient for the plant to produce spontaneous nodule-like structures on root systems in absence of rhizobia. The next approach was to determine whether overexpression of *AUK* could influence the nodule number upon inoculation with rhizobia, and whether any modulation of the nodule number would be maintained over time. An increased number of nodules were observed in A17 hairy roots expressing the *pLjUBI:AUK-GFP* construct in comparison to wild-type at 14 dpi (Figure 4.4a). This increase was sustained at 21 dpi (Figure 4.4b) and at a late timepoint of 60 dpi (Figure 4.4c). It was also examined whether there might be an increased number of young vs. mature nodules at this 60 dpi timepoint, which could suggest a progressed stage of nodulation in these roots, however there was not a significant difference. The results confirm that AUK plays a role in nodulation and that spontaneous Ca^{2+} oscillation observed in *AUK-OE* might prime and hypothetically modulate the early signaling to enhance nodule formation.

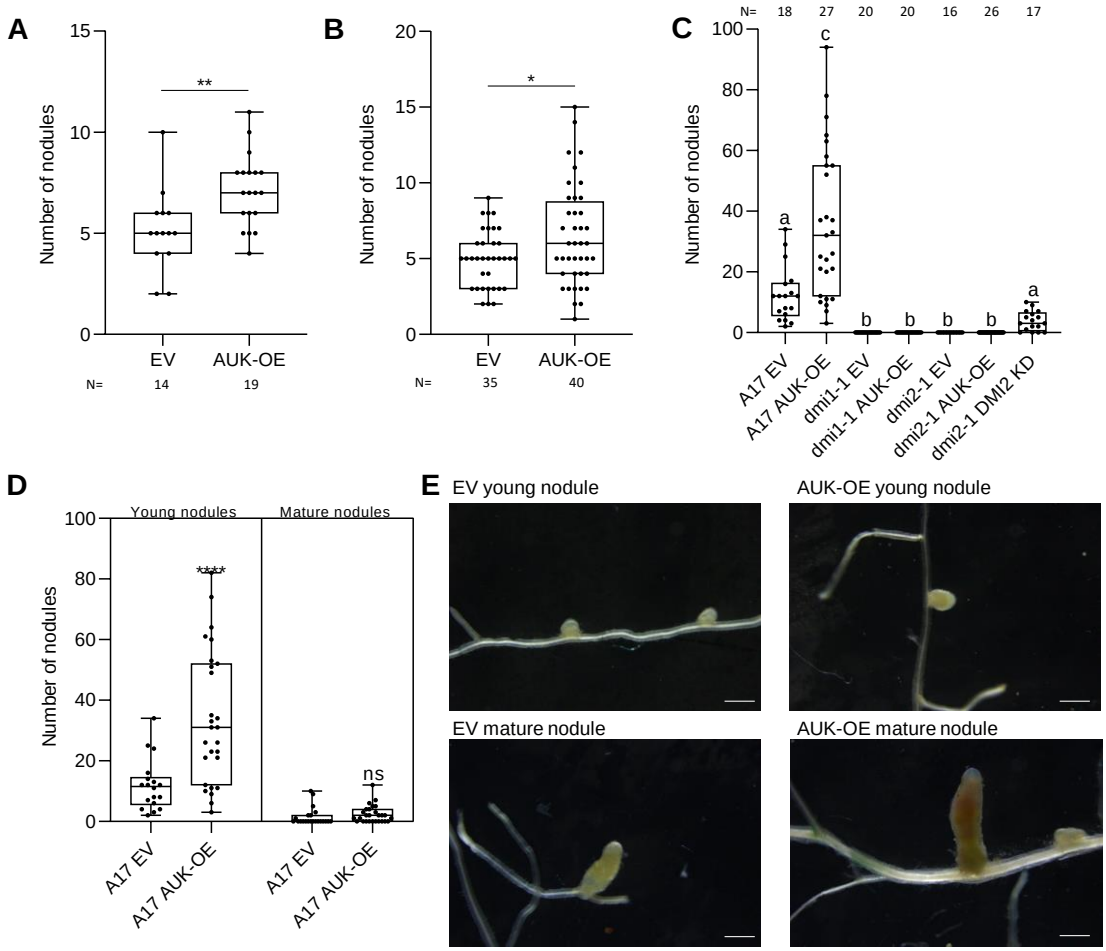

Figure 4.4. *AUK* overexpression leads to increased nodulation.

A. Number of nodules from hairy roots of A17 *M. truncatula* transformed with empty vector (EV) or *pUBI:AUK-GFP* on TerraGreen and sand 14 dpi with *Sm*2011 *LacZ*. Data are from 2

reps and n number is indicated below the x-axis. Statistical test performed was an unpaired t-test (** indicates $p<0.01$). **B.** Number of nodules from hairy roots of A17 *M. truncatula* transformed with empty vector (EV) or *pUBI:AUK-GFP* on TerraGreen and sand 21 dpi with *Sm*2011 *LacZ.* Data are from 3 reps and n is indicated below the x-axis. Statistical test performed was an unpaired t-test (* indicates $p<0.05$). **C.** Number of nodules from hairy roots of A17 or *dmi1-1 M. truncatula* transformed with empty vector (EV) or *pUBI:AUK-GFP* on TerraGreen and sand 60 dpi with *Sm*2011 *LacZ.* Data are from 3 reps and n is indicated above. ANOVA was performed followed by Tukey's post-hoc test. Different letters indicate significance. **D.** Number of mature and elongated nodules for data presented in (C). Statistical test performed was an unpaired t-test (**** indicates $p<0.0001$). **E.** Representative pictures of young and mature nodules on hairy roots from (C) and (D). Scale bar indicates 500 µm.

The results thus far have shown AUK to play a role in nuclear Ca^{2+} oscillation that is dependent on DMI1, but downstream of DMI2. To determine whether these genetic interactions also account for nodulation efficiency, *AUK* was overexpressed in the *dmi1-1* and *dmi2-1* mutant backgrounds and examined nodule number. Neither of these mutants produce nodules in presence of *Sm*2011 (Wais *et al.,* 2000). Consistent with the absence of nuclear Ca^{2+} oscillation observed in *dmi1-1/AUK-OE*, no nodules or nodule-like structures were formed in *dmi1-1* roots overexpressing *AUK* (Figure 4.5). Interestingly, in the *dmi2-1* mutants, one or two nodule-like structures were observed in 3 plants at 100 dpi (Figure 4.5). This result is consistent with the inefficient Ca^{2+} oscillation and suggests that the AUK-induced spontaneous oscillation is sufficient for production of nodule-like structures, but not generation of a fully developed, infected nodule. It is important to note that at the 100 dpi timepoint, there was not a significant difference in nodule number between the EV and AUK-OE transformed roots. This may point to a role for AUK involvement in early signaling in nodulation, which may not be sustained as time progresses. In addition, at this timepoint, the plants are not very happy in trays, and this result could simply be based on overcrowding of the root system or lack of nutrients, which may not be seen in larger trays. Overall, the nodulation results corroborate those seen with Ca^{2+} oscillation, situating AUK upstream of DMI1 and downstream of DMI2.

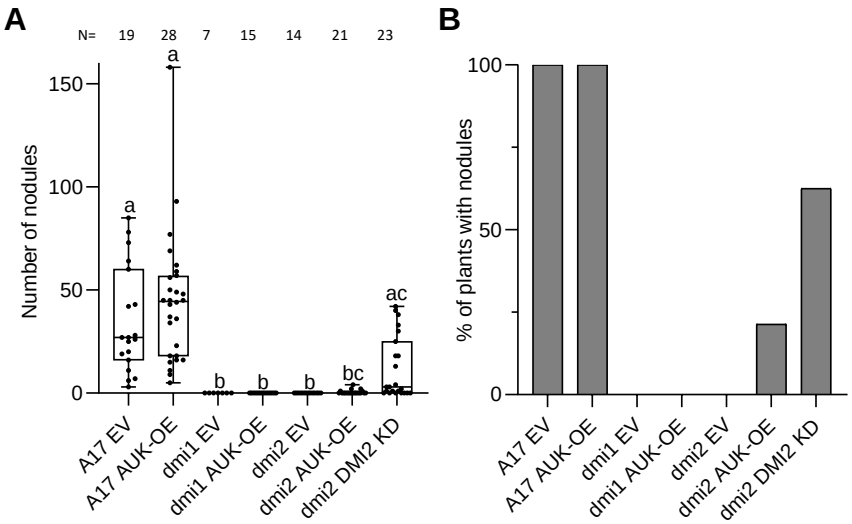

Figure 4.5. *AUK-OE* nodulation is dependent on DMI1 and downstream of DMI2

A. Number of nodules from hairy roots of A17 or *dmi1-1 M. truncatula* transformed with empty vector (EV) or *pUBI:AUK-GFP* on TerraGreen and sand 100 dpi with *Sm*2011 *LacZ*. N indicated above the graph. Data are from 3. ANOVA was performed followed by Tukey's post-hoc test. Different letters indicate significance ($p<0.05$). **B.** Data from (A) represented as bar graph showing percentage of plants with nodule-like structures.

4.2.2.4- AUK *overexpression results in increased AM colonization*

To determine whether AUK plays a role in the common symbiosis pathway, the AM colonization of wild-type roots overexpressing *AUK* was assessed. The roots were planted in TerraGreen and sand mix with 1:10 ratio of AM inoculum to TerraGreen and sand. Colonization was determined using the grid intersection method (Giovannetti & Mosse, 1980) and colonization was determined based on fungal structures of intraradical hyphae (IRH), arbuscules (ARB) and vesicles (VES). Timepoints were chosen based on percentage colonization of arbuscules, with an early timepoint determined to be when arbuscule colonization reached ~10% in the empty vector-transformed roots and a later timepoint when arbuscule colonization reached 30% in the EV-transformed roots. At the early timepoint, the *AUK-OE* roots were not significantly different in AM colonization than wild-type (Figure 4.6a). At the 30% EV colonization timepoint, *AUK-OE* roots had significantly higher numbers of IRH and ARB (Figure 4.6b). This result revealed that overexpression of *AUK* can positively influence AM colonization, and therefore strongly suggest that AUK is a new component of the common symbiosis pathway.

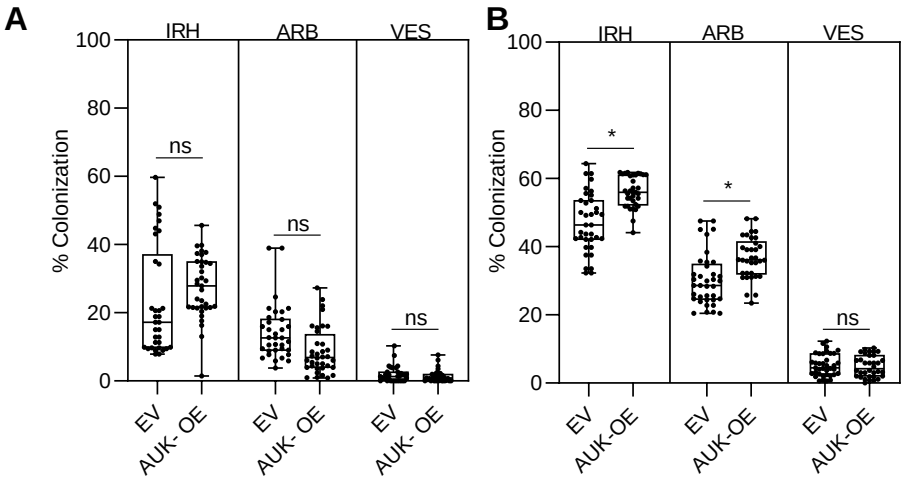

Figure 4.6. *AUK* overexpression results in increased AM colonization dependent on DMI1

A. AM colonization 3-4 weeks post inoculation with AM inoculum in A17 roots transformed with empty vector (EV) or *pUBI:AUK-GFP*. **B.** AM colonization 6-8 weeks post inoculation with AM inoculum in A17 roots transformed with empty vector (EV) or *pUBI:AUK-GFP*. Data are from 3 reps and n= 34-37 plants total. Statistical test performed for all was unpaired t-test (significance value *, $p<0.05$). IRH, intraradical hyphae; ARB, arbuscules; VES, vesicles.

4.2.3- Screening of AUK EMS mutants

To further dissect the role of AUK and its possible kinase activity in endosymbiosis, the *M. truncatula* EMS population was screened for lines with point mutations in the kinase domain of AUK to try and identify either a kinase dead (KD) or gain-of-function (GoF) mutant. From this screening, lines with seven different kinase domain mutations were obtained, selected, and genotyped to homozygosity (Table 4.2). A multiple sequence alignment of the kinase domain of AUK including structurally related kinases (identified from a Swiss Model search), the *Arabidopsis* ortholog of AUK and *Mt*DMI2 was performed using Clustal Omega to identify whether the SNP mutations in the EMS lines were in any conserved or important kinase domain residues (Figure 4.7). Several of these were of particular interest including a E601K mutation in the conserved kinase APE motif, which serves to stabilize the activation loop, and in many kinases is required for kinase activity (Taylor & Kornev, 2011).

Another mutation of interest was G627R, which is a highly conserved glycine amino acid, and a G>E mutation in this residue in DMI2 results in the *dmi2-4* mutant, which does not have nodules, but does have AM colonization (Endre *et al.*, 2002).

Table 4.2. Summary table of AUK EMS mutant line number, point mutation and segregation

EMS mutant line name	Nucleotide mutation	Amino acid mutation	Segregation ratio
auk-6	C2177T	P526L	10:7:1 (WT:het:hmz)
auk-5	G2285G	G562E	Seeds received were homozygous
auk-1/auk^{GoF}	C2293T	P565S	7:9:5 (WT:het:hmz)
auk-4	G2401A	E601K	Seeds received were homozygous
auk-3	G2416A	V606M	15:20:11 (WT:het:hmz)
auk-2	G2479A	G627R	4:11:3 (WT:het:hmz)
auk-7	G2494A	V632I	Seeds received were homozygous

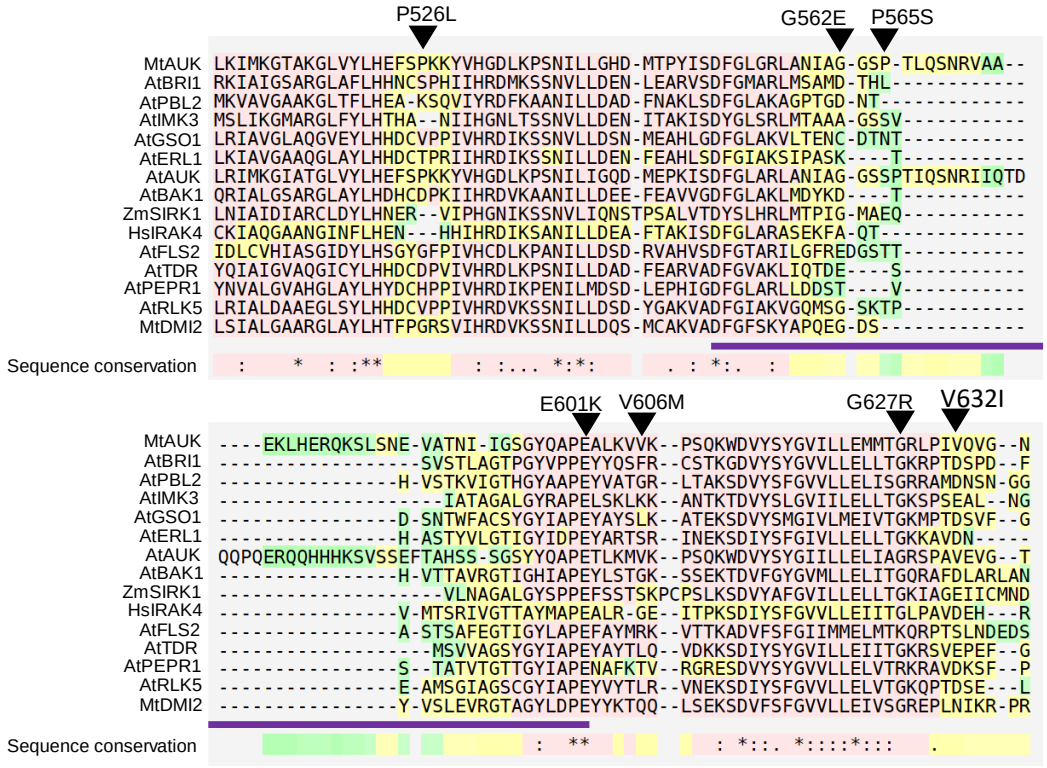

Figure 4.7. Analysis of AUK EMS mutant lines with point mutations in the kinase domain
Alignment of AUK with structurally-related kinases as determined from a Swiss Model search and including *At*AUK and *Mt*DMI2. Black arrowheads indicate the position of the EMS point mutations. The kinase activation loop is indicated by the purple line from the conserved kinase DFG motif to the conserved APE motif. Level of conservation is indicated underneath with red indicating high conservation, yellow intermediate and green low among the indicated kinases.

4.2.3.1- Examining root system architecture in auk^{GoF}

The first thing observed was that one line in particular, designated *auk-1*, line had a severe impact on root system architecture (Figure 4.8), showing much shorter, thickened roots. The mutation in *auk-1* corresponded to P565S amino acid substitution within the activation loop of the kinase. The proline residue P565S is located at the beginning of the kinase activation loop, and in AUK and its *Arabidopsis* ortholog there is an extended section of the activation loop, which does not exist in the other structurally related kinases included within my initial alignment (Figure 4.7). A segregating population at 14 dpi with rhizobia was examined for root system architecture phenotypes of primary root length, number of lateral roots per cm primary root and lateral root lengths. Interestingly, those plants homozygous for the *auk-1* mutation displayed a shorter primary root length and shorter lateral roots, however there was no significant difference between the number of lateral roots between WT, heterozygous and

homozygous mutant plants (Figure 4.16a-c). The root system architecture phenotypes were also investigated at a later timepoint of 25 dpi. At this timepoint, the primary root length of the homozygous mutant plants had caught up to that of the wild-type and heterozygous, however the distribution of lateral root length was still significantly shorter (Figure 4.16d-f). These results suggest that AUK plays a role in the development of primary and lateral roots, but not in the organ initiation of lateral root primordia.

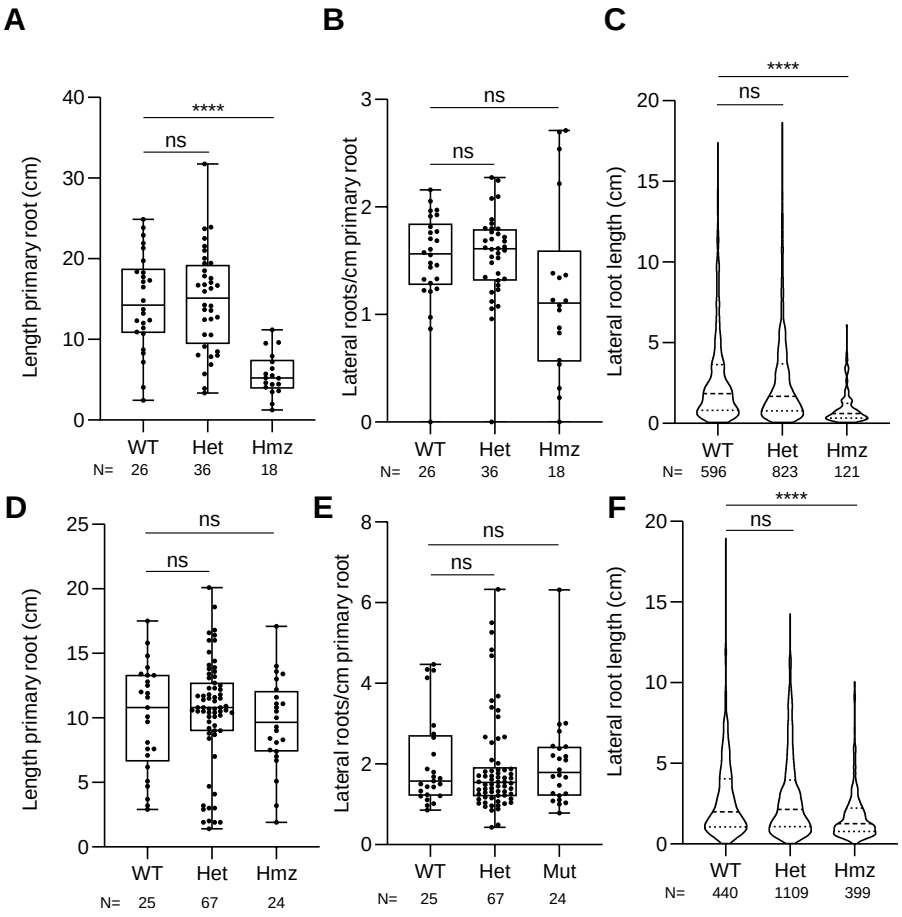

Figure 4.8. Analysis of segregating *auk*^{GoF} mutants in root system architecture.

A. Length of primary root (cm) in a segregating population of *auk*^{GoF} at 14 dpi with *Sm*2011. **B.** Number of lateral roots normalized to length of primary root (lateral roots per cm primary root) for the *auk*^{GoF} segregating population at 14 dpi in (A). **C.** Distribution of lengths of lateral roots (cm) for the segregating *auk*^{GoF} population at 14 dpi. **D.** Length of primary root (cm) in a segregating population of *auk*^{GoF} at 25 dpi with *Sm*2011. **E.** Number of lateral roots normalized to length of primary root (lateral roots per cm primary root) for the *auk*^{GoF} segregating population in (A). **F.** Distribution of lengths of lateral roots (cm) for the segregating *auk*^{GoF} population. N number for each genotype is indicated below the x-axis. Statistical test performed is an ANOVA followed by Dunnett's posthoc test (****, $p<0.0001$).

4.2.3.2- Nodulation in AUK EMS mutant lines

As a first step in determining whether the mutations impact AUK function, the nodulation phenotype was examined at 14 dpi (Figure 4.9a). In addition to the aforementioned *auk*-1 line, most of the mutations influenced the amount of root system (Figure 4.9b), and thus nodule number was corrected relative to root dry mass (Figure 4.9c). Following this correction, two of the mutations were found to have an impact on nodule number, the *auk-1* line, which had significantly increased number of nodules, and *auk-4*, with the mutation within the conserved APE motif, which had significantly fewer nodules (Figure 4.7). All of the lines assessed had pink nodules, thus nitrogen fixation does not appear to be perturbed, although quantitative assessment by acetylene reduction assay would be required to fully come to this conclusion. As discussed in Section 4.2.3.1, the roots of the P565S mutant were significantly altered, with many nodule structures and bumps all over a smaller, thickened root system (Figure 4.9d). It was interesting to note the decreased root dry mass of all of the mutations, however these lines were not backcrossed, and thus may have been the result of pleiotropic mutations affecting genes other than *AUK*.

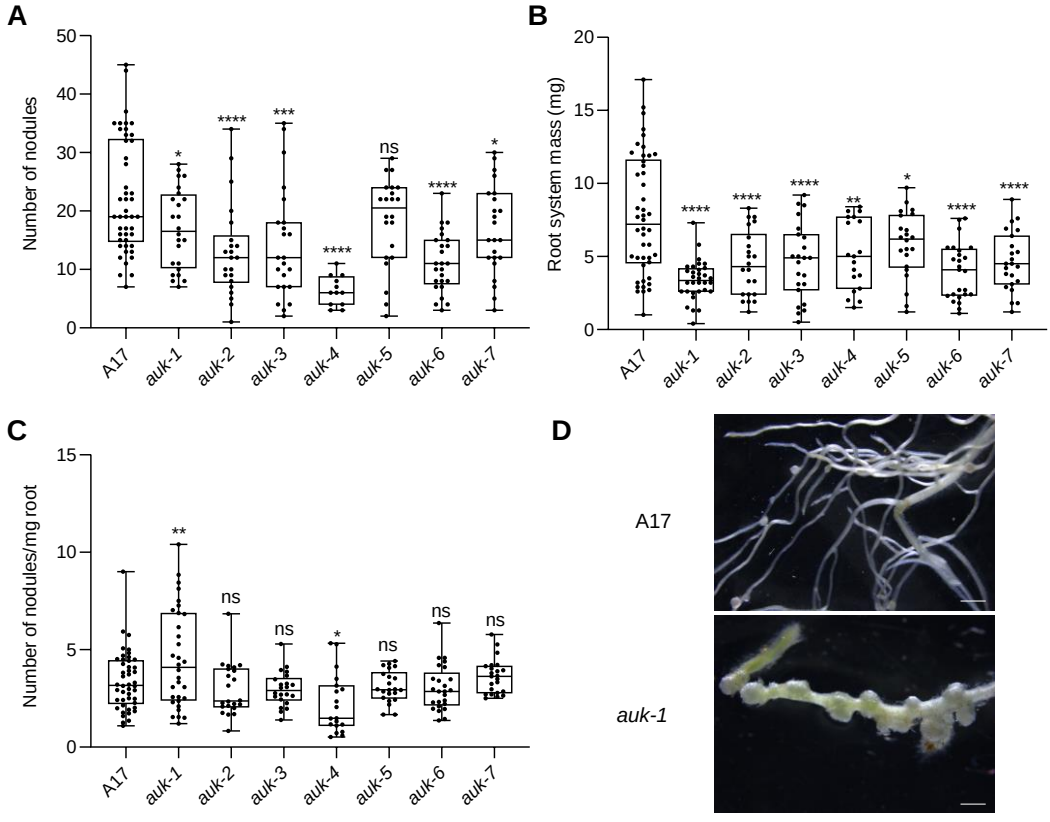

Figure 4.9. Analysis of nodulation in *AUK* EMS mutant lines

A. Number of nodules at 14 dpi with *Sm*2011. **B.** Dry mass of root system from plants measured in (A). **C.** Number of nodules/mg root corrected from (A) and (B) at 14 dpi. **D.** Nodule phenotype of A17 and *auk-1* nodules and root system. Scale bar represents 2 mm.

Statistics used are a one-way ANOVA followed by Dunnett's posthoc test (*, $p<0.05$; **, $p<0.01$; ****, $p<0.0001$). Data are from two biological reps.

Based on the increased nodulation phenotype observed in the *auk-1* line, it could be hypothesized that this allele might be acting as a gain-of-function mutation. The *AUK-OE* experiments had resulted in increased nodule number in presence of rhizobia and generation of spontaneous nodule-like structures in absence of rhizobia. Thus, experiments were set up with *auk-1* lines to examine whether spontaneous nodule-like structures were produced. Indeed, following 10 weeks of growth in sterile phytaboxes, the roots of *auk-1* lines had many nodule-like structures (Figure 4.10), similar to those observed in *auk-1* inoculated with rhizobia (Figure 4.9) and to those seen in *AUK-OE* spontaneous nodulation experiments (Figure 4.3). Due to the increase in nodulation and spontaneous nodule-like structures formed in *auk-1*, the line was designated as a gain-of-function mutation and will hereafter be referred to as *auk*^{GoF}.

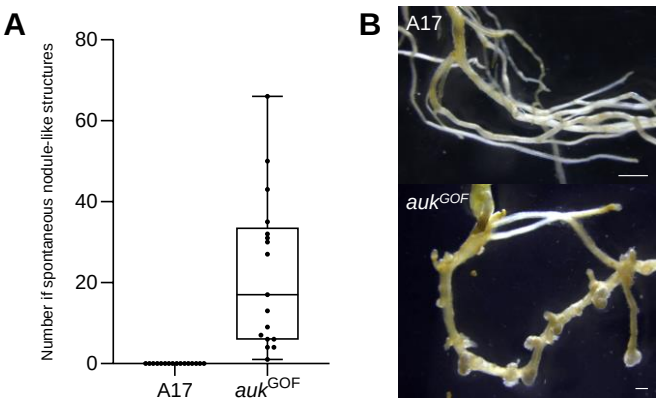

Figure 4.10. *auk*^{GoF} produces spontaneous nodule-like structures

A. Number of spontaneous nodule-like structures produced in wild-type A17 and *auk*^{GoF} mutant following 8 weeks on TerraGreen and sand in absence of rhizobia. **B.** Representative picture of root system and nodule-like structures on *auk*^{GoF} roots from (A). Data are from 2 biological reps. Scale bar represents 2 mm.

To confirm that *AUK* was the causal gene for the spontaneous nodule-like structure formation in absence of rhizobia and of the increase in nodulation in presence of rhizobia, each phenotype was assessed by segregating populations of approximately 120 plants each. For the spontaneous nodulation experiments, only those plants which were homozygous for the *auk*^{GoF} allele had spontaneous nodules (Figure 4.11). In addition, only those plants homozygous for the *auk*^{GoF} allele had a significantly higher number of nodules at 14 dpi with rhizobia when corrected for root system mass (Figure 4.12). Root phenotypes were as seen in previous experiments, with only the homozygous *auk*^{GoF} plants displaying shorter, thickened root

systems with many nodules (Figure 4.11-12). These results indicate that the mutation within *AUK* is responsible for the increased nodulation and spontaneous nodule phenotypes and suggests that the mutation in *auk*^{GoF} is recessive.

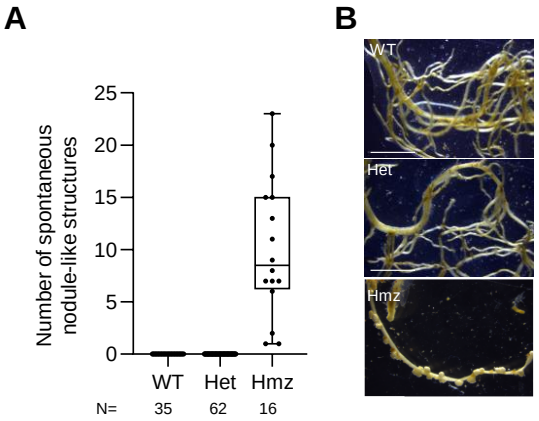

Figure 4.11. Homozygous *auk*^{GoF} mutants produce spontaneous nodule-like structures.

A. Number of nodule-like structures in segregating population (WT, Het, Hmz) after 8 weeks on TerraGreen and sand in absence of rhizobia. N number for each genotype is indicated below the x-axis. **B.** Representative picture of root system from (A).

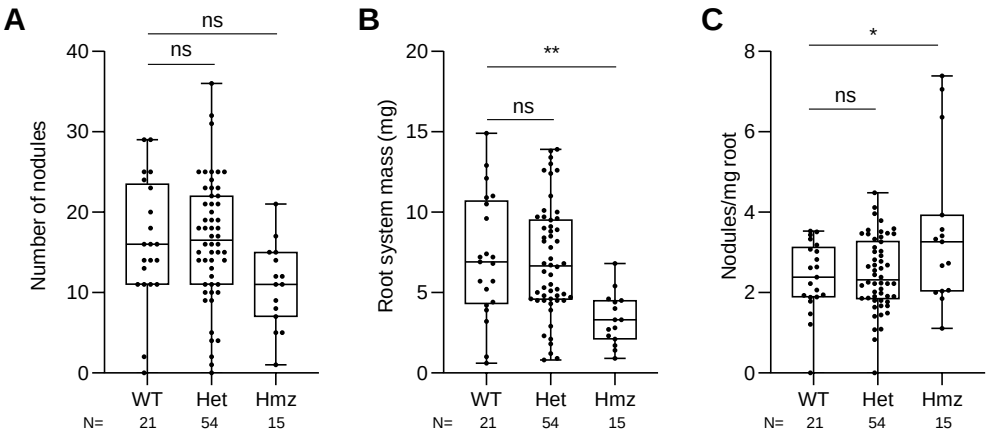

Figure 4.12. Homozygous *auk*^{GoF} mutants produce an increased number of nodules with rhizobial inoculation.

A. Number of nodules at 14dpi with *Sm*2011. **B.** Dry mass of root system from (A) in mg. **C.** Number of nodules/mg root corrected from (A) and (B) at 14 dpi. Statistical test is one-way ANOVA (*, $p<0.05$; **, $p<0.01$). N number for each genotype is indicated below the x-axes.

4.2.3.3- Examining nuclear Ca^{2+} oscillation in auk^{GoF}

To further assess the effect of the mutation in *auk^{GoF}* allele on AUK function related to Ca^{2+} signaling, the next step was to examine nuclear Ca^{2+} oscillation in *auk^{GoF}* roots transformed with the Ca^{2+} reporter, nuclear localized *(NLS):YC3.6*. Ca^{2+} imaging experiments were performed in absence of Nod factor. Excitingly, there were spontaneous nuclear Ca^{2+} oscillations in 3 out of 10 root systems analyzed (Figure 4.13), which corroborated the experiments performed with the *AUK-OE* lines and provided further evidence for AUK playing an important role in the generation of nuclear Ca^{2+} oscillation. To confirm this result, *auk^{GoF}* was backcrossed with A17::*YC3.6* and the Ca^{2+} phenotype of the homozygous mutant line auk^{GoF} stably expressing *YC3.6* was analyzed. In agreement with the previous result from hairy roots (Figure 4.13), spontaneous Ca^{2+} oscillations were recorded in 4 out of 8 plants (Figure 4.14). It is important to note that not all of the plants had spontaneous Ca^{2+} oscillation, which could be due to some of the plants being stressed, or poorer expression of the *YC3.6* so that it wasn't at the level of proper detection. It would also be important to analyze these Ca^{2+} oscillations in comparison to those of the overexpression in hairy roots. Taken together, these results demonstrate that the *auk^{GoF}* allele can autoactivate the nuclear Ca^{2+} oscillation.

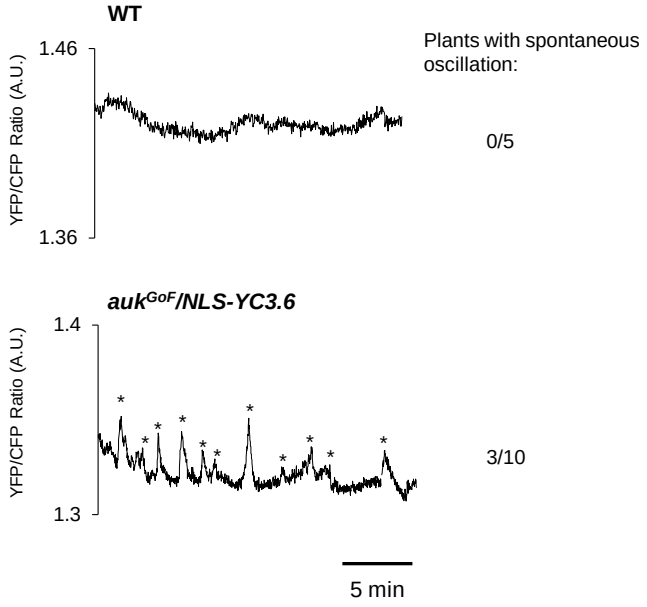

Figure 4.12. *auk^{GoF}* mutants produce spontaneous nuclear Ca^{2+} oscillations

Representative traces of nuclear Ca^{2+} oscillation (YFP/CFP ratio) in WT and *auk^{GoF}* mutants transformed with *NLS-YC3.6.* Number of plants tested showing spontaneous oscillation is indicated to the right of the traces. Spontaneous spikes are indicated with asterisks above the trace. 5 min is indicated by the scale bar.

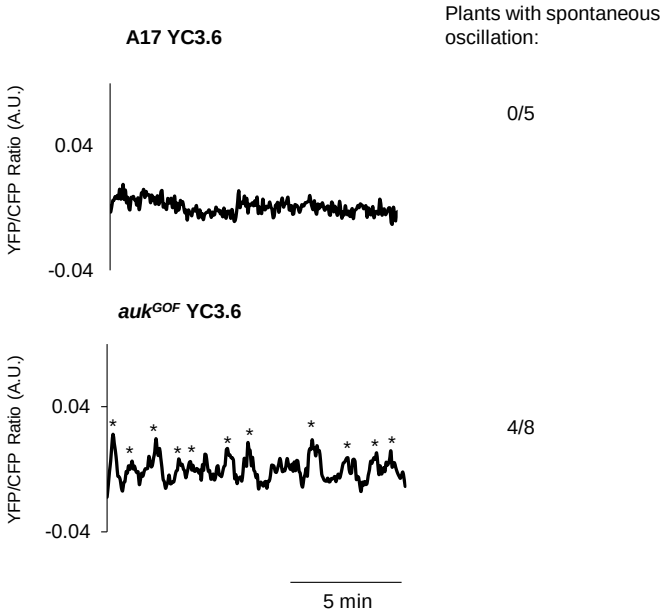

Figure 4.13. Stable *auk*^{GoF} x *YC3.6* lines have spontaneous nuclear Ca^{2+} oscillation

Nuclear Ca^{2+} oscillation (YFP/CFP ratio) in WT and *auk*^{GoF} mutants in stable lines with *YC3.6*. Number of plants tested showing spontaneous oscillation is indicated to the right of the traces. Spontaneous spikes are indicated with asterisks above the trace. 5 min is indicated by the scale bar.

4.2.3.4- Examining AM colonization in auk^{GoF}

Given the autoactive Ca^{2+} oscillation and spontaneous nodulation phenotype of *auk^{GoF}*, it was important to next determine whether the autoactive allele was also autoactive in permitting colonization of AM fungi. Within the experiment, the EMS mutant lines were included to determine whether other conserved residues within the kinase domain might perturb AUK function in AM colonization. As observed with *AUK-OE*, *auk^{GoF}* had increased AM colonization, resulting in a significantly increased number of all three structures: IRH, ARB and VES (Figure 4.15). The *auk-4* line carrying the mutation E601K within the APE motif did not have a phenotype, indicating that this conserved kinase motif may not be important within the symbiosis response for colonization by AM fungi. Interestingly, the G627R mutation present in the *auk-2* line resulted in lower AM colonization, with fewer of all three structures: IRH, ARB and VES, indicating that this residue might specifically impair AM colonization. However, analysis of a segregating population of *auk-2* will be required to confirm this result as it had not been backcrossed at the time of these experiments.

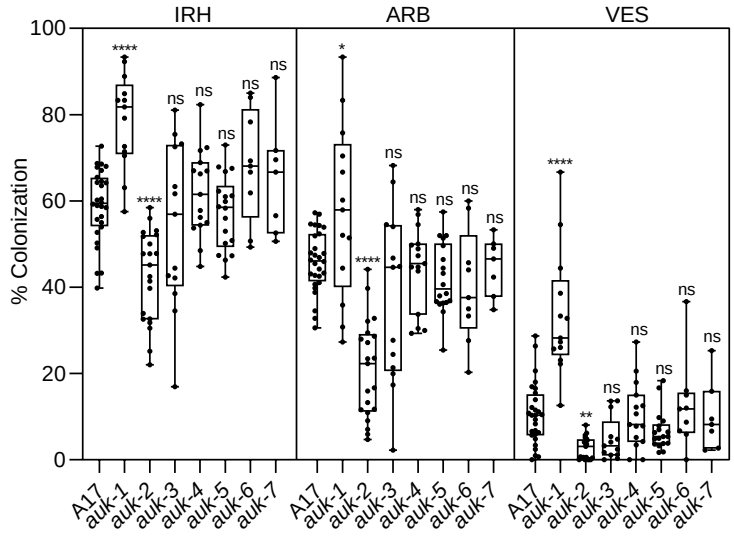

Figure 4.15. Analysis of AM colonization in AUK EMS lines

Percentage colonization in A17 and the indicated AUK EMS lines at 6 wpi with AM inoculum. Structures of intraradical hyphae (IRH), arbuscules (ARB) and vesicles (VES) were counted using the grid intersection method. Data are from 2 biological reps. Statistical tests used are a one-way ANOVA (**, $p<0.01$; ****, $p<0.0001$) related to the A17 wild-type.

In addition to an increased nodulation phenotype, initial screening experiments for the *auk-1* EMS mutant line showed that it displayed increased AM colonization, with significantly increased intraradical hyphae, arbuscules and vesicles. As with the nodulation phenotype, it was important to confirm *auk^{GoF}* allele as the causative mutation for this phenotype, and thus

an experiment with a segregating population of 120 plants was set up with AM inoculum at a ratio of 1:5 Terragreen and sand to AM inoculum. As observed with the initial line screening, only those plants homozygous for the *auk*^{GoF} allele displayed significantly increased AM colonization of IRH and ARB structures (Figure 4.16). These results indicate that as with nodulation, the *auk*^{GoF} allele is what is responsible for the increased AM colonization and this phenotype is recessive. Once again, the roots in these AM colonization experiments were smaller for the *auk*^{GoF} line, however the grid-intersect method for counting AM structures each time the root crosses a grid takes into account possible differences in root size so that it is a percentage of the entire root. Thus, the root length should not have an impact on the overall colonization percentage. In combination with the nodulation results, these experiments indicate that AUK plays an important role in both rhizobia and AM symbioses.

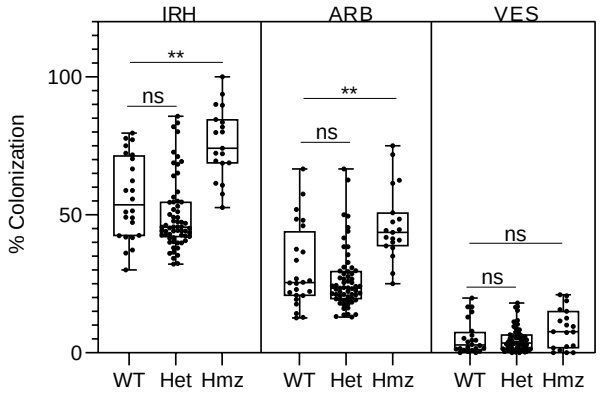

Figure 4.16. Homozygous *auk*^{GoF} mutants have increased AM colonization.

Percentage colonization of a segregating population of *auk*^{GoF} lines at 6 wpi with AM inoculum. Structures of intraradical hyphae (IRH), arbuscules (ARB) and vesicles (VES) were counted using the grid intersection method. Data are from 2 biological reps. Statistical tests used are a one-way ANOVA (**, $p<0.01$).

4.3- Discussion

In this chapter, phenotypic characterization is presented demonstrating a role of AUK in endosymbiosis signaling with both nitrogen-fixing rhizobia bacteria and AM fungi. CRISPR-Cas9 knockout of *AUK* in hairy roots abolished nodulation, indicating AUK is required for nodule organogenesis. Overexpressing *AUK* in *M. truncatula* hairy roots resulted in spontaneous nuclear Ca^{2+} oscillation, likely resulting in spontaneous nodule-like structures in absence of rhizobia, and in increased nodule number upon inoculation. Importantly, epistasis analysis of nuclear Ca^{2+} oscillation and nodulation indicated that AUK function is dependent on DMI1 as no nuclear Ca^{2+} oscillation was observed when overexpressing *AUK* in a *dmi1-1* mutant before or after addition of NF, and no nodule structures were observed, even at 100 dpi. The same experiments overexpressing *AUK* in a *dmi2-1* mutant produced spontaneous

nuclear Ca^{2+} oscillation and the presence of a few nodule-like structures at 100 dpi, indicating AUK functions downstream of DMI2, but DMI2 is still required for perception and proper induction of NF-induced nuclear Ca^{2+} and nodulation. In addition, overexpression of *AUK* resulted in increased AM colonization with a higher number of IRH and ARB, indicating a role for AUK in the common symbiosis signaling pathway for both endosymbionts.

Analyses of EMS mutant lines with mutations in the AUK kinase domain unfortunately did not enable identification of a knockout mutation. However, it did lead to identification of a gain-of-function mutation, which resulted in similar phenotypes to those seen in the overexpression experiments. These included the generation of spontaneous nuclear Ca^{2+} oscillations and spontaneous nodule-like structures, as well as increased nodulation with rhizobia and increased AM colonization. These phenotypes were confirmed using segregating populations, where only plants which were homozygous for the auk^{GoF} allele showed the above phenotypes, indicating that the mutation within *AUK* is responsible for the phenotypes, and that they are genetically recessive. This is an interesting concept that a recessive gene can result in such a drastic gain-of-function phenotype. However, the finding that AUK self-associate may hold the key to understanding this phenomenon. Having a mixture of wild-type and mutant AUK acting together may impact the function of the gain-of-function AUK, thus impairing its potential activation activity. There may also be differential effects in the epidermis and cortex and a future assessment of the requirement of AUK within each cell layer could help narrow down this effect. It is also imperative to test whether the *auk-1* mutation can be complemented genetically in addition to the action of overexpressing AUK^{GOF} within WT A17 hairy roots.

Additionally, the auk^{GoF} homozygous mutants had severely altered root system architecture, with shorter primary root and lateral roots; there was the same number of lateral roots relative to wild-type. This would suggest that AUK perhaps plays a role not in the lateral root initiation, but in its further length and development. Given that the *Arabidopsis* ortholog, *At*ZAR1 plays a role in asymmetric cell division in the embryo (Yu et al., 2016), it would be interesting to examine whether cell division is perturbed in the auk^{GoF} mutant. Overall, these results indicated an important role for AUK in both forms of endosymbiosis, but also in lateral root development, and thus proper functioning through a WT AUK may be important for root growth. Two other EMS mutants were analyzed. *auk-2* was observed to have reduced AM colonization in comparison to wild-type, and *auk-4*, had fewer nodules upon rhizobial inoculation. These results could signify a possible role for separating signaling for establishment of AM vs. rhizobial symbioses, particularly with *auk-4* mutation mutating the conserved kinase APE motif. However, this phenotype has not been confirmed via segregating populations, and thus at present is purely hypothetical as the phenotype may result from

another background mutation from the EMS. It will be important to confirm these results with segregating populations from a backcross.

The CRISPR-Cas9 system was employed in hairy roots to determine the effect of *AUK* knockout. Because of the prolific nature of hairy roots, there were multiple root system populations emerging from the same callus. Thus, it was important to count nodules per root system, rather than per plant, and root systems with and without nodules were sent for sequencing to determine whether there was a correlation with the cutting action of Cas9. This is indeed what was observed: that only those root systems lacking nodules showed Cas9 alleles cutting on both strands (Figure 4.1), indicating functional AUK is necessary for nodule development. Importantly, the sgRNAs were chosen to cut upstream of the kinase domain, but not right at the beginning of the gene, which implied that the kinase domain, or possibly kinase activity is important for the function of AUK in nodulation. Phenotyping results are summarized in Table 4.2.

Table 4.2. Summary of results for AUK phenotyping

Phenotype	**Summary of Results**
Ca^{2+} oscillation	-*AUK-OE* has spontaneous calcium oscillation -*dmi1/AUK-OE* does not have spontaneous or NF-induced oscillation -*dmi2/AUK-OE* as spontaneous, but not NF-induced oscillation -*auk-1/NLS-YC* has spontaneous oscillation -*auk-1 YC3.6* has spontaneous oscillation
Spontaneous nodulation	-*AUK-OE* has spontaneous nodule-like structures -*auk-1* has spontaneous nodule-like structures -in a segregating population, only hmz *auk-1* has spontaneous nodule-like structures
Nodulation	-*AUK-OE* has increased nodulation at 14, 21 and 60 dpi, but not 100 dpi -*dmi1/AUK-OE* has no nodules at 60 or 100 dpi -*dmi2/AUK-OE* has few nodules at 100 dpi -*aukcas9* has no nodules -*auk-1* has increased nodulation -*auk-4* has fewer nodules (but not backcrossed) -in a segregating population, only hmz *auk-1* has increased nodulation
AM colonization	-*AUK-OE* has increased AM colonization at 30% wild-type colonization, but not 10% -*auk-1* has increased AM colonization at 30% wild-type colonization -*auk-2* has decreased AM colonization at 30% wild-type colonization -in a segregating population, only hmz *auk-1* has increased AM colonization

Root system architecture	-At 14 dpi, hmz *auk-1* has shorter primary and lateral root length, but same number of lateral roots -At 25 dpi, hmz *auk-1* has shorter lateral root length, but same length primary root and same number of lateral roots

Further genetic analysis was carried out with the overexpression of *AUK* in hairy roots under the *pLj*UBI constitutive promoter. It is important to note that constitutive expression can result in aberrant phenotypes as the *AUK* gene may have been expressed in tissues or at developmental stages when it would not be under the control of its own promoter. The identification of a gain-of-function mutant showing the same phenotypes as the over-expressor experiments was a confirmation of the phenotypes of spontaneous Ca^{2+} oscillation and nodulation, and that inoculated nodulation and AM colonization were indeed resulting from the action of AUK. It would be of interest in the future to assess the infection phenotype of the auk^{GoF} mutant to identify whether there is increased infection leading to the increased nodulation phenotype. This could be especially important as infection and nodulation can be uncoupled (Madsen *et al.,* 2010), indicating the need to determine whether AUK simply plays a role in generation of the nodule-like structure rather than the infection process *per se*. Additionally, analysis of early signaling genes in nodulation, such as *ENOD11, NIN,* and *NFYA1/2,* as well as AM marker genes *PT4, NADP oxidase,* and *SbtM4* would be useful to determine whether the auk^{GoF} induces signaling genes in absence of symbiont, and whether the spontaneous Ca^{2+} oscillation observed in this mutant is sufficient to activate these symbiotic genes.

The timing of the phenotypes is important to note to place AUK within the common symbiosis signaling pathway. AUK seemed to act early in nodulation, with increased nodulation phenotype observed at 14 dpi, which is considered an early timepoint, whereas at 100 dpi with transformed roots overexpressing *AUK* there was no significant difference from the EV. The opposite case was observed with AM colonization, where a significantly higher percentage colonization in AUK-OE was only observed at approximately 30% wild-type colonization, not the earlier 10%.

The epistasis analysis of Ca^{2+} oscillation, nodulation, and AM colonization of *AUK* overexpression in the *dmi1* and *dmi2* mutant backgrounds placed AUK upstream of DMI1 nuclear Ca^{2+}, but downstream of DMI2 perception at the plasma membrane. Along with its co-localization and association with DMI1, this indicates that AUK could be functioning to activate DMI1 to induce nuclear Ca^{2+}. A previous study suggested, based on HEK cell experiments with LjCASTOR, that DMI1 could be functioning as a Ca^{2+} channel mediating the nuclear Ca^{2+} (Kim *et al.,* 2019). However, *CASTOR* does not complement *dmi1* (Chen *et al.,* 2009), and a more recent study with a constitutively active variant of DMI1 suggests that

DMI1 rather functions as an activator of CNGC to generate the nuclear Ca^{2+} oscillation (Liu *et al.,* 2022). This is important in relation to this study, as it corroborates the basis of the hypothesis with mastoparan activation of symbiosis-like nuclear Ca^{2+} in the *dmi1* mutant (Sun *et al.,* 2007); that CNGC15 is more likely the Ca^{2+} channel, however DMI1 is serving to activate it in the context of symbioses. This activation could be through AUK-induced phosphorylation changing the configuration of the DMI1 channel, allowing it to activate the Ca^{2+} generation by CNGC15.

There is interplay between phytohormone pathways in regulating root development, as well as accommodation of endosymbionts, with the proposal that nodulation has co-opted the lateral root development program (Dong *et al.,* 2021; Franssen *et al.,* 2015; Schiessl *et al.,* 2019; Soyano *et al.,* 2019, 2021). Thus, it would be interesting to further investigate via RNAseq the expression of genes perturbed in the auk^{GoF} mutant both in context of nodulation and lateral root development.

Overall, this chapter presents the requirement for AUK in nodulation and its important role in regulation of nuclear Ca^{2+} oscillation leading to nodulation and AM colonization. A gain-of-function mutation within the activation loop of the kinase domain could induce Ca^{2+} oscillation and nodule formation spontaneously, in the absence of rhizobia, with the action of AUK dependent on DMI1, but downstream of DMI2 perception. A potential role for AUK in root system architecture is also explored.

5- Mechanistic analysis of AUK interaction with DMI1

5.1- Introduction

In the previous chapters, it was demonstrated that AUK interacts with DMI1 using *in vitro* and *in planta* experiments. Using CRISPR-Cas9 and the phenotypical analysis of an AUK gain-of-function mutant, it was further demonstrated that AUK is required to modulate nuclear Ca^{2+} oscillation, nodulation, and arbuscular mycorrhizal colonization. The action of AUK was shown to function downstream of DMI2, but dependent on DMI1. The *auk*^{GoF} mutant presents spontaneous Ca^{2+} spiking and spontaneous nodule organogenesis, demonstrating that the gain-of-function mutation is sufficient to activate the ion channels and generate nuclear Ca^{2+} oscillation. Interestingly, *AUK*^{GoF} carries a mutation at the start of an extension within the kinase activation loop. Although the function of this extension is not known, it could be hypothesized that AUK might activate DMI1 through phosphorylation.

In both prokaryotes and eukaryotes, phosphorylation by protein kinases is one of the most widespread posttranslational modifications. It is a highly dynamic process and is one of the earliest responses in many signaling pathways in plants and animals. Phosphorylation can also be reversed by protein phosphatases, although plant genomes tend to encode more protein kinases than phosphatases (Li & Liu, 2021), indicating protein kinases as a mechanism for encoding signal specificity. Phosphorylation involves addition of a phosphate group via an ester bond with the hydroxyl groups of serine, threonine or tyrosine residues, with serine as the most commonly phosphorylated residue at 80-85% of the sites in *Arabidopsis* (van Wijk *et al.*, 2014). There have also been reports of phosphorylation on histidine and aspartate residues in two-component phosphorelay signaling pathways (Besant & Attwood, 2009; Lohrmann & Harter, 2002), and of arginine for which the function is thus far unknown (Trentini *et al.*, 2014).

RLKs account for a large proportion of the kinases in plants, and in *Arabidopsis* account for nearly 2.5% of protein coding genes (Shiu & Bleecker, 2001). These typically have a large extracellular domain for ligand binding, a transmembrane domain, and a catalytic domain in the cytoplasm. Phosphorylation can modulate activity of downstream targets within a signaling pathway. Kinases can either be membrane-bound or soluble. A typical signal transduction pathway for RLKs is the activation at the membrane via ligand-binding, a cascade of phosphorylation events including auto- and transphosphorylation of downstream targets, often a receptor-like cytoplasmic kinase (RLCK), which dissociates from the receptor complex and translocates to the nucleus where it can activate or inactivate transcription factors. Protein phosphorylation status can also dictate its subcellular localization or polarization, such as in the case of the CAMEL-CANAR complex where CAMEL phosphorylation of PIN1 cytoplasmic loop dictates its trafficking and polarization (Hajný *et al.*, 2020). Phosphorylation

in many signaling pathways can be a way to transmit or amplify signal through systematic activation by enzymes and second messengers. Plasma membrane localized receptors such as LRR-RLKs and LysM-RLKs function both in signal perception and then their kinase activity activates downstream kinases in a phosphorylation cascade, eventually catalyzing phosphorylation of transcription factors or metabolic enzymes for signal response. One example that nicely illustrates activation of targets through phosphorylation and phosphorylation control of localization is in brassinosteroid signaling, Brassinosteroid (BR) binding to the extracellular domain of BRASSINOSTEROID INSENSITIVE1 (BRI1) induces its association with BRI1 ASSOCIATED RECEPTOR KINASE1 (BAK1), catalyzing transphosphorylation between the two (Kinoshita *et al.,* 2005; Wang *et al.,* 2008). This leads to activation of the BRI1 kinase and dissociation from the inhibitor BRI1 KINASE INHIBITOR1 (BKI1) (Wang & Chory, 2006), which phosphorylates its downstream BR-SIGNAKING KINASES (BSK) substrates (Tang *et al.,* 2008). Increased BR signaling results in inactivation of BRASSINOSTEROID INSENSITIVE2 (BIN2) (Li & Nam, 2002). BIN2 phosphorylates BRASSINOZOLE RESISTANT 1 (BZR1) and BRI1 EMS SUPPRESSOR (BES1), which expels them from the nucleus where they are retained in the cytoplasm by 14-3-3 proteins (Gampala *et al.,* 2007; He *et al.,* 2002; Ryu *et al.,* 2007, 2010). Phosphoproteomic screens have identified many proteins possessing several different phosphorylation sites catalyzed by unique protein kinases. This allows for integration of information from different signalling pathways for the appropriate plant response. Such is the case for SPEECHLESS (SPCH), a hub for regulating cell fate with roles in stomata formation (Gudesblat *et al.,* 2012), which is phosphorylated at different residues by MAPKs, BIN2 and SnRK2s to suppress its function (Houbaert *et al.,* 2018; Lampard *et al.,* 2008; Yang *et al.,* 2022). It is also stabilized by phosphorylation by two other kinases CDKA;1 and KIN10, on different residues (Han *et al.,* 2020; Yang *et al.,* 2015). Unique phosphocodes have also been observed for the a remorin protein StREM1.3 in responding to viruses (Rocher *et al.,* 2022), for AhSYMRK dictating its auto- and transphosphorylation (Bhattacharya *et al.,* 2019), and for BAK1 allowing it to function in either immunity or brassinosteroid signaling (Perraki *et al.,* 2018). Protein disordered regions have been shown as overrepresented in phosphoproteomic screens (Christian *et al.,* 2012), indicating the necessity of phosphorylation to stabilize the protein, possibly allowing it to interact with downstream signaling partners or in the case of transcription factors, allowing DNA-binding through addition negative charge accumulation (Kirchler *et al.,* 2010; Ni *et al.,* 2013).

In this chapter, the effect of the gain-of-function mutation on AUK is investigated via homology modelling and whether AUK could modulate DMI1 function via phosphorylation is explored. Experiments performed to gain more structural insights into the perturbation by

the amino acid substitution and show preliminary experiments leading to the postulate that AUK can phosphorylate DMI1 *in planta* at specific residues are explored.

5.2- Results

5.2.1- Predicting effects of AUK^{GoF} mutation on protein structure

In Chapter 4, AUK^{GoF} was shown to induce spontaneous nuclear Ca^{2+} oscillation leading to spontaneous nodules, increased nodulation upon inoculation with rhizobia, and increased AM colonization. This P>S mutation is located at the beginning of the kinase activation loop, which an alignment shows is of extended length in comparison to the activation loop of structurally-related kinases. To determine what might be the function of this mutation, the predicted structure of AUK was retrieved from Alphafold (Figure 5.1a). A superposition of AUK with *Zm*SIRK1 (PDB: 5uv4), which was determined by Swiss Model to be structurally similar to AUK, indicated that this extended kinase activation loop did not align, and the Alphafold structure indicated that the loop was entirely disordered (Figure 5.1b). Thus, it was difficult to predict a function of the mutated proline residue.

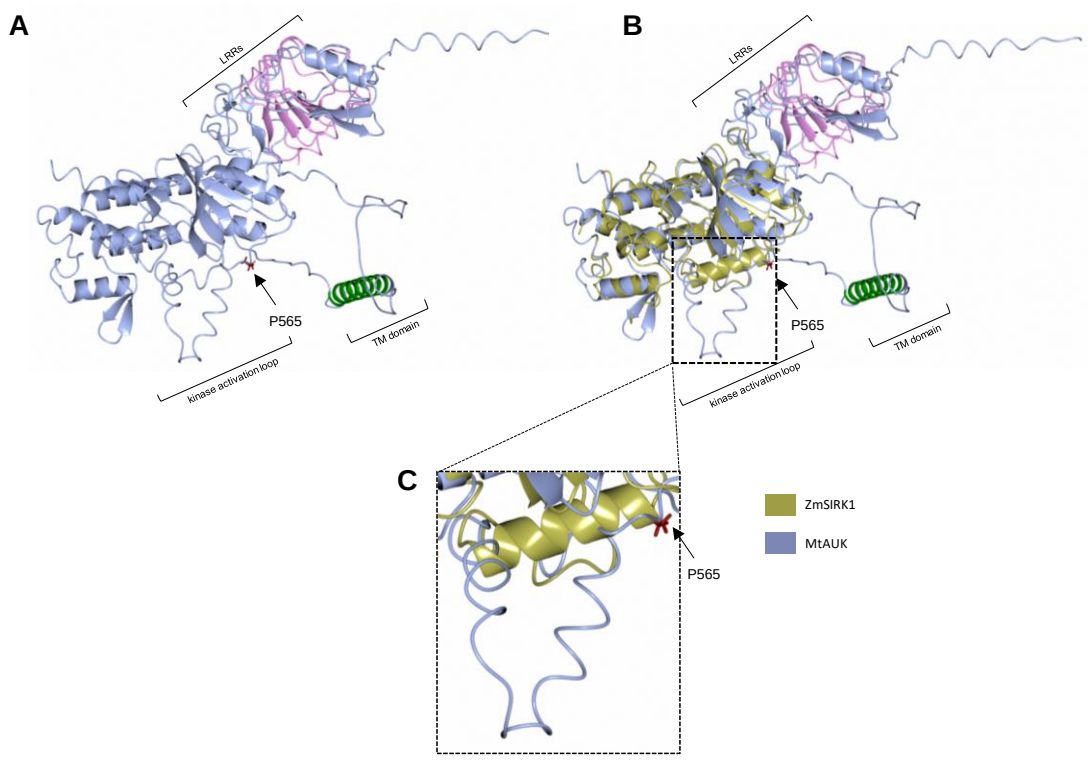

Figure 5.1. Structural analysis of AUK

A. Full-length AUK predicted structure from Alphafold 2.0. Pink indicates LRRs, green indicates the transmembrane domain and blue indicates the N- and C-termini. Residue P565 is highlighted in crimson. **B**. Superposition of the AUK kinase domain (blue) with that of *Zm*SIRK1 (yellow). Residue P565 is indicated in crimson at the beginning of an extended

kinase activation loop, which does not superpose onto the *Zm*SIRK1 structure. **C.** Zoom on the activation loop indicated in (B).

Due to the difficulty of prediction of the effect of mutating P565 from the disordered region within the protein predicted structure, attempts were made to purify and crystallize the wild-type AUK and AUK^{GoF}. It was possible to purify AUK^{GoF} kinase domain from *E.coli* to similar high concentration as the wild-type variant (Figures 3.4, 5.2a). Crystal screens were first set up with just the wild-type AUK at two concentrations, 5 mg/mL and 10 mg/mL, to assess in preliminary crystal screens which concentration would give a good mixture of precipitation and clear droplets, with approximately half of the droplets showing precipitate, and half clear. The first screen attempted was the KISS screen (Molecular Dimensions), which can establish conditions that are easily optimized, and the MORPHEUS® screen (Molecular Dimensions), which is suggested for screening of membrane proteins, and several other structurally-related protein kinases. These initial screens did not yield any hits; however it was determined that 10 mg/mL was a good concentration to have sitting drops with a 50:50 mix of droplets with precipitation or clear (Figure 5.2b). Thus, 10 mg/mL concentration was used to set up a further three crystal screens with both the wild-type and AUK^{GoF} kinase domain: PACT Premier™, which is a screen of different pHs with PEG concentration and different ions, JCSG Plus™ screen, which includes different salts and PEG concentrations and Basic Chemicals Screen (BCS) Additives screens (all from Molecular Dimensions), which contains more unusual agents, proven successful with many proteins. It was hypothesized that perhaps the wild-type variant disordered region results in protein instability, but the mutation might serve to stabilize the protein in an active form, potentially creating less disorder and allowing crystal formation. Unfortunately, no hits were observed in these additional screens with either wild-type or AUK^{GoF} beyond some precipitation and salt crystals, and thus it was impossible to progress further to determine the protein structure. Given the determination of a good concentration to use in screens, it would be good in future to set up additional crystallization screens, possibly with hanging drop crystallization as well as the possible use of adenylyl-imidodiphosphate (AMP-PNP) or the kinase in complex with interacting proteins that may bind and stabilized the disordered activation loop to try to stabilize for crystallization.

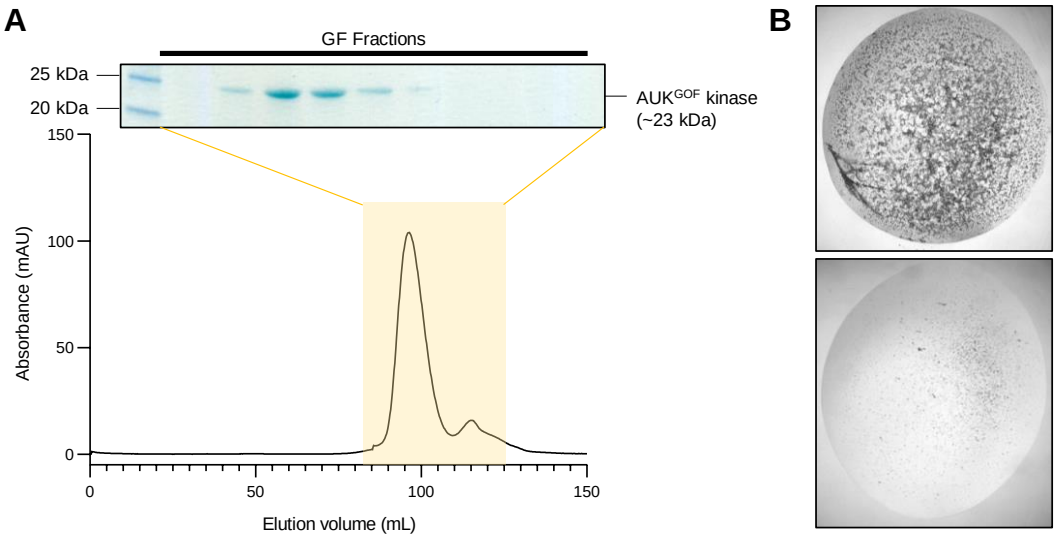

Figure 5.2. Purification and crystallization of AUK^{GoF}

A. Elution trace of AUK^{GoF} kinase domain (~23 kDa size) after expression in *E. coli* and purification using IMAC followed by gel filtration with Superdex S200 16/60 gel filtration column. The chromatograph shows absorbance values (AU) for protein as it was eluted from the column (elution volume, mL). The yellow box indicates fractions that were collected for SDS-PAGE purification assessment, shown above. **B**. Representative sitting drop pictures from PACT Premier crystal screen taken by RockMaker™ Imager. Top shows precipitation and bottom panel shows a clear droplet.

5.2.2- Full-length AUK can be expressed in *Sf9* insect cells and purified

Given the lack of success with crystallizing the kinase domain of AUK, another possibility was to determine the structure of full-length AUK via cryo-EM. The full-length AUK, however, is only 78 kDa, and thus would likely be too small to have good resolution for cryo-EM of a single unit. However, previous purifications and evidence in Y2H system had indicated oligomerization of AUK (Figure 3.1c), which could allow for large enough protein structure determination via cryo-EM. Although actual determination of cryo-EM structure was outside the scope of timing within the PhD project, experimentation with expressing the full-length AUK in insect cells and small-scale purification was done to determine its feasibility for cryo-EM in the future (Figure 5.3).

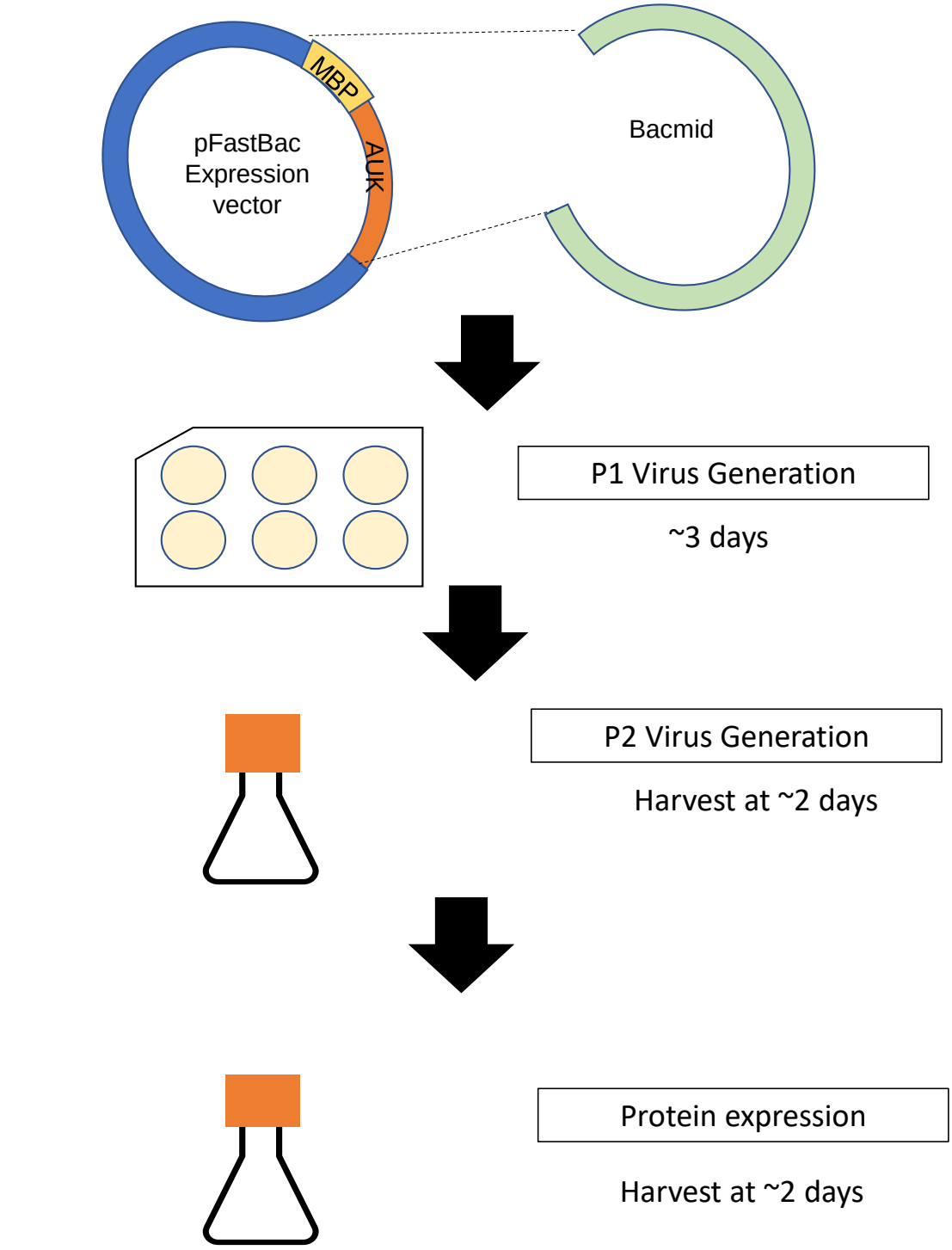

Figure 5.3. Purification scheme for AUK full-length from *Sf*9 insect cells.

Full-length AUK was first subcloned into pFastBac expression vector with an MBP tag and then into Bacmid from DH10Bac cells. Generation of the virus through P1 and P2 stages is indicated followed by protein expression and harvesting.

InFusion cloning was used to subclone full-length AUK into pOPINM to retrieve an MBP tag in-frame and then further subcloning was done MBP-AUK into pFastBac for expression in *Sf9* insect cells. After production of P1 and P2 viral amplification, virus was used to infect 50 mL small-scale insect cells to test expression and purification over an MBP-Trap column. The workflow for insect cell protein expression and small-scale purification is indicated in a diagram in Figure 5.3. It was observed that AUK could be expressed in the insect cells, and it could be purified and eluted from the MBP column as full-length with soybean polar lipids in the elution buffer (Figure 5.4). Thus, this work indicates that it could be possible for larger scale expression and purification perhaps from 1-2 L, of full-length AUK from insect cells for further determination of oligomerization status and possible structural determination in the future.

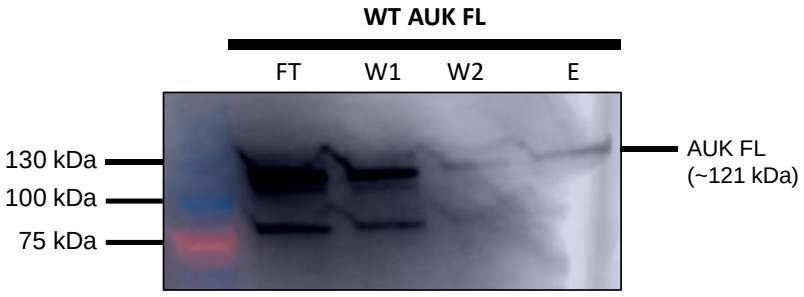

Figure 5.4. Small-scale purification of full-length AUK from insect cells
Immunoblot using α-MBP of full-length MBP-AUK (~121 kDa size) purified from 50 mL small-scale protein expression in *Sf*9 insect cells following elution from an MBPTrap column. Ft, flow-through, W1 and W2, washes, E, elution.

5.2.3- AUK^{GoF} associates with DMI1

As the AUK gain-of-function mutation is within the kinase activation loop, it could be hypothesized that it might be mimicking either constitutive phosphorylation within the activation loop to activate the kinase activity, or the binding of an interaction partner to stabilize the disordered region to activate kinase activity. This activation of kinase activity may then lead to phosphorylation of DMI1 through its interaction with AUK, subsequently activating the DMI1 channel activity for production of nuclear Ca^{2+} oscillation. To determine whether this was a possibility, it was important to confirm that the AUK^{GoF} mutation did not hinder the interaction between AUK and DMI1. As the kinase domain of AUK was able to be purified with the P565S mutation (Figure 5.2a), this was first used for a BLItz assay to determine the binding affinity *in vitro.* It was determined that the K_D value was not significantly different between wild-type and AUK^{GoF} interaction with DMI1 (Figure 5.5a-d), confirming that *in vitro* the gain-of-function mutation does not affect AUK kinase domain

interaction with DMI1 C-terminus. It was also important to perform *in planta* experiments to confirm that within the biological context of symbiotic *M. truncatula* root system, the full-length proteins associate. Indeed, a co-IP experiment in *Sm*2011 inoculated *M. truncatula* hairy roots confirmed that AUK^{GoF} could associate with DMI1, but not with the negative control DMI3 (Figure 5.5e). Thus, the gain-of-function mutation does not have an impact on AUK interaction with DMI1, suggesting that it may promote constitutive activation of the kinase domain and enable constitutive phosphorylation activity to occur.

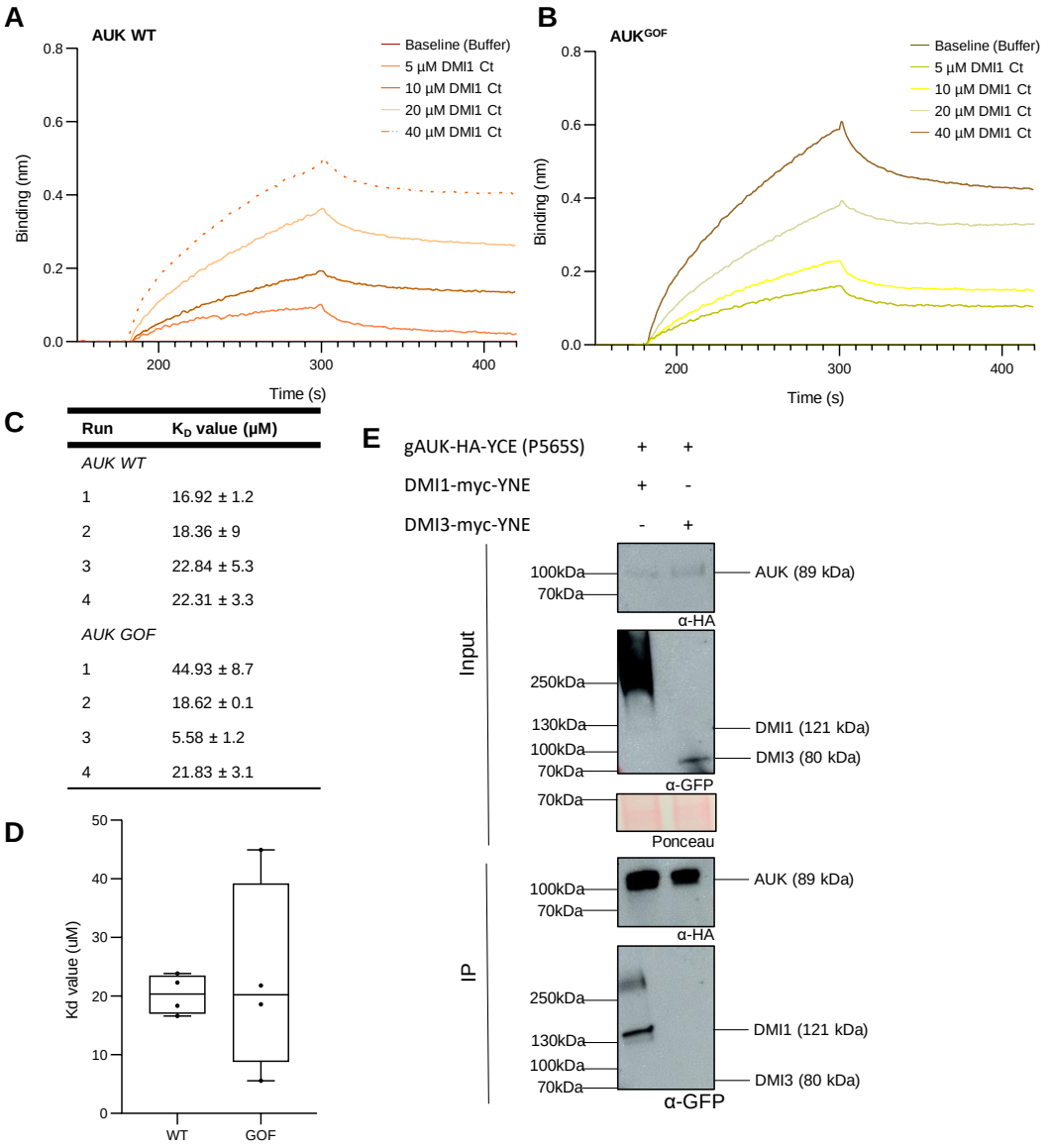

Figure 5.5. DMI1 associates with AUK via BLItz and co-IP in *M. truncatula* hairy roots

A-B. DMI1 association K_D values were determined for AUK kinase domain by BLItz assay. Baseline was established with A4 buffer and 20 µM His-MBP-AUK (A) or His-MBP-AUK^{GoF} C-terminus attached to Ni^{2+}-NTA tips. Purified untagged DMI1 C-terminus was assessed for binding to AUK WT and GoF kinase domain at 5 µM, 10 µM, 20 µM, and 40 µM. Data shown are averages for 4 replicates from 2 separate protein purifications. **C.** Table indicating the K_D

values from each BLItz assay with wild-type and GoF AUK. **D.** K_D values for WT and GoF AUK kinase domain interaction with DMI1 C-terminus from A-C. Statistical test performed was unpaired t-test. **E.** co-immunoprecipitation from *M. truncatula* hairy roots inoculated with *Sm*2011 for 14 days. Immunoprecipitation was done with α-HA beads (μMacs) and immunoblotting with α-HA to observe AUK and α-GFP N-term to observe DMI1 or DMI3. Input and IP samples are shown and Ponceau is included to show equal loading.

5.2.4- Assessing phosphorylation of DMI1 by AUK

The above results suggest that AUK interaction with DMI1 might modulate and activate channel activity through phosphorylation. As both proteins could be purified from *E. coli* (Figures 3.3-3.4), this was first tested this through an *in vitro* kinase assay using AUK kinase domain and DMI1 C-terminus. ProQ Diamond gel stain was used for detection of phosphoproteins. Interestingly, phosphorylated DMI1 was observed even in absence of AUK (Figure 5.6), indicating DMI1 might be phosphorylated in *E. coli* by endogenous kinases. This is plausible as DMI1 shows structural homology with the bacterial MthK channels (Peiter *et al.*, 2007), and thus the phosphorylation machinery may be present in bacterial species. Autophosphorylation of AUK kinase domain was also observed in presence of ATP without addition of DMI1 to the experiment (Figure 5.6), which is unsurprising as AUK self-associates (Figure 3.1c), and many RLKs function through oligomerization and activation of their kinase activation loop through autophosphorylation (Oh *et al.*, 2018; Wang *et al.*, 2008). To avoid DMI1 phosphorylation in *E. coli*, attempts were made to co-express DMI1 with a lambda phosphatase, however this resulted in the *E.coli* growing much slower, and despite 24 h induction with IPTG and 16 L of *E.coli*, only very low amounts of DMI1 could be purified. This may indicate that DMI1 phosphorylation functions to stabilize the protein. Additionally, the slow *E.coli* growth could result from the inhibition of phosphorylation by important bacterial proteins which require phosphorylation for optimal growth.

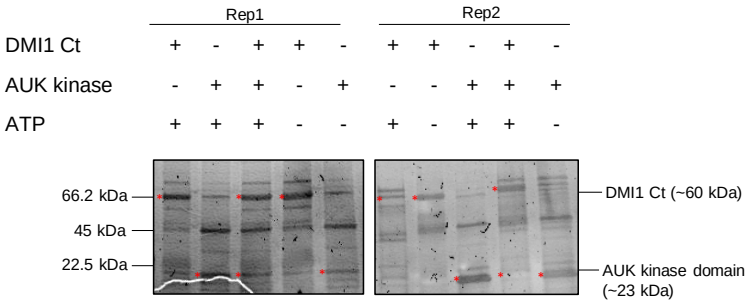

Figure 5.6. Phosphorylation of DMI1 and AUK

ProQ Diamond phosphoprotein stain gel with purified untagged DMI1 Ct and AUK kinase domain loaded in wells as indicated with and without ATP. Imaged on a Typhoon fluorescence

imager. Phosphorylation assay was repeated twice with similar results. Asterisks indicate the expected band size.

As a result of the problems detailed above with *in vitro* experiments, it became imperative to look at phosphorylation using *in planta* experiments. As overexpression of both the wild-type and gain-of-function AUK led to spontaneous activation of nuclear Ca^{2+} oscillation in *M. truncatula* roots, AUK or AUK^{GoF} was next co-expressed with DMI1 in *M. truncatula* hairy roots both inoculated and uninoculated with *Sm*2011 to determine whether similar phosphorylation sites could be identified. Overexpression of DMI1 was used with an empty vector as negative control to determine AUK-specific phosphorylation sites. This experiment required the planting of 100 well-transformed plants per line in TerraGreen and sand mix for 1 week followed by 14 d growth after inoculation before digging out the plants. Around 5 g root material was used for each construct and condition. Figure 5.7 depicts the workflow for this *M. truncatula* hairy roots IP followed by LC-MS/MS.

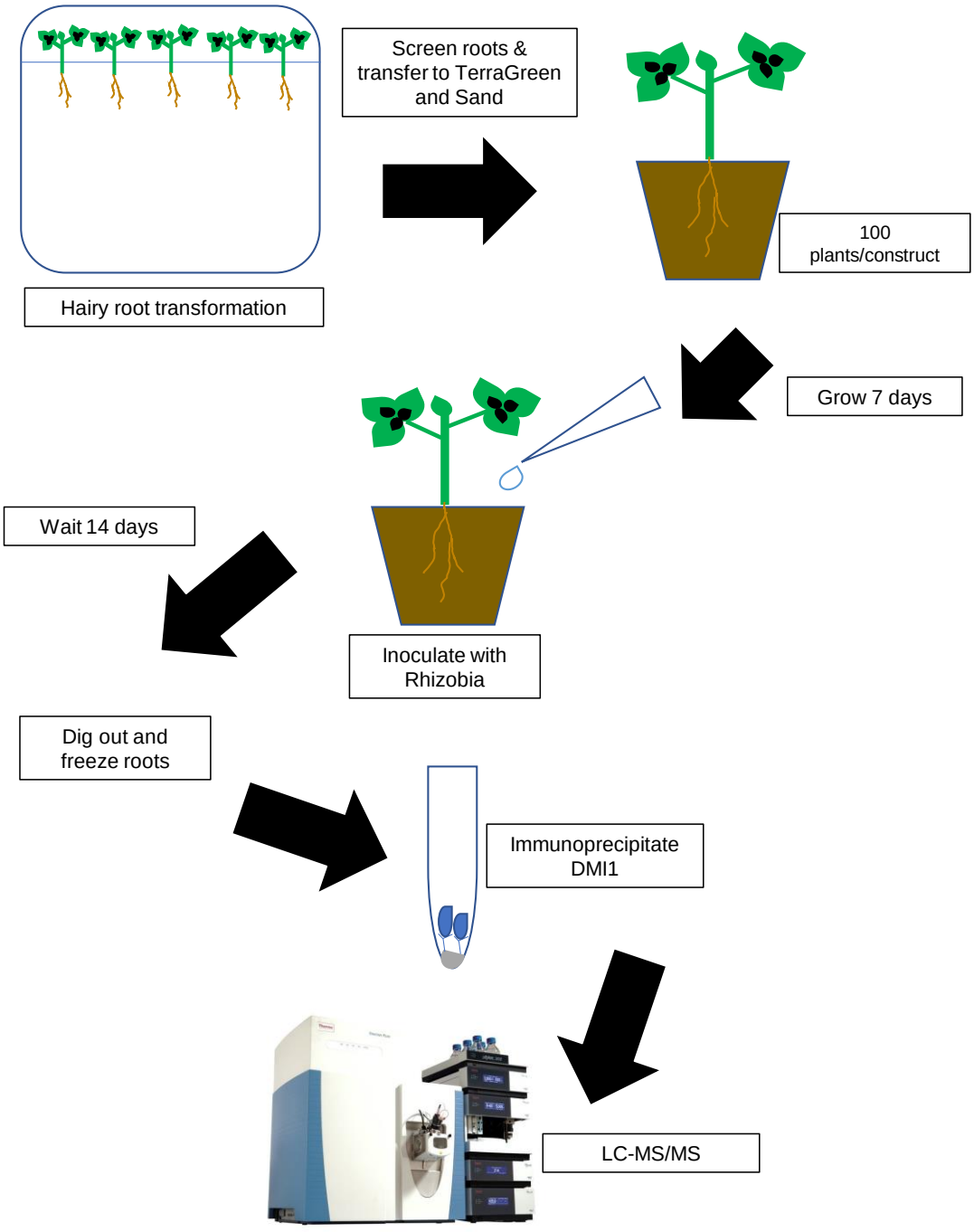

Figure 5.7. Workflow for identification of phosphopeptides from *M. truncatula* hairy roots

DMI1 was immunoprecipitated using ChromoTek Myc-trap beads and the immunoprecipitation of DMI1 was assessed by anti-GFP Nterm immunoblotting (Figure 5.8). In parallel, a Coomassie gel was run and the band corresponding to DMI1 was excised and prepared for trypsin digestion and LC-MS/MS. The latter was performed by Gerhard Saalbach and Carlo Oliveria Martins of JIC proteomics facility. Putative phosphorylation on serine threonine and tyrosine residues was assessed as AUK is predicted by Interpro scan to be a

dual-specificity kinase, with potential for transphosphorylation of serine, threonine and tyrosine residues on its target substrate. In order to observe the T24 phosphosite which was known to be phosphorylated in *L. japonicus* (Zhang *et al.*, 2019), the peptide threshold had to be dropped to 20% peptide confidence with 99% protein confidence. Thus, the localization of the phosphosites was difficult to determine with precision within the phosphopeptide, and the findings were deemed inconclusive. Overall, this experiment will need to be repeated in the future to identify specific residues phosphorylated in DMI1 by AUK^{GoF}. Possible amendments to the method could include use of more starting material for the immunoprecipitation or the elimination of the in-gel trypsin digest, which can affect protein yield and impact large membrane proteins.

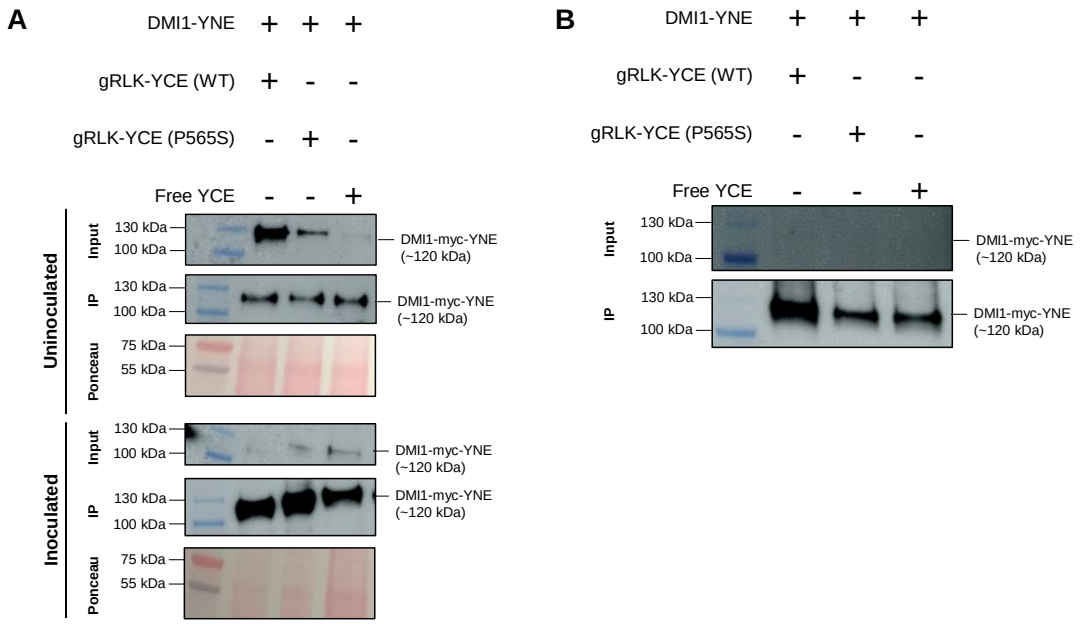

Figure 5.8. Immunoprecipitation of DMI1-myc-YNE in *M. truncatula* hairy roots and *N. benthamiana* leaves for analysis of phosphorylation sites.

Immunoprecipitation of root tissue expressing DMI1-myc-YNE with the indicated constructs, gRLK-HA-YCE (WT), gRLK-HA-YCE (565S) from *M. truncatula* uninoculated and inoculated with Sm2011 **(A)** and from *N. benthamiana* leaves **(B)**. Bands of DMI1 were extracted from 10% SDS-PAGE gel for LC-MS/MS analysis of phosphorylated residues.

As DMI1 and AUK associate in *N. benthamiana* leaves at the nuclear envelope (Chapter 3.2.5), and as previous studies have examined phosphorylation in both *Arabidopsis* roots and *N. benthamiana* leaves and identified similar sites (Piquerez *et al.*, 2014), AUK or AUK^{GoF} were co-expressed with DMI1 in *N. benthamiana* leaves and DMI1 was immunoprecipitated (Figure 5.8). LC-MS/MS analysis revealed several phosphosites with high confidence level and higher protein coverage than the experiments in *M. truncatula* roots. This led to the identification of constitutive phosphorylation in S4, T24, S27, S70, T71, and

S72 as well as AUK-specific sites S115, S772, S774 (Table 5.1, Figure 5.9). Using the structure of *M. truncatula* DMI1 C-terminus (Liu *et al.*, 2022), it could be seen that these sites are accessible and could conceivably be phosphorylated by AUK (Figure 5.10). However, the AUK-specific sites S115, S772 and S774 were not present in the AUK^{GoF}. This may have resulted from the low abundance of phosphopeptides seen (2-3 peptides each), or there may be specific factors in *N. benthamiana* leaves which may inhibit correct protein folding or interaction to facilitate the phosphorylation of AUK^{GoF} in comparison to the wild-type variant.

Table 5.1. List of phosphopeptides identified in *N. benthamiana* leaves (+, identified; NC, no coverage; *, phosphorylated residue)

Phosphosite	Phosphopeptide	DMI1+gAUK (WT)	DMI1 + gAUK (GoF)	DMI1+Free YCE
S4	[M].AKS*NEESSNLNVMNKPPLK.[K]	+	+	+
T24	[K].TKT*LPSLNLR.[V]	+	+	+
S27	[K].TKTLPS*LNLR.[V]	+		+
S70	[K].TDFSEQQWNYPSFLGIGS*TSR.[K]	+	+	+
T71	[K].TDFSEQQWNYPSFLGIGST*SR.[K]	+	+	+
S72	[K].TDFSEQQWNYPSFLGIGSTS*R.[K]	+	+	+
S115	[K].TTSSLLPQPSS*SSITK.[Q]	+		
S732	[R].DTKS*TSLR.[L]	NC	NC	+
S772	[R].NLVS*VSR.[I]	+		
S774	[R].NLVSVS*R.[I]	+		

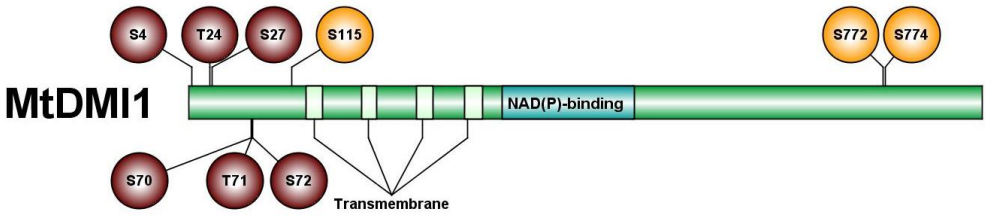

Figure 5.9. Phosphosites identified on DMI1 in *N. benthamiana* leaves

A. Position of phosphosites determined by immunoprecipitation of DMI1-myc-YNE indicated in Table 5.1. Constitutive phosphosites are indicated in crimson and AUK-specific in orange above the protein diagram.

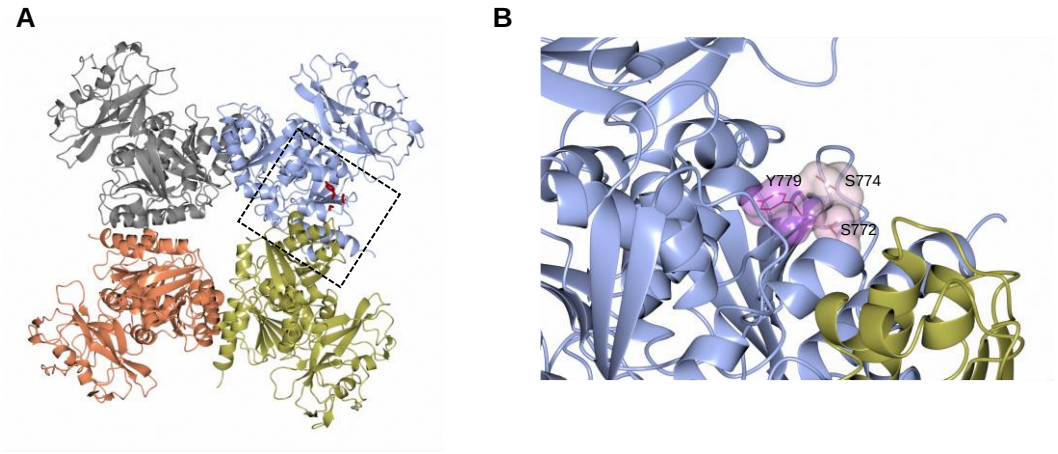

Figure 5.10. Phosphorylated residues identified on DMI1 C-terminus are solvent accessible

Structural model of DMI1 C-terminus derived from the PDB 7vm8 from (Liu *et al.*, 2022). **A.** indicates position of the identified C-terminal phosphorylation sites within one of the 4 tetrameric units of DMI1 in crimson. **B.** Close-up denoted by the dashed line in (**A)**. Space filling model indicates the accessibility of the residues on a scale of red to blue, with S772 and S774 very solvent accessible.

Future work should include repeating the experiment in *M. truncatula* roots to confirm the AUK-specific phosphorylation sites as well as generation of phosphodead and phosphomimetic DMI1 mutants to test the function of those sites on DMI1 function via complementation of the *dmi1-1* mutant. It will also be important to back this up with localization studies to ensure that mutation of the phosphorylation sites does not simply inhibit correct nuclear envelope localization of DMI1 as phosphorylation has been shown to play a role in dictating subcellular localization for some plant proteins (Gampala *et al.*, 2007; Hajný *et al.*, 2020; Ryu *et al.*, 2007, 2010). Overall, these phosphorylation experiments have shown preliminary evidence that AUK may be phosphorylating residues in the C-terminus of DMI1, which may be required to activate the nuclear Ca^{2+} oscillation.

5.3- Discussion

This chapter presents analysis of the mechanism by which AUK association with DMI1 might be functioning to activate nuclear Ca^{2+} oscillation in endosymbiosis signaling, with a focus on phosphorylation mechanisms. It shows that the AUK^{GoF} mutant still associates with DMI1 at a similar binding affinity to the wild-type. This mutation affects a residue at the beginning of the kinase activation loop, which is extended in comparison to conserved kinase domains in structurally-related (as determined by Swiss-Model) plant protein kinases. Since this region does not map onto existing protein kinase structures, and kinase activation loops are often

disordered without phosphorylation or binding of other interacting proteins, it is difficult to predict the precise impact of this mutation. Therefore, preliminary crystal screening attempts are presented to determine the structure of the AUK kinase domain, which although unsuccessful, provided information about future steps to perform to possibly generate crystals. In addition, it was shown that full-length AUK can be purified from insect cells, and thus could serve as a tool in future structural studies, perhaps by cryo-EM. Finally, preliminary evidence is presented that AUK can phosphorylate DMI1. *In vitro* study has shown that DMI1 is phosphorylated in *E. coli*, and this phosphorylation may stabilize it for purification. In addition, preliminary evidence is provided for autophosphorylation of AUK. *In planta* experiments in *N. benthamiana* leaves have provided evidence for putative AUK-specific phosphorylation sites within the C-terminus of DMI1. Conclusions from this chapter are summarized in Figure 5.11.

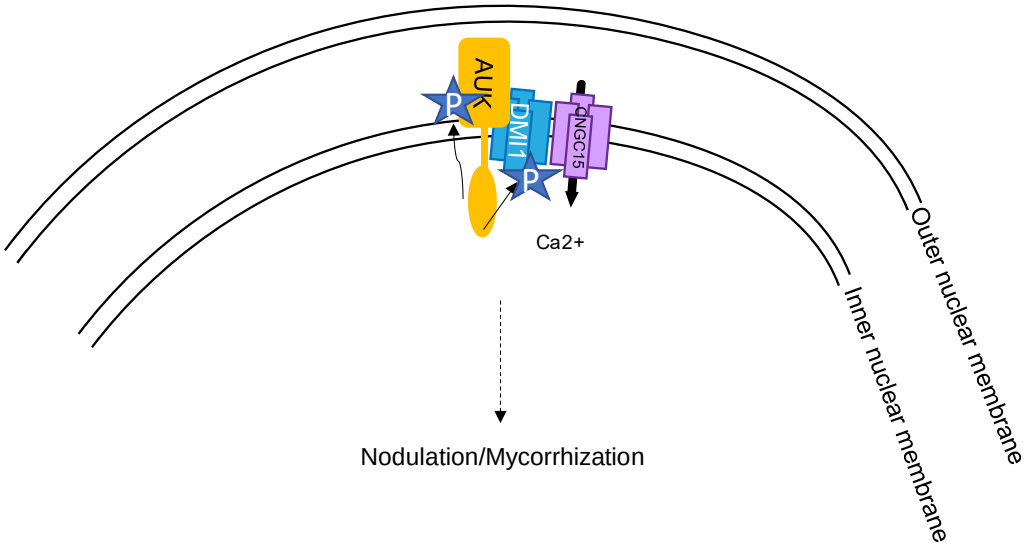

Figure 5.11- Summary of AUK phosphorylation of DMI1.
AUK autophosphorylates and putative AUK-specific phosphorylation sites have been identified on DMI1, S772 and S774 that may activate the nuclear calcium oscillation and allow nodulation and mycorrhization in the presence of symbiont Nod or Myc factors.

For protein kinase activation, a segment of the kinase domain, termed the activation loop, is often phosphorylated, and this phosphorylation can allow for a change in conformation via interaction between the negatively charged phosphate and positively charged amino acids within the activation segment. The activation segment is defined as the region between and including the conserved DFG and APE residue motifs, which typically consists of 20-40 residues. Interestingly, in AUK there are 51 residues in the activation segment (Figure 4.7). Within this activation segment, many kinases are regulated by phosphorylation of one or more residues. This phosphorylation generally stabilizes the active conformation for substrate

binding, and in the inactive, unphosphorylated state this region is typically disordered (Goldberg *et al.,* 1996; Meng *et al.,* 2002; Sicheri *et al.,* 1997). This disorder may also contribute to the difficulty in crystallization of the AUK kinase domain. Additionally, it is possible that this extended activation loop may serve as a binding area for interacting proteins or positioning of the substrate to allow phosphorylation. Thus, the use of a phosphomimic version of AUK within the activation loop or purification and crystallization with a yet unknown interacting partner within this disordered activation loop region may function to stabilize it allowing for crystallization. The addition of AMP-PNP has also been used for crystallization of kinase domains for structural analysis, and thus this could also aid in protein crystallization (Aquino *et al.,* 2017).

It is important to note that an AUK mutant with 15 residues of the extended activation loop deleted maintained the ability to associate with DMI1 in BiFC experiments (Figure 3.8). It could be hypothesized that the proline to serine mutation induces a conformational change within the AUK kinase domain, which mimics or constitutively activates the binding of an interacting partner to activate the kinase activity, corresponding to the spontaneous phenotypes observed with the *auk*^{GoF} mutant. The BLItz and co-IP experiments indicated that AUK^{GoF} has the same binding affinity to DMI1 as the wild-type variant. Notably, the K_D value is lower in these BLItz experiments than those observed in Chapter 3. This may result from the change in which interacting partner was attached to the Ni^{2+}-NTA tips. In the earlier case, DMI1 was attached to the tip, but here tagged AUK kinase domain and untagged DMI1 was used. In BLItz, it is recommended for the smaller protein to be affixed to the tip, with the larger one in binding solution for sensitivity of the incident light (Shah & Duncan, 2014). Thus, the experiments here may be more accurate than those BLItz experiments in Chapter 3. In addition, the AUK^{GoF} mutant had a more variable K_D value, although the average binding affinity was not significantly different. This could indicate that the protein adopts a less stable conformation than the wild-type, impacting its ability to bind DMI1.

In *in vitro* phosphorylation experiments, there was evidence for autophosphorylation of AUK kinase domain. This was expected based on previously presented results, where AUK kinase domain could self-associate via Y2H (Chapter 3). The self-association of RLKs has been commonly presented in the literature, and it is thought that this allows for a high concentration of kinase domains at the site of signal transduction to increase the opportunity for autophosphorylation within the kinase activation loop (Jafari *et al.,* 2021; Needham *et al.,* 2016). The *L. japonicus* AUK has been shown in phosphoproteomic studies to be phosphorylated within the activation loop (Zhang *et al.,* 2019), and thus this could be an autophosphorylation site allowing activation of the kinase domain when enough of the AUK is concentrated, perhaps through use binding at scaffolds, and present at the nuclear envelope site of symbiosis signaling. It would be interesting to send the AUK kinase domain for LC-

MS/MS to determine the autophosphorylation site and whether it matches that seen in *L. japonicus* phosphoproteomic experiments (Zhang *et al.,* 2019).

Interestingly, the DMI1 C-terminus was determined to be phosphorylated in *E.coli* in addition to the *in planta* experiments in *N. benthamiana* and putatively in *M. truncatula*. It would be interesting to examine the *E.coli*-induced phosphorylation sites by LC-MS/MS and compare them to those *in planta* to see if there may be conservation among systems. Excitingly, several AUK-induced phosphorylation sites were indicated in the C-terminus of DMI1 when expressed in *N. benthamiana*, which was pulled out as interacting with DMI1 in the initial Y2H screen, and we have shown *in vitro* and *in vivo* evidence for interaction. It was interesting to note that these AUK-specific phosphorylation sites were only seen in the overexpression of the wild-type, not the AUK^{GoF}. There could be several reasons for this. Firstly, the phosphopeptides were of low abundance, seen only 2 or 3 times in each construct. Secondly, *N. benthamiana* leaves are a very different system than *M. truncatula* roots. Thus, the AUK^{GoF} mutation might alter the folding of the AUK protein, which may render it susceptible to binding or inhibition by other proteins that AUK may not encounter within the endogenous environment of the *M. truncatula* roots.

Future work will involve generating phosphodead and phosphomimetic versions of single and higher-order mutations and testing their ability to complement nodulation and nuclear Ca^{2+} oscillation in the Nod^- *dmi1-1* mutant. Overall, the work presented in this chapter provides preliminary evidence for phosphorylation of DMI1 by AUK, providing a basis for further identification of a mechanism by which AUK may be activating nuclear Ca^{2+} oscillation, and subsequently endosymbiosis, through its interaction with DMI1.

6- General Discussion

Many advancements in the knowledge surrounding the components involved in symbiotic nuclear Ca^{2+} oscillation have been made in the past several decades. Genetic screens have identified molecular players involved in the perception of symbiotic factors as well as the identity of ion channels located at the nuclear envelope to generate the nuclear Ca^{2+} oscillation required for the generation of association between host plant and symbiont. Although experiments and pharmacological studies have revealed possible modes of transducing the signal to the nucleus, the knowledge on the identity of players and mechanisms involved in this link leading to activation and regulation of the nuclear Ca^{2+} oscillation is still lacking.

Following a Y2H screen of putative interactors with DMI1, the main objective of this thesis was to investigate the interaction with an LRR-RLK, termed AUK, determine its role in root symbioses with rhizobia and AM fungi, and uncover whether AUK may function mechanistically to activate or regulate symbiosis-induced Ca^{2+} oscillation through its interaction with DMI1. AUK was determined to localize to the nuclear envelope, be expressed in root hairs, and confirmed to associate with DMI1 using several different *in vitro* and *in planta* interaction assays (Chapter 3). The role of AUK was characterized in rhizobia and AM colonization through analysis of its knockout by CRISPR and overexpression in hairy roots as well as through analysis of EMS mutants in the AUK kinase domain, which identified a gain-of-function mutant (Chapter 4). Importantly, AUK was determined to be required for the generation of nodule structures and its overexpression and gain-of-function mutant led to spontaneous Ca^{2+} oscillation and nodule-like structures in absence of rhizobia, as well as increased nodulation and AM colonization in presence of the respective symbionts. The gain-of-function mutant also implicated a role for AUK in root system architecture. In Chapter 5, a possible mechanism was investigated for AUK-induced nuclear Ca^{2+} oscillation through its interaction with DMI1 and presented preliminary evidence for AUK-specific phosphorylation sites.

6.1- A role for AUK in symbiosis and root development

In Chapter 4, a role for AUK was presented in positively regulating nodulation and AM colonization. In addition, the overexpression of *AUK* and its gain-of-function mutant induced spontaneous Ca^{2+} oscillation and spontaneous organogenesis of nodule-like structures, as well as increased nodulation and AM colonization upon inoculation with rhizobia and AM fungi, respectively. Epistasis analysis positioned AUK upstream of DMI1, but downstream of DMI2 within the symbiosis signaling pathway. This is a relatively unique position, as the only other factor identified acting between DMI2 and DMI1 for the nuclear Ca^{2+} oscillation is HMGR1

(Venkateshwaran *et al.,* 2015), implying an important possibility for AUK to function as a link between symbiosis factor perception and the subsequent nuclear Ca^{2+} oscillation.

The *auk*^{GoF} mutant also had an impact on root system architecture, affecting early elongation of the primary roots and length of lateral roots, although lateral root initiation was unaffected. Development of both nodule and lateral root structures require complex spatiotemporal regulation within the root epidermis and cortex. Lateral root primordia develop from cells in the pericycle and adjacent endodermis, where cell divisions form the root meristem (Xiao *et al.,* 2019). For nodule development, there is cell division in the pericycle and endodermis, but also within the root cortex, which is the primary tissue layer involved in the nodule organogenesis (Xiao *et al.,* 2014).

The formation of a nodule seems to have recruited several players from the lateral root development programme. This includes *PLETHORA (PLT)* genes, which are required in *A. thaliana* for maintenance of the root meristem (Aida *et al.,* 2004; Galinha *et al.,* 2007). *PLT* genes are expressed in *M. truncatula* nodule primordia and in nodule vasculature (Franssen *et al.,* 2015). Another common element in the development of nodules and lateral roots is the complex interplay between auxin and cytokinin phytohormones. Cytokinin has been shown to inhibit lateral root development (Bielach *et al.,* 2012; Gonzalez-Rizzo *et al.,* 2006; Laplaze *et al.,* 2007; Lohar *et al.,* 2004), but promote nodule organogenesis (Murray *et al.,* 2007; Plet *et al.,* 2011; Tirichine *et al.,* 2007), where mutation of the cytokinin receptor CRE1 leads to increased lateral root emergence, but decreased nodulation (Gonzalez-Rizzo *et al.,* 2006; Herrbach *et al.,* 2017). In nodulation, a gain-of-function mutant version of the cytokinin receptor *Lj*LHK1/*Mt*CRE1 can activate cortical cell division, leading to spontaneous pseudonodules (Murray *et al.,* 2007; Tirichine *et al.,* 2007), as can exogenous application of cytokinin (Gauthier-Coles *et al.,* 2019; Heckmann *et al.,* 2011). *Lj*LHK1/*Mt*CRR1 induces expression of *NIN*, which induces cortical cell division, even in absence of infection (Soyano *et al.,* 2013; Vernié *et al.,* 2015). *NIN* has been shown to be essential for infection and formation of nodule primordia (Schauser *et al.,* 1999), and it is a direct target of CYCLOPS, the interacting partner of the nuclear Ca^{2+} decoder CCaMK (Singh *et al.,* 2014). In common between the early stages of development of lateral roots and nodules is the activation of auxin maxima (Schiessl *et al.,* 2019). Cytokinin regulates expression of auxin biosynthesis genes through expression of *NIN* and the auxin-related transcription factor, *ASYMMETRIC LEAVES2-LIKE18 (ASL18)/LATERAL ORGAN BOUNDARIES DOMAIN16 (LBD16),* a component required for the first asymmetric division during the initiation of lateral roots (Goh *et al.,* 2012; Okushima *et al.,* 2007). NIN regulates the expression of *ASL18/LBD16* through an intronic cis-element conserved in legumes to activate cortical cell division by interacting with NUCLEAR FACTOR-Y (NF-Y), another transcription factor, whose expression is also regulated by NIN (Soyano *et al.,* 2019). Thus, the nodule development programme seems to

have co-opted NIN, ASL/LBD16 and NF-Y from the lateral root development (Schiessl *et al.*, 2019; Soyano *et al.*, 2021).

Additional components involved in both lateral root and nodule organogenesis are the SHORTROOT (SHR)-SCARECROW(SCR) module, which are GRAS transcription factors involved in primary root stem cell differentiation and maintenance of root radial patterning (Helariutta *et al.*, 2000; Di Laurenzio *et al.*, 1996; Sabatini *et al.*, 2003) and in lateral root formation (Lucas *et al.*, 2011; Malamy & Benfey, 1997). A recent report by Dong *et al.*, (2021) found the SHR-SCR module to be essential for cortical cell divisions during nodulation. *SCR* was found to be expressed in the endodermis and cortex, and *SHR* accumulated within cortical cells. Expression of *MtSHR* in epidermis and cortex was increased by infection, which also induced *MtSCR*. Additionally, the overexpression of *MtSHR* could induce cortical cell division leading to the formation of nodule-like structures, dependent on *SCR*.

Given the spontaneous induction of nodule-like structures in the auk^{GoF} mutant, and the inhibition of growth of primary and lateral roots, one could envisage AUK as being important within both growth or organogenesis pathways. It would be interesting to determine whether genes involved in auxin and cytokinin biosynthesis and other common regulators of lateral roots and nodules, such as *NIN, ASL18/LBD16, NF-Y,* and *SHR-SCR* are differentially expressed within wild-type and auk^{GoF} during the formation of nodules and of lateral roots. Given the identified role of DMI1 and nuclear Ca^{2+} in primary root development in *Arabidopsis* (Leitão *et al.*, 2019), one could envisage that the interaction of AUK with DMI1 and the role for AUK in nuclear Ca^{2+} oscillation may serve to regulate the nuclear Ca^{2+} oscillation required for both the root development program as well as symbiosis.

The infection programme of both rhizobia and AM fungi requires complex regulation of different cell layers. For both, the perception and beginning of infection occurs within the epidermis. The generation of both the infection thread and pre-penetration apparatus initiates within the epidermal cells to guide progression of the symbiont colonization (Brewin, 2004; Genre *et al.*, 2005, 2008). As colonization progresses, there is cortical cell division in both symbiotic processes (Carotenuto *et al.*, 2019; Reid *et al.*, 2017; Russo *et al.*, 2019). In nodule organogenesis, this occurs at the same time as infection growth and the nodule organ accommodates the bacteria for nitrogen fixation. In AM fungal colonization, the fungus traverses through epidermal and cortical cell layers to reach the inner cortex, where arbuscules develop and are accommodated by split cell formation from previous changes during the reactivation of the cell cycle (Genre *et al.*, 2005, 2008; Russo *et al.*, 2019).

AUK expression was found in epidermal cells, using analysis of *pAUK:NLS-GFP* and its role in Ca^{2+} oscillation, suggesting an epidermal role for *AUK*. However, its generation of spontaneous nodule-like structures also points to a function within the root cortex. Thus, future work to delineate the expression pattern of *AUK* in the epidermis and cortex, and its

requirement in these cell layers during different stages of infection by rhizobia and AM fungi, as well as in root development, will be of great interest. It could also lead to finer understanding of the role of the nuclear Ca^{2+} at different stages of organogenesis and symbiosis. Possible experiments to use for this could be further analysis the *AUK* expression pattern using promoter::GUS experiments across a time-course of rhizobia infection or AM colonization as well as targeted CRISPR to knock out *AUK* within simply the epidermis or cortex to determine its necessity in these cell layers for symbiosis.

6.2- Regulation of nodulation

The production of nodule structures is energetically costly for the plant, and thus they must restrict the nodule number to an optimum to balance nitrogen acquisition with carbon expenditure. Nodule number is tightly controlled by local feedback and systemic long-distance signaling between the root and shoot, called autoregulation of nodulation (AON) (Caetano-Anollés & Gresshoff, 1991; Krusell *et al.*, 2002). In *M. truncatula*, upon sufficient rhizobial infection, there is expression of *CLAVATA3/EMBRYO-SURROUNDING REGION (CLE) 12/13* peptides. The CLE12/13 have been shown to act in the shoot where they are perceived by an LRR-RLK *Mt*SUNN to negatively regulate nodule number (Mortier *et al.*, 2010, 2012; Schnabel *et al.*, 2005). A second pathway exists whereby high nitrate conditions induce the expression of root-derived *C-TERMINALLY ENCODED PEPTIDES* (*CEPs)* to systemically inhibit nodule number. Although both the CLE and CEP pathways independently control nodule number, they both recruit the same downstream factors: the shoot-derived miR2111 and the root-derived TOO MUCH LOVE (TML), a Kelch repeat-containing F-box protein, to modulate nodulation (Gautrat *et al.*, 2019, 2020; Huault *et al.*, 2014; Imin *et al.*, 2013; Laffont *et al.*, 2019; Mohd-Radzman *et al.*, 2016; Tsikou *et al.*, 2018). As mentioned above, cytokinin and NIN contribute to cortical cell division in nodule organogenesis. In *L. japonicus* they can also contribute to negative feedback on nodule organogenesis and infection through induction of CLE peptides and the AON pathway (Soyano *et al.*, 2014). Lin *et al.*, (2021) discovered that in *L. japonicus* nitrate was inhibitory to cytokinin biosynthesis, with high nitrate causing lower expression of several cytokinin biosynthesis genes and ectopic cytokinin application overriding nitrate inhibition of nodule maturation and nitrogen fixation. Interestingly, a recent study by Chen *et al.*, (2022) found that the PUP family of cytokinin transporters exported cytokinin from nodules leading to stimulation of shoot growth, as a way of coordinating the plant shoot growth and development based on the level of available soil nitrogen. The auk^{GoF} mutant has an excessive number of nodules and nodule-like structures both in presence and absence of rhizobia, respectively. In correlation with a resource-balancing effect, the mutant plant is stunted (data not shown), indicative of more carbon resources going into root organogenesis than above-ground growth and development. This may suggest that

constitutively active AUK is contributing in some way in these pathways, contributing to regulation of nodule number. To this end, it would be interesting to determine through RNA-seq whether the gain-of-function mutant affects cytokinin biosynthesis genes and players involved in the AON pathway.

6.3- Activation of protein kinases

Many protein kinases are subject to complex regulation to control the timing and level of their signaling. Under resting conditions, they are often inactive and require stimulus-induced signal transduction to facilitate their activation. A characteristic structure of a protein kinase includes an activation loop, typically 20-40 amino acids long, extending from the DFG (Asp-Phe-Gly) amino acid motif to a conserved APE (Ala-Pro-Glu) (Modi & Dunbrack, 2019). Typically, without protein kinase activation, this activation loop segment is disordered (Nolen *et al.*, 2004). To activate the kinase, there is typically phosphorylation within the activation loop, which can be either autophosphorylation by the protein kinase itself, or transphosphorylation by another protein kinase (Adams, 2003). The activation allows binding of substrate within a cleft formed by this loop. The bound substrate can form interactions with the HRD (His-Arg-Asp) motif within the catalytic loop of the protein kinase (Modi & Dunbrack, 2019). When not phosphorylated, the activation loop can occupy the kinase active site, effectively blocking access by the substrate. The first structure determined for an active protein kinase was for that of protein kinase A (PKA) (Adams *et al.*, 1995). It was shown to be activated through phosphorylation of a single threonine residue, causing an increase in catalysis and rebinding of an inhibitory PKA regulatory subunit. Another example can be seen in the x-ray crystal structure of InRK tyrosine kinase insulin receptor, which shows that a phosphorylated activation loop is well-ordered and forms contacts with positively charged side chains, with the active site accessible for the substrate. When not phosphorylated, there is a significant shift in the placement of the activation loop, autoinhibiting substrate binding at the active site by sitting in that loop (Hubbard, 1997). Phosphoproteomic analyses in *L. japonicus* have shown a phosphorylation site for the *Lj*AUK within its activation loop (Zhang *et al.*, 2019), suggesting that this site may be required for activation of AUK kinase activity, although further work would be needed to confirm the necessity of phosphorylation of this site and its potential role in AUK function in endosymbiosis.

In addition, several kinases require binding of an interaction partner within the activation loop to facilitate their activation and kinase activity. An example of this is the Aurora-A oncogene-associated Ser/Thr kinase in mitosis in animals. It requires binding of another factor TPX2 with interactions with both the N-terminal lobe and kinase activation loop of the Aurora-A kinase (Dodson & Bayliss, 2012). The binding of TPX2 could increase the catalytic activity by a factor of 15-fold. As presented in Chapter 5, AUK is a somewhat atypical

protein kinase, consisting of an extension within the activation loop, making it 51 amino acids in length, in comparison with the typical 20-40 amino acids (Modi & Dunbrack, 2019). Evidence is provided within this chapter that AUK may possess autophosphorylation activity. The gain-of-function mutation affects a proline at the beginning of the extension within the activation loop. It could be hypothesized that the mutation of proline to serine might serve to mimic structural changes induced either by phosphorylation or by binding of an activating partner. The *Arabidopsis* AUK also has this extension within the kinase activation loop (Figure 4.7). Its autophosphorylation has been shown to be dependent on the binding of a G beta subunit of the heterotrimeric G protein signaling cascade and a calmodulin (Yu *et al.,* 2016). This was determined via deletion of a putative G-beta binding site, which corresponds to the extended region of the kinase activation loop in AUK and the deletion of a calmodulin binding site with experiments performed by co-expression of the proteins within *E.coli*. However, as the alignment in Chapter 5 indicates, the amino acid sequence in the putative G-beta binding site in the extended activation loop is not highly conserved, and thus it remains to be seen how *Mt*AUK is activated and whether the mechanism of activation requires a yet unknown interacting partner.

6.4- Complex formation and signaling at plant membranes

In Chapter 3, AUK was identified as an interacting partner of DMI1 at the nuclear envelope. DMI1 is a tetrameric ion channel, which forms as complex with CNGC15 at the nuclear envelope to coordinate symbiotic nuclear Ca^{2+} oscillation (Ané *et al.,* 2004; Charpentier *et al.,* 2016; Del Cerro *et al.,* 2022; Kim *et al.,* 2019; Riely *et al.,* 2007). It is common for proteins to function in a complex at plant membranes to coordinate a signal transduction cascade. About 20-30% of proteins are predicted to possess transmembrane domains (Krogh *et al.,* 2001). The requirement for DMI1 in symbiosis-induced nuclear Ca^{2+} oscillation (Chabaud *et al.,* 2011; Kosuta *et al.,* 2008; Miwa *et al.,* 2006; Oldroyd, Mitra, *et al.,* 2001; Sieberer *et al.,* 2009; Wais *et al.,* 2000; Walker *et al.,* 2000), and the production of symbiosis-like Ca^{2+} oscillation from application of the mastoparan analog Mas7 in a *dmi1* mutant (Sun *et al.,* 2007) prompted hypotheses that DMI1 is not the Ca^{2+} channel, itself, but modulates the Ca^{2+} oscillation via its interaction with CNGC15 (Charpentier *et al.,* 2016; Peiter *et al.,* 2007). Mathematical modelling has also indicated a role for DMI1 primarily as a counter-ion channel, however its initial conductance is required for Ca^{2+} flow and simultaneous activity of DMI1 and CNGC15 is likely required to sustain the nuclear Ca^{2+} oscillation (Charpentier *et al.,* 2013, 2016; Granqvist *et al.,* 2012). A recent report found that a constitutively active form of DMI1 can promote CNGC15 channel activity and Ca^{2+} oscillation (Liu *et al.,* 2022), providing further evidence for the role of DMI1 to modulate the nuclear Ca^{2+} oscillation. Thus, it is tempting to

speculate that AUK interaction with DMI1 might function to activate the conductance of DMI1 to activate the Ca^{2+} oscillation, perhaps through phosphorylation.

Within membranes, proteins are not homogenously distributed, but rather form discrete regions of high concentrations in conjunction with lipids, called microdomains. Microdomain organization and dynamics vary depending on different stimuli (Takahashi *et al.,* 2013), and bring together components of a signal transduction pathway to ensure signal robustness and specificity (Gronnier *et al.,* 2019; Jacobson *et al.,* 2019). This has been shown to be important for plant immune signaling, with FLS2 localization into discrete puncta (Bücherl *et al.,* 2017), and FERONIA acting as a scaffold bringing together FLS2 and BAK1 and LRXs in RALF signaling (Gronnier *et al.,* 2022). In symbiosis, it has been reported that *MtSYMREM1*, which encodes a remorin, is upregulated within nodules in response to Nod factor and associates with NFP, LYK3 and DMI2, suggesting the role of a scaffold protein essential for Nod factor-induced symbiosis signaling (Lefebvre *et al.,* 2010). The addition of AUK, localized to the nuclear envelope and associating with DMI1 suggests more compartmentalization of the nuclear Ca^{2+} oscillation. In several signaling pathways, the binding of a ligand can induce oligomerization of membrane proteins as a first step in transducing intracellular signals (Wang *et al.,* 2018). There can also be dimerization in absence of a ligand, for instance with BRI1, where approximately 20% of BRI1 molecules in the plasma membrane exist within homo-dimers in absence of ligand, as determined by dual-colour fluorescence cross correlation spectroscopy for single molecule detection in living plant cells (Hink *et al.,* 2008). Y2H experiments and gel filtration from *E.coli* expression and purification indicated a dimerization of AUK kinase domain, similarly to that of BRI1 (Wang *et al.,* 2005). This could indicate that dimerization of AUK and its possible concentration within microdomains at the nucleus may serve to activate the kinase activity via close proximity increasing the opportunity for transphosphorylation events.

Given AUK classification as an LRR-RLK, it was hypothesized that its association with DMI1 could contribute to kinase activity and that phosphorylation may serve to regulate the channel activity. In Chapter 5, preliminary evidence was provided for several AUK-specific phosphorylation sites on DMI1 in *N. benthamiana* leaves. Several plant ion channels have been found to associate with protein kinases and phosphoproteomic screens have identified several ion channel phosphorylation sites, however few studies have identified the functional and mechanistic relevance of these phosphorylation events. One channel that has been extensively studied is the S-type anion channel, SLOW ANION CHANNEL1 (SLAC1), which is preferentially expressed in guard cells and plays a role in stomatal closure (Negi *et al.,* 2008; Vahisalu *et al.,* 2008). Within the ABA signaling pathway, SLAC1 has been shown to be phosphorylated on its N-terminal Ser120 by a SnRK2 kinase, OPEN STOMATA1 (OST1) (Geiger *et al.,* 2009; Lee *et al.,* 2009; Vahisalu *et al.,* 2010). The PP2C-type

phosphatase ABA INSESNSITIVE1 (ABI1) can inhibit this phosphorylation independently of its phosphatase activity by direct interaction with OST1 (Geiger *et al.,* 2009; Lee *et al.,* 2009). Additionally, CPK6 was also found to phosphorylate the N-terminal Ser59 on SLAC1, once again dephosphorylated by ABI1 (Brandt *et al.,* 2012). An additional C-terminal phosphorylation site was identified on SLAC1, Thr513 (Lee *et al.,* 2009), as well as phosphorylation by CBL1/CIPK23 (Maierhofer *et al.,* 2014). Each of these studies claimed the phosphorylation served to activate the channel activity, however all of them were performed by co-expression in oocytes. *In planta* experiments by Brandt *et al.,* (2015) showed it was possible to complement the *slac1* mutant with SLAC1 S59A or S120A, which still had ABA-induced stomatal closure. However, combined mutation severely impaired activity, indicating that phosphorylation of these residues is important for stomatal closure. The authors also presented that CPK activation occurred through S59, and OST1 through S120. Initial structural studies of *At*SLAC1 and *Bd*SLAC1 were unable to resolve the structure of the N- and C-terminal ends, precluding mechanistic determination of channel regulation by kinase/phosphatase activity (Chen *et al.,* 2010; Deng *et al.,* 2021). A recent structure of the inactive *At*SLAC1 was determined by cryo-EM (Li *et al.,* 2022). The N- and C-terminal segments of the kinase appear to form a plug-like structure attached to the transmembrane domain to block the channel pore and maintain it within a closed, inactive state. Even in the absence of S59 phosphorylation, breaking the plug-transmembrane domain interaction was found to noticeably activate the channel. The authors propose that phosphorylation of SLAC1 within its N- and C-terminus might lead to structural rearrangements to dissociate the cytosolic domain from the transmembrane domain, releasing its inhibition of the channel pore. Additionally, the K^+ channel AKT1 in *A. thaliana* is phosphorylated in response to change in K^+ availability and under conditions of stress, dependent on the CBL1/9 and CIPK23 (Hirsch *et al.,* 1998; Lee *et al.,* 2007; Xu *et al.,* 2006). These kinases were shown to interact with AKT1 and activate its K^+ influx in *Xenopus* oocytes, where expressed on its own AKT1 does not have any current (Xu *et al.,* 2006). Structural analysis of the AKT1 channel has provided evidence that the phosphorylated AKT1 adopts a 4-fold symmetric conformation of its cytoplasmic domain, which is a conformational change in symmetry associated with its activation, with mutations causing this symmetry switch causing activation independently of phosphorylation (Lu *et al.,* 2022). This study provided evidence for phosphorylation-induced activation of the K^+ channel through conformational change within the channel.

With the observation of AUK-specific phosphorylation sites on DMI1 in *N. benthamiana* leaves, it will be important to assess the phosphorylation status of DMI1 in *M. truncatula* and further test the functional relevance of putative specific phosphorylation sites through complementation experiments of nodulation, Ca^{2+} oscillation and AM colonization within the *dmi1* mutant, with single and multiple mutations for phosphodead (mutation to an

alanine) and phosphomimic (mutation to an aspartate) versions. If the phosphodead mutation versions do not complement the *dmi1* phenotype for lack of colonization and nuclear Ca^{2+}, it could indicate a role for the phosphorylation of these sites in symbiosis signaling. It is tempting to speculate that the phosphorylation of sites within the C-terminus of DMI1 might function to produce a conformational change and activation, which in turn activates and modulates the Ca^{2+} channel activity in CNGC15s. This could be consistent with DMI1 acting as a regulator of the Ca^{2+} channel activity, as suggested by the finding that the constitutively active DMI1 requires CNGC15s in HEK293 cells (Liu *et al.*, 2022), and with the requirement of DMI1 for symbiosis-induced nuclear Ca^{2+} in symbiosis, despite the *dmi1* symbiosis-like nuclear Ca^{2+} induction by Mas7 (Sun *et al.*, 2007; Wais *et al.*, 2000), and also fitting with mathematical modelling suggesting simultaneous activation of DMI1 and CNGC15s (Charpentier *et al.*, 2013, 2016).

6.5- Link to animal nuclear Ca^{2+} signaling

Although the knowledge behind mechanisms involved in encoding and decoding of nuclear Ca^{2+} oscillations is little in plants, many of the experiments and inhibitors used in the field are based on the breadth of knowledge on nuclear Ca^{2+} that have been gained from the animal field. Of particular interest to the symbiosis field is the regulation of large conductance, Ca^{2+}-activated potassium (BK) channels, which have structural homology to DMI1. BK channels are involved in a wide variety of processes in animals, including muscle contraction, neural transmission and hearing (Cui *et al.*, 2009). They are activated by membrane depolarization and elevation of intracellular Ca^{2+} and their activation leads to membrane repolarization and closing of voltage dependent Ca^{2+} channels with which they are in close proximity to reduce calcium entry into the cell (Schubert & Nelson, 2001). BK channels are composed of a membrane spanning domain with 7 transmembrane segments and a large C-terminal cytoplasmic domain with two RCK domains, where 4 subunits form a gating ring of 8 RCK domains (Meera *et al.*, 1997; Wallner *et al.*, 1996). In addition to activation by voltage and calcium, BK channels have also been found to be regulated by several protein kinases including the cAMP-dependent protein kinase A (PKA) (Liu *et al.*, 2009; Tian *et al.*, 2001; Zhou *et al.*, 2001), protein kinase C (PKC) (Barman *et al.*, 2004; Liu *et al.*, 2009; Wu *et al.*, 2007; Zhou *et al.*, 2001), the cGMP-dependent PKG (Hall & Armstrong, 2000; Wu *et al.*, 2007) and cSrc (Alioua *et al.*, 2002) that function to activate or inactivate the channel depending on the system. In addition, BK channels possess auxiliary subunits, including LRR domain-containing auxiliary γ subunits, which consist of an LRR domain, a transmembrane domain and a short intracellular C-terminal tail (comparison with DMI1 detailed in Figure 6.1; Chen *et al.*, 2022). These subunits play important roles in the expression, trafficking and modulation of BK channel activity.

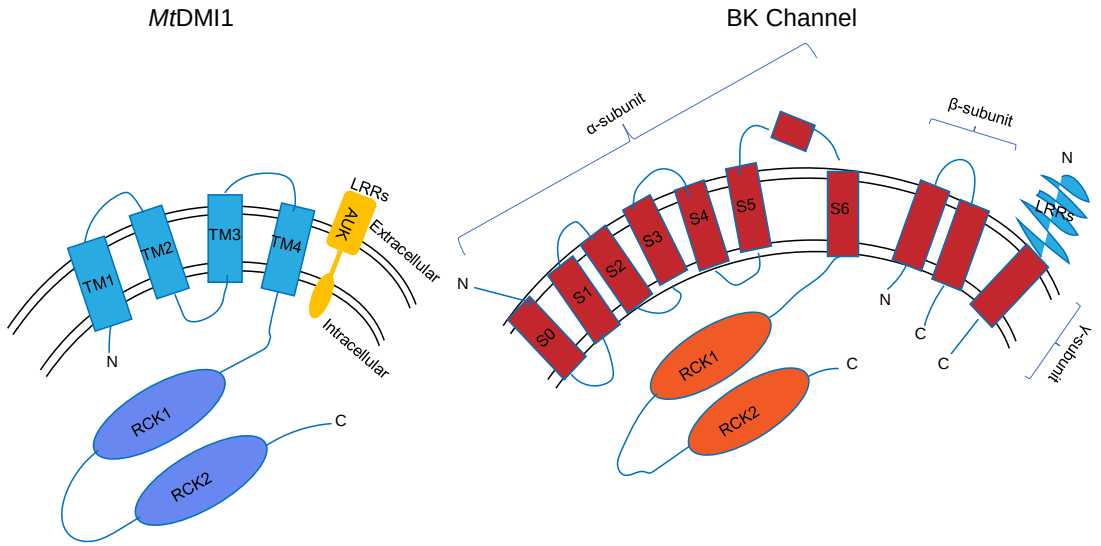

Figure 6.1. Comparison between *Mt*DMI1 and mammalian BK channel membrane topology.

Membrane topology for DMI1 and BK channel membrane topology indicating the transmembrane domains and RCK domains. DMI1 is shown with AUK as its auxiliary unit. BK channel consists of an α, β, and γ- subunit indicated, and the γ-subunit possesses LRRs in the extracellular space.

Interesting parallels between this BK channel system and that of DMI1 and AUK in symbiosis can be drawn. Firstly, DMI1 interaction and potential modulation of CNGC15s calcium activity as discussed above (Charpentier *et al.*, 2016; Liu *et al.*, 2022). Secondly, the BK channels can be regulated by Ca^{2+} binding, and DMI1 possesses two Ca^{2+} binding pockets, which to control channel activation dependent on Ca^{2+} binding (Kim *et al.*, 2019). Finally, the potential for phosphorylation by AUK by an LRR-RLK might serve in the plant symbiosis system to bring together the LRR subunits, combined with kinase activity as an auxiliary unit for activation and modulation of the activity of DMI1.

6.6- Conclusions and future perspectives

Although much is known about perception of symbiotic factors at the plasma membrane and about the involvement and players involved in generation of the nuclear Ca^{2+} oscillation at the nucleus, there is little understanding about what might be linking these to activate the nuclear-localized ion channels. Overall results of this thesis are illustrated in Figure 6.2. In this thesis, the association of DMI1 with an LRR-RLK auxiliary unit of DMI1 termed AUK was confirmed through several heterologous, *in vitro*, and *in planta* experiments. *AUK* was also identified as a required for nodulation and observed that *AUK* overexpression and a gain-of-

function *auk* mutant can contribute to spontaneous nuclear Ca^{2+} spiking and spontaneous nodulation in absence of rhizobia. The *auk* mutant has increased nodulation and AM colonization upon inoculation with the appropriate symbiont. The gain-of-function mutation also leads to alteration in root system architecture, indicating a possible dual role in nodule vs. lateral root development, although further study is required. Finally, preliminary evidence is provided for autophosphorylation of AUK and for AUK-specific phosphorylation sites on DMI1, which may function to regulate channel activity. Important future experiments should include the analysis of *AUK* gene expression in epidermis vs cortex as well as its requirement in these tissue layers throughout different stages of infection, nodulation, AM colonization and lateral root development, as well as the further analysis of the putative role of the AUK-specific DMI1 phosphosites through *dmi1* complementation experiments. Taken together, this thesis presents a novel player in the symbiosis signaling pathway, adding another piece to the puzzle of how symbiosis-induced nuclear Ca^{2+} is regulated.

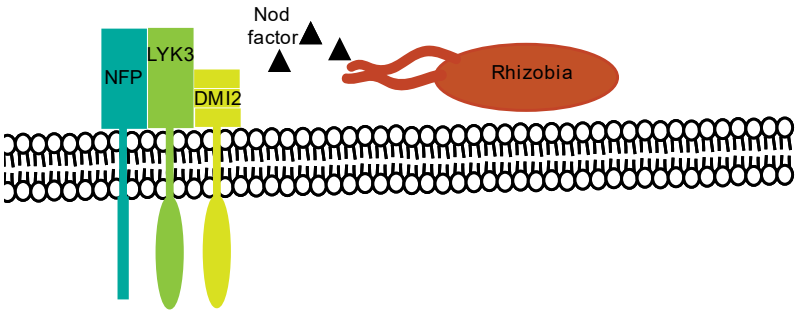

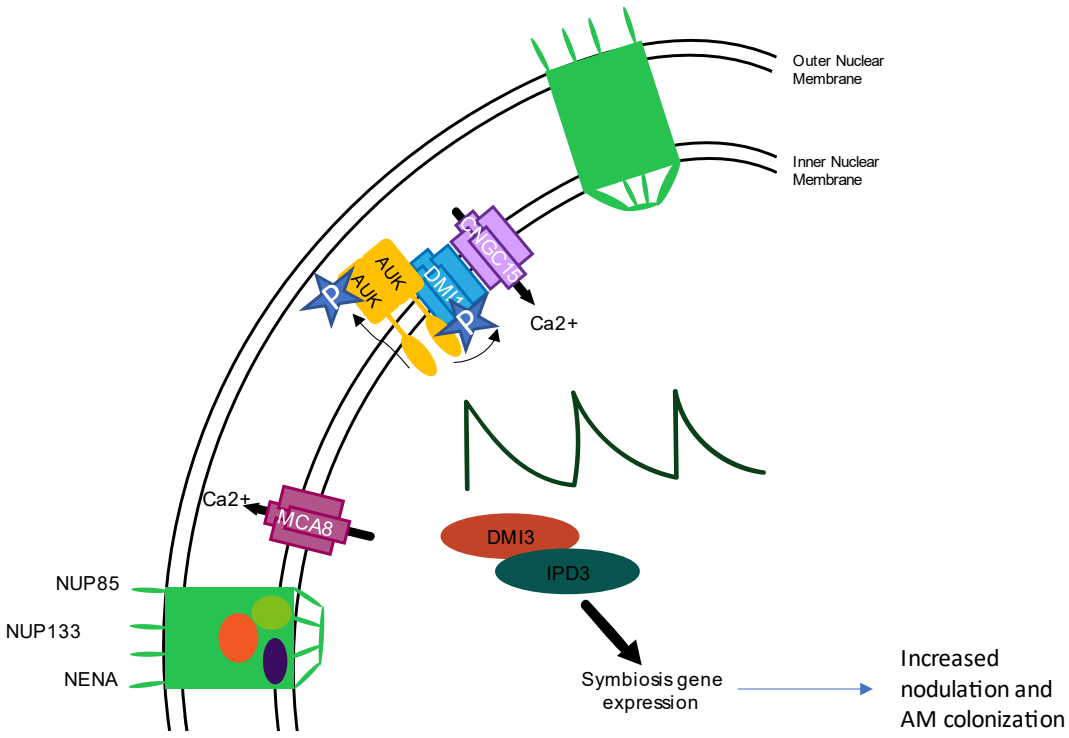

Figure 6.2. Overall summary diagram.

AUK is a novel component of the symbiosis signaling pathway. In *M. truncatula* root hairs, it localizes to the nuclear envelope where it associates with DMI1. Evidence from this thesis indicates that it forms an oligomer and can autophosphorylate itself and transphosphorylate DMI1. This phosphorylation may be activating the nuclear calcium oscillation resulting in symbiosis gene expression and allowing association with the rhizobial or AM fungal symbiont.

References

Adams, J. A. (2003). Activation loop phosphorylation and catalysis in protein kinases: Is there functional evidence for the autoinhibitor model? *Biochemistry*, *42*(3), 601–607.

Adams, J. A., McGlone, M. L., Gibson, R., & Taylor, S. S. (1995). Phosphorylation modulates catalytic function and regulation in the camp-dependent protein kinase. *Biochemistry*, *34*(8), 2447–2454.

Aida, M., Beis, D., Heidstra, R., Willemsen, V., Blilou, I., Galinha, C., Nussaume, L., Noh, Y.-S., Amasino, R., & Scheres, B. (2004). The *PLETHORA* genes mediate patterning of the Arabidopsis root stem cell niche. *Cell*, *119*(1), 109–120.

Akamatsu, A., Nagae, M., Nishimura, Y., Romero Montero, D., Ninomiya, S., Kojima, M., Takebayashi, Y., Sakakibara, H., Kawaguchi, M., & Takeda, N. (2021). Endogenous gibberellins affect root nodule symbiosis via transcriptional regulation of *NODULE INCEPTION* in *Lotus japonicus*. *The Plant Journal*, *105*(6), 1507–1520.

Akiyama, K., & Hayashi, H. (2006). Strigolactones: chemical signals for fungal symbionts and parasitic weeds in plant roots. *Annals of Botany*, *97*(6), 925–931.

Akiyama, K., Matsuzaki, K., & Hayashi, H. (2005). Plant sesquiterpenes induce hyphal branching in arbuscular mycorrhizal fungi. *Nature*, *435*(7043), Article 7043.

Alioua, A., Mahajan, A., Nishimaru, K., Zarei, M. M., Stefani, E., & Toro, L. (2002). Coupling of c-Src to large conductance voltage- and Ca^{2+}-activated K^+ channels as a new mechanism of agonist-induced vasoconstriction. *Proceedings of the National Academy of Sciences*, *99*(22), 14560–14565.

Ané, J.-M., Kiss, G. B., Riely, B. K., Penmetsa, R. V., Oldroyd, G. E. D., Ayax, C., Lévy, J., Debellé, F., Baek, J.-M., Kalo, P., Rosenberg, C., Roe, B. A., Long, S. R., Dénarié, J., & Cook, D. R. (2004). *Medicago truncatula* DMI1 required for bacterial and fungal symbioses in legumes. *Science*, *303*(5662), 1364–1367.

Antolín-Llovera, M., Ried, M. K., & Parniske, M. (2014). Cleavage of the SYMBIOSIS RECEPTOR-LIKE KINASE ectodomain promotes complex formation with NOD FACTOR RECEPTOR 5. *Current Biology*, *24*(4), 422–427.

Aquino, B., Couñago, R. M., Verza, N., Ferreira, L. M., Massirer, K. B., Gileadi, O., & Arruda, P. (2017). Structural characterization of maize SIRK1 kinase domain reveals an unusual architecture of the activation segment. *Frontiers in Plant Science*, *8*, 852.

Arrighi, J.-F., Barre, A., Ben Amor, B., Bersoult, A., Soriano, L. C., Mirabella, R., de Carvalho-Niebel, F., Journet, E.-P., Ghérardi, M., Huguet, T., Geurts, R., Dénarié, J., Rougé, P., & Gough, C. (2006). The *Medicago truncatula* lysine motif-receptor-like kinase gene family includes NFP and new nodule-expressed genes. *Plant Physiology*, *142*(1), 265–279.

Barker, D., Bianchi, S., Blondon, F., Dattee, Y., Duc, G., Essad, S., Flament, P., Gallusci, P., Génier, G., Guy, P., Muel, X., Tourneur, J., Dénarié, J., & Huguet, T. (1990). *Medicago truncatula*, a model plant for studying the molecular genetics of the Rhizobium-legume symbiosis. *Plant Molecular Biology Reporter*, *8*, 40–49.

Barman, S. A., Zhu, S., & White, R. E. (2004). PKC activates BKCa channels in rat pulmonary arterial smooth muscle via cGMP-dependent protein kinase. *American Journal of Physiology-Lung Cellular and Molecular Physiology*, *286*(6), L1275–L1281.

Batistič, O., Waadt, R., Steinhorst, L., Held, K., & Kudla, J. (2010). CBL-mediated targeting of CIPKs facilitates the decoding of calcium signals emanating from distinct cellular stores. *The Plant Journal*, *61*(2), 211–222.

Ben Amor, B., Shaw, S. L., Oldroyd, G. E. D., Maillet, F., Penmetsa, R. V., Cook, D., Long, S. R., Dénarié, J., & Gough, C. (2003). The NFP locus of *Medicago truncatula* controls an early step of Nod factor signal transduction upstream of a rapid calcium flux and root hair deformation. *The Plant Journal*, *34*(4), 495–506.

Bender, K. W., Dobney, S., Ogunrinde, A., Chiasson, D., Mullen, R. T., Teresinski, H. J., Singh, P., Munro, K., Smith, S. P., & Snedden, W. A. (2013). The calmodulin-like protein CML43 functions as a salicylic-acid-inducible root-specific Ca^{2+} sensor in Arabidopsis. *Biochemical Journal*, *457*(1), 127–136.

Benedito, V. A., Torres-Jerez, I., Murray, J. D., Andriankaja, A., Allen, S., Kakar, K., Wandrey, M., Verdier, J., Zuber, H., Ott, T., Moreau, S., Niebel, A., Frickey, T., Weiller, G., He, J., Dai, X., Zhao, P. X., Tang, Y., & Udvardi, M. K. (2008). A gene expression atlas of the model legume *Medicago truncatula*. *The Plant Journal*, *55*(3), 504–513.

Besant, P. G., & Attwood, P. V. (2009). Detection and analysis of protein histidine phosphorylation. *Molecular and Cellular Biochemistry*, *329*(1), 93–106.

Besserer, A., Bécard, G., Jauneau, A., Roux, C., & Séjalon-Delmas, N. (2008). GR24, a synthetic analog of strigolactones, stimulates the mitosis and growth of the arbuscular mycorrhizal fungus *Gigaspora rosea* by boosting its energy metabolism. *Plant Physiology*, *148*(1), 402–413.

Besserer, A., Puech-Pagès, V., Kiefer, P., Gomez-Roldan, V., Jauneau, A., Roy, S., Portais, J.-C., Roux, C., Bécard, G., & Séjalon-Delmas, N. (2006). Strigolactones stimulate arbuscular mycorrhizal fungi by activating mitochondria. *PLOS Biology*, *4*(7), e226.

Bhattacharya, A., Paul, A., Chakrabarti, D., & DasGupta, M. (2019). Gatekeeper–activation loop cross-talk determines distinct autoactivation states of SYMBIOSIS RECEPTOR KINASE. *Biochemistry*, *58*(19), 2419–2431.

Bielach, A., Podlešáková, K., Marhavý, P., Duclercq, J., Cuesta, C., Müller, B., Grunewald, W., Tarkowski, P., & Benková, E. (2012). Spatiotemporal regulation of lateral root organogenesis in Arabidopsis by cytokinin. *The Plant Cell*, *24*(10), 3967–3981.

Bojar, D., Martinez, J., Santiago, J., Rybin, V., Bayliss, R., & Hothorn, M. (2014). Crystal structures of the phosphorylated BRI1 kinase domain and implications for brassinosteroid signal initiation. *The Plant Journal*, *78*(1), 31–43.

Bonfante, P., & Genre, A. (2010). Mechanisms underlying beneficial plant–fungus interactions in mycorrhizal symbiosis. *Nature Communications*, *1*(1), Article 1.

Boudsocq, M., Willmann, M. R., McCormack, M., Lee, H., Shan, L., He, P., Bush, J., Cheng, S.-H., & Sheen, J. (2010). Differential innate immune signalling via Ca^{2+} sensor protein kinases. *Nature*, *464*(7287), Article 7287.

Brandt, B., Brodsky, D. E., Xue, S., Negi, J., Iba, K., Kangasjärvi, J., Ghassemian, M., Stephan, A. B., Hu, H., & Schroeder, J. I. (2012). Reconstitution of abscisic acid activation of SLAC1 anion channel by CPK6 and OST1 kinases and branched ABI1 PP2C phosphatase action. *Proceedings of the National Academy of Sciences*, *109*(26), 10593–10598.

Brandt, B., Munemasa, S., Wang, C., Nguyen, D., Yong, T., Yang, P. G., Poretsky, E., Belknap, T. F., Waadt, R., Alemán, F., & Schroeder, J. I. (2015). Calcium specificity signaling mechanisms in abscisic acid signal transduction in Arabidopsis guard cells. *ELife*, *4*, e03599.

Breakspear, A., Liu, C., Roy, S., Stacey, N., Rogers, C., Trick, M., Morieri, G., Mysore, K. S., Wen, J., Oldroyd, G. E. D., Downie, J. A., & Murray, J. D. (2014). The root hair "infectome" of *Medicago truncatula* uncovers changes in cell cycle genes and reveals a requirement for auxin signaling in rhizobial infection. *The Plant Cell*, *26*(12), 4680–4701.

Brewin, N. J. (2004). Plant cell wall remodelling in the rhizobium–legume symbiosis. *Critical Reviews in Plant Sciences*, *23*(4), 293–316.

Broghammer, A., Krusell, L., Blaise, M., Sauer, J., Sullivan, J. T., Maolanon, N., Vinther, M., Lorentzen, A., Madsen, E. B., Jensen, K. J., Roepstorff, P., Thirup, S., Ronson, C. W., Thygesen, M. B., & Stougaard, J. (2012). Legume receptors perceive the rhizobial lipochitin oligosaccharide signal molecules by direct binding. *Proceedings of the National Academy of Sciences*, *109*(34), 13859–13864.

Bücherl, C. A., Jarsch, I. K., Schudoma, C., Segonzac, C., Mbengue, M., Robatzek, S., MacLean, D., Ott, T., & Zipfel, C. (2017). Plant immune and growth receptors share common signalling components but localise to distinct plasma membrane nanodomains. *ELife*, *6*, e25114.

Bürstenbinder, K., Möller, B., Plötner, R., Stamm, G., Hause, G., Mitra, D., & Abel, S. (2017). The IQD family of calmodulin-binding proteins links calcium signaling to microtubules, membrane subdomains, and the nucleus. *Plant Physiology*, *173*(3), 1692–1708.

Caetano-Anollés, G., & Gresshoff, P. M. (1991). Efficiency of nodule initiation and autoregulatory responses in a supernodulating soybean mutant. *Applied and Environmental Microbiology*, *57*(8), 2205–2210.

Capoen, W., Sun, J., Wysham, D., Otegui, M. S., Venkateshwaran, M., Hirsch, S., Miwa, H., Downie, J. A., Morris, R. J., Ané, J.-M., & Oldroyd, G. E. D. (2011). Nuclear membranes control symbiotic calcium signaling of legumes. *Proceedings of the National Academy of Sciences of the United States of America*, *108*(34), 14348–14353.

Cárdenas, L., Feijó, J. A., Kunkel, J. G., Sánchez, F., Holdaway-Clarke, T., Hepler, P. K., & Quinto, C. (1999). Rhizobium Nod factors induce increases in intracellular free calcium and extracellular calcium influxes in bean root hairs. *The Plant Journal*, *19*(3), 347–352.

Cárdenas, L., Vidali, L., Domínguez, J., Pérez, H., Sánchez, F., Hepler, P. K., & Quinto, C. (1998). Rearrangement of actin microfilaments in plant root hairs responding to *rhizobium etli* NODULATION SIGNALS1. *Plant Physiology*, *116*(3), 871–877.

Carotenuto, G., Volpe, V., Russo, G., Politi, M., Sciascia, I., de Almeida-Engler, J., & Genre, A. (2019). Local endoreduplication as a feature of intracellular fungal accommodation in arbuscular mycorrhizas. *New Phytologist*, *223*(1), 430–446.

Catoira, R., Galera, C., de Billy, F., Penmetsa, R. V., Journet, E. P., Maillet, F., Rosenberg, C., Cook, D., Gough, C., & Dénarié, J. (2000). Four genes of *Medicago truncatula* controlling components of a Nod factor transduction pathway. *The Plant Cell*, *12*(9), 1647–1666.

Cebolla, A., María Vinardell, J., Kiss, E., Oláh, B., Roudier, F., Kondorosi, A., & Kondorosi, E. (1999). The mitotic inhibitor ccs52 is required for endoreduplication and ploidy-dependent cell enlargement in plants. *The EMBO Journal*, *18*(16), 4476–4484.

Chabaud, M., Genre, A., Sieberer, B. J., Faccio, A., Fournier, J., Novero, M., Barker, D. G., & Bonfante, P. (2011). Arbuscular mycorrhizal hyphopodia and germinated spore exudates trigger Ca^{2+} spiking in the legume and nonlegume root epidermis. *New Phytologist*, *189*(1), 347–355.

Chabaud, M., Venard, C., Defaux-Petras, A., Bécard, G., & Barker, D. G. (2002). Targeted inoculation of *Medicago truncatula in vitro* root cultures reveals *MtENOD11* expression during early stages of infection by arbuscular mycorrhizal fungi. *New Phytologist*, *156*(2), 265–273.

Charon, C., Johansson, C., Kondorosi, E., Kondorosi, A., & Crespi, M. (1997). Enod40 induces dedifferentiation and division of root cortical cells in legumes. *Proceedings of the National Academy of Sciences*, *94*(16), 8901–8906.

Charon, C., Sousa, C., Crespi, M., & Kondorosi, A. (1999). Alteration of *ENOD40* expression modifies *Medicago truncatula* root nodule development induced by *Sinorhizobium meliloti*. *The Plant Cell*, *11*(10), 1953–1965.

Charpentier, M., Bredemeier, R., Wanner, G., Takeda, N., Schleiff, E., & Parniske, M. (2008). *Lotus japonicus* CASTOR and POLLUX are ion channels essential for perinuclear calcium spiking in legume root endosymbiosis. *The Plant Cell*, *20*(12), 3467–3479.

Charpentier, M., & Oldroyd, G. E. D. (2013). Nuclear calcium signaling in plants. *Plant Physiology*, *163*(2), 496–503.

Charpentier, M., Sun, J., Martins, T. V., Radhakrishnan, G. V., Findlay, K., Soumpourou, E., Thouin, J., Véry, A.-A., Sanders, D., Morris, R. J., & Oldroyd, G. E. D. (2016). Nuclear-localized cyclic nucleotide–gated channels mediate symbiotic calcium oscillations. *Science*, *352*(6289), 1102–1105.

Charpentier, M., Sun, J., Wen, J., Mysore, K. S., & Oldroyd, G. E. D. (2014). Abscisic acid promotion of arbuscular mycorrhizal colonization requires a component of the PROTEIN PHOSPHATASE 2A complex. *Plant Physiology*, *166*(4), 2077–2090.

Charpentier, M., Vaz Martins, T., Granqvist, E., Oldroyd, G. E. D., & Morris, R. J. (2013). The role of DMI1 in establishing Ca^{2+} oscillations in legume symbioses. *Plant Signaling & Behavior*, *8*(2), e22894.

Charron, D., Pingret, J.-L., Chabaud, M., Journet, E.-P., & Barker, D. G. (2004). Pharmacological evidence that multiple phospholipid signaling pathways link rhizobium Nodulation factor perception in *Medicago truncatula* root hairs to intracellular responses, including Ca^{2+} spiking and specific *ENOD* gene expression. *Plant Physiology*, *136*(3), 3582–3593.

Chen, C., Fan, C., Gao, M., & Zhu, H. (2009). Antiquity and function of CASTOR and POLLUX, the twin ion channel-encoding genes key to the evolution of root symbioses in plants. *Plant Physiology*, *149*(1), 306–317.

Chen, G., Li, Q., & Yan, J. (2022). The leucine-rich repeat domains of BK channel auxiliary γ subunits regulate their expression, trafficking, and channel-modulation functions. *Journal of Biological Chemistry*, *298*(3), 101664.

Chen, Y., Hu, L., Punta, M., Bruni, R., Hillerich, B., Kloss, B., Rost, B., Love, J., Siegelbaum, S. A., & Hendrickson, W. A. (2010). Homologue structure of the SLAC1 anion channel for closing stomata in leaves. *Nature*, *467*(7319), Article 7319.

Chen, Y., Liu, J., Lin, J., Roswanjaya, Y. P., Nadzieja, M., Buron, F., Kohlen, W., Geisler, M., Stougaard, J., & Reid, D. (2022). Cytokinin synthesis and export from symbiotic root nodules coordinates shoot growth with nitrogen fixation (p. 2022.12.03.518951). *bioRxiv*.

Choi, M. S., Kim, M. C., Yoo, J. H., Moon, B. C., Koo, S. C., Park, B. O., Lee, J. H., Koo, Y. D., Han, H. J., Lee, S. Y., Chung, W. S., Lim, C. O., & Cho, M. J. (2005). Isolation of a calmodulin-binding transcription factor from rice *(Oryza sativa* L.). *The Journal of Biological Chemistry*, *280*(49), 40820–40831.

Christian, J.-O., Braginets, R., Schulze, W., & Walther, D. (2012). Characterization and prediction of protein phosphorylation hotspots in *Arabidopsis thaliana*. *Frontiers in Plant Science*, *3*.

Clapham, D. E. (2007). Calcium signaling. *Cell*, *131*(6), 1047–1058.

Crespi, M. d., Jurkevitch, E., Poiret, M., d'Aubenton-Carafa, Y., Petrovics, G., Kondorosi, E., & Kondorosi, A. (1994). Enod40, a gene expressed during nodule organogenesis, codes for a non-translatable RNA involved in plant growth. *The EMBO Journal*, *13*(21), 5099–5112.

Cui, J., Yang, H., & Lee, U. S. (2009). Molecular mechanisms of BK channel activation. *Cellular and Molecular Life Sciences : CMLS*, *66*(5), 852–875.

Dammann, C., Ichida, A., Hong, B., Romanowsky, S. M., Hrabak, E. M., Harmon, A. C., Pickard, B. G., & Harper, J. F. (2003). Subcellular targeting of nine calcium-dependent protein kinase isoforms from Arabidopsis. *Plant Physiology*, *132*(4), 1840–1848.

de Ruijter, N. C. A., Rook, M. B., Bisseling, T., & Emons, A. M. C. (1998). Lipochito-oligosaccharides re-initiate root hair tip growth in *Vicia sativa* with high calcium and spectrin-like antigen at the tip. *The Plant Journal*, *13*(3), 341–350.

Del Cerro, P., Cook, N. M., Huisman, R., Dangeville, P., Grubb, L. E., Marchal, C., Ho Ching Lam, A., & Charpentier, M. (2022). Engineered CaM2 modulates nuclear calcium oscillation and enhances legume root nodule symbiosis. *Proceedings of the National Academy of Sciences of the United States of America*, *119*(13), e2200099119.

Demidchik, V., Shabala, S., Isayenkov, S., Cuin, T. A., & Pottosin, I. (2018). Calcium transport across plant membranes: Mechanisms and functions. *New Phytologist*, *220*(1), 49–69.

Den Hartog, M., Musgrave, A., & Munnik, T. (2001). Nod factor-induced phosphatidic acid and diacylglycerol pyrophosphate formation: A role for phospholipase C and D in root hair deformation. *The Plant Journal*, *25*(1), 55–65.

den Hartog, M., Verhoef, N., & Munnik, T. (2003). Nod factor and elicitors activate different phospholipid signaling pathways in suspension-cultured alfalfa cells. *Plant Physiology*, *132*(1), 311–317.

Den Herder, J., Vanhee, C., De Rycke, R., Corich, V., Holsters, M., & Goormachtig, S. (2007). Nod factor perception during infection thread growth fine-tunes nodulation. *Molecular Plant-Microbe Interactions*, *20*(2), 129–137.

Deng, Y., Kashtoh, H., Wang, Q., Zhen, G., Li, Q., Tang, L., Gao, H., Zhang, C., Qin, L., Su, M., Li, F., Huang, X., Wang, Y., Xie, Q., Clarke, O. B., Hendrickson, W. A., & Chen, Y. (2021). Structure and activity of SLAC1 channels for stomatal signaling in leaves. *Proceedings of the National Academy of Sciences*, *118*(18), e2015151118.

Dodson, C. A., & Bayliss, R. (2012). Activation of Aurora-A kinase by protein partner binding and phosphorylation are independent and synergistic. *The Journal of Biological Chemistry*, *287*(2), 1150–1157.

Dong, W., Zhu, Y., Chang, H., Wang, C., Yang, J., Shi, J., Gao, J., Yang, W., Lan, L., Wang, Y., Zhang, X., Dai, H., Miao, Y., Xu, L., He, Z., Song, C., Wu, S., Wang, D., Yu, N., & Wang, E. (2021). An SHR–SCR module specifies legume cortical cell fate to enable nodulation. *Nature*, *589*(7843), Article 7843.

Dubrovsky, J. G., Sauer, M., Napsucialy-Mendivil, S., Ivanchenko, M. G., Friml, J., Shishkova, S., Celenza, J., & Benková, E. (2008). Auxin acts as a local morphogenetic trigger to specify lateral root founder cells. *Proceedings of the National Academy of Sciences*, *105*(25), 8790–8794.

Ehrhardt, D. W., Wais, R., & Long, S. R. (1996). Calcium spiking in plant root hairs responding to rhizobium nodulation signals. *Cell*, *85*(5), 673–681.

Emsley, P., Lohkamp, B., Scott, W. G., & Cowtan, K. (2010). Features and development of Coot. *Acta Crystallographica. Section D, Biological Crystallography*, *66*(Pt 4), 486–501.

Endre, G., Kereszt, A., Kevei, Z., Mihacea, S., Kaló, P., & Kiss, G. B. (2002). A receptor kinase gene regulating symbiotic nodule development. *Nature*, *417*(6892), Article 6892.

Engstrom, E. M., Ehrhardt, D. W., Mitra, R. M., & Long, S. R. (2002). Pharmacological analysis of Nod factor-induced calcium spiking in *Medicago truncatula*. Evidence for the requirement of type IIA calcium pumps and phosphoinositide signaling. *Plant Physiology*, *128*(4), 1390–1401.

Esseling, J. J., Lhuissier, F. G. P., & Emons, A. M. C. (2003). Nod factor-induced root hair curling: continuous polar growth towards the point of Nod factor application. *Plant Physiology*, *132*(4), 1982–1988.

Etemadi, M., Gutjahr, C., Couzigou, J.-M., Zouine, M., Lauressergues, D., Timmers, A., Audran, C., Bouzayen, M., Bécard, G., & Combier, J.-P. (2014). Auxin perception is required for arbuscule development in arbuscular mycorrhizal symbiosis1. *Plant Physiology*, *166*(1), 281–292.

Felsenstein, J. (1985). Confidence limits on phylogenies: an approach using the bootstrap. *Evolution*, *39*(4), 783–791.

Floss, D. S., Levy, J. G., Lévesque-Tremblay, V., Pumplin, N., & Harrison, M. J. (2013). DELLA proteins regulate arbuscule formation in arbuscular mycorrhizal symbiosis. *Proceedings of the National Academy of Sciences*, *110*(51), E5025–E5034.

Foo, E., Ross, J. J., Jones, W. T., & Reid, J. B. (2013). Plant hormones in arbuscular mycorrhizal symbioses: An emerging role for gibberellins. *Annals of Botany*, *111*(5), 769–779.

Franssen, H. J., Xiao, T. T., Kulikova, O., Wan, X., Bisseling, T., Scheres, B., & Heidstra, R. (2015). Root developmental programs shape the *Medicago truncatula* nodule meristem. *Development*, *142*(17), 2941–2950.

Fujishige, N. A., Kapadia, N. N., De Hoff, P. L., & Hirsch, A. M. (2006). Investigations of Rhizobium biofilm formation. *FEMS Microbiology Ecology*, *56*(2), 195–206.

Gage, D. J. (2002). Analysis of infection thread development using *GFP*- and *DsRed*-expressing *Sinorhizobium meliloti. Journal of Bacteriology*, *184*(24), 7042–7046.

Galinha, C., Hofhuis, H., Luijten, M., Willemsen, V., Blilou, I., Heidstra, R., & Scheres, B. (2007). PLETHORA proteins as dose-dependent master regulators of Arabidopsis root development. *Nature*, *449*(7165), Article 7165.

Gampala, S. S., Kim, T.-W., He, J.-X., Tang, W., Deng, Z., Bai, M.-Y., Guan, S., Lalonde, S., Sun, Y., Gendron, J. M., Chen, H., Shibagaki, N., Ferl, R. J., Ehrhardt, D., Chong, K., Burlingame, A. L., & Wang, Z.-Y. (2007). An essential role for 14-3-3 proteins in brassinosteroid signal transduction in Arabidopsis. *Developmental Cell*, *13*(2), 177–189.

Gauthier-Coles, C., White, R. G., & Mathesius, U. (2019). Nodulating legumes are distinguished by a sensitivity to cytokinin in the root cortex leading to pseudonodule development. *Frontiers in Plant Science*, *9*.

Gautrat, P., Laffont, C., & Frugier, F. (2020). COMPACT ROOT ARCHITECTURE 2 promotes root competence for nodulation through the mir2111 systemic effector. *Current Biology*, *30*(7), 1339-1345.e3.

Gautrat, P., Mortier, V., Laffont, C., De Keyser, A., Fromentin, J., Frugier, F., & Goormachtig, S. (2019). Unraveling new molecular players involved in the

autoregulation of nodulation in *Medicago truncatula*. *Journal of Experimental Botany*, *70*(4), 1407–1417.

Geiger, D., Scherzer, S., Mumm, P., Stange, A., Marten, I., Bauer, H., Ache, P., Matschi, S., Liese, A., Al-Rasheid, K. A. S., Romeis, T., & Hedrich, R. (2009). Activity of guard cell anion channel SLAC1 is controlled by drought-stress signaling kinase-phosphatase pair. *Proceedings of the National Academy of Sciences*, *106*(50), 21425–21430.

Genre, A., Chabaud, M., Balzergue, C., Puech-Pagès, V., Novero, M., Rey, T., Fournier, J., Rochange, S., Bécard, G., Bonfante, P., & Barker, D. G. (2013). Short-chain chitin oligomers from arbuscular mycorrhizal fungi trigger nuclear Ca^{2+} spiking in *Medicago truncatula* roots and their production is enhanced by strigolactone. *New Phytologist*, *198*(1), 190–202.

Genre, A., Chabaud, M., Faccio, A., Barker, D. G., & Bonfante, P. (2008). Prepenetration apparatus assembly precedes and predicts the colonization patterns of arbuscular mycorrhizal fungi within the root cortex of both *Medicago truncatula* and *Daucus carota*. *The Plant Cell*, *20*(5), 1407–1420.

Genre, A., Chabaud, M., Timmers, T., Bonfante, P., & Barker, D. G. (2005). Arbuscular mycorrhizal fungi elicit a novel intracellular apparatus in *Medicago truncatula* root epidermal cells before infection. *The Plant Cell*, *17*(12), 3489–3499.

Gibelin-Viala, C., Amblard, E., Puech-Pages, V., Bonhomme, M., Garcia, M., Bascaules-Bedin, A., Fliegmann, J., Wen, J., Mysore, K. S., le Signor, C., Jacquet, C., & Gough, C. (2019). The *Medicago truncatula* LysM receptor-like kinase LYK9 plays a dual role in immunity and the arbuscular mycorrhizal symbiosis. *New Phytologist*, *223*(3), 1516–1529.

Giovannetti, M., & Mosse, B. (1980). An evaluation of techniques for measuring vesicular arbuscular mycorrhizal infection in roots. *The New Phytologist*, *84*(3), 489–500.

Gleason, C., Chaudhuri, S., Yang, T., Muñoz, A., Poovaiah, B. W., & Oldroyd, G. E. D. (2006). Nodulation independent of rhizobia induced by a calcium-activated kinase lacking autoinhibition. *Nature*, *441*(7097), Article 7097.

Goedhart, J., Hink, M. A., Visser, A. J. W. G., Bisseling, T., & Gadella Jr, T. W. J. (2000). *In vivo* fluorescence correlation microscopy (FCM) reveals accumulation and immobilization of Nod factors in root hair cell walls. *The Plant Journal*, *21*(1), 109–119.

Goh, T., Joi, S., Mimura, T., & Fukaki, H. (2012). The establishment of asymmetry in Arabidopsis lateral root founder cells is regulated by LBD16/ASL18 and related LBD/ASL proteins. *Development*, *139*(5), 883–893.

Goldberg, J., Nairn, A. C., & Kuriyan, J. (1996). Structural basis for the autoinhibition of CALCIUM/CALMODULIN-DEPENDENT PROTEIN KINASE I. *Cell*, *84*(6), 875–887.

Gomez, S. K., Javot, H., Deewatthanawong, P., Torres-Jerez, I., Tang, Y., Blancaflor, E. B., Udvardi, M. K., & Harrison, M. J. (2009). *Medicago truncatula* and *Glomus intraradices* gene expression in cortical cells harboring arbuscules in the arbuscular mycorrhizal symbiosis. *BMC Plant Biology*, *9*(1), 10.

Gonzalez-Rizzo, S., Crespi, M., & Frugier, F. (2006). The *Medicago truncatula* CRE1 cytokinin receptor regulates lateral root development and early symbiotic interaction with *Sinorhizobium meliloti*. *The Plant Cell*, *18*(10), 2680–2693.

Granqvist, E., Sun, J., Op den Camp, R., Pujic, P., Hill, L., Normand, P., Morris, R. J., Downie, J. A., Geurts, R., & Oldroyd, G. E. D. (2015). Bacterial-induced calcium oscillations are common to nitrogen-fixing associations of nodulating legumes and non-legumes. *New Phytologist*, *207*(3), 551–558.

Granqvist, E., Wysham, D., Hazledine, S., Kozlowski, W., Sun, J., Charpentier, M., Martins, T. V., Haleux, P., Tsaneva-Atanasova, K., Downie, J. A., Oldroyd, G. E. D., & Morris, R. J. (2012). Buffering capacity explains signal variation in symbiotic calcium oscillation. *Plant Physiology*, *160*(4), 2300–2310.

Gronnier, J., Franck, C. M., Stegmann, M., DeFalco, T. A., Abarca, A., von Arx, M., Dünser, K., Lin, W., Yang, Z., Kleine-Vehn, J., Ringli, C., & Zipfel, C. (2022). Regulation of immune receptor kinase plasma membrane nanoscale organization by a plant peptide hormone and its receptors. *ELife*, *11*, e74162.

Gronnier, J., Legrand, A., Loquet, A., Habenstein, B., Germain, V., & Mongrand, S. (2019). Mechanisms governing subcompartmentalization of biological membranes. *Current Opinion in Plant Biology*, *52*, 114–123.

Groth, M., Takeda, N., Perry, J., Uchida, H., Dräxl, S., Brachmann, A., Sato, S., Tabata, S., Kawaguchi, M., Wang, T. L., & Parniske, M. (2010). NENA, a *Lotus japonicus* homolog of Sec13, is required for rhizodermal infection by arbuscular mycorrhiza fungi and rhizobia but dispensable for cortical endosymbiotic development. *The Plant Cell*, *22*(7), 2509–2526.

Guan, Q., Wu, J., Yue, X., Zhang, Y., & Zhu, J. (2013). A nuclear calcium-sensing pathway is critical for gene regulation and salt stress tolerance in Arabidopsis. *PLOS Genetics*, *9*(8), e1003755.

Gudesblat, G. E., Schneider-Pizoń, J., Betti, C., Mayerhofer, J., Vanhoutte, I., van Dongen, W., Boeren, S., Zhiponova, M., de Vries, S., Jonak, C., & Russinova, E. (2012). SPEECHLESS integrates brassinosteroid and stomata signalling pathways. *Nature Cell Biology*, *14*(5), Article 5.

Gutjahr, C., Novero, M., Guether, M., Montanari, O., Udvardi, M., & Bonfante, P. (2009). Presymbiotic factors released by the arbuscular mycorrhizal fungus *Gigaspora margarita* induce starch accumulation in *Lotus japonicus* roots. *New Phytologist*, *183*(1), 53–61.

Gutjahr, C., & Parniske, M. (2013). Cell and developmental biology of arbuscular mycorrhiza symbiosis. *Annual Review of Cell and Developmental Biology*, *29*, 593–617.

Hajný, J., Prát, T., Rydza, N., Rodriguez, L., Tan, S., Verstraeten, I., Domjan, D., Mazur, E., Smakowska-Luzan, E., Smet, W., Mor, E., Nolf, J., Yang, B., Grunewald, W., Molnár, G., Belkhadir, Y., De Rybel, B., & Friml, J. (2020). Receptor kinase module targets PIN-dependent auxin transport during canalization. *Science*, *370*(6516), 550–557.

Hall, S. K., & Armstrong, D. L. (2000). Conditional and unconditional inhibition of calcium-activated potassium channels by reversible protein phosphorylation. *Journal of Biological Chemistry*, *275*(6), 3749–3754.

Han, C., Liu, Y., Shi, W., Qiao, Y., Wang, L., Tian, Y., Fan, M., Deng, Z., Lau, O. S., De Jaeger, G., & Bai, M.-Y. (2020). KIN10 promotes stomatal development through stabilization of the SPEECHLESS transcription factor. *Nature Communications*, *11*(1), Article 1.

Harris, J. M., Wais, R., & Long, S. R. (2003). *Rhizobium*-induced calcium spiking in *Lotus japonicus*. *Molecular Plant-Microbe Interactions*, *16*(4), 335–341.

Hayashi, T., Banba, M., Shimoda, Y., Kouchi, H., Hayashi, M., & Imaizumi-Anraku, H. (2010). A dominant function of CCaMK in intracellular accommodation of bacterial and fungal endosymbionts. *The Plant Journal*, *63*(1), 141–154.

Hayashi, T., Shimoda, Y., Sato, S., Tabata, S., Imaizumi-Anraku, H., & Hayashi, M. (2014). Rhizobial infection does not require cortical expression of upstream common symbiosis genes responsible for the induction of Ca^{2+} spiking. *The Plant Journal*, *77*(1), 146–159.

He, J., Benedito, V. A., Wang, M., Murray, J. D., Zhao, P. X., Tang, Y., & Udvardi, M. K. (2009). The *Medicago truncatula* gene expression atlas web server. *BMC Bioinformatics*, *10*, 441.

He, J.-X., Gendron, J. M., Yang, Y., Li, J., & Wang, Z.-Y. (2002). The GSK3-like kinase BIN2 phosphorylates and destabilizes BZR1, a positive regulator of the brassinosteroid signaling pathway in Arabidopsis. *Proceedings of the National Academy of Sciences*, *99*(15), 10185–10190.

He, Y., Zhou, J., Shan, L., & Meng, X. (2018). Plant cell surface receptor-mediated signaling – a common theme amid diversity. *Journal of Cell Science*, *131*(2), jcs209353.

Heckmann, A. B., Sandal, N., Bek, A. S., Madsen, L. H., Jurkiewicz, A., Nielsen, M. W., Tirichine, L., & Stougaard, J. (2011). Cytokinin induction of root nodule primordia in *Lotus japonicus* is regulated by a mechanism operating in the root cortex. *Molecular Plant-Microbe Interactions*, *24*(11), 1385–1395.

Helariutta, Y., Fukaki, H., Wysocka-Diller, J., Nakajima, K., Jung, J., Sena, G., Hauser, M.-T., & Benfey, P. N. (2000). The *SHORT-ROOT* gene controls radial patterning of the Arabidopsis root through radial signaling. *Cell*, *101*(5), 555–567.

Heldin, C.-H. (1995). Dimerization of cell surface receptors in signal transduction. *Cell*, *80*(2), 213–223.

Herrbach, V., Chirinos, X., Rengel, D., Agbevenou, K., Vincent, R., Pateyron, S., Huguet, S., Balzergue, S., Pasha, A., Provart, N., Gough, C., & Bensmihen, S. (2017). Nod factors potentiate auxin signaling for transcriptional regulation and lateral root formation in *Medicago truncatula*. *Journal of Experimental Botany*, *68*(3), 569–583.

Herrbach, V., Remblière, C., Gough, C., & Bensmihen, S. (2014). Lateral root formation and patterning in *Medicago truncatula*. *Journal of Plant Physiology*, *171*(3), 301–310.

Higashijima, T., Burnier, J., & Ross, E. M. (1990). Regulation of *Gi* and *Go* by mastoparan, related amphiphilic peptides, and hydrophobic amines. Mechanism and structural determinants of activity. *Journal of Biological Chemistry*, *265*(24), 14176–14186.

Hink, M. A., Shah, K., Russinova, E., Vries, S. C. de, & Visser, A. J. W. G. (2008). Fluorescence fluctuation analysis of *Arabidopsis thaliana* SOMATIC EMBRYOGENESIS RECEPTOR-LIKE KINASE and BRASSINOSTEROID INSENSITIVE 1 receptor oligomerization. *Biophysical Journal*, *94*(3), 1052–1062.

Hirsch, A. M., Larue, T. A., & Doyle, J. (1997). Is the legume nodule a modified root or stem or an organ *sui generis*? *Critical Reviews in Plant Sciences*, *16*(4), 361–392.

Hirsch, R. E., Lewis, B. D., Spalding, E. P., & Sussman, M. R. (1998). A role for the AKT1 potassium channel in plant nutrition. *Science*, *280*(5365), 918–921.

Hoffmann, B., Trinh, T. H., Leung, J., Kondorosi, A., & Kondorosi, E. (1997). A new *Medicago truncatula* line with superior *in vitro* regeneration, transformation, and symbiotic properties isolated through cell culture selection. *Molecular Plant-Microbe Interactions*, *10*(3), 307–315.

Horváth, B., Yeun, L. H., Domonkos, A., Halász, G., Gobbato, E., Ayaydin, F., Miró, K., Hirsch, S., Sun, J., Tadege, M., Ratet, P., Mysore, K. S., Ané, J.-M., Oldroyd, G. E. D., & Kaló, P. (2011). *Medicago truncatula* IPD3 is a member of the common symbiotic signaling pathway required for rhizobial and mycorrhizal symbioses. *Molecular Plant-Microbe Interactions: MPMI*, *24*(11), 1345–1358.

Houbaert, A., Zhang, C., Tiwari, M., Wang, K., de Marcos Serrano, A., Savatin, D. V., Urs, M. J., Zhiponova, M. K., Gudesblat, G. E., Vanhoutte, I., Eeckhout, D., Boeren, S.,

Karimi, M., Betti, C., Jacobs, T., Fenoll, C., Mena, M., de Vries, S., De Jaeger, G., & Russinova, E. (2018). POLAR-guided signalling complex assembly and localization drive asymmetric cell division. *Nature*, *563*(7732), Article 7732.

Huault, E., Laffont, C., Wen, J., Mysore, K. S., Ratet, P., Duc, G., & Frugier, F. (2014). Local and systemic regulation of plant root system architecture and symbiotic nodulation by a receptor-like kinase. *PLOS Genetics*, *10*(12), e1004891.

Hubbard, S. R. (1997). Crystal structure of the activated insulin receptor tyrosine kinase in complex with peptide substrate and ATP analog. *The EMBO Journal*, *16*(18), 5572–5581.

Imin, N., Mohd-Radzman, N. A., Ogilvie, H. A., & Djordjevic, M. A. (2013). The peptide-encoding CEP1 gene modulates lateral root and nodule numbers in *Medicago truncatula*. *Journal of Experimental Botany*, *64*(17), 5395–5409.

Ishida, S., Yuasa, T., Nakata, M., & Takahashi, Y. (2008). A Tobacco Calcium-Dependent Protein Kinase, CDPK1, Regulates the Transcription Factor REPRESSION OF SHOOT GROWTH in Response to Gibberellins. *The Plant Cell*, *20*(12), 3273–3288.

Jabaji-Hare, S., Deschene, A., & Kendrick, B. (1984). Lipid content and composition of vesicles of a vesicular-arbuscular mycorrhizal fungus. *Mycologia*, *76*(6), 1024–1030.

Jacobson, K., Liu, P., & Lagerholm, B. C. (2019). The lateral organization and mobility of plasma membrane components. *Cell*, *177*(4), 806–819.

Jafari, N., Del Rio, J., Akimoto, M., Byun, J. A., Boulton, S., Moleschi, K., Alsayyed, Y., Swanson, P., Huang, J., Martinez Pomier, K., Lee, C., Wu, J., Taylor, S. S., & Melacini, G. (2021). Noncanonical protein kinase A activation by oligomerization of regulatory subunits as revealed by inherited Carney complex mutations. *Proceedings of the National Academy of Sciences*, *118*(21), e2024716118.

Jauregui, E., Du, L., Gleason, C., & Poovaiah, B. W. (2017). W342F mutation in CCaMK enhances its affinity to calmodulin but compromises its role in supporting root nodule symbiosis in *Medicago truncatula*. *Frontiers in Plant Science*, *8*.

Jin, Y., Liu, H., Luo, D., Yu, N., Dong, W., Wang, C., Zhang, X., Dai, H., Yang, J., & Wang, E. (2016). DELLA proteins are common components of symbiotic rhizobial and mycorrhizal signalling pathways. *Nature Communications*, *7*, 12433.

Journet, E. p., Pichon, M., Dedieu, A., De Billy, F., Truchet, G., & Barker, D. g. (1994). *Rhizobium meliloti* Nod factors elicit cell-specific transcription of the *ENOD12* gene in transgenic alfalfa. *The Plant Journal*, *6*(2), 241–249.

Journet, E.-P., El-Gachtouli, N., Vernoud, V., de Billy, F., Pichon, M., Dedieu, A., Arnould, C., Morandi, D., Barker, D. G., & Gianinazzi-Pearson, V. (2001). *Medicago truncatula ENOD11*: A novel RPRP-encoding early nodulin gene expressed during

mycorrhization in arbuscule-containing cells. *Molecular Plant-Microbe Interactions*, *14*(6), 737–748.

Kanamori, N., Madsen, L. H., Radutoiu, S., Frantescu, M., Quistgaard, E. M. H., Miwa, H., Downie, J. A., James, E. K., Felle, H. H., Haaning, L. L., Jensen, T. H., Sato, S., Nakamura, Y., Tabata, S., Sandal, N., & Stougaard, J. (2006). A nucleoporin is required for induction of Ca^{2+} spiking in legume nodule development and essential for rhizobial and fungal symbiosis. *Proceedings of the National Academy of Sciences*, *103*(2), 359–364.

Kelner, A., Leitão, N., Chabaud, M., Charpentier, M., & de Carvalho-Niebel, F. (2018). Dual color sensors for simultaneous analysis of calcium signal dynamics in the nuclear and cytoplasmic compartments of plant cells. *Frontiers in Plant Science*, *9*.

Kevei, Z., Lougnon, G., Mergaert, P., Horváth, G. V., Kereszt, A., Jayaraman, D., Zaman, N., Marcel, F., Regulski, K., Kiss, G. B., Kondorosi, A., Endre, G., Kondorosi, E., & Ané, J.-M. (2007). 3-HYDROXY-3-METHYLGLUTARYL COENZYME A REDUCTASE1 interacts with NORK and is crucial for nodulation in *Medicago truncatula*. *The Plant Cell*, *19*(12), 3974–3989.

Kim, S., Zeng, W., Bernard, S., Liao, J., Venkateshwaran, M., Ane, J.-M., & Jiang, Y. (2019). Ca^{2+}-regulated Ca^{2+} channels with an RCK gating ring control plant symbiotic associations. *Nature Communications*, *10*, 3703.

Kinoshita, T., Caño-Delgado, A., Seto, H., Hiranuma, S., Fujioka, S., Yoshida, S., & Chory, J. (2005). Binding of brassinosteroids to the extracellular domain of plant receptor kinase BRI1. *Nature*, *433*(7022), Article 7022.

Kirchler, T., Briesemeister, S., Singer, M., Schütze, K., Keinath, M., Kohlbacher, O., Vicente-Carbajosa, J., Teige, M., Harter, K., & Chaban, C. (2010). The role of phosphorylatable serine residues in the DNA-binding domain of Arabidopsis bZIP transcription factors. *European Journal of Cell Biology*, *89*(2), 175–183.

Knight, M. R., Campbell, A. K., Smith, S. M., & Trewavas, A. J. (1991). Transgenic plant aequorin

reports the effects of touch and cold-shock and elicitors on cytoplasmic calcium. *Nature,*

352(6335), Article 6335.

Kosuta, S., Chabaud, M., Lougnon, G., Gough, C., Dénarié, J., Barker, D. G., & Bécard, G. (2003). A diffusible factor from arbuscular mycorrhizal fungi induces symbiosis-specific *MtENOD1*1 expression in roots of *Medicago truncatula*. *Plant Physiology*, *131*(3), 952–962.

Kosuta, S., Hazledine, S., Sun, J., Miwa, H., Morris, R. J., Downie, J. A., & Oldroyd, G. E. D. (2008). Differential and chaotic calcium signatures in the symbiosis signaling

pathway of legumes. *Proceedings of the National Academy of Sciences of the United States of America*, *105*(28), 9823–9828.

Krogh, A., Larsson, B., von Heijne, G., & Sonnhammer, E. L. L. (2001). Predicting transmembrane protein topology with a hidden markov model: Application to complete genomes. *Journal of Molecular Biology*, *305*(3), 567–580.

Krusell, L., Madsen, L. H., Sato, S., Aubert, G., Genua, A., Szczyglowski, K., Duc, G., Kaneko, T., Tabata, S., de Bruijn, F., Pajuelo, E., Sandal, N., & Stougaard, J. (2002). Shoot control of root development and nodulation is mediated by a receptor-like kinase. *Nature*, *420*(6914), Article 6914.

Kudla, J., Becker, D., Grill, E., Hedrich, R., Hippler, M., Kummer, U., Parniske, M., Romeis, T., & Schumacher, K. (2018). Advances and current challenges in calcium signaling. *New Phytologist*, *218*(2), 414–431.

Kumar, S., Stecher, G., Li, M., Knyaz, C., & Tamura, K. (2018). MEGA X: Molecular Evolutionary

Genetics Analysis across Computing Platforms. *Molecular Biology and Evolution*, *35*(6),

1547–1549.

Lachaud, C., Da Silva, D., Cotelle, V., Thuleau, P., Xiong, T. C., Jauneau, A., Brière, C., Graziana, A., Bellec, Y., Faure, J.-D., Ranjeva, R., & Mazars, C. (2010). Nuclear calcium controls the apoptotic-like cell death induced by d-erythro-sphinganine in tobacco cells. *Cell Calcium*, *47*(1), 92–100.

Laffont, C., Huault, E., Gautrat, P., Endre, G., Kalo, P., Bourion, V., Duc, G., & Frugier, F. (2019). Independent regulation of symbiotic nodulation by the SUNN negative and CRA2 positive systemic pathways. *Plant Physiology*, *180*(1), 559–570.

Lakatos, L., Szittya, G., Silhavy, D., & Burgyán, J. (2004). Molecular mechanism of RNA silencing suppression mediated by p19 protein of tombusviruses. *The EMBO Journal*, *23*(4), 876–884.

Lampard, G. R., MacAlister, C. A., & Bergmann, D. C. (2008). Arabidopsis stomatal initiation is controlled by MAPK-mediated regulation of the bHLH SPEECHLESS. *Science*, *322*(5904), 1113–1116.

Laplaze, L., Benkova, E., Casimiro, I., Maes, L., Vanneste, S., Swarup, R., Weijers, D., Calvo, V., Parizot, B., Herrera-Rodriguez, M. B., Offringa, R., Graham, N., Doumas, P., Friml, J., Bogusz, D., Beeckman, T., & Bennett, M. (2007). Cytokinins act directly on lateral root founder cells to inhibit root initiation. *The Plant Cell*, *19*(12), 3889–3900.

Larrainzar, E., Riely, B. K., Kim, S. C., Carrasquilla-Garcia, N., Yu, H.-J., Hwang, H.-J., Oh, M., Kim, G. B., Surendrarao, A. K., Chasman, D., Siahpirani, A. F., Penmetsa,

R. V., Lee, G.-S., Kim, N., Roy, S., Mun, J.-H., & Cook, D. R. (2015). Deep sequencing of the *Medicago truncatula* root transcriptome reveals a massive and early interaction between Nodulation factor and ethylene signals. *Plant Physiology*, *169*(1), 233–265.

Laurenzio, L. D., Wysocka-Diller, J., Malamy, J. E., Pysh, L., Helariutta, Y., Freshour, G., Hahn, M. G., Feldmann, K. A., & Benfey, P. N. (1996). The *SCARECROW* gene regulates an asymmetric cell division that is essential for generating the radial organization of the Arabidopsis root. *Cell*, *86*(3), 423–433.

Lecourieux, D., Lamotte, O., Bourque, S., Wendehenne, D., Mazars, C., Ranjeva, R., & Pugin, A. (2005). Proteinaceous and oligosaccharidic elicitors induce different calcium signatures in the nucleus of tobacco cells. *Cell Calcium*, *38*(6), 527–538.

Lee, S. C., Lan, W., Buchanan, B. B., & Luan, S. (2009). A protein kinase-phosphatase pair interacts with an ion channel to regulate ABA signaling in plant guard cells. *Proceedings of the National Academy of Sciences*, *106*(50), 21419–21424.

Lee, S. C., Lan, W.-Z., Kim, B.-G., Li, L., Cheong, Y. H., Pandey, G. K., Lu, G., Buchanan, B. B., & Luan, S. (2007). A protein phosphorylation/dephosphorylation network regulates a plant potassium channel. *Proceedings of the National Academy of Sciences*, *104*(40), 15959–15964.

Lefebvre, B., Timmers, T., Mbengue, M., Moreau, S., Hervé, C., Tóth, K., Bittencourt-Silvestre, J., Klaus, D., Deslandes, L., Godiard, L., Murray, J. D., Udvardi, M. K., Raffaele, S., Mongrand, S., Cullimore, J., Gamas, P., Niebel, A., & Ott, T. (2010). A remorin protein interacts with symbiotic receptors and regulates bacterial infection. *Proceedings of the National Academy of Sciences*, *107*(5), 2343–2348.

Leitão, N., Dangeville, P., Carter, R., & Charpentier, M. (2019). Nuclear calcium signatures are associated with root development. *Nature Communications*, *10*, 4865.

Leppyanen, I. V., Shakhnazarova, V. Y., Shtark, O. Y., Vishnevskaya, N. A., Tikhonovich, I. A., & Dolgikh, E. A. (2018). Receptor-like kinase LYK9 in *Pisum sativum* L. is the CERK1-like receptor that controls both plant immunity and AM symbiosis development. *International Journal of Molecular Sciences*, *19*(1), Article 1.

Lerouge, P., Roche, P., Faucher, C., Maillet, F., Truchet, G., Promé, J. C., & Dénarié, J. (1990). Symbiotic host-specificity of *Rhizobium meliloti* is determined by a sulphated and acylated glucosamine oligosaccharide signal. *Nature*, *344*(6268), Article 6268.

Lévy, J., Bres, C., Geurts, R., Chalhoub, B., Kulikova, O., Duc, G., Journet, E.-P., Ané, J.-M., Lauber, E., Bisseling, T., Dénarié, J., Rosenberg, C., & Debellé, F. (2004). A putative Ca^{2+} and Calmodulin-dependent protein kinase required for bacterial and fungal symbioses. *Science*, *303*(5662), 1361–1364.

Li, J., & Nam, K. H. (2002). Regulation of brassinosteroid signaling by a GSK3/SHAGGY-like kinase. *Science*, *295*(5558), 1299–1301.

Li, J., Wen, J., Lease, K. A., Doke, J. T., Tax, F. E., & Walker, J. C. (2002). BAK1, an Arabidopsis LRR receptor-like protein kinase, interacts with BRI1 and modulates brassinosteroid signaling. *Cell*, *110*(2), 213–222.

Li, P., & Liu, J. (2021). Protein phosphorylation in plant cell signaling. *Plant Phosphoproteomics: Methods and Protocols* (pp. 45–71). Springer US.

Li, Y., Ding, Y., Qu, L., Li, X., Lai, Q., Zhao, P., Gao, Y., Xiang, C., Cang, C., Liu, X., & Sun, L. (2022). Structure of the Arabidopsis guard cell anion channel SLAC1 suggests activation mechanism by phosphorylation. *Nature Communications*, *13*(1), Article 1.

Liao, J., Singh, S., Hossain, M. S., Andersen, S. U., Ross, L., Bonetta, D., Zhou, Y., Sato, S., Tabata, S., Stougaard, J., Szczyglowski, K., & Parniske, M. (2012). Negative regulation of CCaMK is essential for symbiotic infection. *The Plant Journal*, *72*(4), 572–584.

Limpens, E., Franken, C., Smit, P., Willemse, J., Bisseling, T., & Geurts, R. (2003). LysM domain receptor kinases regulating rhizobial Nod factor-induced infection. *Science*, *302*(5645), 630–633.

Lin, J., Roswanjaya, Y. P., Kohlen, W., Stougaard, J., & Reid, D. (2021). Nitrate restricts nodule organogenesis through inhibition of cytokinin biosynthesis in *Lotus japonicus*. *Nature Communications*, *12*, 6544.

Liu, C.-W., & Murray, J. D. (2016). The role of flavonoids in nodulation host-range specificity: An update. *Plants*, *5*(3), Article 3.

Liu, G.-Z., Pi, L.-Y., Walker, J. C., Ronald, P. C., & Song, W.-Y. (2002). Biochemical characterization of the kinase domain of the rice disease resistance receptor-like kinase XA21*. *Journal of Biological Chemistry*, *277*(23), 20264–20269.

Liu, H., Ding, Y., Zhou, Y., Jin, W., Xie, K., & Chen, L.-L. (2017). CRISPR-P 2.0: An improved CRISPR-Cas9 tool for genome editing in plants. *Molecular Plant*, *10*(3), 530–532.

Liu, H., Lin, J.-S., Luo, Z., Sun, J., Huang, X., Yang, Y., Xu, J., Wang, Y.-F., Zhang, P., Oldroyd, G. E. D., & Xie, F. (2022). Constitutive activation of a nuclear-localized calcium channel complex in *Medicago truncatula*. *Proceedings of the National Academy of Sciences*, *119*(34), e2205920119.

Liu, H., & Naismith, J. H. (2008). An efficient one-step site-directed deletion, insertion, single and multiple-site plasmid mutagenesis protocol. *BMC Biotechnology*, *8*, 91.

Liu, J., Deng, J., Zhu, F., Li, Y., Lu, Z., Qin, P., Wang, T., & Dong, J. (2018). The MtDMI2-MtPUB2 negative feedback loop plays a role in nodulation homeostasis. *Plant Physiology*, *176*(4), 3003–3026.

Liu, W., Wei, Y., Sun, P., Wang, W.-H., Kleyman, T. R., & Satlin, L. M. (2009). Mechanoregulation of BK channel activity in the mammalian cortical collecting duct: Role of protein kinases A and C. *American Journal of Physiology-Renal Physiology*, *297*(4), F904–F915.

Lohar, D. P., Schaff, J. E., Laskey, J. G., Kieber, J. J., Bilyeu, K. D., & Bird, D. McK. (2004). Cytokinins play opposite roles in lateral root formation, and nematode and Rhizobial symbioses. *The Plant Journal*, *38*(2), 203–214.

Lohrmann, J., & Harter, K. (2002). Plant two-component signaling systems and the role of response regulators. *Plant Physiology*, *128*(2), 363–369.

Lu, Y., Yu, M., Jia, Y., Yang, F., Zhang, Y., Xu, X., Li, X., Yang, F., Lei, J., Wang, Y., & Yang, G. (2022). Structural basis for the activity regulation of a potassium channel AKT1 from Arabidopsis. *Nature Communications*, *13*(1), Article 1.

Lucas, M., Swarup, R., Paponov, I. A., Swarup, K., Casimiro, I., Lake, D., Peret, B., Zappala, S., Mairhofer, S., Whitworth, M., Wang, J., Ljung, K., Marchant, A., Sandberg, G., Holdsworth, M. J., Palme, K., Pridmore, T., Mooney, S., & Bennett, M. J. (2011). SHORT-ROOT regulates primary, lateral, and adventitious root development in Arabidopsis. *Plant Physiology*, *155*(1), 384–398.

Luginbuehl, L. H., & Oldroyd, G. E. D. (2017). Understanding the arbuscule at the heart of endomycorrhizal symbioses in plants. *Current Biology*, *27*(17), R952–R963.

Madsen, E. B., Madsen, L. H., Radutoiu, S., Olbryt, M., Rakwalska, M., Szczyglowski, K., Sato, S., Kaneko, T., Tabata, S., Sandal, N., & Stougaard, J. (2003). A receptor kinase gene of the LysM type is involved in legume perception of rhizobial signals. *Nature*, *425*(6958), 637–640.

Madsen, L. H., Tirichine, L., Jurkiewicz, A., Sullivan, J. T., Heckmann, A. B., Bek, A. S., Ronson, C. W., James, E. K., & Stougaard, J. (2010). The molecular network governing nodule organogenesis and infection in the model legume *Lotus japonicus.* *Nature Communications*, *1*(1), Article 1.

Maierhofer, T., Diekmann, M., Offenborn, J. N., Lind, C., Bauer, H., Hashimoto, K., S. Al-Rasheid, K. A., Luan, S., Kudla, J., Geiger, D., & Hedrich, R. (2014). Site- and kinase-specific phosphorylation-mediated activation of SLAC1, a guard cell anion channel stimulated by abscisic acid. *Science Signaling*, *7*(342), ra86–ra86.

Maillet, F., Poinsot, V., André, O., Puech-Pagès, V., Haouy, A., Gueunier, M., Cromer, L., Giraudet, D., Formey, D., Niebel, A., Martinez, E. A., Driguez, H., Bécard, G., &

Dénarié, J. (2011). Fungal lipochitooligosaccharide symbiotic signals in arbuscular mycorrhiza. *Nature*, *469*(7328), Article 7328.

Malamy, J. E., & Benfey, P. N. (1997). Organization and cell differentiation in lateral roots of *Arabidopsis thaliana*. *Development*, *124*(1), 33–44.

Mbengue, M., Camut, S., de Carvalho-Niebel, F., Deslandes, L., Froidure, S., Klaus-Heisen, D., Moreau, S., Rivas, S., Timmers, T., Hervé, C., Cullimore, J., & Lefebvre, B. (2010). The *Medicago truncatula* E3 ubiquitin ligase PUB1 interacts with the LYK3 symbiotic receptor and negatively regulates infection and nodulation. *The Plant Cell*, *22*(10), 3474–3488.

McAinsh, M. R., & Hetherington, A. M. (1998). Encoding specificity in Ca^{2+} signalling systems. *Trends in Plant Science*, *3*(1), 32–36.

McAinsh, M. R., & Pittman, J. K. (2009). Shaping the calcium signature. *New Phytologist*, *181*(2), 275–294.

McNicholas, S., Potterton, E., Wilson, K. S., & Noble, M. E. M. (2011). Presenting your structures: The CCP4mg molecular-graphics software. *Acta Crystallographica. Section D, Biological Crystallography*, *67*(Pt 4), 386–394.

Meera, P., Wallner, M., Song, M., & Toro, L. (1997). Large conductance voltage- and calcium-dependent K+ channel, a distinct member of voltage-dependent ion channels with seven N-terminal transmembrane segments (S0-S6), an extracellular N terminus, and an intracellular (S9-S10) C terminus. *Proceedings of the National Academy of Sciences*, *94*(25), 14066–14071.

Meng, W., Swenson, L. L., Fitzgibbon, M. J., Hayakawa, K., ter Haar, E., Behrens, A. E., Fulghum, J. R., & Lippke, J. A. (2002). Structure of MITOGEN-ACTIVATED PROTEIN KINASE-ACTIVATED PROTEIN (MAPKAP) KINASE 2 suggests a bifunctional switch that couples kinase activation with nuclear export. *Journal of Biological Chemistry*, *277*(40), 37401–37405.

Messinese, E., Mun, J.-H., Yeun, L. H., Jayaraman, D., Rougé, P., Barre, A., Lougnon, G., Schornack, S., Bono, J.-J., Cook, D. R., & Ané, J.-M. (2007). A novel nuclear protein interacts with the symbiotic DMI3 calcium- and calmodulin-dependent protein kinase of *Medicago truncatula*. *Molecular Plant-Microbe Interactions*, *20*(8), 912–921.

Miller, J. B., Pratap, A., Miyahara, A., Zhou, L., Bornemann, S., Morris, R. J., & Oldroyd, G. E. D. (2013). CALCIUM/CALMODULIN-DEPENDENT PROTEIN KINASE Is negatively and positively regulated by calcium, providing a mechanism for decoding calcium responses during symbiosis signaling. *The Plant Cell*, *25*(12), 5053–5066.

Mitra, R. M., Gleason, C. A., Edwards, A., Hadfield, J., Downie, J. A., Oldroyd, G. E. D., & Long, S. R. (2004). A Ca^{2+}/calmodulin-dependent protein kinase required for

symbiotic nodule development: Gene identification by transcript-based cloning. *Proceedings of the National Academy of Sciences*, *101*(13), 4701–4705.

Miwa, H., Sun, J., Oldroyd, G. E. D., & Downie, J. A. (2006). Analysis of Nod-factor-induced calcium signaling in root hairs of symbiotically defective mutants of *Lotus japonicus*. *Molecular Plant-Microbe Interactions*, *19*(8), 914–923.

Miyawaki, A., Llopis, J., Heim, R., McCaffery, J. M., Adams, J. A., Ikura, M., & Tsien, R. Y. (1997).

Fluorescent indicators for Ca^{2+}based on green fluorescent proteins and calmodulin. *Nature*,

388(6645), Article 6645.

Modi, V., & Dunbrack, R. L. (2019). Defining a new nomenclature for the structures of active and inactive kinases. *Proceedings of the National Academy of Sciences*, *116*(14), 6818–6827.

Mohd-Radzman, N. A., Laffont, C., Ivanovici, A., Patel, N., Reid, D., Stougaard, J., Frugier, F., Imin, N., & Djordjevic, M. A. (2016). Different pathways act downstream of the CEP peptide receptor CRA2 to regulate lateral root and nodule development. *Plant Physiology*, *171*(4), 2536–2548.

Montero, H., Choi, J., & Paszkowski, U. (2019). Arbuscular mycorrhizal phenotyping: The dos and don'ts. *The New Phytologist*, *221*(3), 1182–1186.

Mortier, V., De Wever, E., Vuylsteke, M., Holsters, M., & Goormachtig, S. (2012). Nodule numbers are governed by interaction between CLE peptides and cytokinin signaling. *The Plant Journal*, *70*(3), 367–376.

Mortier, V., Den Herder, G., Whitford, R., Van de Velde, W., Rombauts, S., D'haeseleer, K., Holsters, M., & Goormachtig, S. (2010). CLE peptides control *Medicago truncatula* nodulation locally and systemically. *Plant Physiology*, *153*(1), 222–237.

Moser, M., Kirkpatrick, A., Groves, N. R., & Meier, I. (2020). LINC-complex mediated positioning of the vegetative nucleus is involved in calcium and ROS signaling in Arabidopsis pollen tubes. *Nucleus*, *11*(1), 149–163.

Munnik, T., van Himbergen, J. A. J., ter Riet, B., Braun, F.-J., Irvine, R. F., van den Ende, H., & Musgrave, A. (1998). Detailed analysis of the turnover of polyphosphoinositides and phosphatidic acid upon activation of phospholipases C and D in Chlamydomonas cells treated with non-permeabilizing concentrations of mastoparan. *Planta*, *207*(1), 133–145.

Murakami, Y., & Mizuguchi, K. (2010). Applying the Naïve Bayes classifier with kernel density estimation to the prediction of protein–protein interaction sites. *Bioinformatics*, *26*(15), 1841–1848.

Murray, J. D., Karas, B. J., Sato, S., Tabata, S., Amyot, L., & Szczyglowski, K. (2007). A cytokinin perception mutant colonized by rhizobium in the absence of nodule organogenesis. *Science*.

Nam, K. H., & Li, J. (2002). BRI1/BAK1, a receptor kinase pair mediating brassinosteroid signaling. *Cell*, *110*(2), 203–212.

Needham, S. R., Roberts, S. K., Arkhipov, A., Mysore, V. P., Tynan, C. J., Zanetti-Domingues, L. C., Kim, E. T., Losasso, V., Korovesis, D., Hirsch, M., Rolfe, D. J., Clarke, D. T., Winn, M. D., Lajevardipour, A., Clayton, A. H. A., Pike, L. J., Perani, M., Parker, P. J., Shan, Y., Shaw, D.E., & Martin-Fernandez, M. L. (2016). EGFR oligomerization organizes kinase-active dimers into competent signalling platforms. *Nature Communications*, *7*(1), Article 1.

Negi, S., Ivanchenko, M. G., & Muday, G. K. (2008). Ethylene regulates lateral root formation and auxin transport in *Arabidopsis thaliana*. *The Plant Journal: For Cell and Molecular Biology*, *55*(2), 175–187.

Nguyen Ba, A. N., Pogoutse, A., Provart, N., & Moses, A. M. (2009). NLStradamus: A simple Hidden Markov Model for nuclear localization signal prediction. *BMC Bioinformatics*, *10*(1), 202.

Ni, W., Xu, S.-L., Chalkley, R. J., Pham, T. N. D., Guan, S., Maltby, D. A., Burlingame, A. L., Wang, Z.-Y., & Quail, P. H. (2013). Multisite light-induced phosphorylation of the transcription factor pif3 is necessary for both its rapid degradation and concomitant negative feedback modulation of photoreceptor phyB levels in Arabidopsis. *The Plant Cell*, *25*(7), 2679–2698.

Nolen, B., Taylor, S., & Ghosh, G. (2004). Regulation of protein kinases: Controlling activity through activation segment conformation. *Molecular Cell*, *15*(5), 661–675.

Oh, E.-S., Lee, Y., Chae, W. B., Rameneni, J. J., Park, Y.-S., Lim, Y. P., & Oh, M.-H. (2018). Biochemical analysis of the role of leucine-rich repeat receptor-like kinases and the carboxy-terminus of receptor kinases in regulating kinase activity in *Arabidopsis thaliana* and *Brassica oleracea*. *Molecules : A Journal of Synthetic Chemistry and Natural Product Chemistry*, *23*(1), 236.

Okushima, Y., Fukaki, H., Onoda, M., Theologis, A., & Tasaka, M. (2007). ARF7 and ARF19 regulate lateral root formation via direct activation of LBD/ASL genes in Arabidopsis. *The Plant Cell*, *19*(1), 118–130.

Oláh, B., Brière, C., Bécard, G., Dénarié, J., & Gough, C. (2005). Nod factors and a diffusible factor from arbuscular mycorrhizal fungi stimulate lateral root formation in *Medicago truncatula* via the DMI1/DMI2 signalling pathway. *The Plant Journal*, *44*(2), 195–207.

Oldroyd, G. E. D., Engstrom, E. M., & Long, S. R. (2001). Ethylene inhibits the Nod factor signal transduction pathway of *Medicago truncatula*. *The Plant Cell*, *13*(8), 1835–1849.

Oldroyd, G. E. D., Mitra, R. M., Wais, R. J., & Long, S. R. (2001). Evidence for structurally specific negative feedback in the Nod factor signal transduction pathway. *The Plant Journal*, *28*(2), 191–199.

Osman, A. (2004). Yeast two-hybrid assay for studying protein-protein interactions. *Methods in Molecular Biology (Clifton, N.J.)*, *270*, 403–422.

Ovchinnikova, E., Journet, E.-P., Chabaud, M., Cosson, V., Ratet, P., Duc, G., Fedorova, E., Liu, W., den Camp, R. O., Zhukov, V., Tikhonovich, I., Borisov, A., Bisseling, T., & Limpens, E. (2011). IPD3 controls the formation of nitrogen-fixing symbiosomes in pea and *Medicago* Spp. *Molecular Plant-Microbe Interactions*, *24*(11), 1333–1344.

Pauly, N., Knight, M. R., Thuleau, P., Graziana, A., Muto, S., Ranjeva, R., & Mazars, C. (2001). The nucleus together with the cytosol generates patterns of specific cellular calcium signatures in tobacco suspension culture cells. *Cell Calcium*, *30*(6), 413–421.

Pauly, N., Knight, M. R., Thuleau, P., van der Luit, A. H., Moreau, M., Trewavas, A. J., Ranjeva, R., & Mazars, C. (2000). Control of free calcium in plant cell nuclei. *Nature*, *405*(6788), Article 6788.

Peiter, E., Sun, J., Heckmann, A. B., Venkateshwaran, M., Riely, B. K., Otegui, M. S., Edwards, A., Freshour, G., Hahn, M. G., Cook, D. R., Sanders, D., Oldroyd, G. E. D., Downie, J. A., & Ané, J.-M. (2007). The *Medicago truncatula* DMI1 protein modulates cytosolic calcium signaling. *Plant Physiology*, *145*(1), 192–203.

Penmetsa,V, , & Cook, D.J., (1997). A legume ethylene-insensitive mutant hyperinfected by its rhizobial symbiont. *Science (New York, N.Y.)*, *275*(5299), 527–530.

Perraki, A., DeFalco, T. A., Derbyshire, P., Avila, J., Séré, D., Sklenar, J., Qi, X., Stransfeld, L., Schwessinger, B., Kadota, Y., Macho, A. P., Jiang, S., Couto, D., Torii, K. U., Menke, F. L. H., & Zipfel, C. (2018). Phosphocode-dependent functional dichotomy of a common co-receptor in plant signalling. *Nature*, *561*(7722), Article 7722.

Peters, N. K., Frost, J. W., & Long, S. R. (1986). A plant flavone, luteolin, induces expression of *Rhizobium meliloti* nodulation genes. *Science*, *233*(4767), 977–980.

Pimprikar, P., & Gutjahr, C. (2018). Transcriptional regulation of arbuscular mycorrhiza development. *Plant and Cell Physiology*, *59*(4), 678–695.

Pingret, J.-L., Journet, E.-P., & Barker, D. G. (1998). Rhizobium Nod factor signaling: evidence for a g protein–mediated transduction mechanism. *The Plant Cell*, *10*(5), 659–671.

Piquerez, S. J. M., Balmuth, A. L., Sklenář, J., Jones, A. M. E., Rathjen, J. P., & Ntoukakis, V. (2014). Identification of post-translational modifications of plant protein complexes. *Journal of Visualized Experiments : JoVE*, *84*, 51095.

Plet, J., Wasson, A., Ariel, F., Le Signor, C., Baker, D., Mathesius, U., Crespi, M., & Frugier, F. (2011). MtCRE1-dependent cytokinin signaling integrates bacterial and plant cues to coordinate symbiotic nodule organogenesis in *Medicago truncatula*. *The Plant Journal*, *65*(4), 622–633.

Radutoiu, S., Madsen, L. H., Madsen, E. B., Felle, H. H., Umehara, Y., Grønlund, M., Sato, S., Nakamura, Y., Tabata, S., Sandal, N., & Stougaard, J. (2003). Plant recognition of symbiotic bacteria requires two LysM receptor-like kinases. *Nature*, *425*(6958), Article 6958.

Rao, V. S., Srinivas, K., Sujini, G. N., & Kumar, G. N. S. (2014). Protein-protein interaction detection: methods and analysis. *International Journal of Proteomics*, *2014*, 147648.

Redmond, J. W., Batley, M., Djordjevic, M. A., Innes, R. W., Kuempel, P. L., & Rolfe, B. G. (1986). Flavones induce expression of nodulation genes in Rhizobium. *Nature*, *323*(6089), Article 6089.

Reid, D., Nadzieja, M., Novák, O., Heckmann, A. B., Sandal, N., & Stougaard, J. (2017). Cytokinin biosynthesis promotes cortical cell responses during nodule development. *Plant Physiology*, *175*(1), 361–375.

Ried, M. K., Antolín-Llovera, M., & Parniske, M. (2014). Spontaneous symbiotic reprogramming of plant roots triggered by receptor-like kinases. *ELife*, *3*, e03891.

Riely, B. K., Lougnon, G., Ané, J.-M., & Cook, D. R. (2007). The symbiotic ion channel homolog DMI1 is localized in the nuclear membrane of *Medicago truncatula* roots. *The Plant Journal*, *49*(2), 208–216.

Rightmyer, A. P., & Long, S. R. (2011). Pseudonodule formation by wild-type and symbiotic mutant *Medicago truncatula* in response to auxin transport inhibitors. *Molecular Plant-Microbe Interactions®*, *24*(11), 1372–1384.

Rocher, M., Simon, V., Jolivet, M.-D., Sofer, L., Deroubaix, A.-F., Germain, V., Mongrand, S., & German-Retana, S. (2022). StREM1.3 REMORIN protein plays an agonistic role in potyvirus cell-to-cell movement in *N. benthamiana*. *Viruses*, *14*(3), Article 3.

Rodrigues, C. H., Pires, D. E., & Ascher, D. B. (2018). DynaMut: Predicting the impact of mutations on protein conformation, flexibility and stability. *Nucleic Acids Research*, *46*(W1), W350–W355.

Roth, L. E., & Stacey, G. (1989). Bacterium release into host cells of nitrogen-fixing soybean nodules: The symbiosome membrane comes from three sources. *European Journal of Cell Biology*, *49*(1), 13–23.

Routray, P., Miller, J. B., Du, L., Oldroyd, G., & Poovaiah, B. W. (2013). Phosphorylation of S344 in the calmodulin-binding domain negatively affects CCaMK function during bacterial and fungal symbioses. *The Plant Journal*, *76*(2), 287–296.

Russo, G., Carotenuto, G., Fiorilli, V., Volpe, V., Chiapello, M., Van Damme, D., & Genre, A. (2019). Ectopic activation of cortical cell division during the accommodation of arbuscular mycorrhizal fungi. *New Phytologist*, *221*(2), 1036–1048.

Ryu, H., Kim, K., Cho, H., & Hwang, I. (2010). Predominant actions of cytosolic BSU1 and nuclear BIN2 regulate subcellular localization of BES1 in brassinosteroid signaling. *Molecules and Cells*, *29*(3), 291–296.

Ryu, H., Kim, K., Cho, H., Park, J., Choe, S., & Hwang, I. (2007). Nucleocytoplasmic shuttling of BZR1 mediated by phosphorylation is essential in Arabidopsis brassinosteroid signaling. *The Plant Cell*, *19*(9), 2749–2762.

Sabatini, S., Heidstra, R., Wildwater, M., & Scheres, B. (2003). SCARECROW is involved in positioning the stem cell niche in the Arabidopsis root meristem. *Genes & Development*, *17*(3), 354–358.

Sagan, M., Morandi, D., Tarenghi, E., & Duc, G. (1995). Selection of nodulation and mycorrhizal mutants in the model plant *Medicago truncatula* (Gaertn.) after *γ*-ray mutagenesis. *Plant Science*, *111*(1), 63–71.

Saha, S., Dutta, A., Bhattacharya, A., & DasGupta, M. (2014). Intracellular catalytic domain of SYMBIOSIS RECEPTOR KINASE hyperactivates spontaneous nodulation in absence of rhizobia. *Plant Physiology*, *166*(4), 1699–1708.

Saito, K., Yoshikawa, M., Yano, K., Miwa, H., Uchida, H., Asamizu, E., Sato, S., Tabata, S., Imaizumi-Anraku, H., Umehara, Y., Kouchi, H., Murooka, Y., Szczyglowski, K., Downie, J. A., Parniske, M., Hayashi, M., & Kawaguchi, M. (2007). NUCLEOPORIN85 is required for calcium spiking, fungal and bacterial symbioses, and seed production in *Lotus japonicus*. *The Plant Cell*, *19*(2), 610–624.

Saitou, N., & Nei, M. (1987). The neighbor-joining method: A new method for reconstructing phylogenetic trees. *Molecular Biology and Evolution*, *4*(4), 406–425.

Sanders, D., Brownlee, C., & Harper, J. F. (1999). Communicating with calcium. *The Plant Cell*, *11*(4), 691–706.

Sanders, D., Pelloux, J., Brownlee, C., & Harper, J. F. (2002). Calcium at the crossroads of signaling. *The Plant Cell*, *14*(suppl_1), S401–S417.

Sathyanarayanan, P. V., Siems, W. F., Jones, J. P., & Poovaiah, B. W. (2001). Calcium-stimulated autophosphorylation site of plant chimeric calcium/calmodulin-dependent protein kinase . *Journal of Biological Chemistry*, *276*(35), 32940–32947.

Schauser, L., Roussis, A., Stiller, J., & Stougaard, J. (1999). A plant regulator controlling development of symbiotic root nodules. *Nature*, *402*(6758), Article 6758.

Scheres, B., Wiel, C. V. D., Zalensky, A., Horvath, B., Spaink, H., Eck, H. V., Zwartkruis, F., Wolters, A.-M., Gloudemans, T., Kammen, A. V., & Bisseling, T. (1990). The *ENOD12* gene product is involved in the infection process during the pea-rhizobium interaction. *Cell*, *60*(2), 281–294.

Schiessl, K., Lilley, J. L. S., Lee, T., Tamvakis, I., Kohlen, W., Bailey, P. C., Thomas, A., Luptak, J., Ramakrishnan, K., Carpenter, M. D., Mysore, K. S., Wen, J., Ahnert, S., Grieneisen, V. A., & Oldroyd, G. E. D. (2019). NODULE INCEPTION recruits the lateral root developmental program for symbiotic nodule organogenesis in *Medicago truncatula*. *Current Biology: CB*, *29*(21), 3657-3668.e5.

Schnabel, E., Journet, E.-P., de Carvalho-Niebel, F., Duc, G., & Frugoli, J. (2005). The *Medicago truncatula SUNN* gene encodes a CLV1-like leucine-rich repeat receptor kinase that regulates nodule number and root length. *Plant Molecular Biology*, *58*(6), 809–822.

Schubert, R., & Nelson, M. T. (2001). Protein kinases: Tuners of the BKCa channel in smooth muscle. *Trends in Pharmacological Sciences*, *22*(10), 505–512.

Semple, J. I., Sanderson, C. M., & Campbell, R. D. (2002). The jury is out on 'guilt by association' trials. *Briefings in Functional Genomics*, *1*(1), 40–52.

Shah, N. B., & Duncan, T. M. (2014). Bio-layer interferometry for measuring kinetics of protein-protein interactions and allosteric ligand effects. *Journal of Visualized Experiments : JoVE*, *84*, 51383.

Shaw, S. L., & Long, S. R. (2003). Nod factor elicits two separable calcium responses in *Medicago truncatula* root hair cells. *Plant Physiology*, *131*(3), 976–984.

Shimomura, O., & Johnson, F. H. (1970). Calcium binding, quantum yield, and emitting molecule in aequorin bioluminescence. *Nature*, *227*(5265), 1356–1357.

Shimomura, O., Johnson, F. H., & Morise, H. (1974). Mechanism of the luminescent intramolecular reaction of aequorin. *Biochemistry*, *13*(16), 3278–3286.

Shiu, S.-H., & Bleecker, A. B. (2001). Receptor-like kinases from *Arabidopsis* form a monophyletic gene family related to animal receptor kinases. *Proceedings of the National Academy of Sciences*, *98*(19), 10763–10768.

Shrestha, A., Zhong, S., Therrien, J., Huebert, T., Sato, S., Mun, T., Andersen, S. U., Stougaard, J., Lepage, A., Niebel, A., Ross, L., & Szczyglowski, K. (2021). *Lotus japonicus* NUCLEAR FACTOR YA1, a nodule emergence stage-specific regulator of auxin signalling. *The New Phytologist*, *229*(3), 1535–1552.

Sicheri, F., Moarefi, I., & Kuriyan, J. (1997). Crystal structure of the Src family tyrosine kinase Hck. *Nature*, *385*(6617), Article 6617.

Sieberer, B. J., Chabaud, M., Fournier, J., Timmers, A. C. J., & Barker, D. G. (2012). A switch in Ca^{2+} spiking signature is concomitant with endosymbiotic microbe entry into cortical root cells of *Medicago truncatula*. *The Plant Journal*, *69*(5), 822–830.

Sieberer, B. J., Chabaud, M., Timmers, A. C., Monin, A., Fournier, J., & Barker, D. G. (2009). A nuclear-targeted cameleon demonstrates intranuclear Ca^{2+} spiking in *Medicago truncatula* root hairs in response to rhizobial Nodulation factors. *Plant Physiology*, *151*(3), 1197–1206.

Singh, S., Katzer, K., Lambert, J., Cerri, M., & Parniske, M. (2014). CYCLOPS, A DNA-binding transcriptional activator, orchestrates symbiotic root nodule development. *Cell Host & Microbe*, *15*(2), 139–152.

Singh, S., & Parniske, M. (2012). Activation of calcium- and calmodulin-dependent protein kinase (CCaMK), the central regulator of plant root endosymbiosis. *Current Opinion in Plant Biology*, *15*(4), 444–453.

Smit, P., Limpens, E., Geurts, R., Fedorova, E., Dolgikh, E., Gough, C., & Bisseling, T. (2007). *Medicago* LYK3, an entry receptor in rhizobial nodulation factor signaling. *Plant Physiology*, *145*(1), 183–191.

Soyano, T., Hirakawa, H., Sato, S., Hayashi, M., & Kawaguchi, M. (2014). NODULE INCEPTION creates a long-distance negative feedback loop involved in homeostatic regulation of nodule organ production. *Proceedings of the National Academy of Sciences*, *111*(40), 14607–14612.

Soyano, T., Kouchi, H., Hirota, A., & Hayashi, M. (2013). NODULE INCEPTION directly targets NF-Y subunit genes to regulate essential processes of root nodule development in *Lotus japonicus*. *PLOS Genetics*, *9*(3), e1003352.

Soyano, T., Liu, M., Kawaguchi, M., & Hayashi, M. (2021). Leguminous nodule symbiosis involves recruitment of factors contributing to lateral root development. *Current Opinion in Plant Biology*, *59*, 102000.

Soyano, T., Shimoda, Y., Kawaguchi, M., & Hayashi, M. (2019a). A shared gene drives lateral root development and root nodule symbiosis pathways in *Lotus*. *Science (New York, N.Y.)*, *366*(6468), 1021–1023.

Stael, S., Wurzinger, B., Mair, A., Mehlmer, N., Vothknecht, U. C., & Teige, M. (2012). Plant organellar calcium signalling: An emerging field. *Journal of Experimental Botany*, *63*(4), 1525–1542.

Stougaard, J., Abildsten, D., & Marcker, K. A. (1987). The *Agrobacterium rhizogenes* pRi TL-DNA segment as a gene vector system for transformation of plants. *Molecular and General Genetics MGG*, *207*(2), 251–255.

Stracke, S., Kistner, C., Yoshida, S., Mulder, L., Sato, S., Kaneko, T., Tabata, S., Sandal, N., Stougaard, J., Szczyglowski, K., & Parniske, M. (2002). A plant receptor-like kinase required for both bacterial and fungal symbiosis. *Nature*, *417*(6892), Article 6892.

Sun, J., Miller, J. B., Granqvist, E., Wiley-Kalil, A., Gobbato, E., Maillet, F., Cottaz, S., Samain, E., Venkateshwaran, M., Fort, S., Morris, R. J., Ané, J.-M., Dénarié, J., & Oldroyd, G. E. D. (2015). Activation of symbiosis signaling by arbuscular mycorrhizal fungi in legumes and rice. *The Plant Cell*, *27*(3), 823–838.

Sun, J., Miwa, H., Downie, J. A., & Oldroyd, G. E. D. (2007). Mastoparan activates calcium spiking analogous to nod factor-induced responses in *Medicago truncatula* root hair cells. *Plant Physiology*, *144*(2), 695–702.

Sun, W., Cao, Y., Jansen Labby, K., Bittel, P., Boller, T., & Bent, A. F. (2012). Probing the Arabidopsis flagellin receptor: FLS2-FLS2 association and the contributions of specific domains to signaling function. *The Plant Cell*, *24*(3), 1096–1113.

Suzaki, T., Yano, K., Ito, M., Umehara, Y., Suganuma, N., & Kawaguchi, M. (2012). Positive and negative regulation of cortical cell division during root nodule development in *Lotus japonicus* is accompanied by auxin response. *Development*, *139*(21), 3997–4006.

Takahashi, D., Kawamura, Y., & Uemura, M. (2013). Detergent-resistant plasma membrane proteome to elucidate microdomain functions in plant cells. *Frontiers in Plant Science*, *4*.

Takeda, N., Handa, Y., Tsuzuki, S., Kojima, M., Sakakibara, H., & Kawaguchi, M. (2015). Gibberellins interfere with symbiosis signaling and gene expression and alter colonization by arbuscular mycorrhizal fungi in *Lotus japonicus*. *Plant Physiology*, *167*(2), 545–557.

Takeda, N., Maekawa, T., & Hayashi, M. (2012). Nuclear-localized and deregulated calcium- and calmodulin-dependent protein kinase activates rhizobial and mycorrhizal responses in *Lotus japonicus*. *The Plant Cell*, *24*(2), 810–822.

Tang, W., Kim, T.-W., Oses-Prieto, J. A., Sun, Y., Deng, Z., Zhu, S., Wang, R., Burlingame, A. L., & Wang, Z.-Y. (2008). BSKs mediate signal transduction from the receptor kinase BRI1 in Arabidopsis. *Science*, *321*(5888), 557–560.

Taylor, S. S., & Kornev, A. P. (2011). Protein kinases: Evolution of dynamic regulatory proteins. *Trends in Biochemical Sciences*, *36*(2), 65–77.

Tian, L., Duncan, R. R., Hammond, M. S. L., Coghill, L. S., Wen, H., Rusinova, R., Clark, A. G., Levitan, I. B., & Shipston, M. J. (2001). Alternative splicing switches potassium channel sensitivity to protein phosphorylation. *Journal of Biological Chemistry*, *276*(11), 7717–7720.

Tian, W., Hou, C., Ren, Z., Wang, C., Zhao, F., Dahlbeck, D., Hu, S., Zhang, L., Niu, Q., Li, L., Staskawicz, B. J., & Luan, S. (2019). A calmodulin-gated calcium channel links pathogen patterns to plant immunity. *Nature*, *572*(7767), 131–135.

Timmers, A. C., Auriac, M. C., & Truchet, G. (1999). Refined analysis of early symbiotic steps of the *Rhizobium-Medicago* interaction in relationship with microtubular cytoskeleton rearrangements. *Development*, *126*(16), 3617–3628.

Tirichine, L., Imaizumi-Anraku, H., Yoshida, S., Murakami, Y., Madsen, L. H., Miwa, H., Nakagawa, T., Sandal, N., Albrektsen, A. S., Kawaguchi, M., Downie, A., Sato, S., Tabata, S., Kouchi, H., Parniske, M., Kawasaki, S., & Stougaard, J. (2006). Deregulation of a Ca^{2+}/calmodulin-dependent kinase leads to spontaneous nodule development. *Nature*, *441*(7097), Article 7097.

Tirichine, L., Sandal, N., Madsen, L. H., Radutoiu, S., Albrektsen, A. S., Sato, S., Asamizu, E., Tabata, S., & Stougaard, J. (2007). A gain-of-function mutation in a cytokinin receptor triggers spontaneous root nodule organogenesis. *Science*, *315*(5808), 104–107.

Trentini, D. B., Fuhrmann, J., Mechtler, K., & Clausen, T. (2014). Chasing phosphoarginine proteins: development of a selective enrichment method using a phosphatase trap. *Molecular & Cellular Proteomics*, *13*(8), 1953–1964.

Truchet, G., Roche, P., Lerouge, P., Vasse, J., Camut, S., de Billy, F., Promé, J.-C., & Dénarié, J. (1991). Sulphated lipo-oligosaccharide signals of *Rhizobium meliloti* elicit root nodule organogenesis in alfalfa. *Nature*, *351*(6328), Article 6328.

Tsikou, D., Yan, Z., Holt, D. B., Abel, N. B., Reid, D. E., Madsen, L. H., Bhasin, H., Sexauer, M., Stougaard, J., & Markmann, K. (2018). Systemic control of legume susceptibility to rhizobial infection by a mobile microRNA. *Science*, *362*(6411), 233–236.

Tsyganova, A. V., Kitaeva, A. B., Tsyganov, V. E., Tsyganova, A. V., Kitaeva, A. B., & Tsyganov, V. E. (2017). Cell differentiation in nitrogen-fixing nodules hosting symbiosomes. *Functional Plant Biology*, *45*(2), 47–57.

Vahisalu, T., Kollist, H., Wang, Y.-F., Nishimura, N., Chan, W.-Y., Valerio, G., Lamminmäki, A., Brosché, M., Moldau, H., Desikan, R., Schroeder, J. I., & Kangasjärvi, J. (2008). SLAC1 is required for plant guard cell S-type anion channel function in stomatal signalling. *Nature*, *452*(7186), Article 7186.

Vahisalu, T., Puzõrjova, I., Brosché, M., Valk, E., Lepiku, M., Moldau, H., Pechter, P., Wang, Y.-S., Lindgren, O., Salojärvi, J., Loog, M., Kangasjärvi, J., & Kollist, H. (2010). Ozone-triggered rapid stomatal response involves the production of reactive oxygen species, and is controlled by SLAC1 and OST1. *The Plant Journal*, *62*(3), 442–453.

van Batenburg, F. H. D., Jonker, R., & Kijne, J. W. (1986). Rhizobium induces marked root hair curling by redirection of tip growth: A computer simulation. *Physiologia Plantarum*, *66*(3), 476–480.

van Brussel, A. A. N., Bakhuizen, R., van Spronsen, P. C., Spaink, H. P., Tak, T., Lugtenberg, B. J. J., & Kijne, J. W. (1992). Induction of pre-infection thread structures in the leguminous host plant by mitogenic lipo-oligosaccharides of Rhizobium. *Science*, *257*(5066), 70–72.

Van de Velde, W., Guerra, J. C. P., Keyser, A. D., De Rycke, R., Rombauts, S., Maunoury, N., Mergaert, P., Kondorosi, E., Holsters, M., & Goormachtig, S. (2006). Aging in legume symbiosis. A molecular view on nodule senescence in *Medicago truncatula*. *Plant Physiology*, *141*(2), 711–720.

van der Luit, A. H., Olivari, C., Haley, A., Knight, M. R., & Trewavas, A. J. (1999). Distinct calcium signaling pathways regulate calmodulin gene expression in tobacco. *Plant Physiology*, *121*(3), 705–714.

van Spronsen, P., Bakhuizen, R., van, B. A., & Kijne, J. W. (1994). Cell wall degradation during infection thread formation by the root nodule bacterium *Rhizobium leguminosarum* is a two-step process. *European Journal of Cell Biology*, *64*(1), 88–94.

van Wijk, K. J., Friso, G., Walther, D., & Schulze, W. X. (2014). Meta-analysis of *Arabidopsis thaliana* phospho-proteomics data reveals compartmentalization of phosphorylation motifs. *The Plant Cell*, *26*(6), 2367–2389.

Varma Penmetsa, R., Uribe, P., Anderson, J., Lichtenzveig, J., Gish, J.-C., Nam, Y. W., Engstrom, E., Xu, K., Sckisel, G., Pereira, M., Baek, J. M., Lopez-Meyer, M., Long, S. R., Harrison, M. J., Singh, K. B., Kiss, G. B., & Cook, D. R. (2008). The *Medicago truncatula* ortholog of Arabidopsis EIN2, sickle, is a negative regulator of symbiotic and pathogenic microbial associations. *The Plant Journal*, *55*(4), 580–595.

Venkateshwaran, M., Jayaraman, D., Chabaud, M., Genre, A., Balloon, A. J., Maeda, J., Forshey, K., den Os, D., Kwiecien, N. W., Coon, J. J., Barker, D. G., & Ané, J.-M. (2015). A role for the mevalonate pathway in early plant symbiotic signaling. *Proceedings of the National Academy of Sciences of the United States of America*, *112*(31), 9781–9786.

Vernié, T., Camut, S., Camps, C., Rembliere, C., de Carvalho-Niebel, F., Mbengue, M., Timmers, T., Gasciolli, V., Thompson, R., le Signor, C., Lefebvre, B., Cullimore, J., & Hervé, C. (2016). PUB1 interacts with the receptor kinase DMI2 and negatively regulates rhizobial and arbuscular mycorrhizal symbioses through its ubiquitination activity in *Medicago truncatula*. *Plant Physiology*, *170*(4), 2312–2324.

Vernié, T., Kim, J., Frances, L., Ding, Y., Sun, J., Guan, D., Niebel, A., Gifford, M. L., de Carvalho-Niebel, F., & Oldroyd, G. E. D. (2015). The NIN transcription factor coordinates diverse nodulation programs in different tissues of the *Medicago truncatula* root. *The Plant Cell*, *27*(12), 3410–3424.

Waas, W. F., & Dalby, K. N. (2002). Transient protein-protein interactions and a random-ordered kinetic mechanism for the phosphorylation of a transcription factor by EXTRACELLULAR-REGULATED PROTEIN KINASE 2. *Journal of Biological Chemistry*, *277*(15), 12532–12540.

Wais, R. J., Galera, C., Oldroyd, G., Catoira, R., Penmetsa, R. V., Cook, D., Gough, C., Dénarié, J., & Long, S. R. (2000). Genetic analysis of calcium spiking responses in nodulation mutants of *Medicago truncatula*. *Proceedings of the National Academy of Sciences of the United States of America*, *97*(24), 13407–13412.

Walker, S. A., Viprey, V., & Downie, J. A. (2000). Dissection of nodulation signaling using pea mutants defective for calcium spiking induced by Nod factors and chitin oligomers. *Proceedings of the National Academy of Sciences*, *97*(24), 13413–13418.

Wallner, M., Meera, P., & Toro, L. (1996). Determinant for *β*-subunit regulation in high-conductance voltage-activated and Ca^{2+}-sensitive K^+ channels: An additional transmembrane region at the N terminus. *Proceedings of the National Academy of Sciences*, *93*(25), 14922–14927.

Walter, A., Mazars, C., Maitrejean, M., Hopke, J., Ranjeva, R., Boland, W., & Mithöfer, A. (2007). Structural requirements of jasmonates and synthetic analogues as inducers of Ca^{2+} signals in the nucleus and the cytosol of plant cells. *Angewandte Chemie International Edition*, *46*(25), 4783–4785.

Wang, L., Xue, Y., Xing, J., Song, K., & Lin, J. (2018). Exploring the spatiotemporal organization of membrane proteins in living plant cells. *Annual Review of Plant Biology*, *69*(1), 525–551.

Wang, X., & Chory, J. (2006). Brassinosteroids regulate dissociation of BKI1, a negative regulator of BRI1 signaling, from the plasma membrane. *Science (New York, N.Y.)*, *313*(5790), 1118–1122.

Wang, X., Goshe, M. B., Soderblom, E. J., Phinney, B. S., Kuchar, J. A., Li, J., Asami, T., Yoshida, S., Huber, S. C., & Clouse, S. D. (2005). Identification and functional analysis of *in vivo* phosphorylation sites of the Arabidopsis BRASSINOSTEROID-INSENSITIVE1 receptor kinase. *The Plant Cell*, *17*(6), 1685–1703.

Wang, X., Kota, U., He, K., Blackburn, K., Li, J., Goshe, M. B., Huber, S. C., & Clouse, S. D. (2008). Sequential transphosphorylation of the BRI1/BAK1 receptor kinase complex impacts early events in brassinosteroid signaling. *Developmental Cell*, *15*(2), 220–235.

Wang, X., Li, X., Meisenhelder, J., Hunter, T., Yoshida, S., Asami, T., & Chory, J. (2005). Autoregulation and homodimerization are involved in the activation of the plant steroid receptor BRI1. *Developmental Cell*, *8*(6), 855–865.

Waterhouse, A., Bertoni, M., Bienert, S., Studer, G., Tauriello, G., Gumienny, R., Heer, F. T., de Beer, T. A. P., Rempfer, C., Bordoli, L., Lepore, R., & Schwede, T. (2018). SWISS-MODEL: Homology modelling of protein structures and complexes. *Nucleic Acids Research*, *46*(W1), W296–W303.

Wu, H.-C., Luo, D.-L., Vignols, F., & Jinn, T.-L. (2012). Heat shock-induced biphasic Ca^{2+} signature and *Os*CaM1-1 nuclear localization mediate downstream signalling in acquisition of thermotolerance in rice (*Oryza sativa* L.). *Plant, Cell & Environment*, *35*(9), 1543–1557.

Wu, S.-N., Wang, Y.-J., & Lin, M.-W. (2007). Potent stimulation of large-conductance Ca^{2+}-activated K^+ channels by rottlerin, an inhibitor of protein kinase C-δ, in pituitary tumor (GH3) cells and in cortical neuronal (HCN-1A) cells. *Journal of Cellular Physiology*, *210*(3), 655–666.

Xiao, T. T., Schilderink, S., Moling, S., Deinum, E. E., Kondorosi, E., Franssen, H., Kulikova, O., Niebel, A., & Bisseling, T. (2014). Fate map of *Medicago truncatula* root nodules. *Development*, *141*(18), 3517–3528.

Xiao, T. T., van Velzen, R., Kulikova, O., Franken, C., & Bisseling, T. (2019). Lateral root formation involving cell division in both pericycle, cortex and endodermis is a common and ancestral trait in seed plants. *Development*, *146*(20), dev182592.

Xie, F., Murray, J. D., Kim, J., Heckmann, A. B., Edwards, A., Oldroyd, G. E. D., & Downie, J. A. (2012). Legume pectate lyase required for root infection by rhizobia. *Proceedings of the National Academy of Sciences*, *109*(2), 633–638.

Xu, J., Li, H.-D., Chen, L.-Q., Wang, Y., Liu, L.-L., He, L., & Wu, W.-H. (2006). A protein kinase, interacting with two calcineurin B-like proteins, regulates K+ transporter AKT1 in Arabidopsis. *Cell*, *125*(7), 1347–1360.

Yang, K.-Z., Jiang, M., Wang, M., Xue, S., Zhu, L.-L., Wang, H.-Z., Zou, J.-J., Lee, E.-K., Sack, F., & Le, J. (2015). Phosphorylation of serine 186 of bHLH transcription factor SPEECHLESS promotes stomatal development in Arabidopsis. *Molecular Plant*, *8*(5), 783–795.

Yang, X., Gavya S, L., Zhou, Z., Urano, D., & Lau, O. S. (n.d.). Abscisic acid regulates stomatal production by imprinting a SnRK2 kinase–mediated phosphocode on the master regulator SPEECHLESS. *Science Advances*, *8*(40), eadd2063.

Yano, K., Yoshida, S., Müller, J., Singh, S., Banba, M., Vickers, K., Markmann, K., White, C., Schuller, B., Sato, S., Asamizu, E., Tabata, S., Murooka, Y., Perry, J., Wang, T. L., Kawaguchi, M., Imaizumi-Anraku, H., Hayashi, M., & Parniske, M. (2008).

CYCLOPS, a mediator of symbiotic intracellular accommodation. *Proceedings of the National Academy of Sciences*, *105*(51), 20540–20545.

Yoro, E., Suzaki, T., Toyokura, K., Miyazawa, H., Fukaki, H., & Kawaguchi, M. (2014). A positive regulator of nodule organogenesis, NODULE INCEPTION, acts as a negative regulator of rhizobial infection in *Lotus japonicus*. *Plant Physiology*, *165*(2), 747–758.

Yu, T.-Y., Shi, D.-Q., Jia, P.-F., Tang, J., Li, H.-J., Liu, J., & Yang, W.-C. (2016). The Arabidopsis receptor kinase ZAR1 is required for zygote asymmetric division and its daughter cell fate. *PLOS Genetics*, *12*(3), e1005933.

Yuan, P., Jewell, J. B., Behera, S., Tanaka, K., & Poovaiah, B. W. (2020). Distinct molecular pattern-induced calcium signatures lead to different downstream transcriptional regulations via AtSR1/CAMTA3. *International Journal of Molecular Sciences*, *21*(21), Article 21.

Yuan, S., Zhu, H., Gou, H., Fu, W., Liu, L., Chen, T., Ke, D., Kang, H., Xie, Q., Hong, Z., & Zhang, Z. (2012). A ubiquitin ligase of SYMBIOSIS RECEPTOR KINASE involved in nodule organogenesis. *Plant Physiology*, *160*(1), 106–117.

Zhang, G., Yang, J., Chen, X., Zhao, D., Zhou, X., Zhang, Y., Wang, X., & Zhao, J. (2021). Phospholipase D- and phosphatidic acid-mediated phospholipid metabolism and signaling modulate symbiotic interaction and nodulation in soybean (*Glycine max*). *The Plant Journal*, *106*(1), 142–158.

Zhang, Y. (2008). I-TASSER server for protein 3D structure prediction. *BMC Bioinformatics*, *9*, 40.

Zhang, Z., Ke, D., Hu, M., Zhang, C., Deng, L., Li, Y., Li, J., Zhao, H., Cheng, L., Wang, L., & Yuan, H. (2019). Quantitative phosphoproteomic analyses provide evidence for extensive phosphorylation of regulatory proteins in the rhizobia–legume symbiosis. *Plant Molecular Biology*, *100*(3), 265–283.

Zhou, X.-B., Arntz, C., Kamm, S., Motejlek, K., Sausbier, U., Wang, G.-X., Ruth, P., & Korth, M. (2001). A molecular switch for specific stimulation of the BKCa Channel by cGMP and cAMP kinase. *Journal of Biological Chemistry*, *276*(46), 43239–43245.